Reversible solid oxide cells in microgrids and peer-to-peer energy markets

Timothy Hutty

Thesis submitted to the University of Sheffield for the degree of Doctor of Philosophy

The University of Sheffield

Department of Chemical and Biological Engineering

September 2022

Acknowledgements

I'd like to thank Prof. Solomon Brown, PhD Supervisor, University of Sheffield – for his wisdom, good advice and (especially) patience.

I would also like to thank my wife, for putting up with this whole thing.

S.D.G.

Funding

Grateful acknowledgement is made of the financial support of the Engineering and Physical Sciences Research Council (EPSRC) in the form of the 'Energy Storage and its Applications' Centre for Doctoral Training under grant code EP/L0168/18; also of the Electric Power Research Institute.

Abstract

The drive to decarbonise energy systems is leading to increased deployment of renewable generation; such generation is typically intermittent, leading to difficulties in matching supply and demand. Whilst battery storage and related technologies can address intermittency on a short timescale, longer timescales will likely require storage of energy as hydrogen (or perhaps other fuels). Reversible solid oxide cells (rSOCs) embody both electrolyser and fuel cell in one device; that is, they can convert both power to gas, and gas to power - when combined with hydrogen storage, an energy store is the result. They also boast superior efficiency to the rival alkaline and PEM technologies, whilst the high-grade heat given off during fuel cell operation provides an interesting opportunity to supply heat demand.

This project aims to assess the possible application of rSOCs as electrical energy storage for the residential sector. Simulation models are developed to investigate the techno-economic benefits of the technology, principally as a store for solar power. In the first two results chapters, these models are combined with global optimisation in order to investigate the optimal sizing of the energy storage system, and the choice of energy storage technology (rSOC versus battery). Findings indicate challenging economics for electrical energy storage with the rSOC. Battery storage and / or oversizing of generation is often a more cost-efficient way to address the intermittency of generation, with the rSOC an optimal selection only when a high degree of self-sufficiency is required of the system, leading to a need for seasonal energy storage; even in this case, the financial metrics (payback period, net present value) for the rSOC are not entirely encouraging.

A secondary theme of the work is peer-to-peer (P2P) trading, whereby electricity (and perhaps heat) can be traded between customers, rather than with the utility company only. P2P is introduced to the modelling in the last two results chapters, using an agent-based approach to model the P2P market. Electrification of transport and heat will introduce large loads to the electricity network in the future, but these loads are expected to have a degree of flexibility; P2P provides the incentive to synchronise these flexible loads with local generation, as far as possible. As such, P2P may be seen as competing with energy storage as a solution to intermittency, or as synergetic. The third results chapter demonstrates the efficacy of P2P in conjunction with solar PV and energy storage using electric vehicle batteries (‘V2H’). Financial savings are demonstrated across technology penetration scenarios, and for all classes of participant in the market. In the fourth results chapter, the rSOC returns, participating in a simulated P2P market alongside EV chargers, PV and heat pumps. For this work, a novel P2P model is constructed on the basis of continuous double auction, along with strategies for bidding with flexible devices or energy storage. It is demonstrated that the P2P electricity trading gains significant profits for the rSOC owners, as well as bringing environmental and technical benefits. In future work, it is hoped to recombine results of the P2P market with the earlier work on optimal technology choice and sizing.

Declaration

I, the author, confirm that the Thesis is my own work. I am aware of the University's Guidance on the Use of Unfair Means (www.sheffield.ac.uk/ssid/unfair-means). This work has not been previously been presented for an award at this, or any other, university.

The thesis includes the text of three publications of which I am the main author. These are reproduced with the permission of Elsevier. The published works are as follows:

> Hutty, T. D., Dong, S., & Brown, S. (2020). Suitability of energy storage with reversible solid oxide cells for microgrid applications. *Energy Conversion and Management*, *226*, 113499. https://doi.org/10.1016/j.enconman.2020.113499
>
> Hutty, T. D., Dong, S., Lee, R., & Brown, S. (2021). Long term energy storage with reversible solid oxide cells for microgrid applications. *Energy Reports*, *7*, 24–33. https://doi.org/10.1016/j.egyr.2021.02.059
>
> Hutty, T. D., Pena-Bello, A., Dong, S., Parra, D., Rothman, R., & Brown, S. (2021). Peer-to-peer electricity trading as an enabler of increased PV and EV ownership. *Energy Conversion and Management*, *245*, 114634. https://doi.org/10.1016/j.enconman.2021.114634

A further text has been prepared for publication, but not yet submitted to a journal.

Contents

Table of acronyms

Acronym	Definition	Acronym	Definition
ADMM	Alternating direction method of multipliers	MH	Metal hydride
ASHP	Air source heat pump	MILP	Mixed integer linear programming
ASR	Area specific resistance	MMR	Mid-market rate
BESS	Battery energy storage system	NG	Natural gas
CAES	Compressed air energy storage	NPC	Net present cost
CCS	Carbon capture and storage	NPV	Net present value
CDA	Continuous double auction	NTS	National Travel Survey
CES	Community energy storage	OOP	Object oriented programming
CHG	Compressed hydrogen gas	P2G	Power to gas
CHP	Combined heat and power	P2G2P	Power to gas to power
COE	Cost of electricity	P2P	Peer-to-peer
COP	Coefficient of performance	PCM	Phase change material
CSP	Concentrated solar power	PEM	Proton exchange membrane / Polymer electrolyte membrane
DHI	Direct horizontal irradiance	PHS	Pumped hydropower storage
DHW	Domestic hot water	PTSC	Parabolic trough solar collector
DSM	Demand side management	PV	Photovoltaic
EBI	Energy balance index	RSOC	Reversible solid oxide cell
EC	Electrolyser cell	RT	Round trip
EV	Electric vehicle	SDR	Supply demand ratio
FC	Fuel cell	SOC	Solid oxide cell
G2P	Gas to power	SOEC	Solid oxide electrolyser cell
GHG	Greenhouse gas	SOFC	Solid oxide fuel cell
GHI	Global horizontal irradiance	SSR	Self-sufficiency ratio
HDD	Heating degree day	TES	Thermal energy storage
HESS	Hydrogen energy storage system	V1G	Smart EV charging
HHV	Higher heating value	V2G	Vehicle to grid
LCOS	Levelised cost of storage	V2H	Vehicle to home
LHV	Lower heating value	V2X	Vehicle to anything
LSGM	Lanthanum strontium magnesium gallate	YSZ	Yttrium-stabilised zirconia
LSM	Lanthanum strontium manganite	ZI	Zero intelligence

1. Introduction

In order to mitigate the threat of climate change, it is urgently necessary for energy systems around the world to move away from the carbon intensive fossil fuels upon which they have largely depended in the past. Renewable electricity generation (wind, solar, hydropower, biomass) has the potential to displace generation from fossil fuels. However, wind and solar energy in particular suffer from the problem of intermittency [1]–[3], meaning that the available supply of electricity may not match the demand. Thus energy storage technologies may have an increasing role to play in future energy systems, storing renewable energy when it is available, for consumption when it is required.

Of existing energy storage technologies, most are ill-adapted to store energy for sufficient time periods, or in sufficient bulk, to compensate for fluctuations in renewable output beyond a timescale of hours or days. By contrast, power to gas ('P2G'), the use of electricity to synthesise a gas fuel such as hydrogen or methane, has potential to provide storage of weeks' or months' duration, enabling heavier reliance on renewables by the energy system as a whole. This would typically be accomplished by splitting water with an electrolyser to produce hydrogen gas, which can be stored and subsequently converted back to power using a fuel cell or internal combustion engine. Key difficulties for this form of energy storage are high expense and low round-trip efficiency.

Solid oxide cells (SOCs), although less technologically mature than alkaline or PEM cells, potentially offer superior energy conversion efficiencies both as electrolysers (P2G) and as fuel cells (G2P). Furthermore, it is possible for an SOC to operate reversibly, with a single device able to operate alternately as fuel cell and electrolyser; in this case, it is termed a 'reversible solid oxide cell' or rSOC. SOCs also have a capability to work directly with carbonaceous gases, including methane, a capability not shared by alkaline or PEM cells; use of methane rather than hydrogen as the energy storage medium may offer higher round-trip efficiency, and also enable difficulties with the storage and transport of hydrogen gas to be sidestepped.

A secondary theme of the project is peer-to-peer (P2P) energy trading. This innovation allows for the trading of electricity (and perhaps heat) between customers; compare the current paradigm where energy can only be purchased from, and perhaps sold to, the supplier. P2P trading is potentially a powerful tool to help shift demand to synchronise with local energy generation. For this reason, P2P trading could perhaps offer a rival solution to energy storage such as the rSOC – or perhaps prove to be complementary; either way, the study of the rSOC in tandem with P2P trading should provide a novel and interesting area to investigate.

1.1 Objectives

The objective of this project is to assess the efficacy and cost of rSOCs for providing energy storage at the 'distributed' scale – for instance at suburban/residential level. The core of the project will use the multi-paradigm simulation software AnyLogic [4] to carry out simulation of such a local scale system, seeking to optimise its design and its control. The agent-based simulation paradigm available in AnyLogic is well-adapted to the simulation of complex modern electrical systems, where the interaction of different components is less predictable than in traditional systems with centralised generation; the ability to model such interactions between components and observe the overall emergent behaviour is a key feature of agent-based modelling (see Chapter 2.11).

Observed benefits of the rSOC will be weighed against costs, to determine whether there is a strong case for this technology. Benefits should be considered to include self-sufficiency and environmental benefits, as well as possible economic advantages. A key priority is that the rSOC should not be assessed in isolation, but should be compared to other storage options, particularly battery storage as this is the most prevalent form of energy storage at the present time (other than pumped hydropower). Ultimately, it is the objective of the project to assess the utility of the rSOC in a distributed energy context with energy demands for heat, power and mobility all considered, and to identify whether a synergy can be found between the rSOC and a P2P energy trading market.

1.2 Thesis structure

This thesis is presented in a ‘publication’ format. Chapter 2 presents the background and literature surrounding both rSOCs and P2P energy trading. Chapter 3 provides an overview of the publications; the publications themselves occupy chapters 4 – 7. Conclusions and a discussion of future work are found in Chapters 8 and 9.

2. Literature Review

2.1 Introduction

This chapter relates the background information and academic literature relevant to the present work. The first (and larger) portion of the chapter focuses on **reversible solid oxide cells** (rSOCs) and surrounding topics. The latter sections (2.10 and 2.11) consider **peer-to-peer** (P2P) electricity trading and **agent-based modelling**, before the chapter concludes in Section 2.12.

In this thesis, rSOCs are considered primarily for the application to **electrical energy storage**, and accordingly this chapter begins with an overview of electrical energy storage in 2.2.1. **Energy storage** is simply defined as the storage of energy available at one time for use at a later time; *electrical* energy storage is distinguished by the fact that the stored energy is recovered as electricity, rather than in other forms (such as heat or kinetic energy). In 2.2.1 the motivations for electrical energy storage are discussed, as well as the challenges inherent in achieving bulk storage for long periods of time. One possible approach to achieving bulk storage is the synthesis of fuels (especially, but not limited to, hydrogen) using electricity; this is often termed **power-to-gas** ‘P2G’ and is discussed in 2.2.2. P2G may be used for electrical energy storage provided the synthesised fuel can be reconverted into electricity (power-to-gas-to-power ‘P2G2P’); this is the mode by which an rSOC could provide electrical energy storage. P2G2P would conventionally be achieved using separate **electrolyser** and **fuel cell** devices, and accordingly these technologies are discussed in 2.2.2.1. An energy storage system based on P2G2P also requires storage of the fuel itself; in the case of hydrogen, this is not straightforward, and so in 2.2.2.2 approaches for **hydrogen storage** are discussed.

With the context of electrical energy storage and P2G established, sections 2.3 to 2.5 focus on the **rSOC**, discussing its chemistry and thermodynamics (2.3); its high-level characterisation (2.4); and the body of literature covering system level modelling and plant design – which forms a high proportion of the available rSOC literature (2.5).

2.6 covers mainly **microgrid** applications for energy storage using hydrogen, including the small amount of academic literature previously published on rSOCs in this context. A **microgrid** may be defined as a small local cluster of electrical loads, generation and possibly storage; it may be stand-alone or grid-connected, but typically aims to achieve a measure of independence from the grid, and grid-connected systems may be capable of ‘islanded’ mode where the microgrid operates fully independently [5]. The applications for rSOCs considered in this thesis are at microgrid scale; utility scale energy storage using rSOC has been considered in the literature, for instance by Sigurjonsson and Clausen [6] and by Zhang et al [7] but is mainly outside of the scope of this work. The microgrids considered in this work are envisaged for the **distribution** level, meaning they would likely be downstream of primary substations and distribution transformers – in simple terms, they would be at the level of a street or community. Note that in 2.6, owing to the scarcity of academic work on applications for rSOCs, the scope is widened to include some of the literature on other fuel cell and electrolyser technology for microgrids.

Whilst 2.6 is concerned with academic literature, 2.7 provides an overview of some of the real-world trials of rSOC, and hydrogen energy storage more generally. 2.8 gives a brief overview of future developments for the rSOC, before 2.9 concludes this part of the literature review.

Peer-to-peer (P2P) energy trading is a secondary theme of this work, and this topic is discussed in 2.10. P2P energy trading enables consumers to trade energy with one another (i.e., their peers) rather than with the energy supplier only [8]. The ability to trade P2P can incentivise the shifting of electrical load to better align with the availability of renewable generation, increasing efficiency and cutting costs; as such, in some ways it can be seen as a rival to energy storage. On the other hand, a P2P market might offer better financial reward for power exported from an rSOC or other energy store.

Section 2.11 gives a brief overview of the agent-based philosophy of modelling, which is employed in parts of this work – particularly in conjunction with P2P. **Agent-based modelling** typically involves the interactions of many entities ('agents') which are programmed to behave in certain ways, often pursuing their own self-interest; an emergent picture of the overall outcome can then be obtained. Finally, 2.12 provides an overall conclusion to Chapter 2.

2.2 Background

2.2.1 Overview of electrical energy storage

Approaches to handling the intermittency of renewable energy sources may be grouped into four broad categories: *flexible generation*, *interconnection*, *demand side management* and *energy storage*. *Flexible generation,* the dominant solution at present, involves the ramping up or down of conventional thermal power plants to accommodate the lack or surplus of renewable energy. The ability to do this relies on having a stockpile of fuel – usually a fossil fuel. *Interconnection* allows for the import/export of electricity with adjoining geographic areas. *Demand side management* seeks to reschedule electrical loads to better match the availability of electricity generation. Here our focus is on *energy storage*, which enables surplus renewable electricity to be stored until needed. [9].

Various forms of electrical energy storage are extant, with different capabilities and applications. They may be classified loosely according to the duration for which energy is stored – as shown in Figure 2.1. Flywheels and supercapacitors provide short bursts of power lasting only seconds or minutes, and are thus used to ensure quality of power rather than shifting appreciable amounts of energy in time [9]–[11]. Batteries of various kinds occupy the middle ground; typically these store energy for time periods on the order of hours [9], making them suitable (for instance) for storing solar power generated during the day for consumption in the evening. Lead acid batteries were at one time the most prevalent choice, but lithium ion batteries are gaining momentum, partly thanks to the improvements in performance and reductions in cost that have accompanied their use in electric vehicles. Battery energy storage may be deployed at the level of a single household but larger 'grid-scale' deployments are also increasingly seen. High temperature molten salt batteries (such as the sodium sulphur battery) have potential for industrial or grid-scale applications; they offer the advantages of durability and long cycle life, and employ materials which are cheap and abundant [12].

In conventional batteries, capacity in terms of both energy and power is tied to the area of the electrodes. By contrast, in flow batteries, the solid electrodes of conventional batteries are replaced with liquid 'anolyte' and 'catholyte' which circulate past a membrane. Thus, the cross-sectional area of the membrane dictates the achievable power, whilst energy storage capacity depends on the total volume

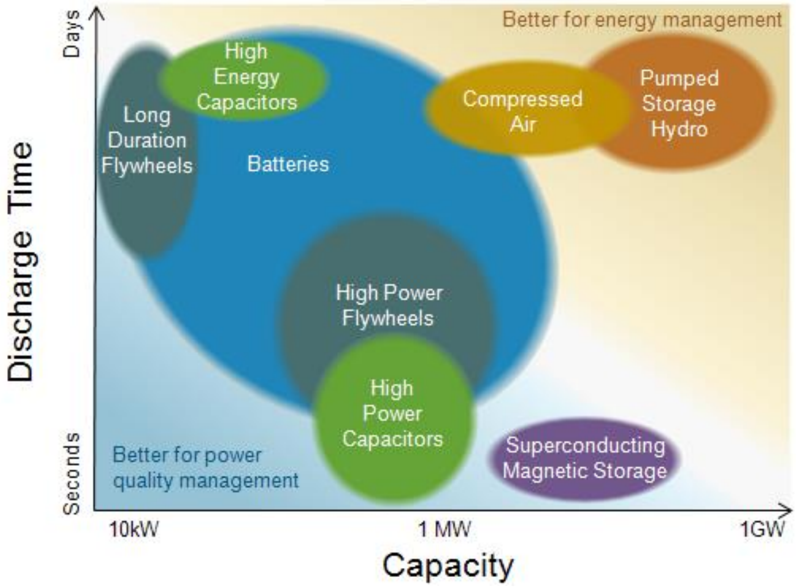

Figure 2.1 This image from the US Energy Information Administration [13] shows the approximate capabilities of mainstream technologies for electrical energy storage, with discharge time plotted against power. None of the technologies shown are considered suitable for the storage of energy for weeks or months.

of the tanks for storage of anolyte and catholyte. Power and energy capacity can therefore be varied independently; furthermore, self-discharge is minimal since anolyte and catholyte are stored in separate tanks. [9], [11]. Flow batteries also offer the advantage of a long lifetime. However, low energy/power density, inferior cycle efficiency (in comparison with conventional batteries) and high cost are all concerns [11]. Flow batteries are closely related to the reversible fuel cells which are the focus of the present work.

For the storage of electrical energy ‘in bulk’, pumped hydropower storage (PHS), whereby energy is stored gravitationally by pumping water uphill between reservoirs at different altitudes, is currently the only mature and widespread technology. The largest pumped storage facilities can store tens of GWh of electricity [10], compared to hundreds of MWh for the largest battery storage facilities to date [14], [15]. Indeed, pumped hydropower accounts for the vast majority of energy storage capacity installed globally [11], [16]. Round-trip efficiency can be somewhat above 80% [3], [9]. The only other bulk-storage technology to be implemented at comparable scale is compressed air energy storage (CAES) using underground caverns; the number of large-scale CAES pilot projects is in single figures as of 2022, with many projects cancelled in recent years [17], [18]. CAES suffers a much lower round-trip efficiency than pumped hydro [3], [16]. Both storage technologies are geographically constrained in where they can be sited [9], [19] and are only really feasible when implemented at large scale – whereas the concern of this present work is with storage that can be implemented at a distributed scale – e.g. at the level of a household / street / district.

Of the energy storage technologies listed (not exhaustively) above, none offer the prospect of storing electricity in sufficient volume, or for sufficient duration, to compensate for longer term fluctuations in renewable output – i.e. on the scale of weeks, months or seasons. Thus, flexible generation or perhaps interconnection would always be required in conjunction with them. Power to gas is a possible technology for shifting large amounts of energy across these longer time periods, and this will now be discussed.

2.2.2 Power to gas

Power to gas (P2G) is the use of electricity to synthesise a gas fuel. Most commonly this involves the splitting of water to produce hydrogen (although syngas or methane may also be produced via co-electrolysis of CO_2 [20]–[22]). Such gas might then be used for heating applications [23] but here our interest is in the reconversion of stored gas back into electricity (i.e. 'power-to-gas-to-power'). To achieve this, one typically needs an electrolyser for the production of hydrogen; some means of storing the hydrogen; and either a fuel cell or a gas turbine that consumes the stored hydrogen to generate electricity. [9].

There are various reasons why P2G is attractive as an energy storage technology. Firstly (unless stored cryogenically) the gas retains its stored energy indefinitely; there is no self-discharge. Secondly, achievable energy density is high: 2500 kWh / m^3 for hydrogen compressed to 700 bar, which compares with an upper limit of 700 kWh / m^3 for lithium ion batteries. Thirdly, energy storage capacity can be added relatively cheaply, since this simply entails providing more storage tanks [24]; as with flow batteries, energy and power capacity are decoupled [9]. Together these attributes suggest the possibility for long term storage of energy (compare PHS / CAES which tend to operate on cycles of at most a few days) [3], [22].

A key challenge for hydrogen as an electrical storage technology is poor round-trip (i.e. power to gas to power) efficiency [25]. This is typically expected to be below 50% [3], [10]; indeed, pilot hydrogen energy storage plants have reported efficiencies in the 20s of percent [26], [27]. Further concerns are high costs and high rates of degradation for electrolysers and fuel cells, necessitating frequent replacement [22]. It should be noted that at present, global hydrogen production is mostly via steam reformation of methane; this is cheaper than electrolysis, but emits CO_2, unless used in conjunction with carbon capture and storage (CCS) [28].

As an aside, it is worth noting that, whilst electrolysis remains the most important method for splitting water, there are a number of other technologies undergoing research. At very high temperatures (2500 °C and above) water molecules disassociate into hydrogen and oxygen through *thermolysis* with no electrical work required. The necessity for such high temperatures makes this a challenging approach in practice. However, by the use of intermediate chemical reactions forming a '*thermochemical cycle'*, water can be split at lower temperatures; around 850 °C to 1000 °C. Corrosion is a challenge, as is the provision of the high grade heat needed - concentrated solar power is one possible heat source [29][28]. Meanwhile photoelectrochemical cells aim to integrate photovoltaic generation and electrolysis within one device, producing hydrogen from water and sunlight; this technology is still under development [1]. Electrolysers and fuel cells remain the core technologies for energy storage with P2G; an overview of the most important types is provided in the next section.

2.2.2.1 Electrolyser / fuel cell technologies

Electrolysers use electrical power to split water into hydrogen and oxygen. Other reactions are also possible; for instance, solid oxide electrolyser cells can split CO_2 into carbon monoxide and oxygen. Conversely, fuel cells generate electricity from the oxidation of a fuel (usually hydrogen). It is important to note that the conversion of fuel to electrical power can in theory be performed much more efficiently by a fuel cell than by a heat engine (i.e. an internal combustion engine); this is because the heat engine is limited by the Carnot efficiency [20].

Fuel cells and electrolysers are fundamentally the same device operating in opposite modes. Nonetheless it is more common for cells to be designed and optimised for one mode of use only; in Gahleitner's 2012 review of hydrogen energy storage schemes, separate ('discrete') devices were invariably used for power-to-gas and gas-to-power [30]. Cells that are designed to be used in both modes are referred to as 'unitised' or 'reversible'; the term 'regenerative' is also used, although this may also be used of a *system* that can perform in both electrolysis and fuel cell modes, whilst using discrete cells for these roles [31][32].

The different types of fuel cells / electrolytic cells are distinguished principally by the electrolyte employed; the following are the most important types [33]:

- alkaline fuel cell / electrolyser
- proton exchange membrane (PEM) fuel cell / electrolyser
- phosphoric acid fuel cell
- molten carbonate fuel cell
- solid oxide fuel cell / electrolyser

Of these, PEM and alkaline cells are currently the most commonly used for stationary energy storage applications [30]. These technologies are the main competitors with solid oxide cells, both for fuel cell *and* electrolysis applications; their attributes are compared to SOCs in Table 2.1. Molten carbonate and phosphoric acid electrolytes are rarely considered for electrolysis.

Alkaline cells generally use an alkaline aqueous solution of potassium hydroxide for the electrolyte. The electrodes are separated by a gas tight diaphragm. Hydroxide anions OH^- carry charge across this diaphragm to balance the half reactions. Alkaline fuel cells are a mature technology with low cost and are relatively easy to mass produce [1]. The corrosive nature of the electrolyte is a disadvantage [34]. Start-up time can be of the order 15-20 minutes [26]. For electrolysis, alkaline cells are the most mature technology, offer the lowest cost, and have tended to be the preferred choice [1], [30], [34]. Large alkaline electrolysers are available capable of producing over 500 Nm^3/h and consuming several MW [29].

PEM cells employ a polymer membrane electrolyte which is conductive of hydrogen cations (that is, protons). PEM may thus stand for *proton-exchange membrane* or *polymer electrolyte membrane*. Rare earth metals (usually platinum) are needed at the electrodes to catalyse the half reactions, and this leads to high costs which are a key challenge for this technology [29][34]. Typical operating temperatures are 50 – 100 °C, although research is underway to allow operation at higher temperatures, allowing higher efficiency operation [1]. PEM fuel cells appear to be the preferred option for conversion of hydrogen to power in pilot energy storage schemes [30]. PEM electrolysers are also gaining popularity [30], with one expert elicitation study [35] predicting that by 2030 they will dominate the electrolysis market jointly with SOEC. PEM cells offer superior kinetics to alkaline cells; they are better able to work at partial loads (down to 5% [36] or even 0% [37] of rated capacity), and have a much faster start-up / response time [26][28][34]. These attributes make them potentially well suited for use with an unpredictable renewable energy source. Power density is also superior [1]. Besides the rarity and high cost of catalyst materials, disadvantages include very low tolerance of impurities and susceptibility to fast degradation [1][28]. Costs per kW appear to be greater than for alkaline technology, but less than SOC.

Phosphoric acids fuel cells, which use an electrolyte of concentrated phosphoric acid, were the first fuel cells to be commercialised. However, their competitiveness is now doubtful as they are costly and relatively inefficient, with an inferior power density. [1]. Molten carbonate fuel cells run at high temperature (600 – 700 °C), employing a molten sodium and potassium carbonate as the electrolyte. Since the transport of charge within the cell relies on carbonate anions, only carbonaceous fuels (syngas or methane) can be used – not pure hydrogen. Advantages are reasonably high efficiency and low capital costs thanks to the lack of rare metal catalysts; however, challenges include poor durability and short lifetime. [1].

Solid oxide cells (SOCs) employ porous solid oxide ceramics as both electrolyte and electrodes. Their high operational temperature (600 - 1000 °C), and ability to work with carbonaceous substances including syngas and methane, distinguish them from PEM and alkaline cells [29], [34]. Carrying out electrolysis at high temperature is attractive as the reaction is more endothermic - this leads to increased efficiency through the recycling of unavoidable joule heat, and also raises the possibility of using an external source of waste heat [29]. SOCs remain an immature technology, particularly for electrolysis [28], [29], [34]. For this reason (as well as difficulties with manufacturing cells at scale, and expense of high-temperature BoP equipment) costs per kW are high [35], [38], [39]. However, the possibility of using SOCs reversibly, with a stack operating as both fuel cell and electrolyser, may allow cost savings [22], [40], [41], and it has also been suggested that reversible operation can actually reduce degradation [42]. An SOC cell or stack capable of such reversible operation will be referred to as rSOC. SOCs and rSOCs will be introduced in greater detail in Section 2.3; first, this overview of power-to-gas will conclude with a summary of hydrogen storage technologies.

Table 2.1. A summary of alkaline, PEM and solid oxide technology for electrolysis and fuel cell applications.

	Alkaline	**PEM**	**SOC**
Operating temp. (°C)	<100 °C [29], [34]	< 140 °C [1], [34]	600 – 1000 °C [29], [34]
Electrolysis efficiency (system level LHV efficiency)	51 - 60% [37] 43 – 67% [43] 63% [44]	46 - 60% [37] 40 - 67% [43] 65% [44]	**highest** 76 - 81% [37] 63 – 76% [43] 82% [44]
Fuel cell electrical efficiency (system level)	45 – 60% [45]	45 – 50% [45]	35 – 60%$_{AC}$; [44] ~50%$_{LHV}$ [46] 45 – 50% [45] 61% [47]
Lifetime	Stack 90000 hours System 20-30 years [28]	Stack 20000 hours System 10-20 years [28]	Stack 40000 hours [28]
Dynamics and flexibility	• 15 minute startup [34] • Min partial load 10-40% [37]	• <15 minute startup [34] • Quick response; suitable for variable load operation [26], [28], [34], [36] • Partial load possibly to 0% [37]	• Start-up from cold: hours [1], [34] • From hot standby: perhaps minutes [48], [49] • Intermittent loads challenging as causes thermal stress [1], [34]
Max. system size	100's MW [1], [28], [37]	Multiple MW [43]	100's kW [43]
Key advantages	• **Most mature technology for electrolysis; reliable, safe, long lifetime** [29], [30], [34]	• **Usually preferred fuel cell** [30] • Suitable for use with intermittent loads • Electrolyser yields highest purity hydrogen [29]	• High efficiency particularly for SOEC [29] • Further boost electrolysis efficiency through use of waste heat [34] • Can work with carbonaceous species • Possible CHP applications • Possible reversible operation
Key challenges	• Inferior dynamic response to PEM electrolyser • Corrosive electrolyte [34]	• Rare, expensive catalyst materials; high cost of membranes [29], [34] • Shorter lifetime for electrolysis [1] [29] • Less scalable than alkaline technology [29]	• Immature technology [29], [34] • Susceptible to rapid degradation especially for electrolysis [29] • Thermal management is challenging • Load changes can cause thermal stress [34] • Shortest lifetime [35] • Difficult to manufacture cells at scale [50]
Costs (whole system CAPEX for electrolysis unless otherwise specified)	**lowest** • 800 – 1500 € / kW [37] • 750 – 1200 € / kW [51] • 700 – 1400 € / kW [35] • 1000 – 1200 € / kW [43]	**medium** • 1400 – 2100 € / kW [37] • 1200 – 1500 € / kW [51] • 800 – 2200 € / kW [35] • 1900 – 2300 € / kW [43]	**highest** • >2000 € / kW [37] 2500 – 8000 € / kW [35] • SOFC system, CAPEX for kW scale system: 2000 – 6600 € / kW [38] • SOFC system, CAPEX for 100-250 kW system: 800 – 1500 € / kW [39] • **Greatest potential for cost reduction**, possibly to 760 € / kW [35]

2.2.2.2 Hydrogen storage technologies

Whilst the gravimetric energy density of hydrogen is very high, at 39.4 kWh_{HHV} / kg (2.5 times the figure for methane), because it is so light its volumetric energy density at normal conditions is low – only 3.5 kWh / Nm^3, one third that of methane [29]. When one considers that a TESLA Powerpack achieves 85 kWh/m^3 even at pack level [52], it will be understood that storage of hydrogen at higher density is necessary in order to achieve a useful energy storage density. The principal storage technologies are:

- Compressed hydrogen gas (CHG): storage of H_2 gas at high pressure and ambient temperature
- Liquid hydrogen
- Sorption
- Liquid carriers (methanol, ammonia, liquid organic hydrogen carriers) [9]

CHG has overwhelmingly been the approach taken in pilot hydrogen storage schemes; CHG was used in 88% of the demonstration hydrogen storage plants in Gahleitner's 2012 review paper [30]. The highest storage pressure encountered by this review was 420 bar, although most projects used 200 bar or below. Makridis gives 800 bar as the upper pressure limit for existing lightweight composite cylinders [53]. Gahleitner notes that extra storage density at higher pressures comes at the expense of efficiency. The advantages of the CHG approach lie in its simplicity and scalability, technological maturity and low cost. The energy needed for compression is of course a consideration. Ghosh et al [26] state that using a metal membrane compressor, only 9% of the hydrogen's stored energy was needed for compression to 120 bar. Running an electrolyser at high pressure can reduce or eliminate the need for subsequent compression, and increase efficiency [29][34].

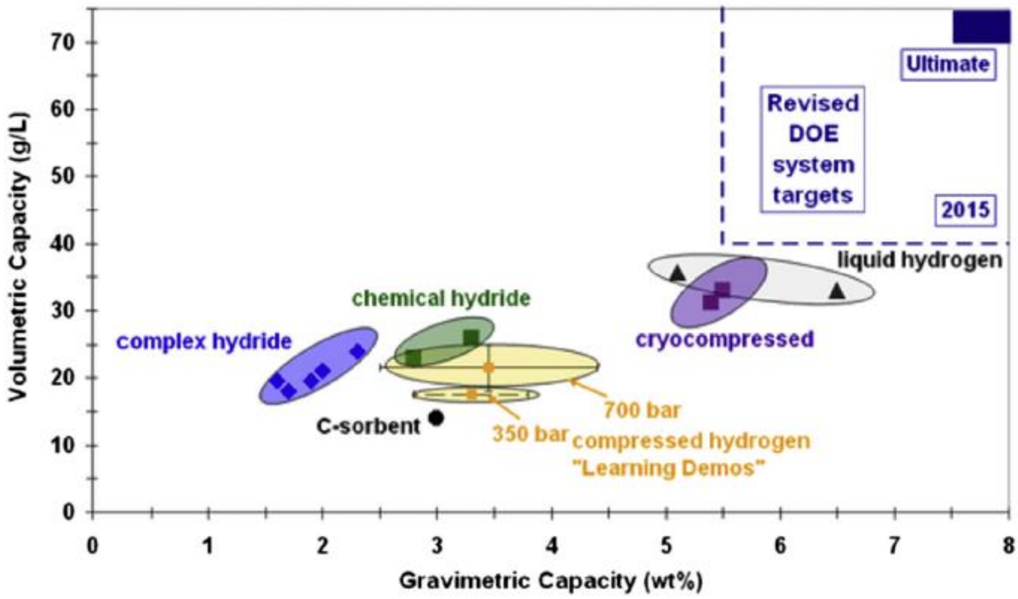

Figure 2.2. The gravimetric and volumetric capacities of various hydrogen storage technologies. (The targets shown are the US Department of Energy's targets for automotive applications.) [55]. Reproduced by permission.

Liquid hydrogen offers a very high energy density of nearly 2800 kWh/m^3; compression to 800 bar would be needed to match this with hydrogen gas [53]. Unfortunately there are many disadvantages that tend to outweigh this. To liquefy hydrogen, it must be cooled to 21°K. The energy needed to achieve this is at least 30% of the hydrogen's lower heating value [1][54], implying a severe impact on round-
trip efficiency of the storage system. Furthermore, it is very difficult, if not impossible, to prevent the hydrogen from boiling off; it has been reported that 2-3% of the stored hydrogen is inevitably vented per day [1]. For long-term energy storage liquid hydrogen is thus a very unlikely choice, especially when space is not at a premium. Cryo-compression of hydrogen involves the storage of hydrogen at low temperature *and* high pressure, and may combine some of the merits of both approaches – but this again is of more interest for vehicular applications [55].

Hydrogen may also be stored in certain solids through absorption or adsorption. In absorption/chemisorption hydrogen atoms are integrated within the lattice of the absorbent material, whereas in adsorption/physisorption, hydrogen binds to the surface of the adsorbent material. [1]. Certain metals, including magnesium, lithium and sodium, are able to absorb hydrogen within their metallic structures, forming metal hydrides. It is these materials which have provoked the most interest for storage of hydrogen in solid carriers; metal hydrides were used in five of the pilot plants reviewed by Gahleitner, being the only technology employed other than CHG [30]. According to Dutta [56], magnesium is the material attracting most interest, although many different metal hydrides are available. Magnesium is able to store 7.6 wt.% hydrogen [56], which implies an energy density above 4 MWh / m^3 for this storage material. It is important to note that hydrogen tends to bind strongly with metal hydrides; as a result moderately high temperatures (150 – 600°C depending on the material [1]) are needed to retrieve it. Conversely, the absorption of hydrogen will be exothermic. In fact this has potential to complement the thermal management of a hydrogen energy storage system, since endothermic electrolysis can use heat produced by the hydride store, whilst exothermic fuel cells can supply heat to release hydrogen. This idea is explored in [57]. Simplicity and lack of moving parts are among the advantages of hydrogen storage in metal hydrides [1]. However slow reaction kinetics are a concern [58].

Figure 2.3. Tanks of compressed hydrogen at the HARI project, West Beacon farm, Loughborough. 2856 Nm^3 of hydrogen is stored at 137 bar, providing the farm with around three weeks of storage (3.8 MWh). Image: [27]. Reproduced by permission.

Adsorbents considered for hydrogen storage include carbon materials (such as graphite, carbon nanotubes and Buckyballs) as well as zeolites. Adsorption offers lower energy density (volumetric and gravimetric) than absorption, but may offer a faster reaction kinetic and less problems with thermal management, as binding is weaker than for absorbent storage media [1].

Finally, the difficulties of storing hydrogen may be bypassed through conversion to an energy carrier which is more energy dense and easier to handle, such as methanol or ammonia; Siemens is currently running a pilot project using the Haber-Bosch process to store green hydrogen as ammonia [59]. Methane is also easier to transport and store than hydrogen [3], [22], and there is considerable interest in the use of solid oxide technology to synthesise methane via the coelectrolysis of water and CO_2 [60]–[65].

2.3 Introduction to SOCs and rSOCs

The electrodes and electrolytes of SOCs are made of porous solid oxide ceramics. They operate at intermediate to high temperature (600 - 1000 °C), such temperatures being necessary to attain sufficient ionic conductivity. They potentially offer the highest efficiency available from any electrolyser or fuel cell [28], [40], [50]; however, the technology is significantly less mature than either PEM or alkaline cells – particularly for electrolysis [28], [29], [34]. Because of the high temperature operation, rare metal catalysts are not required, which is potentially a significant advantage over PEM cells [66][33]. Another advantage is their ability to work with various fuels, not only hydrogen: natural gas, syngas or even ammonia can all be used in solid oxide fuel cells (SOFCs) [20], [33], [66], [67]; conversely, solid oxide electrolyser cells (SOECs), besides being able to split water into H_2 and O_2, can also split CO_2 to produce carbon monoxide and oxygen, or co-electrolyse CO_2 and water to produce syngas or methane [20][21]. The tolerance of solid oxide cells to impurities in the fuel is also superior to that of PEM cells [33].

2.3.1 Chemistry and materials

Most commonly, the electrolyte in a solid oxide cell conducts negatively charged oxygen ions. In fuel cell mode, the reactions in the cell proceed as follows: at the oxygen electrode, oxygen is reduced to

O^{2-} and these anions migrate across the electrolyte to the anode. At the anode, the fuel is oxidised and combines with O^{2-} to form water (or CO_2 in the case that the fuel is CO). Thus, the half-reactions for a solid oxide cell working with hydrogen are:

$$\text{Anode: } H_2 + O^{2-} \leftrightarrow H_2O + 2e^-$$

$$\text{Cathode: } \frac{1}{2}O_2 + 2e^- \leftrightarrow O^{2-}$$

$$\text{Overall: } H_2 + \frac{1}{2}O_2 \leftrightarrow H_2O$$

[1]

In fuel cell mode these reactions run from left to right; in electrolysis mode, from right to left.

Proton conducting ceramic electrolytes for SOCs also exist; however they generally display inferior performance to the O^{2-} conducting electrolytes and have accordingly attracted less interest [1][68].

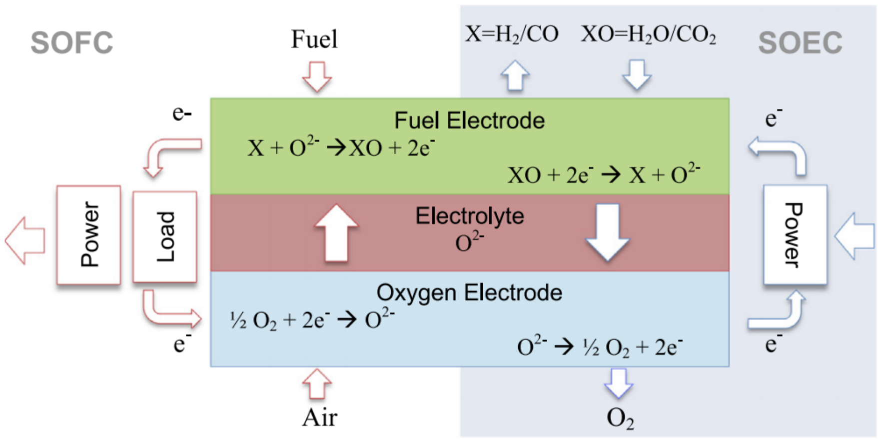

Figure 2.4. Schematic of a solid oxide cell [40]. The cell is depicted as a reversible cell, with fuel cell mode shown on the left and electrolyser mode on the right. The fuel produced / consumed is either pure hydrogen or syngas. Reproduced by permission.

As for all fuel cells, the electrolyte of a SOC must be highly ionically conductive, but not conductive of electrons; furthermore it must be stable in both oxidising and reducing environments. The most common material used is yttrium stabilised zirconia (YSZ), although many other materials have been considered [29][40][68]. YSZ only achieves adequate ionic conductivity at high temperatures (750 °C – 1000 °C); if lower temperature operation is desired, alternatives must be sought; LSGM (a lanthanum gallate doped with strontium and magnesium) is one of these [40].

Since (in contrast with PEM or alkaline cells) the reactants are in gas phase, the electrodes of a solid oxide cell must be highly porous, maximising the solid / gas interface [29], whilst being electronically and ionically conductive. For the fuel electrode, a cermet of nickel and the electrolyte material is most commonly used. Nickel is readily oxidised when using an SOC for electrolysis, one of the reasons why this application is more challenging for SOCs. [68]. For the oxygen electrode, common materials are lanthanum strontium manganite (LSM), or a mixture of LSM and YSZ. Again, LSM exhibits worse stability during electrolysis than fuel cell mode.

Solid oxide cells may be produced in either planar or tubular designs. The tubular design may offer superior mechanical strength and resistance to thermal shock; nonetheless the planar design remains more common [42][40]. Manufacture of large cells is challenging, and in any case smaller cells are less susceptible to fail when subjected to thermal shock [50].

2.3.2 Thermodynamics

Figure 2.5 shows why carrying out electrolysis at high temperatures can be desirable; the electrolysis reaction is increasingly endothermic at higher temperatures, with a greater proportion of the overall energy requirement supplied from heat. For a solid oxide electrolyser cell (SOEC) operating at 1000 °C this proportion is as high as 40.1% [29]. This enables the electrolysis to be highly efficient, as the joule heat inevitably produced within the cell may be recycled by the reaction. If an external source of waste heat can be used, the electrical efficiency can be increased still further.

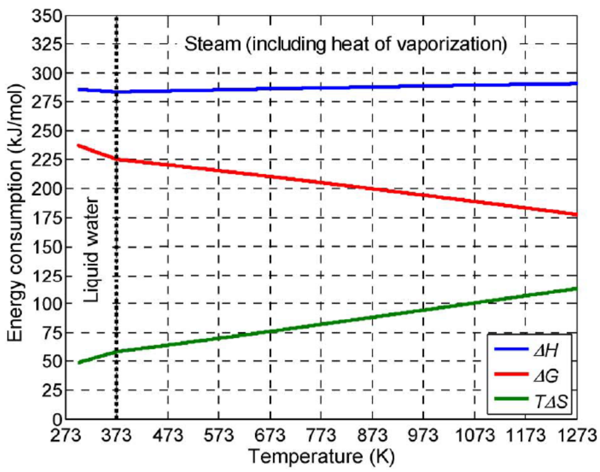

Figure 2.5. The theoretical energy requirements for electrolysis at different temperatures [29]. ΔG (Gibb' free energy) is the portion of the energy that must be provided by electrical work. TΔS, the product of temperature and entropy change, is the energy that may be supplied by heat. It will be seen that electrolysis at higher temperatures is more endothermic, with a higher proportion of the overall energy requirement ΔH provided as heat. Figure reproduced by permission; © 2012 IEEE.

This may be understood in terms of the 'thermo-neutral voltage'; this is the voltage whereby each unit of charge is given precisely enough energy to supply both the necessary heat and the necessary electrical work for the electrolysis reaction. Operation at the thermoneutral voltage keeps the cell in thermal equilibrium; above the thermoneutral voltage the cell generates heat; below it, the cell is endothermic. According to [29] most commercial electrolysers are designed to operate close to the thermo-neutral voltage, so that the current provides all required heat. However, there is also the potential to run electrolysis below the thermoneutral voltage if a source of high-grade heat (e.g. waste heat from industry or a nuclear power station) can be supplied, in which case the electrical efficiency can be brought above 100% [21], [42], [60].

For a SOFC, operation is inevitably exothermic [42], [63], [69], theoretically returning heat and work in the same proportions as shown in Figure 2.5. This naturally leads to the question of whether the heat from SOFC mode could be stored and subsequently used to boost the efficiency of SOEC mode in a reversible cell [69]. Phase change materials can provide such thermal storage at high temperatures, as discussed in [60] and [70], although it is dubious whether storage duration is long enough to be useful. It can also be noted that certain hydrogen storage technologies (metal hydride and CHG) can achieve a good synergy with an rSOC, since the storage of hydrogen is exothermic and its release endothermic. Such heat may be used to assist with steam production if not the direct supply of heat to the stacks.

A further possibility for boosting thermodynamic performance is to work with methane as the storage medium. Steam reformation of methane is endothermic, whereas the reverse reaction (methanation of syngas) is exothermic. If coelectrolysis of CO_2 and H_2O is used to produce syngas, methanation can therefore provide some heat to the electrolysis reaction – the overall reaction is more reversible. Conversely, steam reformation during fuel cell mode can absorb heat from the oxidation reaction. Such an approach potentially allows for high round-trip efficiency and has attracted considerable interest; it will be discussed further in Section 2.5. [60], [63].

2.4 Assessment of rSOC characteristics for high level modelling

The section discusses some of the characteristics of rSOCs that are expected to be relevant for high-level modelling and techno-economic analysis, with the aim of informing future modelling work.

2.4.1 Capacity

The largest rSOC systems constructed have had capacity below 200 kW_{AC} for electrolysis mode [49]; a 720 kW electrolysis project is in the pipeline as of late 2021 [71]. Contrast this with the more mature PEM technology, where electrolysis projects in the order of 10 MW are planned or operational [72]–[74]. Saarinen et al [75] recommend that large rSOC systems be constructed in modules of at most 100 kW, to minimise the impact of cell failures on the plant.

Capacity is invariably higher for SOEC mode than SOFC mode. This partly reflects the round-trip efficiency of the rSOC, but may also be the result of using a higher current density in SOEC mode [76]. Table 2.2 gives the power in each mode of some rSOCs found in the literature.

Table 2.2. Reported rSOC capacity by mode.

Reference	SOEC nominal load (kW)	SOFC nominal load (kW)	Ratio	Notes
[77]	14.3	5.4	2.65 : 1	Experimental
[78]	80	15	5.33 : 1	Experimental
[46]	150	30	5 : 1	Experimental
[79]	-	-	4 : 1	Modelling assumption
[80]	-	-	5 : 1	Modelling assumption

2.4.2 Flexibility

2.4.2.1 Partial load range

SOC systems cannot in general operate at indefinitely small partial loads, a consequence of the need to maintain stable temperature. (PEM systems, by contrast, can viably operate at very low partial loads below 5% [36], [37]. Different sources give a variety of values for minimum attainable partial loads; these are given in Table 2.3.

Table 2.3 . Reported attainable partial load for SOC.

Reference	Minimum partial load SOFC	Minimum partial load SOEC	Notes
[81]	40%	33%	4 kW_{SOEC} / 1 kW_{SOFC} stack. Experimental.
[78]	23%	58%	Experimental.
[82]	-	24%	Experimental.
[83]	14%	14%	Modelling assumption.
[77]	30% / 20%*	10%*	Experimental *required external heat supply
[46], [49], [84], [85]	40% 0% with efficiency penalty	50%	Experimental (GrInHy project)
[86]	-	5%	Advertised
[87]	50%	-	Advertised

2.4.2.2 Full shutdown versus hot standby

Safely warming up an SOC stack from room temperature to the operational temperature (at least 600°C) takes multiple hours [1], [34]. Heating and cooling the stack over this temperature range causes it to degrade faster [88]–[90]. For this reason, it is generally accepted that full shutdown of an SOC system should be rare (Nousch et al suggest only 21 full thermal cycles in a stack's lifetime [89]); instead, systems are designed with a 'hot standby' / 'hot idle' mode. This generally entails a slight cooling of the stack, and operation at a reduced loadpoint to minimise energy consumption. Sunfire's SOC stacks appear to use a hot standby temperature of 500 – 550 °C, compared to a operational temperature of 750°C [91]; standby temperatures in the range 400 – 600°C are seen in other literature [88], [92]. For an rSOC, standby mode could correspond to operation at the lowest possible partial load in either electrolysis or fuel cell mode; alternatively, temperature could be maintained by external supply of heat. Aicart et al [81] give the operating modes for the rSOC system developed for the SMARTHYES prototype, where the standby mode corresponds to approximately 10% partial load in SOEC mode. Mottaghizadeh et al [93] present an SOEC system where standby corresponds to ca. 5% partial load, with heat also needing to be supplied; in [94] 10% partial load is assumed for standby mode of an SOFC.

It is important to note that, in contrast to the multiple hours required to begin operation from cold shutdown, SOC systems require only minutes to start from the hot idle state [81], [86].

2.3.2.3 Degradation and lifetime

Degradation of SOCs is widely reported to be more rapid and severe for SOEC than for SOFC, with this degradation occurring principally at the oxygen electrode [29], [67], [68], [95]. The review by Zhang et al [1] suggests a stack lifetime of no more than 40000 hours for SOEC; still superior to PEM electrolysers, but inferior to alkaline; from the review by Wang et al [68] it seems clear that outcomes can vary considerably according to the materials used. By contrast, SOFC can have a reasonably long lifetime: Jülich Research Centre reported that their SOFC stack operated for 93000 hours continuously [96].

Generally, voltage degradation for SOC is of the order 1% per thousand hours (that is, 1%/kh). The GrInHy project have reported degradation of 0.8%/kh, after 5000 hours of reversible operation of their 150 kW rSOC plant [46], [49], [84], [85]. Aicart et al [81] reversibly operated a 4.8 kW stack of 25 cells over 800 hours, and found voltage degradation for the cells to be 0.9 – 2.4%/kh, excluding four damaged cells. Nechache and Hody [76] measured the voltage degradation of a ca. 5 kW stack in electrolysis mode only; voltage degradation was 4.1%/kh; but 1.3%/kh excluding the worst cell. The degradation of commercial SOCs made by Ceres is reported to be 1%/kh [97].

An interesting and still controversial question is whether reversible operation of an rSOC, with frequent cycling between modes, might possibly counteract degradation mechanisms – or accelerate them. The literature does not yet offer a firm conclusion. Graves et al [98] found that the deterioration in the microstructure of the oxygen-electrode/electrolyte interface, observed when performing continual electrolysis at high current density, was no longer observed when cycling between fuel cell and electrolysis modes. In fact, Ohmic resistance actually *decreased* after 4000 hours of cycling. Chen et al [99] found very similar results: degradation of an LSM oxygen electrode during electrolyser mode was reversed during fuel cell mode. Reflex Energy also report that daily cycling of their 80 kW ‘Smart Energy Hub’ technology significantly reduces degradation [100]. However, research published by NASA in 2010 [101] found degradation when cycling between modes to be worse than continuous electrolysis (the researchers noted that this contradicted the received wisdom). Experimental work by Choi et al [102] and Hong et al [103] also found cycling between modes gave rise to worse degradation. It is of course possible that degradation is associated with dynamics of the actual switch between modes; in this case controlling the mode-switching appropriately may solve the problem, as discussed in [104].

2.4.2 Costs

Owing to the immaturity of the technology, costs for SOC / rSOC installations are rather uncertain [35]. Some of the estimates for whole system CAPEX in the literature have been collated in Table 2.1. Balance of plant can be a significant proportion of costs; [105] suggests that BoP is 2/3 of the cost for a 250 kW SOFC system, and for rSOC it is reasonable to expect BoP to account for a still greater portion. What is fairly clear is that for now, costs per kW are higher than for alkaline or PEM cells; however, there is also considerable scope for costs to fall in the future [35]. It seems reasonable to estimate system costs as at least €2000 / kW on the basis of [35], [37], [38], although [39] suggests that large SOFC systems for CHP (combined heat and power) can get below €1000 / kW. [44] points out that cost per kW is not the whole story, claiming that SOEC is already cost-competitive thanks to its higher efficiency.

Some of the research papers presenting detailed system designs for energy storage with rSOCs (see Chapter 2) include some economic analysis. For instance, estimates given in [61] and [64] for the whole system CAPEX of a distributed scale energy storage plant fall in the range 233 - 452 [1864 – 3616] $/kW [$/kWh]. For comparison, it is worth bearing in mind that the average cost of lithium-ion batteries at pack level was $176/kWh in 2018, and is expected to eventually fall below $100 / kWh [106].

2.4.3 Conclusions

The challenges that SOCs face in avoiding excessive degradation from sudden temperature swings will need to be considered in modelling. This is likely to mean limiting the amount of mode-switching, and perhaps constraining ramp-rate. Concerning standby and on/off modes, the literature seems clear that transitions to and from a fully off cold state should be rare. An assumption that hot standby mode is used should be appropriate for high-level modelling. Concerning stack lifetime, the rSOC technology apparently still has ground to make. Nonetheless, with some optimism expressed in the literature that reversible operation can even extend lifetime, it may be reasonable to assume that lifetime will eventually rival that currently displayed by SOFC.

2.5 rSOCs – system level modelling

In this section, we examine the various systems for energy storage using rSOCs that have been proposed in the literature. Different approaches are distinguished by:

- the gas stored: hydrogen, syngas or methane;
- the proposed method for storage (compression / metal hydride);
- the approach to thermal management, including possible use of thermal energy storage;

Accordingly, these studies tend to involve the modelling of the whole proposed storage system including all balance-of-plant components. The modelling of individual components is often simplified, for instance by the application of zero-dimensional lumped models. In most cases the predicted round-trip efficiency is calculated; some researchers also include an assessment of the cost of storage for the proposed system.

A great deal of interest in the literature has arisen from an idea which seems to have originally been due to Bierschenk et al [107]; this idea involves the coelectrolysis of CO_2 and water in an rSOC at intermediate temperature (650 °C), allowing the produced syngas to undergo methanation within the stack. This offers a number of advantages: methane gas allows for higher energy storage density than hydrogen with less compression. Furthermore, the exothermic methanation reaction can help with the supply of heat to the endothermic electrolysis reaction, allowing a lower voltage to be used. Conversely, steam reformation of methane in fuel cell mode makes the overall reaction a little less exothermic; overall, the storage cycle is closer to being isentropic.

The difficulty with this approach lies in the particular conditions (lower temperature and high pressure) needed for methanation to take place. The usual YSZ electrolyte does not have sufficient ionic conductivity at 650 °C, so alternatives such as doped lanthanum-gallate (LSGM) must be used. Despite the challenges, this approach to energy storage using rSOCs has attracted a great deal of interest since, with several papers modelling energy storage plants at system level and/or undertaking economic analyses. Wendel et al [62] used an LSGM electrolyte, and conducted experiments using a button cell to validate a cell-level numerical model for the proposed SOC. The modelling suggested that a current density of 0.32 A/cm^2 would achieve the targeted round-trip efficiency of 80%, with this efficiency dropping off linearly as current density increased. This figure did not include balance of plant considerations. It was felt that further improvements were needed to enable operation at higher current densities (>0.4A/cm^2) and lower temperatures (600 °C). [60] discusses the application of this technology to a stand-alone energy storage system with tanks to hold both fuel and exhaust. A system level model incorporating all balance of plant components was constructed. In a 'base case' scenario operating the rSOC stack at 650 °C and 20 bar pressure, the model predicted a system level roundtrip efficiency of 72.6%. It was noted that the roundtrip efficiency was strongly influenced by system thermal integration. The researchers also commented on the playoff between storage density and roundtrip efficiency; the fuel mix generated at the optimal conditions for efficiency was not the most energy dense possible.

The application of the system at a distributed scale (100 kW, 800 kWh) is discussed in [61]. Different system configurations were considered, including the question of whether to store water as vapour or liquid. Storage of water as vapour was predicted to achieve higher round trip efficiency (almost 74%), but at the cost of lower storage density and higher capital cost. [64] extends this work. A techno-economic analysis put the capital cost of the distributed storage plant at \$422 - \$452 / kWh, and the LCOS just below 20 ¢/ kWh. The estimated roundtrip efficiency was 53% for this study, although this was considered to be 'a conservative lower limit'. [63] discusses the implementation of the aforementioned design at a large scale, employing caverns for storage of methane and CO_2. A 250 MW, 500 GWh store was proposed, which would undergo just 44 cycles over a 20 year lifetime, achieving an estimated electricity cost of around $0.03 / kWh - comparable to pumped hydropower. [65] also considers a large megawatt scale storage facility; here, only CO_2 would be stored locally, with the gas grid used for storage of CH_4. Simulations of this plant suggested a round-trip efficiency of 79.6%$_{DC}$ – a higher figure than seen in previous studies, which was attributed to lower current density and extra methane formation. However, lab experiments could not replicate the modelled level of methane formation during electrolysis.

Ren et al [108] present an rSOC system intended for grid energy storage. In the proposed system the mix of fuel and exhaust (hydrogen and steam) always remains in the pressurised vessel containing the fuel cells. The advantages of this design were considered to be the avoidance of any need to preheat the fuel entering the SOC stack, the avoidance of contamination, and a more uniform temperature in the stack. Bronze was used as a phase change material to prevent overheating in fuel cell mode, and provide heat during the endothermic electrolysis mode. The researchers carried out modelling using Matlab / Simulink, building from a cell level model to a system model incorporating the stack, the thermal storage and the inverter providing the AC grid connection. The maximum round trip efficiency was found to be 64%. It should be noted that the application envisaged for the system was cycles over 'short time periods, such as hours'. This is presumably dictated by the use of phase change thermal storage and the restriction on storage capacity resulting from keeping the fuel and exhaust within the system. One might be inclined to question whether fuel cells are competitive to operate with such short cycles.

Frank et al [109] describe a 6 kW rSOC energy storage plant. They describe their design as 'particularly environmentally friendly' since no carbonaceous gases are involved. Hydrogen is produced by electrolysis of steam and stored at 70 bar using multistage compression with intermediate cooling. Unconverted steam is condensed so that only hydrogen is stored. Electrolysis takes place slightly below the thermoneutral voltage; thus heating plates are used to maintain the stack at 750 °C. In fuel cell mode the stack temperature is controlled by adjusting the flow of air. As in most designs, heat is exchanged between the inlet and outlet gases. Balance of plant calculations for the proposed design indicated a maximum efficiency of 61.4% in fuel cell mode and 74.3% in electrolyser mode, for a 45.6% round-trip efficiency. With the recycling of heat from the condensers, this could be improved slightly to 51%. These figures were for steady state operation, and do not account for mode switching. The possibility of using thermal storage was mentioned, but to keep the system simple it was not included.

Perna et al [110] considered a distributed scale rSOC energy storage system (100 – 200 kW), with storage of pressurised hydrogen at 200 bar. The thermal balance of the plant was elegantly designed in order to avoid the use of any external heat sources. Preheating of gas streams and steam production were to be achieved using heat exchange with the off-gas, or heat given off by the compression of hydrogen. Also, waste heat produced by the system was to be used for the supply of hot water at 65 °C. Diathermic oil was to be used as a medium for both heat exchange and heat storage. A SOC model was constructed and validated against experimental data, before being incorporated into a modular balance-of-plant model. The electrical round-trip efficiency was predicted to be 60%, and the cogeneration efficiency 91%.

Table 2.4. Summary of studies with system level modelling of rSOC energy storage plants.

Source / institution / year	Notable features	Thermal management	Modelling	Modelling environment	Roundtrip efficiency	Economic analysis
Ren et al [108] / U. of Strathclyde / 2012	H_2 / H_2O mix remains in sealed pressure vessel with cell stack.	PCM (bronze)	0D cell & BoP models	Matlab / Simulink	64%	-
Akikur et al [111] / U. of Malaya / 2014	Cogen. system using concentrated solar power and PV.	CSP for steam generation	Mathematical analysis	-	Co-gen 71%; electrical 38%	Total system CAPEX: c. $6000 / kW; COE: $0.0676 / kWh
di Giorgio and Desideri [112] / Pisa / 2016	Focus on use of TES, and comparison of scenarios with/without storage of water vapour.	Sensible TES using ceramics / PCM with eutectic metal alloy / Steam drum	0D cell & BoP models	Matlab / Simulink	64 – 74%	-
Frank et al [109] / Jülich research centre / 2018	6 kW plant with storage of H_2 at 70 bar.	Heating plates for electrolysis; coupling of heat sources / sinks; possibility of TES noted.	1D cell model; cascade of continuous stirred tank reactors for BoP	Matlab / Simulink / C	51%	-
Perna et al [110] / U. of Cassino / 2018	100 – 200 kW plant storage of H_2 at 200 bar.	Coupling of heat sources and sinks; diathermic oil for TES and heat transfer	0D cell & BoP models	Fortran	60% (91% cogen.)	-
Srikanth et al / Stuttgart / 2018	Study focused on safety / durability under mode switching.	Electric preheater	1D cell model Simple system model (H_2 storage not modelled)	Modelica	42%	-
Giap et al [113] / Daejeon / 2018	rSOC plant using waste heat for electrolysis; storage of H_2 at 22 bar.	Waste heat provides steam	0D cell & BoP models	EBSILON	53.8% with use of waste steam	-
Lototskyy et al [57] / U. Western Cape / 2018	Tri-generation system for coupling with PV generation. Metal hydrides for storage of H_2 & heat.	TES using metal hydrides	0D cell & BoP models	Matlab	Tri-gen 70.6%; electrical 46.7%	-

Table 2.4 continued.

Source / institution / year	Notable features	Thermal management	Modelling	Modelling environment	Roundtrip efficiency	Economic analysis
Wendel et al [60] / Colorado School of Mines / 2015	1 MW scale system with tanks for fuel and exhaust.	Methanation / steam reformation reactions improve efficiency	Draws on 1D cell model.	?	72.6%	-
Wang et al [114] / Beijing / 2019	Distributed energy storage of c. 200 kW; emphasis on detailed cell / stack model.	TES using diathermic oil	3D cell model 0D BoP models	gPROMS / Matlab / DETCHEM	58.3% (system) 72.3% (stack)	
Jensen et al [63] / Tech. U. of Denmark / 2015	Large scale system (250 MW, 500 GWh) with storage of fuel and exhaust underground	Methanation / steam reformation reactions improve efficiency; coupling of heat sources and sinks	1D steady-state cell model; 0D BoP models	?	>70%	CAPEX \$269 / kW Storage cost \$0.03 / kWh
Wendel and Braun [61] / Colorado School of Mines / 2016	Distributed scale system (100 kW / 800 kWh); tanks for fuel and exhaust; comparison of scenarios with/without storage of steam	Methanation / steam reformation reactions improve efficiency; coupling of heat sources and sinks	1D steady-state cell model; 0D BoP models	?	68.3 – 73.7%	CAPEX: \$233 – \$317 /kWh Energy storage cost \$0.088 / kWh-cycle
Butera et al [65] / Technical University of Denmark / 2018	Multi megawatt plant storing CO_2 underground, CH_4 in gas grid.	Methanation / steam reformation reactions improve efficiency	0D cell & BoP models	Dynamic Network Analysis	79.6%$_{DC}$	
Reznicek and Braun [64] / Colorado School of Mines / 2018	Distributed scale system (100 kW / 800 kWh); tanks for fuel and exhaust.	Methanation / steam reformation reactions improve efficiency; coupling of heat sources and sinks	1D steady-state cell model; 0D BoP models	gPROMS ModelBuilder	≥53%	CAPEX: \$422 - \$452 / kWh LCOS \$0.1808 – \$0.196 /kWh

Ullvius and Rokni [115] / Tech. U. of Denmark / 2018	Polygeneration system carrying out desalination and power generation	CSP for steam generation. Waste heat used for DCMD desalination.	0D cell model	Dynamic Network Analysis	42 - 45% electrical	-

In a 2018 paper, Srikanth et al express concern that the ‘simplified block models’ used in [109][62] and others tend to overestimate the performance of rSOC energy storage systems. They note that the zero-dimensional models of cells / stacks may not predict failures caused by local effects; thus unsafe or unrealistic operating conditions are permitted. Accordingly the researchers built a more detailed 1D model of a solid oxide cell in Modelica, and validated this model experimentally using a 10 cell stack in both SOFC and SOEC modes. This model was then incorporated into a simple system level model; this model included thermal balance-of-plant components, but not any kind of hydrogen storage. The research was particularly concerned with safety, and the avoidance of cell failure, during mode switching. On this point, it was concluded that rather than instantaneous switching between modes, the composition of inlet gases should be ramped over one minute, and the temperature of inlet gases over around 10 minutes. The efficiencies predicted for SOEC and SOFC mode were 49% and 87% respectively, for 42% round-trip efficiency.

Giap et al [113] express the opinion that designs intended to produce methane for storage (as discussed above) are likely to suffer faster degradation thanks to the steam reformation and methanation reactions. Instead they consider a system based purely on hydrogen / steam, and their main interest is in the possibility of employing waste steam from industrial processes. The balance-of-plant design was intended to be ‘simple and highly practical’ but not necessarily claimed to be optimal. Storage of hydrogen was to be realised at the unusually low pressure of 22 bar. A zero-dimensional lumped model of the proposed system was constructed in EBSILON software. The round-trip efficiency was predicted by the model to be 53.8%; if the energy to create steam had to be considered, this would fall to 37.9%. The researchers felt that these figures were still too low; one of their recommendations was that the incorporation of thermal energy storage should be considered.

Lototskyy et al [57] considered a distributed rSOC system designed for combined cooling, heating and power, using metal hydrides for storage of both hydrogen and heat. It was proposed that the system would be powered by photovoltaics. Three different types of metal hydride (MH) bed were incorporated in the design. A MH hydrogen and heat storage system would store H_2 and medium grade heat, consuming heat during SOFC mode and releasing it in SOEC mode. A MH hydrogen compressor would supply hot water at 90 °C to the end user, whilst a MH heat pump would supply chilled water. A numerical analysis of the system was conducted, with optimisation of the most sensitive parameters conducted in MATLAB. It was noted that operating SOFC and SOEC at too high an efficiency would lead to a deficit in energy to drive the MH heat management system. The analysis suggested that the thermal management strategy could give a round-trip efficiency of 70.6%, though it should be noted that this is tri-generation efficiency, accounting for the provision of heat and cold; electrical round-trip efficiency would be 46.7%. A concern with this approach would be the unlikelihood of demand for heat and cool aligning with the operation of the hydrogen storage. Furthermore, the system seems to have been designed for a daily cycle which again is a questionable application for hydrogen storage.

Akikur et al [111] present a system combining rSOCs with concentrated solar power and photovoltaics, to be used for combined heat and power. In the proposed system, a parabolic trough solar collector (PTSC) assists with the generation of steam during electrolysis, whilst the PV provides the electric current. In addition to hydrogen, water would also be stored within the system.

A heat store is used to buffer the output of the PTSC, but plays no other role in the thermal management of the plant. Heat exchangers enhance thermal performance by exchanging heat between air leaving and entering the SOC stack. The researchers constructed mathematical models for the PTSC, SOC and PV components, and validated these against results in the literature and in the manufacturer’s data. The model predicted 44.3% efficiency for fuel cell mode (83.6% allowing for cogeneration) and 85.1% efficiency for electrolysis. The electrical round-trip efficiency is thus predicted as around 38%. The researchers also carried out an analysis of the economics for the proposed plant. Capital cost estimates included the various components of the system ($1000 / kW was assumed, perhaps optimistically, for the SOCs). The cost of electricity for this system was computed as $0.0676 / kWh, assuming a twenty year lifetime for the plant as a whole, and a five year lifetime for the SOC module. It should be noted that although a ‘hydrogen storage tank’ is mentioned, neither the technical nor the economic analysis gives detailed consideration to this.

In [112] a system is proposed using thermal energy storage in close contact with the stack. This would be either sensible heat storage using a ceramic material or latent storage using a eutectic metal alloy. Hydrogen would be stored at 108 bar. In similar fashion to [61], two configurations were considered: one in which water vapour would be condensed out of the off-gas, and one in which the vapour would be stored (removing the need for a steam generator). In the first configuration, surplus heat during SOFC mode was transferred to a steam drum in preparation for SOEC mode. This configuration was found to be capable of 72% RT efficiency, with either form of TES. However, electrolysis could not continue for long before external heat was needed for steam generation. The stored vapour configuration could achieve RT efficiency of only 64% - although this would reach 74% if the stack could be pressurised. The evaluation cycles considered in this research were of short duration, with two hours of fuel cell mode followed by electrolysis.

Wang et al [114] considered a distributed scale rSOC energy storage system of around 200 kW capacity, working with hydrogen only (no carbonaceous species). This research used an unusually detailed stack model, enabling the heat distribution in the stack to be monitored in three dimensions. Diathermic oil would be used for thermal storage, as in [110]; hydrogen would be stored at 20 bar. BoP components were modelled using 0D lumped models in gPROMS. Round-trip efficiency was found to be 72.3% at stack level, and 58.3% at whole system level. The research also examined the thermal gradients arising in the stack, which were found to be much higher in SOFC mode. Up to the time of writing, only steady state simulations had been carried out, and the researchers noted the need to conduct dynamic simulations, as well as to conduct economic analysis.

Ullvius and Rokni [115] present a concept for a polygeneration plant using concentrated solar power with rSOC’s and hydrogen storage. The distinguishing feature of this idea is the use of waste heat from the rSOC for carrying out desalination using direct contact membrane distillation. Dish Stirling solar collectors would generate electricity, whilst parabolic trough solar collectors would generate steam for electrolysis. Hydrogen would be stored at pressure in tanks (the precise details are unclear); this would enable the plant to continue operating through the night, and possibly provide longer term storage also. Simulations were undertaken using in-house software Dynamic Network Analysis. The round-trip efficiency of the energy storage component was found to be 42 - 45%, without accounting for the use of waste heat for desalination. A case study was undertaken for a South African location where the plant would generate a constant 500 kW and produce c. 8.5 tonnes of fresh water per day; this design incorporated 70 stacks of 200 rSOC’s. However, simulations were conducted only for one randomly chosen day, with no consideration of the variation in solar resource over the year. The economics of the proposed plant are yet to be studied.

2.6 Extant literature on energy storage using hydrogen in microgrids and distributed energy applications

We now consider some of the literature dealing with the role of hydrogen energy storage in the context of microgrid or distributed applications. Recall that a microgrid is defined as a localised grouping of electrical loads, generation and perhaps storage; a microgrid will generally manage its energy to achieve some measure of independence from the utility grid, and may be capable of functioning completely independently [5]. The studies reviewed here are concerned with the 'high-level' design and simulation of microgrid energy systems, and tend to include models for renewable generation and electrical load as well as the storage components. Accordingly, modelling of the individual components tends to be relatively simple. The objective of these studies is frequently to assess the technical or financial viability of the whole energy system. In some cases optimisation is carried out to determine the best choice of technologies and their capacities and dispatch over time. Only a few studies of this kind have considered rSOCs; more commonly, alkaline / PEM cells are considered, whilst some studies do not even specify the exact technology to be used.

Baldinelli et al [116], noting that rSOC's are considered to have poor load-following capability, accordingly put forward a concept in which rSOC's are hybridised with flywheel energy storage to smooth out short term transients. A case study is presented wherein the hybrid energy storage forms part of a minigrid consisting of a number of homes (2 kW mean demand) and PV generation (11 kW peak). A hydrogen tank would be used for bulk energy storage. PV output is modelled using solar generation profiles constant within each month. The rSOC is modelled in simple fashion using efficiencies for each mode of operation (respectively 85% and 50% for SOEC, SOFC). Preliminary sizing of the flywheel, rSOC and hydrogen tank is done analytically: the flywheel would provide 2.1 kWh of storage, the H_2 tank 25 kWh; the rSOC would have 2.6 kW / 1.14 kW capacity as electrolyser / fuel cell. A control algorithm is proposed to determine charge / discharge of the two energy stores, with the rSOC limited to one cycle per day, to minimise degradation. The algorithm decides the mode for the rSOC according to whether there is a generation surplus / deficit for the entire day, rather than on an instantaneous basis.

It was found that the hybrid energy storage could increase self-consumption from 52.1% to 58.0%; with the bulk storage alone, only 54.5% would be achievable. (N.B. the formula used for self-sufficiency appears to be unconventional.) Interaction with the grid (annual imports + exports) could be reduced from 15.6 MWh to 11.4 MWh (or 13.5 MWh for bulk storage only). Some of the current literature (e.g. [46], [48]) does reveal optimism that SOCs may in fact be capable of a good level of flexibility, possibly obviating the need for storage to be hybridised as described here. No economic assessment was undertaken in this research.

Sorrentino et al [117] designed a microgrid to supply power to an apartment complex in Salerno, Italy. This consisted of an rSOC and hydrogen storage, as well as PV and a vertical axis wind turbine. Thinking along similar lines to [116] the design only allowed for one load point for each mode of the rSOC; the researchers suggested that short term storage should be used to 'manage the transient phases', but this was not included in the model. The rSOC was modelled simply in terms of efficiencies for each mode: for electrolysis the efficiency was given as 0.64, which allowed for the use of some hydrogen to burn for heat; for fuel cell mode the efficiency was 0.7 (which seems implausibly high). The model of the hydrogen storage tank is not reported.

Sizing of the wind, PV generation, and hydrogen storage was optimised using the Excel Solver, the objective function being payback time (plus a penalty term to discourage net accumulation or loss of stored energy over a full year). The capacity of the rSOC appears to have been specified as 28 kW, to cover peak demand of the seven flats. The optimised design would have 11.7 kW of PV, 36.7 kW of wind, and would require 144 kg of H_2 storage (almost 5 MWh). The system would be capable of 3-10 days of full grid independence. It was claimed to achieve a payback period of 11.27 years; however, some of the CAPEX estimation seems very optimistic (rSOC $400 / kW; PV €817 / kW).

Patterson et al [118] used HOMER software ("Hybrid Optimization Model for Electric Renewables" [119]) to optimise the design of a microgrid to supply the Biosphere 2 Village, a research facility located in Arizona, consisting of 28 houses. The design was required to enable 45% of the microgrid's electricity to be procured from embedded renewables (solar photovoltaic panels); to cut its associated CO_2 emissions by 50%, and to keep annual imports from the grid below 120 MWh. Zinc bromine flow batteries and proton exchange membrane (PEM) electrolysers / fuel cells were considered as providers of electrical energy storage. It is unclear why more established technologies such as Li-ion were not considered. HOMER software was used to attempt the optimisation of the following key metrics: economics in terms of net present cost (NPC) and cost of electricity (COE); environmental impact in terms of grid imports and associated CO_2 emissions; and 'autonomy', the length of time the microgrid could function in islanded mode. A communal quick charger for electric vehicles was added to the microgrid's load, with different penetrations of electric car ownership considered. Various combinations of flow batteries and fuel cells were found to be capable of meeting the microgrid's requirements. The cheapest solutions used flow batteries only; however, the researchers felt that a hybrid system combining 63 kW of fuel cells with an 8.75 kWh flow battery was more favourable because of the increased autonomy provided by the hydrogen storage. This hybrid system would cut the microgrid's emissions by almost 80% and its dependence on the grid by over 75%; the COE would be an estimated $0.21 / kWh. Whilst NPC of the hybrid system was only 14% above that of a 50 kWh flow battery system, a large question remains here of whether it could possibly be cost competitive with more conventional battery storage.

In their 2004 paper [120], Khan and Iqbal consider the design of a stand-alone hybrid energy system for a remote off-grid house notionally located in Newfoundland, Canada. This research also employed HOMER. Wind turbines, photovoltaic (PV) modules and diesel generators were the generation technologies considered, whilst storage could be provided by PEM electrolysers and fuel cells, and/or by lead acid batteries. The system was optimised for cost, with sensitivity analyses conducted to vary the capital cost of fuel cells, the cost of diesel, and the wind and solar resource. It was concluded that a wind-diesel-battery system was the cheapest possible solution. However, if the capital costs of PEM fuel cells (estimated to be $3000 / kW at the time) were 35% lower, a wind-diesel-fuel cell-battery system would become financially viable, with the COE estimated at $0.49 / kWh. For an 85% reduction in fuel cost, a system with only wind generation and fuel cell / electrolyser could be optimal, achieving a COE of $0.42 / kWh. Clearly it is difficult to rival the cost-effectiveness of a diesel generator to complement the intermittency of renewable generation – so a secondary objective of minimising emissions could have been interesting here.

Another study using HOMER software was conducted by Shahinzadeh et al [121]. The microgrid under consideration was to be located in Nain, Iran. The considered technologies for generation were wind turbines, solar PV and gas microturbines; storage options were electrolysers / fuel cells and batteries; a connection to the external grid allowed additional flexibility. The net present cost of the energy system was minimised. The capital costs used for fuel cells and electrolysers were significantly lower than in [120] at $1800 / kW and $333 / kW respectively; this price for electrolyser capacity seems implausibly low [35]. Notably, the fuel cells and hydrogen storage were selected by the optimisation, providing 2% of electricity demand across the year. The optimised COE for the energy system was calculated as $0.106 / kWh.

Maroufmashat et al [122] considered the design of a hydrogen powered microgrid for the remote community of Cornwall, Ontario. A novel aspect of the model was the inclusion of hydrogen powered vehicles (HPVs) as well as the electrical load. It was wished to deliver a microgrid capable of two full days in islanded mode; PEM electrolysers and fuel cells would be used with hydrogen storage to store renewable energy (wind and solar). Mixed integer dynamic optimisation was used to determine the installed capacity of each technology, optimising for lowest cost. The optimal design employed 380 kW of solar generation, 6.4 MW of wind, 4 MW of electrolysers and 4 MW of fuel cells. The researchers noted that the cost of the storage system would be excessive at around 70% of the CAPEX of the entire energy system; the fuel cells by themselves contributed 42%, eclipsing the 30% contribution of the installed wind and solar generation. A further ‘vehicle to grid’ scenario was explored in which HPVs could release electricity back to the microgrid. This enabled a reduction in the installed capacity of fuel cells, which nonetheless still contributed 35% to the system cost. The possibility of using waste heat from the electrolyser was also mentioned but does not seem to have been included in the model. COE does not appear to have been calculated for the proposed energy system, making a judgement of its overall financial viability difficult.

A 2011 paper from Kyriakarakos et al [123] discusses the design of a microgrid for deployment on remote islands in the Aegean sea. The conceived microgrid would supply two dwellings with power, and would also power a desalination unit and supply fuel to a hydrogen powered vehicle. Solar PV and wind power would provide renewable energy, with energy storage realised by PEM electrolysers and fuel cells in tandem with metal hydride hydrogen storage – and/or by lead acid batteries. Particle swarm optimisation was used to optimise the sizing of the various components, in order to minimise the capital and maintenance costs of the energy system over twenty years. The optimisation sized the electrolyser at 700 W, the fuel cell at 300 W and the lead acid battery at 48 kWh. (It should be noted that the selection of hydrogen storage by the optimisation was inevitable owing to the inclusion of a hydrogen powered vehicle in the model.) The fuel cell would operate for less than ten hours a year; the researchers argue it cannot be dispensed with as it is needed for security of supply and to avoid deep cycling of the battery. To evaluate the economics of the proposed microgrid, the avoided cost of potable water and petrol was considered, and the cost of electricity generation was compared with a more conventional diesel-battery microgrid. A Monte Carlo method was used to take account of uncertainty in fuel prices et cetera; it was concluded that the hydrogen microgrid was profitable (positive net present value) with around 90% probability.

Nelson, Wang and Nehrir [124][125] considered the design of a stand-alone energy system for implementation in Montana, USA. The research involved unit sizing and cost analysis for two designs: one using conventional battery storage, and one using hydrogen storage with electrolysers and fuel cells. Both designs incorporated wind and PV generation. Batteries were modelled with a simple round-trip efficiency of 85%; electrolysers and fuel cells were assigned efficiencies of 74% and 50% respectively. Designs were constrained to have a loss of power supply probability of below 0.0003. It was found that of the viable solutions, the ones with the least amount of PV generation were most cost effective, owing to the high capital cost of PV modules. Ultimately it was found that the COE for the hydrogen-based energy system was far higher at $0.70 / kWh, with the battery system at only $0.37 / kWh. The factor underlying this was the low round trip efficiency of the hydrogen storage, which led to more generation capacity needing to be installed. For this reason, the hydrogen system was found to have a higher COE even if the fuel cells and electrolysers had zero capital costs.

The researchers therefore emphasised the need for fuel cells and electrolysers to achieve higher efficiencies in order to compete viably with batteries. It has to be pointed out that the modelling did not include the self-discharge of the batteries, and therefore the advantage of the electrolyser/fuel cell system for long term storage would not have been captured. It should also be noted that the costs of PV generation have fallen dramatically since 2005 when the research was published.

Finally, Gabrielli et al [126] used mixed integer linear programming (MILP) to optimise the provision of energy to a district of Zurich, Switzerland. Uniquely among the work reviewed here, the demand for both power and heat was considered. Solar PV and solar thermal were considered as renewable energy sources, with electricity and gas also available to import from the national grid. Energy storage options considered were hydrogen storage using PEM electrolysers and fuel cells, in addition to Li-ion battery storage and hot water sensible thermal storage. The fuel cells and electrolysers were modelled with efficiency depending on power according to an affine approximation, an improvement on simply using a flat efficiency. Battery self-discharge was also taken into account. The optimisation was conducted with two objectives: the minimisation of both cost and CO_2 emissions. Thus a cost/emissions Pareto set was constructed. Notably, the hydrogen storage was not selected by the optimisation when minimising for cost only; indeed it was only selected when emissions cuts of 80% and above were required. For less ambitious curtailment of CO_2, battery storage was chosen as the more cost-effective option. Furthermore, the selection of the hydrogen storage was found to be relatively insensitive to its capital costs.

2.7 Real-world trials of hydrogen energy storage

This section discusses a few of the real-world pilot schemes that have been conducted using hydrogen for stationary energy storage in distributed energy systems. The overwhelming majority of such schemes to date have employed alkaline or PEM electrolysers and fuel cells, and to provide some background, a few of these are discussed first. We then describe the pilots involving rSOCs, which are all recent and as yet are few in number.

What follows is by no means intended to be an exhaustive account; for a more thorough review on pilot schemes with hydrogen energy storage, Gahleitner's review paper [30] is recommended, although this only covers to the year 2012. Here we discuss four schemes that seem particularly relevant to this project. Common themes worth noting are the low round-trip efficiencies that are achieved, and the desirability of hybridising hydrogen energy storage with shorter term storage.

The PHOEBUS demonstration plant at the Central Library of the Jülich Research Centre, Germany, ran for 10 years to 2003 [26]. A 30 kW solar array was used to power an alkaline electrolyser; the oxygen and hydrogen produced were stored in separate pressurised tanks, at 70 bar and 120 bar respectively. The 6 kW fuel cell initially installed was found unreliable and a grid connection was used as a fuel cell simulator instead, before finally a PEM fuel cell was installed. A lead acid battery bank was also installed, with 303 kWh capacity able to supply the load for three days. In fact the battery supplied over half of the final power demand, with the hydrogen storage supplying less than a quarter. The hydrogen storage was noted to have 'very low efficiency', at around 22 to 26%. 'Lessons learned' included that storage of O_2 was perhaps an unnecessary expense, as the fuel cell could have run on air; also that running the electrolyser at high pressure (200 bar) could have reduced the energy cost of compressing hydrogen (from 9% of stored energy to 3%).

The Centre for Renewable Energy Systems Technology (CREST) ran the Hydrogen and Renewables Integration (HARI) project at West Beacon farm, Loughborough, beginning in 2001 [27], [127]. The system was designed to store surplus power from onsite wind, solar and hydro generation. 3.8 MWh_e of hydrogen storage – enough for about three weeks - was realised using an alkaline electrolyser and tanks pressurised to 137 bar. A 20 kWh ZEBRA battery was also used to buffer the variable electricity supplying the electrolyser. Two PEM fuel cells were used for conversion of H_2 to power. One of these

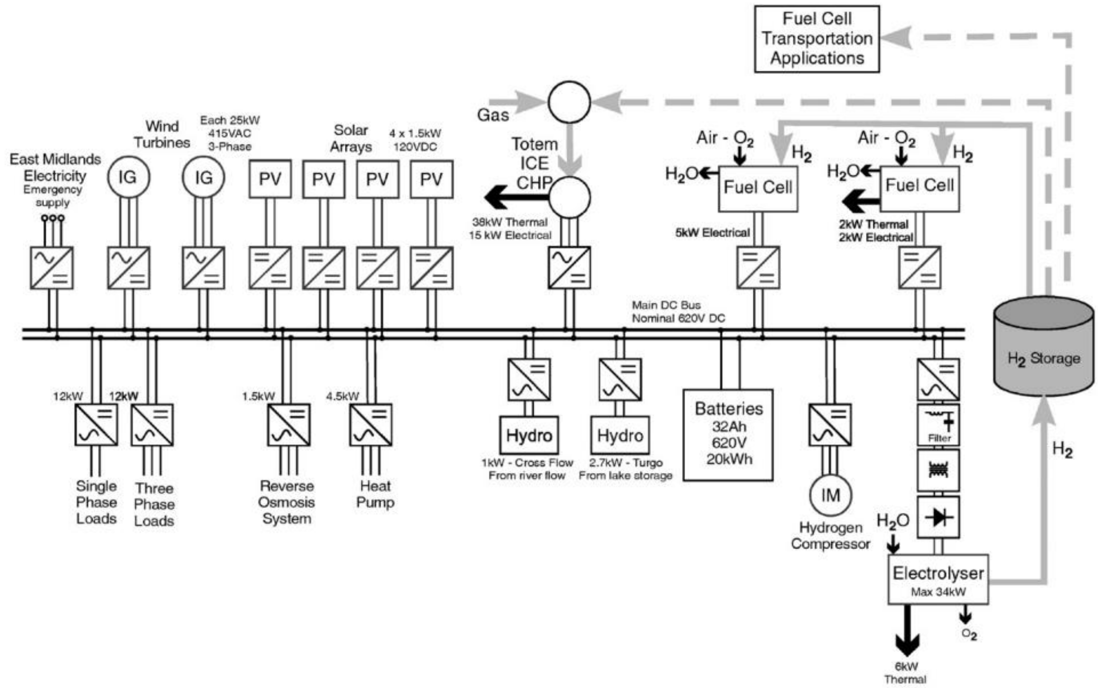

Figure 2.6. Schematic of the stand-alone power system at West Beacon farm [27]. Reproduced by permission.

was designed to output useful heat as well as electricity, but it is unclear if/how this heat was used. Modelling suggested that the hydrogen storage would have a round trip efficiency of only around 25%; it wasn't specified whether this accounted for the possible use of fuel cell heat. The indicative capital cost of the storage system excluding the controls and converters was given as £369000 or £97 / kWh. In the 2007 paper the system was still described as 'not fully operational'.

A wind/hydrogen system launched on the Norwegian island of Utsira in 2004 was used to supply electricity to ten houses [36]. The system used an alkaline electrolyser to produce hydrogen at times of surplus wind power; 2400 Nm^3 of hydrogen could be stored at a pressure of 200 bar (presumably representing several MWh of stored energy). A 10 kW PEM fuel cell was installed, but suffered various failures and degradation over time, so that at the time of writing a 55 kW hydrogen generator was exclusively used in its place. With the production of hydrogen estimated to be only 53% efficient, and the hydrogen engine under 20%, the round-trip efficiency for the hydrogen storage would have been only around 10%. Nevertheless the microgrid, which was also equipped with 5 kWh of flywheel storage and a 50 kWh battery storage system for regulation of frequency and voltage, could achieve two to three days of energy autonomy for the island.

Around 2005, the PURE ('Promoting Unst Renewable Energy') project on Unst in the Shetland Islands became operational, supplying electricity to five business properties [128]. Compressed hydrogen was used as a storage medium for electricity generated by two 15 kW wind turbines. Pains were taken to reduce 'on-demand' electrical load at the beginning of the project; on-demand electrical heating was removed and replaced with storage heaters charged by surplus wind power, and building insulation was substantially improved. These measures reduced the ‘on-demand’ load by 55% and apparently saved the project £40000 in capital costs whilst costing only £3000. The project experienced difficulty in finding a suitable electrolyser, with concerns that alkaline electrolysers are not appropriate for use with an intermittent supply; nonetheless one was eventually chosen that was expected to be efficient under flexible load. The PEM option was considered but dismissed, the cited concerns being degradation, short lifetime and inadequate efficiency at high current density. A 5 kW fuel cell was used for generation, and hydrogen was also stored in hydride cylinders and used in a fuel cell vehicle, and for ‘other applications’. Few other technical details are available.

2.7.1 Real-world trials using rSOCs

To the author’s knowledge, only two pilot schemes have been conducted using rSOCs at the time of writing (assuming that lab-scale work is discounted). A third is under development at the time of writing. The two demonstration projects that have already published results have both involved German SOC manufacturer Sunfire, which has a number of SOC and rSOC products relatively near to commercialisation [129].

The first of these projects was a collaboration between Sunfire and Boeing [24]. This multi-kW scale system, designed with microgrid applications in mind, was commissioned in 2015 and underwent testing at Boeing’s Huntingdon Beach facility in southern California. 1920 cells in stacks of 30 could generate 50 kW in fuel cell mode, and absorb 120 kW in electrolyser mode. The system was apparently online for 1000 hours, although only underwent seven cycles during that time.

Figure 2.7. rSOC energy storage system demonstrated at Boeing Huntingdon Beach. [24]. Reproduced by permission.

Storage of hydrogen was in tanks at about 250 bar. The storage was ‘sized for 12 hours of operation in fuel cell and electrolysis modes’; however the paper stresses that more storage could be added easily and cheaply (cost of tanks was given as $30-$40 / kWh). The compressor used 13% of the total electrical load during electrolysis. Electrolysis was carried out at close to the thermoneutral voltage. In terms of hydrogen’s HHV and neglecting the electricity consumption of the compressor and the steam generator, electrolysis was 99.3% efficient; the more realistic figure, using hydrogen’s LHV and allowing for the compressor and steam generator, was 60.5%. Fuel cell mode was reported to be 49% efficient, indicating a power-to-power round-trip efficiency of about 30%. Apparently, gas burners were also used for start-up and during electrolyser mode, and it is not clear if/how this energy consumption was accounted for. The researchers argue that unfavourable comparisons to battery storage are unfair, given the ‘theoretically infinite’ energy storage capacity. No mention is made of whether any degradation was detected during the tests.

A second trial using Sunfire rSOC technology is reported in [46], [49], [85], [130]; this is the ‘GrInHy’ or ‘Green Industrial Hydrogen’ project. The technology application here is somewhat different, with the 143 kW rSOC installed in a steelworks at Salzgitter, Germany in 2017. This enabled the energy cost of steam generation to be avoided through use of waste steam from the steelworks. Furthermore, generated hydrogen could be used in the steelworks as a reducing agent (in place of coke) and for annealing, as an alternative to using it for electricity generation. Although such industrial applications will not be a focus of this present work, results from GrInHy cast unique light on the current capabilities of rSOC technology, so are of interest.

The rSOC storage had a nominal load of 143 kW_{AC} in electrolyser mode, and generated 30 kW_{AC} in fuel cell mode. The system was operational for 5000 hours overall, with seven full shutdowns needed to exchange BoP components. Efficiency of electrolysis was reported as $84\%_{LHV}$ - although this was subject to improving the power electronics (DC to AC conversion was responsible for the majority of energy losses in this mode). For fuel cell mode, efficiency was $47\%_{LHV}$ for potential round-trip efficiency of nearly 40%. (In practice the device was not used as energy storage as such, since H_2 generated was used in the steelworks and fuel cell mode was primarily run using natural gas.) Other notable results include the achieved level of flexibility, with relatively fast startup (from hot standby) and shutdown times possible, and a good range of achievable partial loads without efficiency penalty; see Table 2.5. Additionally, the degradation of the system was monitored over the duration of its operation; mean ASR degradation was measured at 21 $m\Omega \cdot cm^2$ per thousand hours, equating to voltage degradation of 0.8% per thousand hours in electrolysis mode. The fact that running fuel cell mode using natural gas (rather than stored hydrogen) was considered more cost-effective for this project is worth noting.

Table 2.5 Details pertaining to GrInHy's rSOC system [46], [49], [85], [130].

Mode	Electrolysis	Fuel cell (H_2)`	Fuel cell (NG)
Nominal AC power (kW)	143	30	25
AC efficiency (%$_{LHV}$)	84	47	50
Test regime	1400 hours; 160 on-off cycles	Only used for calibration & monitoring degradation	1000 hours; 60 on-off cycles; mainly 80 – 100% load.
Partial load range	50% - 113% with no efficiency penalty	-	40 – 100% (down to 0% with efficiency penalty)
Startup time (hot standby → 100% load)	24 mins	-	20 mins
Shutdown time (100% load → hot standby)	7 mins	-	up to 6 mins

It is worth briefly mentioning the third major demonstration project to employ Sunfire's SOC technology: HELMETH ('high temperature electrolysis and methanation') [131]. This is purely a power-to-gas project; the SOCs are not used reversibly. The syngas produced by electrolysis undergoes methanation, boosting the overall efficiency of electrolysis – a concept that has attracted a great deal of attention ([60]–[65], [107]). This may be the first project to implement such a concept beyond lab-scale (the HELMETH prototype is 10 kW.) Unlike the concept studied by Braun's research group, here methanation is carried out in a separate component to the SOC stack, but is thermally coupled to it. The system achieved 76%$_{HHV}$ efficiency, with potential to reach 80%$_{HHV}$ at industrial scale.

A third major pilot project using rSOC technology is REFLEX [48], [132], [133], a European project coordinated by CEA-Liten, using rSOCs manufactured by Estonian company Elcogen. This project is currently in development; a Smart Energy Hub located at Envipark, Turin, Italy is to be completed by the end of 2019 with testing in 2020. This will incorporate three rSOC modules for total electrolysis capacity of 120 kW, which will be hybridised with li-ion batteries for shorter term storage. CHG will be stored at 200 bar. The Energy Hub will be co-located with solar and hydro generation and will supply both heat and power. It is of note that the rSOCs are expected to be capable of a reasonable dynamic response; the design allows three load points for each mode, with transition times between these of the order of minutes – see Figure 2.8.

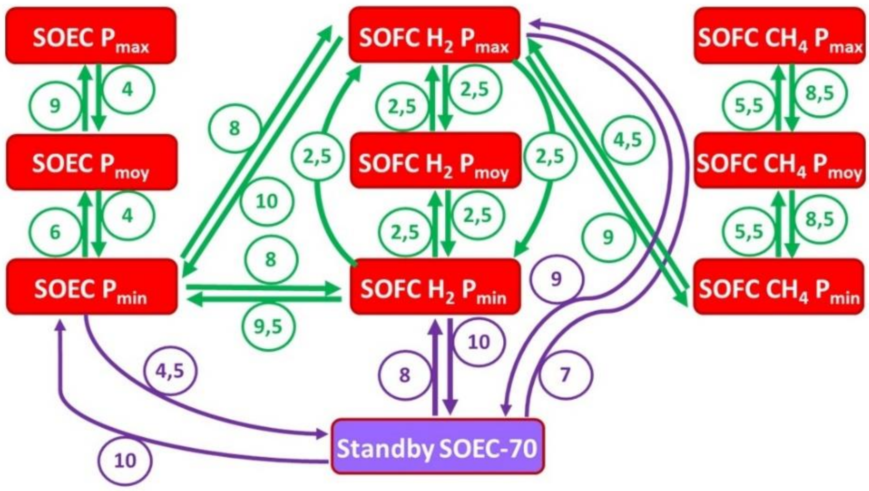

Figure 2.8. Operation modes for the rSOC modules at the REFLEX Smart energy Hub, with expected transition times in minutes. [48].

Having examined some of the hydrogen energy storage trials reported in the literature, a few points may be highlighted.

- The realisation of rSOC energy storage at scale is in its infancy, with no projects pre 2015.
- rSOCs do appear to have proven a superior round-trip efficiency compared to PEM and alkaline technology (but still only 30 – 40%).
- The more complex concepts for thermal integration of rSOC energy storage (see sections 2.3, 2.5) have not been tried at scale
- Almost all pilot hydrogen storage schemes seem to require shorter term energy storage as a buffer.
- Details of costs are generally not available.

2.8 Challenges and future developments for SOC technology

Gomez and Hotza [40] list the challenges for solid oxide technology as: materials properties, materials costs, mechanical strength, electrode stability, delamination, and difficulties with bulk manufacture of complex ceramic parts. Similarly, [50] states that 'the materials problems of SOFCs are profound', and in a 2012 review [42], Laguna-Bercero concluded that materials improvements were needed before commercialisation.

As is to be expected, several of the challenges for solid oxide fuel cells and electrolysers pertain to the high operational temperatures. The time taken to heat up or cool down is considerable – it can even be as much as 12 hours. This limits the applications of the technology, suggesting that it is best deployed where the stack can be in continual use [1][33]. High temperature operation also necessitates balance-of-plant components able to tolerate a high temperature gas stream [134]. It is desirable to keep the temperature of a SOC stack stable, as changes in temperature can lead to mechanical stresses and cracking/flaking in the layers of individual cells [50]. It is therefore difficult to use a SOC as a fuel cell supplying a variable load, or as an electrolyser running on intermittent renewable generation.

[34], [135] both suggest that SOECs should not be coupled to renewable energy sources. However, the proposals for SOC energy storage plants discussed in Section 2.5 seek to address this problem in various ways.

The susceptibility of individual SOCs to thermal shock is minimised by keeping their dimensions small. According to [50], the largest planar SOC to be fabricated was only 20cm by 20cm. Larger cells are in any case inherently more delicate and difficult to manufacture. PEMFC or alkaline technology, by contrast, can use much larger individual cells [50]. This does imply challenges for the scalability of SOC technology.

For a SOEC with O^{2-} conducting electrolyte, it is important to note that the fuel-electrode off-gas consists of both hydrogen and unreacted steam. This is a disadvantage in comparison with PEM or alkaline electrolysers, which can directly produce hydrogen of high purity (99.999% for PEM [1]). The need to separate unreacted steam from hydrogen in a system using SOECs pushes up the capital costs [29]. It is also often necessary to mix hydrogen with the steam supplied to the SOEC, in order to reduce oxidation of the nickel; in the literature the inlet gas is 10-50% H_2 [29], [109], [110], [113].

2.8.1 Future developments for SOCs

As has been stated, the majority of SOCs employ O^{2-} conducting electrolytes. Alternative electrolytes (strontium zirconates) conduct protons H^+ rather than oxygen ions. This can be desirable as pure hydrogen can be obtained, rather than a mixture of hydrogen and unreacted steam. Unfortunately the performance of such cells is still inferior to the more conventional design, but may improve in the future [68][42][29]. Further to this, hybrid electrolytes have also been considered which conduct both oxygen anions *and* protons. Steam is supplied, and hydrogen given off, at both electrodes. This may enable much higher current densities (and hence power densities) to be achieved [136].

Other research has focused on enabling SOCs to run at lower temperatures. This requires that either the electrolyte be made thinner, or use different materials [134]. In [137], Goodenough describes a new solid O^{2-} conducting electrolyte exhibiting high conductivity at room temperature, raising the prospect of solid oxide cells that could operate at 300 °C if not all the way down to room temperature. Clearly this could help to overcome the difficulties associated with high temperature operation: complex and costly balance of plant components, and fast degradation.

2.9 Conclusions on rSOCs

Modelling of rSOCs in the literature typically draws its boundaries around the energy storage system itself (if not the cell or stack). Very few studies have carried out work at higher level than ‘balance of plant’. When real-world applications are considered, very simple assumptions are often made – for instance the assumption of a static electrical load. Hence there is a gap in knowledge as to how well suited these systems are for real-world applications – how well-matched are their properties to the real loads experienced in a distributed energy system?

Studies on hydrogen-based energy storage in the context of microgrids have certainly been performed by many, but there appears to be more interest generally in PEM fuel cells than solid oxide fuel cells. This may be because PEM is considered cheaper [35], easier to implement because of the lower temperatures, or more established. Still, the result is that that the literature lacks much exploration of the possible advantages offered by rSOC: higher efficiency; the incorporation of fuel cell and electrolyser functions in one device; and the potential for CHP applications. It is also the case that the 'microgrid' studies tend to use highly simplified models for fuel cell / electrolyser components, often modelling them simply with a blanket conversion efficiency. In some cases this is to ensure tractability for linear optimisation algorithms. Also, the design of microgrids is often undertaken considering the demand, supply and storage of energy in an aggregated fashion. Storage is assumed to be a communal asset, or its configuration is not specified at all. For this current work, the potential of rSOCs to supply heat as well as power provides an incentive to build a simulation that can capture individual dwellings in more detail.

In general, there is concern that electrolysers with hydrogen storage are an overly expensive storage option [120][122][124][126]. Niche applications, such as the HPVs in [122] and [123] can potentially provide more incentive. There is also naturally more incentive to consider hydrogen storage when the microgrid is remote or completely stand-alone as in [120][123]; when there is a reliable grid connection, as in [126], the incentive diminishes.

2.10 P2P energy trading

In traditional energy systems, households are exclusively consumers of energy, and they buy this exclusively from a large-scale supplier. Peer-to-peer (P2P) energy trading would represent a disruptive shake-up of this paradigm, as it definitionally enables the trade of energy *between* customers. For instance, household A might charge an electric vehicle using solar PV exported from household PV, with this transaction remunerated on a P2P market.

On the road to decarbonisation, the energy system faces various changes, and some of these contribute to the motivation for P2P as an innovation. Such changes include the **decarbonisation of heat**, the **decarbonisation of transport**, and the proliferation of **embedded generation** (mainly PV). For the UK, decarbonisation of heat is likely to involve electrification of the ca. 700 TWh/a [138] of existing heat demand. This is approximately double the existing annual electricity demand, and also brings peak demand roughly quadruple the peak electricity demand (214 GW versus 53 GW for winter 2017 – 18) [139]. Therefore, accommodating electrified heat in the electricity transmission and distribution network is an immense challenge. Decarbonisation of transport using electric vehicles (EVs) would compound these problems, with the distribution grid similarly ill-equipped to meet peak demand for vehicle charging [140]. PV generation can bring clean power generation to homes, but electricity demand is not necessarily well-matched to PV output [141], whilst excessive generation surpluses can disrupt the distribution grid [142].

All of these challenges point to the advantages of managing energy more creatively in localities. A key opportunity is to match locally generated energy to local demands (including for EV charging or heat pumps); achieving this reduces the burden on distribution / transmission grid infrastructure, especially if demand can be shifted temporally to align with generation. Under the existing paradigm, there tends to be no incentive for local generators and consumers of energy to cooperate, since all parties are trading at fixed prices with utility companies; this is where P2P could provide the missing piece of the jigsaw.

Interest in P2P is growing, and companies including Centrica and EDF have carried out pilot schemes for P2P in recent years [143], [144]. A number of platforms for the P2P buying and selling of energy have also been designed, including among others Piclo [145] and Vandebron [146]. In terms of the actual market mechanism through which P2P exchange of power is agreed and paid for, the literature covers a number of different possibilities. These include **centralised control**; **centrally issued price signals**; **auctions** and **iterative markets** – where these categories are not exhaustive and may also overlap. These approaches will now be discussed in more detail.

Under **centralised control**, decisions on which market participants should trade energy are made centrally, in order to optimise the welfare of the entire community. This may entail direct control of EV batteries and other flexible devices by the central coordinator. When the dispatch of the microgrid has been optimised, the coordinator can then dictate how traded energy is remunerated; for instance, a mid-market rate (MMR; halfway between the grid tariff and the feed-in tariff) may be used. Solving the full-scale optimisation problem for an entire P2P community requires that the central coordinator receives detailed information about each participant's forecast demand or generation, and the availability of their devices. As such, this gives rise to concerns about the privacy and the autonomy of participants, as well as the computational complexity of optimising the entire microgrid [147]. Consequently, some researchers have formulated the central optimisation problem in their work, before recasting it as a distributed optimisation [148]–[150]. Oh and Son [151] compared central optimisation of microgrid dispatch with a distributed algorithm, finding that the distributed approach was almost as effective. Centralised optimisation may of course be used as a tool to understand the potential of a local energy market, even if not intended for real-life implementation, as in [152]. In [153], centralised MILP optimisation is used to determine P2P trades of energy between EVs.

Another approach is for microgrid participants to retain full autonomy, whilst the microgrid operator tries to incentivise desirable actions via **centrally issued price signals**. For instance, increasing the microgrid's internal prices should incentivise the reduction of load, or the increase of generation. Under this paradigm, households trade only with the microgrid operator; nonetheless, the tariffs chosen can effectively transfer money between generators and consumers within the microgrid to compensate for energy which is physically shared. Price signals can be issued ahead of time (e.g. day ahead) or in real time. Kim et al [154] consider this approach, with reinforcement learning used to improve the operator's strategy. The approach in general may be interpreted as a Stackelberg game, with the microgrid operator as leader and households as followers [155], [156]; equilibria for such games can be identified through iteration, so that this paradigm overlaps with **iterative markets**.

A natural approach to local energy markets is through the use of **auctions** – especially as microgrid auctions can be designed to emulate traditional energy markets, as in [157]. Double auctions, wherein buyers of energy submit 'ask' prices and sellers submit 'bid' prices are of most interest; auctions may be 'one-shot', with all asks and bids submitted simultaneously, or continuous, where asks and bids are submitted and accepted/rejected on a rolling basis. Auctions may be uniform, with all agreed trades receiving the same clearing price, or discriminatory, with participants receiving different prices [158]. The Brooklyn microgrid operates using a discriminatory double auction [158]. Participants in auctions need to employ some kind of strategy to determine their bid/ask prices, in order to maximise their benefits. For instance, Wang et al [159] modelled a continuous double auction for a microgrid, with participants employing an adaptive learning strategy, incorporating an aggressiveness model; similarly, Marufu et al [160] studied a local energy market with participants employing the adaptive aggressive strategy; Li and Ma [158] compared an 'eyes on best price' strategy with a 'zero-intelligence' strategy. None of these three specifically consider flexible loads or energy storage, however. Zhang et al [161] considered an auction for PV and flexible loads, whereby forecasting uncertainty is paired with load flexibility – although the strategy of bidders in setting prices is unclear. El-Baz et al [147] considered a uniform double auction for microgrid energy sharing, with different bidding strategies for different flexible devices. The P2P market was able to effect a doubling of self-sufficiency, and a decrease in household bill of up to 23%. Meanwhile Block et al [162] contrived a two dimensional auction for heat and power in microgrids, based on call-market trading.

As has been touched on in the above, Game Theory is often a useful tool to approach the study of P2P markets. Participants in such markets are generally competing to serve their own self-interests, so that the market may be modelled as a non-cooperative game, and the problem of choosing a strategy requires identifying a Nash equilibrium; this approach is seen in references [163]–[166]. In some cases, the game theoretic problem is converted to an optimisation problem to be solved iteratively or otherwise [167]–[170]. Stackelberg games with 'leaders' and 'followers' are also frequently used, as already noted [155], [156], [171], [172].

Many papers discuss **iteratively settled markets**, in which feedback from each round of bidding is used by participants to update their new bids; the market is only finally settled if and when it converges, otherwise requiring an exit mechanism of some kind. For instance, Guo et al [148] considered a P2P market with components for both energy and reserve (to address forecasting uncertainty). The consensus method of direct multipliers was used to iterate the market until each pair of participants agreed the volume and price of energy to be traded. In Li et al [158] an iterative process is used to solve a Nash bargaining theory problem in order to settle the market. Kim et al [173] compare two iterative, distributed optimisations for deciding P2P trades: one in which participants collaborate, and one in which they compete in pursuit of their own self-interest.

Liu et al [174] contrived an iterative pricing mechanism for an energy-sharing zone consisting of buildings with PV generation and some adjustable loads. The internal tariffs for import and export of power were functions of the supply-demand ratio (SDR), i.e. the total of all exported power over all buildings, divided by the total of imported power. As such, this pricing mechanism will henceforth be referred to as the SDR tariff; it is the mechanism adopted in the present work, and so will be discussed in more detail. When SDR > 1, prices are low (equal to the grid feed-in tariff), incentivising demand to be increased or supply reduced. For SDR < 1, prices increase towards the cost of grid power, incentivising demand to be reduced or supply increased. Prices are designed so that the operator operates a balanced budget – i.e. all payments effectively flow between households and the utility grid, or between different households, with the operator not profiting. In [174], all of a building's demand was considered reschedulable, but subject to an inconvenience cost, weighted by a parameter reflecting the willingness of a participant to shift load. The final prices and load schedules are decided iteratively. In each round, participants optimise their load schedule relative to the most recently issued internal prices. The new schedules give rise to a new SDR and new prices, and the process repeats until convergence is achieved: viz. prices do not significantly change between iterations. Successful convergence indicates that a kind of Nash equilibrium has been found: every participant cannot further improve their strategy given the strategies chosen by all other participants. Implementing the SDR tariff for a case study with a number of residential and commercial/office buildings, and found that modest technical and economic benefits resulted – these quite dependent on the willingness parameter.

Zhou et al also consider the SDR tariff in [8]. This work was focused on (i) possible approaches to improving the convergence of the iterative market mechanism; and (ii) the comparison of the SDR tariff to alternatives (mid-market rate and bill-sharing). They point out that the iterative market is likely to diverge in the presence of large flexible loads such as EVs or electric water heaters, which can readily be rescheduled without inconvenience. In the absence of convergence controls, demand will always jump to the cheapest timeslots; thus response to the price signal is discontinuous. Step-length control and learning-rate methods were tried to mitigate this problem. Also, technical and economic indices were formulated to facilitate comparison of the different tariffs and convergence aids. Simulations involved 20 households equipped with PV and flexible loads, with one day simulated at a time. Flexible loads considered were water heaters and washing / drying machines in addition to EVs. The methods to improve convergence were both found to be effective, and the SDR pricing tariff was considered to outperform the alternative pricing formulas.

For the modelling of P2P markets incorporated in this thesis, both the iteratively settled market mechanism, and the double auction mechanism, are considered of interest.

2.11 Agent-based modelling approaches

Agent-based modelling has attracted interest lately for the simulation of energy systems. As noted by Ringler et al [175], agent-based modelling lacks a universally agreed definition. In general, it involves the simulation of a complex system by modelling its individual components as distinct *agents*, which interact with each other and with their environment. Typically – but not universally – agents are many in number, and whilst their individual models may well be simple, their interactions give rise to emergent phenomena which may be unforeseeable by the modeller ahead of time. It is often – but not universally - the case that agents are programmed to pursue some individual goal; Kremers suggests that proactive pursuit of such a goal is a defining attribute of a true 'agent' [176]. However, there is no real consensus on this: [177] emphasises that there are many different styles of agent-based modelling: "some [agents] communicate while others live in total isolation, some live in a space while others live without a space, and some learn and adapt while others never change their behaviour patterns…An object that seems to be absolutely passive can be an agent…" Kremers states that even simple objects like an on/off resistive heater can be modelled as agents. He also notes that agent-based modelling is a close relation of object-oriented programming (OOP), whilst lacking the same formal definition and framework. The author's own view is that the pursuit by agents of their own individual goals, and the emergent behaviour that results, is key to the definition of an agent-based model. It can be contrasted with more top-down methods, such as optimisation methods.

An agent-based modelling approach is becoming increasingly more attractive for the simulation of energy systems. As noted in [178], this is because energy systems are moving away from their traditional structure, with large centralised generators distributing power to consumers who are essentially passive; the advent of distributed energy generation (and storage), along with smart-grid type technologies like demand-side management (DSM) and vehicle-to-grid (V2G) mean that customers can no longer be considered as a passive, well-behaved electrical load. Instead they become 'prosumers' and their individual, disaggregated behaviour becomes more significant. Agent-based modelling is well-suited to capturing such complexity. As noted in [176], it also allows social and economic behaviours to be simulated alongside technical aspects.

The most common use of agent-based modelling for questions pertaining to energy systems focuses on economics, with agents interacting via markets. This may be combined with models for the adoption of new technologies. For instance, Ponta et al [179] constructed an agent-based macroeconomic model, with producers of renewable energy or fossil fuel generators taking investment decisions in response to fossil fuel prices and government feed-in tariffs. Mittal et al [180] modelled the adoption of rooftop PV for households, and the feedback effects of such adoption on electricity generators and other stakeholders. Kuznetsova et al [181] constructed an agent-based microgrid model, wherein agents (representing a train station equipped with PV, a district of small businesses and residences, and a local wind farm) vied with each other to maximise revenues from sold energy and minimise costs, with robust optimisation used to tackle uncertainties attached to renewable generation.

Whilst models focused on economics, social aspects or technology adoption are common, agent-based models that mainly address the technical aspects of an energy system are also seen [178], [182]–[185]. For instance, in [178] Gonzalez de Durana et al present a highly generalised and versatile agent-based model, describing the flow of multiple energy carriers (electricity, heat and chemical energy) around a network, with nodes acting as loads or converters of energy between types. The model, which was implemented in AnyLogic, was also intended to be adaptable to a wide range of scales, from the workings of a single electric vehicle, to a smart grid. (There may perhaps be some debate over whether this is truly an agent-based model, or merely an object-oriented one. Ultimately, an agent-based modelling environment is also a good environment to build an object-oriented simulation.) Another example is the work of Bazan and German [186] who present a hybrid simulation for the study of distributed storage and generation of energy in a domestic microgrid, also implemented in AnyLogic; the simulation was used to study the cooperation of multiple houses with a nearby solar park, attempting to approach energy self-sufficiency.

Ultimately, a strength of agent-based modelling is its adaptability to address many different types of question, whether focusing on technical, social or economic aspects. As with OOP, an advantage of constructing a simulation through the creation of various agent types is the ability to develop different sub-models separately, to incrementally improve them, and to deploy them in different places. Inheritance of behaviour by agent-types is another advantage in common with OOP.

The multi-paradigm simulation software AnyLogic [4] is used for most of the modelling work in this project. This provides agent-based simulation functionality, along with discrete-event and system-dynamics modelling paradigms. In this work, the agent-based modelling approach will come to the fore when P2P markets are simulated, particularly in Chapter 7.

2.12 Conclusions

This chapter opened by demonstrating how, despite the broad range of extant electrical energy storage technologies, storing electricity in bulk for long duration storage cycles is challenging, with P2G one of the principal solutions available. Whilst PEM and alkaline cells are currently the main technologies employed as fuel cells and electrolysers for P2G, rSOCs are promising for a number of reasons – these include the higher conversion efficiency; potential CHP applications; comparatively abundant electrode materials; and possible savings from reversible operation, including the possibility that some degradation may be reversed. Foremost among the challenges for rSOC are the difficulties in thermal management and slow dynamic response; also the cost and complexity of high-temperature balance-of-plant equipment, and the difficulty in manufacturing at scale.

It has been seen that rSOC technology is still in its infancy relative to more established technologies, with few pilot plants and no commercialised solutions. Academic literature, meanwhile, has tended to concentrate on plant design, with limited exploration of applications or economic analysis. Furthermore, few studies on rSOC or hydrogen energy storage incorporate all the relevant features of the future energy system: electrified transport and heat as well as distributed generation. The current work aims to address some of these gaps.

This work will focus on the rSOC as electrical energy storage for the residential environment. Utility scale rSOC plants are a long way from being realisable, so a scale of approximately 1 – 1000 kW to operate in such an environment appears a reasonable object for study. Further, the residential sector is the single biggest electricity consuming sector in the UK [187] and will perhaps also see some of the most interesting changes and challenges on the road to decarbonisation. This choice of application means that the most important energy generation to pair with the rSOC will be rooftop PV. The residential setting also makes P2P trading an interesting topic for study in tandem with the rSOC, as it offers another approach for helping to reconcile fluctuating renewable generation with electrical loads; P2P may thus be a complementary or perhaps a rival solution to energy storage. It has been demonstrated that the academic literature on P2P has covered a profusion of market designs and modelling techniques. It is not necessarily an objective of this work to contrive new designs of P2P market, but rather to experiment with simulation of P2P and consider the impact (financial and technical) of P2P alongside energy storage technologies.

The final topic examined in this chapter, agent-based modelling, was shown to be an approach increasingly used in the study of energy systems. Models constructed on this basis have seen use particularly in modelling energy markets and the adoption of new energy technologies. In this work, all modelling will be constructed in an agent-based modelling environment (AnyLogic); it is expected that this agent-based aspect will become most useful in conjunction with the study of P2P markets.

3. Overview of publications

Methodology and results in this thesis are presented in publication format. The first three papers have been published, whilst the fourth is prepared for publication but not yet submitted. Published papers appear exactly as published, except for renumbering of figures, tables etc.

(i) Hutty, T. D., Dong, S., & Brown, S. (2020). Suitability of energy storage with reversible solid oxide cells for microgrid applications. Energy Conversion and Management, 226, 113499. https://doi.org/10.1016/j.enconman.2020.113499

The first paper considers the application of an rSOC system with hydrogen storage for electrical energy storage in a residential microgrid. The rSOC system was based on the Sunfire pilot system [24]; results on the technical performance of this system were available in the literature, but an examination of potential applications had not been made. In this work, the application was storage of distributed (rooftop) solar generation, for supplying the houses' electricity load. Because solar generation naturally has short-term (diurnal) variability, battery energy storage was also considered, with one objective of the work being to identify when the battery storage was adequate, or when the long-term storage with rSOC was an optimal selection.

Optimising the design of seasonal energy storage can be challenging, due to the length of time that the model must cover. Here, the approach taken was to employ a global optimiser (OptQuest [188]). The global optimiser is used to plan the load points for the rSOC and battery over five-day periods on a rolling basis throughout the year. This was superior to a simple greedy algorithm, whilst still fast enough for the 'outer' optimisation of the system design, also using OptQuest, to be viable.

Economics of the optimised microgrid systems were evaluated in terms of CAPEX and simple payback time. Payback times for the systems were generally discouraging. Hybrid energy storage with battery and rSOC was an optimal selection only when (a) required self-sufficiency for the system was high and (b) sizing of the generation was constrained. The novelty of the paper lay in the exploration of an application for rSOC energy storage, which was rare in the literature at the time; and in the comparison between the short-term and long-term energy storage. Siyuan Dong, having contributed to the author's understanding of the AnyLogic software, is credited as the second author in this paper.

(ii) Hutty, T. D., Dong, S., Lee, R., & Brown, S. (2021). Long term energy storage with reversible solid oxide cells for microgrid applications. Energy Reports, 7, 24–33. https://doi.org/10.1016/j.egyr.2021.02.059

The second paper covers similar ground to the first; the main difference in the model is the introduction of a model for EV charging demand, based on the UK National Travel Survey (NTS) [189].

In contrast with the previous paper, in which separate optimisations were run with different constraints for self-sufficiency ratio (SSR), in this paper multi-objective optimisation was used to construct Pareto fronts for payback period against SSR. This method did require simplifying the dispatch model in the simulation, in order to be viable computationally. Economic analysis was extended from the previous paper to include estimation of net present value (NPV), and a greater spread of scenarios for costs and efficiency was considered. Results confirmed the findings of the previous publication; the microgrids designed using the rSOC and battery energy storage invariably had negative NPV and overly long payback period. On the other hand, rSOC was selected for most system designs with SSR above 60%, but only if PV capacity was constrained below 6 kW.

In this paper, a ‘charge when home’ assumption was made for the EVs. This resulted in a peak roughly coincident with the peak in standard electrical load, and poor utilisation of solar power by the EV chargers. Moving forward, it was wished to model EV demand as a flexible load, since failure to consider the potential of demand-shifting can lead to overstating the case for additional energy storage. This was one of the motivating factors to investigate P2P trading in the second half of the project.

Rachel Lee is credited as third author of this paper in recognition of guidance and advice she provided regarding the use of the National Travel Survey. Siyuan Dong is credited as the second author as previously and for the same nature of contribution.

An appendix (not part of the original publication) has been attached to this chapter to give some extra information on the construction of the EV model.

(iii) Hutty, T. D., Pena-Bello, A., Dong, S., Parra, D., Rothman, R., & Brown, S. (2021). Peer-to-peer electricity trading as an enabler of increased PV and EV ownership. *Energy Conversion and Management*, *245*, 114634. https://doi.org/10.1016/j.enconman.2021.114634

The third publication is the product of the author’s first attempts to introduce P2P trading to the microgrid model, and hence to ensure that the benefits of flexible demand are properly considered. The rSOC is not included in this paper (the rSOC topic is picked up again in the final publication). Instead, the paper explores how P2P can contribute to a synergy between PV generation and EVs. The novelty of the paper lies not in the design of the market mechanism, which was derived from the literature; rather the novelty lies in the consideration of the relative merits of smart charging (V1G), vehicle-to-home (V2H) and vehicle-to-grid (V2G) when combined with P2P trading. Also in the estimation of annual savings for households of different categories under different scenarios; and in the combination of the P2P system with a stationary battery energy storage. A chief conclusion from the work was that the combination of P2P electricity trading with V2H can effect particularly interesting household savings and technical benefits. A further notable conclusion was that even at near 100% PV and EV ownership, the P2P trading is beneficial – a result that contradicted some of the existing literature, and was probably a consequence of properly modelling the diversity in EV availability though use of data from the UK National Travel Survey.

In this paper, the MILP model for scheduling flexible devices in response to prices was based on the BASOPRA model developed at University of Geneva [190]. This was originally a model for stationary battery storage; accordingly the author made multiple adjustments to encode the availability of the EV battery, the ‘compulsory’ discharge for travel, and the possibility of rapid charging away from home. The model was also adjusted to allow the export of battery power to the grid, rather than the house only, and some structural changes were made to decrease the number of binary variables. The creators of the original BASOPRA optimisation model, Alejandro Peña-Bello and David Parra, are credited as authors; the remaining authors are credited for their supervisory role.

(iv) Hutty, T. D., Brown, S. P2P trading of heat and power via a continuous double auction.

The final paper, which is prepared for publication but not yet submitted, reunites the topics of rSOCs and P2P energy trading. It also fulfils the project’s objective to create a model for an rSOC application wherein the three key energy demands of electricity, heat and transport are all present.

Whilst the EV battery and travel model was retained from the previous work, the P2P market was redesigned for this paper. In the previous paper, bids by auction participants consist only of the volume of electricity at each timeslot. Although this proved effective for the sharing of PV power for EV charging, it was felt important to have a market structure in which bidders could specify their reserve prices as well as volumes of energy. Therefore, the new market model was constructed as a continuous double auction, which also seems a more realistic model of possible real-world P2P implementations. Because of the presence of energy storage and flexible loads in the market, it was considered important that trading could be carried out simultaneously for all the upcoming timeslots, to assist with the realisation of strategies for these devices. Furthermore, the model allowed simultaneous trading of heat as well as electricity. Strategies were developed to address the interdependence of bids for power and heat, as well as interdependence between bids in different timeslots. The resulting model, a continuous double auction for trade of power and heat across multiple timeslots of the day ahead, is possibly unique in the literature.

This paper demonstrated that the possibility to trade energy P2P is of particular interest for rSOCs in a distributed energy setting. The availability of a P2P tariff substantially higher than the grid feed-in tariff incentivises the rSOC to run SOFC mode at a much higher average load factor. Reliance on grid electricity is reduced both in terms of overall energy import and peak load. Resultant savings for the rSOC owners are in the order of £10’s per week, and heat trading can bring additional financial gain when compared with power trading only. However, participant willingness was not generally 100%, indicating that some auction participants made losses by their P2P trading strategies; also the advantages of heat trading were not clearcut. These issues may indicate that the trading strategies in the model still need further development.

For this work, it was felt advantageous to drop the MILP model from the previous publication, in order to build something more modular, customisable and reusable. The kernel library in Pyomo was employed for development of this model, being more object-oriented than the standard environment library. This new model made it straightforward to add arbitrary devices to a house, or to optimise multiple houses simultaneously. Consequently the BASOPRA model is not credited in this chapter, and the only co-author is Prof. Solomon Brown for his supervisory role.

4. Suitability of energy storage with reversible solid oxide cells for microgrid applications

Timothy D Hutty[a], Siyuan Dong[a], Solomon Brown[a]*

[a]*Department of Chemical and Biological Engineering, University of Sheffield, UK*

Abstract

Reversible solid oxide cells (rSOCs) offer the prospect of long term bulk energy storage using hydrogen or methane fuel. Solid oxide technology, whilst less mature than alkaline and PEM technology, offers superior conversion efficiency - especially for electrolysis. Furthermore, the possibility of using the cells reversibly means that separate 'power-to-gas' and 'gas-to-power' components are not needed, potentially reducing costs. In this work, we consider the suitability of energy storage using rSOCs and/or battery storage for a microgrid consisting of houses equipped with solar PV generation. An agent-based simulation model is developed to assess the performance of such a microgrid. The model enables the microgrid's self-sufficiency to be quantified, and hence the possible cost savings through avoided imports of grid power. Sizing of microgrid components is optimised to determine the most cost-effective design capable of achieving given self-sufficiency ratio. Case studies are considered for England and Texas. Initially, designs are considered with hydrogen energy storage only; subsequently, hybrid energy storage is considered, with a community scale battery working alongside the rSOC. Results suggest that payback periods for pure rSOC systems tend to be unfavourable. However, if prices fall to levels foreseen in the literature, a system designed to achieve 50% grid-independence could pay back its investment costs within 20 years. Systems designed for Texas need relatively less storage, owing to the good year-round solar resource; as such, payback time in Texas is superior to the UK. Hybrid storage with battery + rSOC is found to be preferable to battery only systems when (i) high SSR is required and (ii) large over-capacity of PV generation is not possible.

Keywords: energy storage; reversible solid oxide cell; microgrid; hybrid energy storage; self-sufficiency ratio; rSOC

*Corresponding author.
E-mail address: s.f.brown@sheffield.ac.uk

4.1 Introduction

4.1.1 Reversible solid oxide cells (rSOCs) and their applications

In order to mitigate the threat of climate change, it is urgently necessary for energy systems around the world to move away from the carbon intensive fossil fuels upon which they have largely depended in the past. Renewable electricity generation (wind, solar, hydropower, biomass) has the potential to displace generation from fossil fuels. However, wind and solar energy in particular suffer from the problem of intermittency [1]–[3], meaning that the available supply of electricity may not match the demand. Thus energy storage technologies may have an increasing role to play in future energy systems, storing renewable energy when it is available, for consumption when it is required.

Of existing energy storage technologies, most are ill-adapted to store energy for sufficient time periods, or in sufficient bulk, to compensate for fluctuations in renewable output beyond a timescale of hours or days. By contrast, power to gas ('P2G'), the use of electricity to synthesise a gas fuel such as hydrogen or methane, has potential to provide storage of weeks' or months' duration, enabling heavier reliance on renewables by the energy system as a whole. This would typically be accomplished by splitting water with an electrolyser to produce hydrogen gas, which can be stored and subsequently converted back to power using a fuel cell or internal combustion engine. Key difficulties for this form of energy storage are high expense and low round-trip efficiency.

Solid oxide cells (SOCs), although less technologically mature than the more prevalent alkaline or PEM cells, potentially offer superior energy conversion efficiencies both as electrolysers ('P2G') and as fuel cells ('G2P'). SOCs employ ceramic electrolytes and operate at high temperatures (600 – 1000

°C) [29], [34]. These high operational temperatures are associated with some of the key advantages of SOC technology: higher efficiency, tolerance to fuel impurities [29], abundant electrode materials [33], and possibilities for combined heat and power (CHP) applications [57], [111]. At the same time, high operational temperature is also responsible for long start-up times [1], difficulties in pairing with a dynamic load [34], complex and expensive balance-of-plant (BoP) equipment [39], and rapid degradation of cell materials [29]. It is possible for an SOC to operate reversibly, with a single device able to operate alternately as fuel cell and electrolyser [24]; in this case, it is termed a 'reversible solid oxide cell' or rSOC.

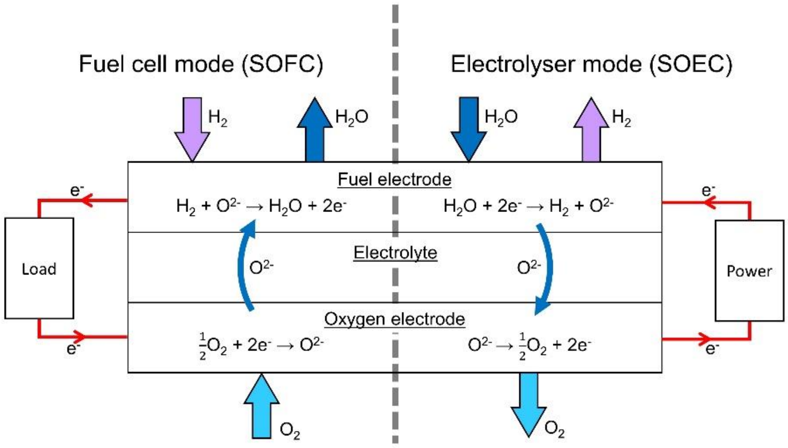

Figure 4.1. Operation of an rSOC working with hydrogen / steam. Fuel cell mode and electrolyser mode are shown respectively left and right.

The operation of an SOC as both a fuel cell ('SOFC') and electrolyser ('SOEC') is illustrated in Figure 4.1. The electrolyte of an SOC is usually conductive of negatively charged oxygen ions. In fuel cell mode, the reactions proceed as follows: at the oxygen electrode, oxygen is reduced to O^{2-} and these anions migrate across the electrolyte to the fuel electrode. At the fuel electrode, the fuel is oxidised and combines with O^{2-} to form steam (or CO_2 in the case that the fuel is CO). In electrolysis mode, the reactions are reversed and the ions and electrons flow in the opposite direction. [1].

SOFC is a more mature technology than SOEC, suffering fewer problems with degradation: the Jülich Research Centre reported that their SOFC stack operated for 93,000 hours continuously [96]. Nonetheless, SOEC is attractive because the electrolysis reaction is increasingly endothermic at high temperature [29]. Electrolysis with SOEC is consequently highly efficient, since the reaction recycles unavoidable Joule heat, and may also use external high temperature heat sources. In particular, SOEC is more efficient than PEM or alkaline electrolysers [37], [43], [44], though degradation represents more of a challenge [1], [29]. There is some evidence though, that reversible use of a cell (i.e. as an rSOC) can actually reverse degradation reactions and prolong the lifetime [42] [99] – but this is still uncertain. Reversible operation can certainly offer a saving in investment costs versus systems with separate devices for P2G and G2P [22], [40], [41]. An overview of the comparison between SOC with the more mature PEM and alkaline technologies is given in Table 4.1.

Whilst energy storage using rSOC remains a relatively immature technology, pilot schemes of significant scale have begun to emerge in recent years. The most significant demonstration projects to date have been conducted using SOC technology from German manufacturer Sunfire [129]. The first of these projects was a collaboration between Sunfire and Boeing; this multi-kW scale system, designed with microgrid applications in mind, was commissioned in 2015, undergoing testing at Boeing's Huntingdon Beach facility in southern California. 1920 cells in stacks of 30 could generate 50 kW in fuel cell mode, and absorb 120 kW in electrolyser mode. Hydrogen storage at 250 bar was sized for cycle durations of only 12 hours, although more storage volume could have been added easily and cheaply. The system was online for 1000 hours of testing, undergoing seven full cycles in that time, and achieved electrolysis efficiency of ca. $60\%_{LHV}$ (allowing for steam generation and hydrogen compression). In comparison, fuel cell mode was found to be $49\%_{LHV}$ efficient, resulting in a round-trip efficiency of around 30%. Whether any degradation was observed over the test's duration is not reported.

Another trial using Sunfire rSOC technology is reported in [46], [49], [84], [85]; this is the 'GrInHy' or 'Green Industrial Hydrogen' project. The 143 kW rSOC was installed at a steelworks, where the ready availability of waste heat enabled the energy cost of steam generation to be avoided. Furthermore, generated hydrogen could be used by the steelworks as a reducing agent (in place of coke) and for annealing. Thanks to the use of waste heat, electrical round-trip efficiency was able to approach 40%.

Table 4.1. Comparison of electrolytes: solid oxide versus alkaline and PEM.

Electrolyte	**Alkaline**	**PEM**	**Solid oxide**
Operating temp. (°C)	<100 °C [29], [34]	< 140 °C [1], [34]	600 – 1000 °C [29], [34]
Electrolysis efficiency (system level)	43 - 67% [37], [43], [44]	40 - 67% [37], [43], [44]	63 - 82% [37], [43], [44]
Fuel cell efficiency (system level)	45 – 60% [45]	45 – 50% [45]	35 – 61% [44]–[47]
Startup time	15 minutes [34]	< 15 minutes [34]	From cold: hours [1], [34] From hot standby: minutes [48], [49]
Dynamics and flexibility	Min partial load 10-40% [37]	Suitable for partial load and variable load operation [26], [28], [34], [36], [37]	Rapid load changes can cause problems due to thermal stress [1], [34].
Key advantages	**Most mature technology for electrolysis; reliable, safe, long lifetime** [29], [30], [34].	**Preferred for fuel cell applications** [30]; electrolyser yields highest purity hydrogen [29].	Use waste heat to boost electrolysis efficiency [34]; work with carbonaceous species; possible CHP applications; possible reversible operation.
Key challenges	Inferior dynamic response to PEM; corrosive electrolyte [34].	Expensive membranes, catalyst materials [29] [34]; less scalable than alkaline technology [29].	Immature technology [29] [34]; rapid degradation especially for SOEC [29] [35]; thermal management is challenging [34].
System cost for electrolysis	**lowest** 700 – 1500 € / kW [35], [37], [43], [51]	**medium** 800 – 2300 € / kW [35], [37], [43], [51]	**highest** >2000 € / kW [37] [35] **Potential for cost reduction**, possibly to 760 € / kW [35]

The rSOC demonstrated a good level of flexibility, with transition between hot standby and 100% load taking respectively 24 and 20 minutes for electrolysis and fuel cell operation; partial load operation down to respectively 50% and 40% was possible with no efficiency penalty. Voltage degradation of 0.8% per thousand hours was observed in electrolysis mode. In practice, it was more economically viable to use generated hydrogen in the steelworks, and run fuel cell mode using CH_4, rather than using the rSOC as a true energy store.

A third notable pilot project is REFLEX [48], [132], [133], a European project coordinated by CEA-Liten, using rSOCs manufactured by Estonian company Elcogen. The project is currently in development, with a 'Smart Energy Hub' to be built at Envipark, Turin, Italy. This will incorporate three rSOC modules for total electrolysis capacity of 120 kW, with storage of CHG at 200 bar, and Li-ion batteries providing shorter term storage. The Smart Energy Hub will be co-located with solar and hydro generation and will supply both heat and power. The stated objective is to achieve $90\%_{LHV}$ efficiency for electrolysis, and $50\%_{LHV}$ for fuel cell operation. Testing of the facility is to take place in 2020.

With sophisticated balance-of-plant (BoP) configurations, it may be possible to improve on the efficiencies observed in these real-world trials - and a great deal of work has been done to model rSOC energy storage at the BoP scale. The thermal management of the plant is key to unlocking higher RT efficiency. Many proposed plants use thermal energy storage (TES) to enable surplus heat from fuel cell mode to supply heat for electrolysis; waste heat from the compression of hydrogen or other heat sources may also be used. For instance, modelling by Giap et al [113] found that the use of industrial waste heat in an rSOC plant could enable RT electrical efficiency to reach 53.8%; the researchers felt this to be too low, recommending the use of TES to boost efficiency further. Ren et al [108] modelled a concept for rSOC energy storage in which fuel and exhaust species would remain always in a pressurised vessel, with bronze used as a phase change material for TES. The system, for which the suggested storage duration was 'short time periods, such as hours', was modelled to achieve round-trip efficiency up to 64%. Perna et al [110] modelled a 100 – 200 kW rSOC energy storage system, wherein coupling of heat sources and sinks, together with the use of diathermic oil for TES, enabled the modelled RT efficiency to reach 60%. The proposed plant would also supply hot water, with cogeneration efficiency of 91%. Lototskyy et al [57] present a novel rSOC system designed for combined cooling, heating and power; various metal hydride beds would be used to store both hydrogen and heat. Their modelling suggested that the system, which was proposed for use with domestic solar PV, could achieve electrical RT efficiency of 46.7%, and tri-generation efficiency of 70.6%. Akikur et al [111] propose a solar + rSOC plant for CHP. Solar PV would provide power for electrolysis, with concentrated solar power providing heat for steam generation. Mathematical modelling suggested electrical round-trip efficiency of around 38%. Economic analysis found that the cost of electricity for the plant would be \$0.0676 / kWh, although the cost of the hydrogen storage component was neglected.

Ullvius and Rokni [115] suggest a rather different approach to extracting additional value from an rSOC plant: the use of waste heat for water desalination using direct contact membrane distillation. Such a system was modelled for deployment on the South African coast, with concentrated solar power providing both heat and power for electrolysis. The plant would export 500 kW of power continually, and also generate 8.5 tonnes of fresh water per day.

Giorgio and Desideri have proposed an rSOC system using TES in close contact with the stack [112]. This would be either sensible heat storage using a ceramic material or latent storage using a eutectic metal alloy. Hydrogen would be stored at 108 bar. In similar fashion to [61], two configurations were considered: one in which water vapour would be condensed out of the off-gas, and one in which the vapour would be stored (removing the need for a steam generator). In the first configuration, surplus heat during SOFC mode was transferred to a steam drum in preparation for SOEC mode. This configuration was found to be capable of 72% RT efficiency, with either form of TES. However, electrolysis could not continue for long before external heat was needed for steam generation. The stored vapour configuration could achieve RT efficiency of only 64% - although this would reach 74% if the stack could be pressurised. The evaluation cycles considered in this research were of short duration, with two hours of fuel cell mode followed by electrolysis.

4.1.2 Hydrogen energy storage for microgrids – existing work

There is a fair amount (e.g. refs [118], [120]–[126]) of extant research on the applications of hydrogen energy storage for distributed scale, microgrid type applications. Such research often includes optimisation of technology choice, sizing, or dispatch over time, and some assessment of the economic case for the storage. Common themes include concerns with high costs; the desirability of hybridisation with shorter term storage; and the extraction of additional value through niche applications such as hydrogen powered vehicles. These studies overwhelmingly consider PEM or alkaline technology, and studies assessing applications of rSOCs are much less numerous. However, Baldinelli et al [116] propose a concept in which rSOCs are hybridised with flywheel energy storage to smooth out short term load fluctuations. A control algorithm is proposed to determine charge / discharge of the two energy stores, and the system's components are sized for a microgrid consisting of a number of homes with PV generation. The hybrid system was able to moderately increase the microgrid's self-sufficiency (from 52.1% to 58.0%); economic analysis was not conducted. Sorrentino et al [117] present a microgrid consisting of an rSOC and hydrogen storage, as well as PV and a vertical axis wind turbine, for the supply of power to an apartment complex. The use of additional short-term storage was recommended but not modelled. Sizing of the microgrid's components was optimised to achieve the lowest possible payback time; the optimal system would store 144 kg (~5 MWh) of hydrogen gas, enabling up to 10 days of grid independence, and was claimed to achieve payback in just over 11 years. However, CAPEX estimates appear to have been rather optimistic (rSOC \$400 / kW; PV €817 / kW).

4.1.3 Novel contribution of this work

Whilst simulations at BoP level are abundant in the literature, studies on actual applications for rSOC energy storage are few. Literature on microgrid applications for hydrogen energy storage typically assumes use of PEM or alkaline technology with separate components for gas-to-power and power-to-gas. Here we consider the design of a microgrid using rSOC specifically. Accordingly, key characteristics of rSOCs (limited partial load capability; limited ramp rate; coupled fuel cell and electrolysis capacity) are included in the model. Whilst there is some extant work on rSOC based microgrids, it gives an incomplete picture, especially on economic aspects. Here we attempt to give a fuller picture, through inclusion of different scenarios for location, cost and performance of the technology. We also obtain some indication of the circumstances under which rSOC can compete with, or complement, battery storage.

The rest of the paper is structured as follows: in Section 4.2, the simulation model constructed in AnyLogic is described, including its various sub-models. Section 4.3 introduced the case studies and presents the results obtained from them; conclusions are summarised in Section 4.4.

4.2 Model construction

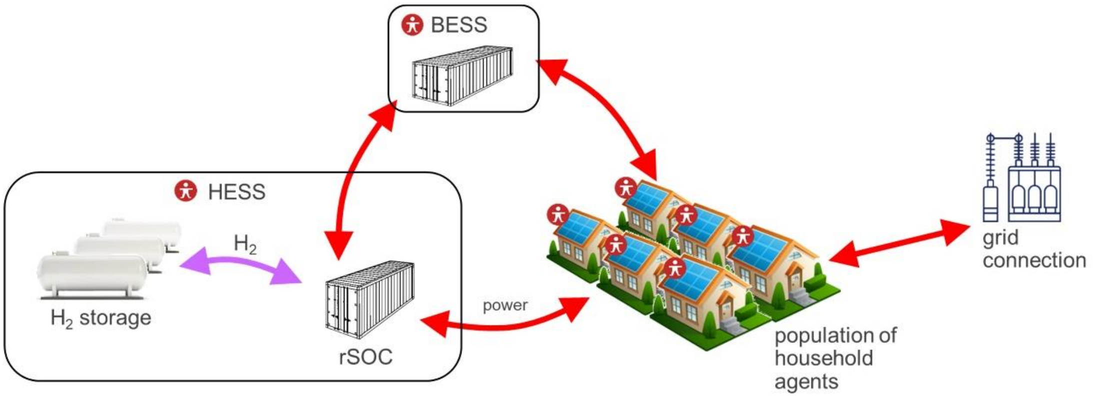

Figure 4.2. Schematic representation of the microgrid model. Most elements of the model are represented as agents (denoted by the red icons).

4.2.1 Overview

The purpose of this work is to simulate how an rSOC energy storage system might perform in a real-world distributed energy context. To this end, a simulation has been constructed of a small distributed energy system (or microgrid), consisting of a residential area with local renewable generation, supported by a hydrogen energy storage system (HESS) using rSOC, and a grid connection. A community battery, which can be used in tandem with the rSOC, is also modelled. A schematic of the simulation is provided in Figure 4.2. This simulation has been implemented using the multi-paradigm simulation programme AnyLogic [4]. Agent-based modelling provides versatility in modelling the components of the microgrid as distinct entities, and readily allows for combination of social or economic models with technical ones. Most elements of the microgrid model are agents (or sub-agents), including individual households – although the behaviour of households on an individual level is not discussed here.

We now present the various sub-models in more detail.

4.2.2 rSOC model

For the present work a detailed BoP model is not desirable. Instead, the rSOC is described by a few key parameters (see Table 4.2): the nominal capacity of the rSOC in each mode; the partial load range; the efficiency and the achievable ramp rate. The efficiency values are intended to incorporate all BoP losses, including power electronic converters and (for electrolysis mode) steam generation.

Table 4.2. Parameters used to characterise the rSOC system.

Parameter	**Symbol**	**Unit**	**Values from** [24], [46]
Electrolyser mode nominal capacity	P_{SOEC}	kW_{AC}	166
Electrolysis efficiency*	η_{SOEC}	MJ / kg_{H2}	172.5
Electrolyser partial load range	-	%	50 … 125%
Fuel cell mode nominal capacity	P_{SOFC}	kW_{AC}	30
Fuel cell nominal efficiency*	η_{SOFC}	MJ / kg_{H2}	60
Fuel cell partial load range	-	%	30 … 100%
Ramp rate	Δ	% of nominal capacity per minute	5%

*including steam production and all BoP other than H_2 compression

The state of the rSOC at a given point in time is described by the partial load percentage, which here we shall represent by μ. This can range from -100% (or below) for electrolysis to +100% for fuel cell mode, where +/-100% are respectively mapped to the nominal loads P_{SOFC} and P_{SOEC} for fuel cell and electrolyser mode. Thus, the AC power either generated (+) or consumed (-) is given by:

$$P_{AC} = \begin{cases} \frac{\mu}{100} \times P_{SOFC} \,, \mu \geq 0 \\ \frac{\mu}{100} \times P_{SOEC} \,, \mu \ < 0 \end{cases} \quad \text{(Eqn. 4.1)}$$

The consumption or production of hydrogen, $\dot{m}_{H2}$ in kg per hour is then given as follows:

$$\dot{m}_{H2} = \begin{cases} \frac{3.6 \times P_{AC}}{\eta_{SOFC}} \,, \quad \mu \geq 0 \\ \frac{3.6 \times P_{AC}}{\eta_{SOEC}} , \mu \ < 0 \end{cases} \quad \text{(Eqn. 4.2)}$$

The rate at which μ can change is limited by the ramprate Δ. Work from GrInHy [49], [84] suggested that their electrolyser could ramp its output by least 10 kW/min, which was about 7% of the nominal 142.9 kW load. Here Δ defaults to a conservative value of 5% of nominal load per minute. When changing mode, the rSOC can pass through ‘forbidden’ load points that are outside the permissible partial load range; however, it is not permitted to remain continually at such load points. It is worth noting that although we allow load to vary continuously in the permitted range, it is also possible that a real system might only have discrete partial load settings.

As a starting point, the rSOC model is parametrised based on the data available from the various trials of Sunfire’s rSOC technology [24], [46]. P_{SOEC} and P_{SOFC} may be scaled up or down, but will be assumed to remain in proportion. With efficiencies of 172.5 MJ/kg_{H2} for electrolysis, and 60 MJ/kg_{H2}

for fuel cell mode, round-trip efficiency is just under 35%, before allowing for the electrical work to compress the hydrogen for storage.

4.2.3 Hydrogen storage model

During electrolysis mode, additional power is required for compression of hydrogen; this is calculated as follows. The isentropic compression energy W for compression of 1 kg of hydrogen between pressures P_1 and P_2 is given in kJ by [191]:

$$W = \frac{\gamma R T}{\gamma - 1}\left(\left(\frac{P_2}{P_1}\right)^{\frac{\gamma-1}{\gamma}} - 1\right)\cdot {M_{H2}}^{-1} \quad \text{(Eqn. 4.3)}$$

where T is temperature in Kelvin, R is the ideal gas constant; $\gamma = 1.41$ is hydrogen's heat capacity ratio and $M_{H2} = 2.014$ g / mol is hydrogen's molar mass. Multi-stage compression with intercooling can allow the required work to be less than the isentropic work. Whilst the specific configuration of compressors and intercoolers is outside the scope of this work, we assume that the hydrogen storage system would be designed with intercooling. Accordingly, we assume that the work of compression can be reduced to 74.5% of the isentropic work, where this proportion is derived from reference [191]. Thus, the mass flow rate of hydrogen $\dot{m}_{H2}$ in kg/hour can be used to find the electrical load P_{comp} for the compression of hydrogen (in kilowatts):

$$P_{comp} = \frac{0.745 \cdot W \cdot \dot{m}_{H2}}{3600} \quad \text{(Eqn. 4.4)}$$

This power is drawn from the microgrid in addition to the power required by the rSOC itself.

4.2.4 Battery model

Table 4.3. Parameters used to characterise the community battery.

Parameter	Symbol	Unit	Default value
Nominal capacity	C_{BESS}	kWh	-
DC to DC efficiency	η_{BESS}	-	0.94 [192]
Inverter efficiency	η_{DCAC}	-	0.95 [49]
Rectifier efficiency	η_{ACDC}	-	0.95 [49]
C rate	R_{BESS}	h^{-1}	2 [193]
Self-discharge rate	Λ	h^{-1}	4.2×10^{-5} [194], [195]
State of charge range	-	%	5 – 95%

The community scale battery energy storage system (BESS) is modelled primarily in terms of its capacity in kWh (C_{BESS}), its achievable C rate (R_{BESS}) and its DC to DC round-trip efficiency η_{BESS}. Unlike for the rSOC, the efficiencies of the power electronic converters are accounted for separately as η_{DCAC} and η_{ACDC}, both equal to 0.95 [49]. Self-discharge is also included, although impact of this is expected to be negligible, with the default value of 4.2×10^{-5} h^{-1} equating to 3% per month. Here the model is parametrised to represent Li-ion battery technology, based on figures from [192], [193].

For simplicity, the losses according to η_{BESS} are modelled as though they occur entirely during the charging of the battery. R_{BESS} is interpreted such that R_{BESS}^{-1} gives the minimum time in hours to either fully charge or discharge the battery. In contrast with the rSOC, there is no lower limit set on the charge / discharge power: i.e. partial load can be varied all the way down to 0%. Similarly, there is no restriction placed on the battery's ramp rate. It is reported in [193] that a 2 MW battery is able to fully reverse its output in 40 milliseconds; this is many orders of magnitude smaller than the time resolution considered here.

Where P_{ch} is the AC power supplied to the battery, P_{dch} is the AC powered discharged from the battery, and E_{BESS} is the electrical energy stored in the battery, the model imposes the following equations (with hours as time unit):

$$\dot{E}_{BESS} = \eta_{BESS} \cdot \eta_{ACDC} \cdot P_{ch} - \frac{P_{dch}}{\eta_{DCAC}} - \Lambda \cdot E_{BESS} \qquad \text{(Eqn. 4.5)}$$

$$0 \leq E_{BESS} \leq C_{BESS} \qquad \text{(Eqn. 4.6)}$$

$$0 \leq P_{ch} \leq \frac{R_{BESS} \cdot C_{BESS}}{\eta_{BESS} \cdot \eta_{ACDC}} \qquad \text{(Eqn. 4.7)}$$

$$0 \leq P_{dch} \leq \eta_{DCAC} \cdot R_{BESS} \cdot C_{BESS} \qquad \text{(Eqn. 4.8)}$$

Equation [5] is modelled using system dynamics, with E_{BESS} represented as a stock, and flows of power in or out according to the charge, discharge and self-discharge terms. A statechart is used to classify the battery as 'empty' once $E_{BESS} \leq 0.05 \cdot C_{BESS}$, 'full' when $E_{BESS} \geq 0.95 \cdot C_{BESS}$, and 'partially charged' otherwise.

4.2.5 PV model

Solar generation profiles are simulated using measured hourly data for global horizontal irradiance (GHI). The model outlined here uses GHI to predict the output of PV panels with arbitrary tilt and orientation. Clearness index k_t is calculated as [196]:

$$k_t = \frac{GHI}{I_{ET} \sin \alpha_s} \qquad \text{(Eqn. 4.9)}$$

where α_s is the sun's altitude above the horizon, and I_{ET} is the normal irradiance above the Earth's atmosphere, which averages 1367 Wm^{-2}, varying by ±3.3% throughout the year. Erbs' model [197] is then employed to predict diffuse fraction k_d from the value of k_t, so that the diffuse horizontal irradiance (DHI) is known. The simplifying assumption is made that diffuse irradiance is distributed evenly across the sky. The total radiation I_{pv} incident on one square metre of tilted panel can now be calculated [198]:

$$I_{pv} = direct\ contribution + diffuse\ contribution + reflected\ contribution$$

$$= \frac{GHI(1 - k_d)}{\sin \alpha_s} \cos \theta_i + GHI \cdot k_d \cdot \frac{1 + cos(\zeta_{pv})}{2} + GHI \cdot R_{gr} \cdot \frac{1 - cos(\zeta_{pv})}{2} \qquad \text{(Eqn. 4.10)}$$

Here, θ_i is the incident angle between the sun's rays and the normal to the tilted PV panel, and R_{gr} is the reflectance of the ground, taken to be 0.2. θ_i is obtained from the sun's azimuth φ_s and altitude α_s, and the panel's azimuth φ_{pv} and tilt ζ_{pv}, as follows [198]:

$$cos(\theta) = sin(\zeta_{pv})cos(\varphi_{pv})cos(\alpha_s)cos(\varphi_s) + sin(\zeta_{pv})sin(\varphi_{pv})cos(\alpha_s)sin(\varphi_s) + cos(\zeta_{pv})sin(\alpha_s) \quad \text{(Eqn. 4.11)}$$

Assuming a fixed efficiency η_{pv} and area A for the PV installation, the generated power P is simply

$$P = \eta \cdot A \cdot I_{pv} \quad \text{(Eqn. 4.12)}$$

5.75 m^2 of PV is assumed to correspond to 1 kW_p capacity [199]. Validation of the PV model was conducted using hourly irradiance data for 2015 recorded at Rothamsted [200], and corresponding PV generation data for a 3.96 kW installation located 5.9 km to the south-west [201]. Modelled and measured generation were compared at daily resolution over the year, and at hourly resolution over a two-week period in June. At daily resolution, the model achieved mean absolute error of 0.769 kWh / day (7.6% of average daily generation). At hourly resolution, mean absolute error was 0.112 kWh/h. The errors observed were checked for correlation with temperature (hourly average; daily min, max and average) and irradiance. No significant correlations were found, suggesting that a simple model with constant efficiency is adequate for the UK climate.

For the results presented below, the model was calibrated by enforcing a capacity factor of 11.8% for a south-facing panel at 40° tilt angle in SE England [202]; this was achieved by setting $\eta_{pv} = 0.1541$. For the SE England case study, houses are assumed to have random orientation, resulting in diversity between the different rooftop PV installations; the *average* capacity factor then becomes ~11.0%.

4.2.6 Control strategies

4.2.6.1 Control of rSOC without BESS

Since time-variable import / export tariffs are not considered in this work, the most cost-effective dispatch of a single energy storage type, whether battery or rSOC, is trivially achieved via a greedy algorithm. At every time step, the energy surplus (or deficit) is calculated, and the energy storage will absorb (or supply) as much of this as possible, as constrained by its capacity, partial load capability, and state of charge.

4.2.6.2 Control of hybrid energy storage

When rSOC and BESS are both used, the control is less trivial, even in the absence of variable tariffs. A naïve approach is to continue to use a greedy algorithm, which preferentially uses the battery because of its superior efficiency. For instance, all surplus generation would be sent to the battery until the battery is full, after which the rSOC would take over. This is an unsatisfactory approach; the two energy stores need to be worked simultaneously, otherwise the rSOC capacity would have to be sized larger to absorb the largest deficits / surpluses by itself.

In this work, the approach taken is to plan the rSOC dispatch in advance, whilst the BESS continues to follow a 'greedy' approach, compensating for the remaining surplus/deficit. Five-day forecasts, at one-hour resolution, are made for electrical load and generation, and passed to a controller agent. Forecasts for load and irradiance assume perfect foreknowledge; PV generation forecast is calculated from irradiance by modelling the many separate solar rooftop installations as just three large arrays at different orientations.

The controller works by setting bounds $\left(P_{max,d}\right)_{1\le d\le 5}$ and $\left(P_{min,d}\right)_{1\le d\le 5}$ on the net load absorbed by the rSOC on each day d of the forecast. For each time step, the rSOC responds to the microgrid's net load as far as possible (see Figure 4.3), as constrained by $P_{min,d}$ and $P_{max,d}$, as well as its partial load capability and the H_2 storage capacity. Remaining load imbalances are then addressed by the battery and the grid connection, in that order. In this way, an hourly schedule $\left(P_{HESS,t}\right)_{0\le t<120}$ for the rSOC net load is produced. The full details of this method are given in the appendix.

Thus, there are ten decision variables for the controller to optimise, $\left(P_{max,d}\right)_{1\le d\le 5}$ and $\left(P_{min,d}\right)_{1\le d\le 5}$. The objective function is defined as the (negative) value of effective energy stored at the end of the forecast period, plus the cost of imported power during the forecast period, as follows:

$$-c_{store}\cdot\left(\frac{\eta_{SOFC}}{3.6}\cdot m_{H2,120}+\eta_{DCAC}\cdot E_{BESS,120}\right)+c_{grid}\cdot\sum_{t=0}^{119}P_{imp,t} \qquad \text{(Eqn. 4.13)}$$

Here, $E_{BESS,120}$ is the final kWh stored in the battery; c_{grid} is the cost of grid-imported power, and c_{store} is the value assigned to energy stored at the end of the forecast period. c_{store} is set to £0.10 for the case study in this work. $c_{store} < c_{grid}$ is essential or the rSOC will never use fuel cell mode.

The controller carries out this optimisation using the OptQuest optimisation engine [188]. OptQuest is well suited to problems with low dimensionality and unknown structure, which is why the controller has been designed in this manner. The controller runs at 6pm every day to update the schedule for the rSOC.

Figures 4.4 and 4.5 show microgrid dispatch over the same three days for microgrids with differently sized energy storage components. Note that the controller produces markedly different schedules in each case. In Figure 4.4, the rSOC is small but the battery large. The controller sets the maximum load negative, close to the minimum (similar to Figure 4.3b), so that electrolysis continues steadily through the night, powered by the battery. The battery manages the day/night cycling, whilst the stored hydrogen climbs continually. In Figure 4.5, the battery is not large enough for this approach. The maximum load is set positive, so that fuel cell mode is active during the night (similar to left hand side of Figure 4.3). The rSOC and battery both contribute to the day/night cycling.

For the microgrid specification in Figure 4.4, the control method described here reduces annual grid imports by around 15% compared to a greedy algorithm.

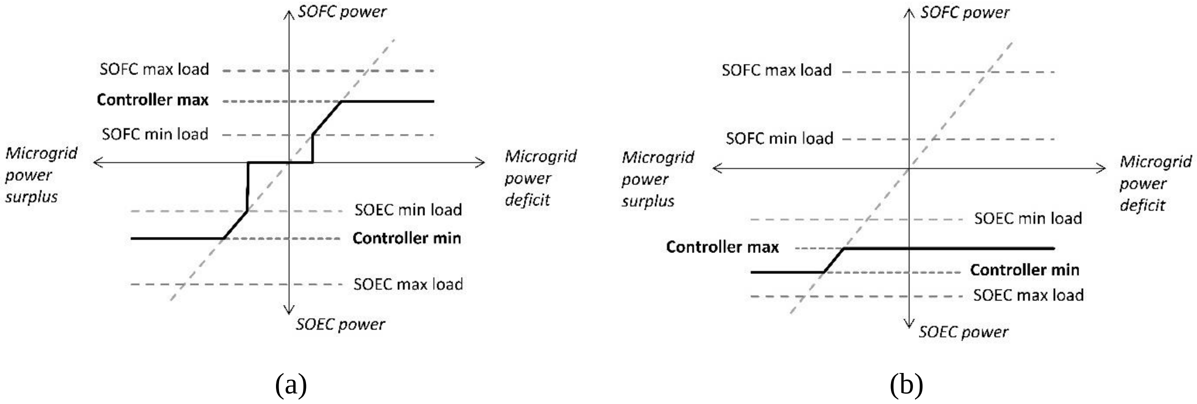

Figure 4.3. Illustrates how the response of the rSOC to the microgrid's deficit / surplus is curtailed by the maximum and minimum daily load imposed by the controller. The rSOC may be permitted to operate in both modes, as in (a), or constrained to operate in only one mode – as in (b), where electrolysis carries on even when the microgrid is in deficit. Operation in one mode throughout the day is likely to occur when battery capacity is large but rSOC capacity is small.

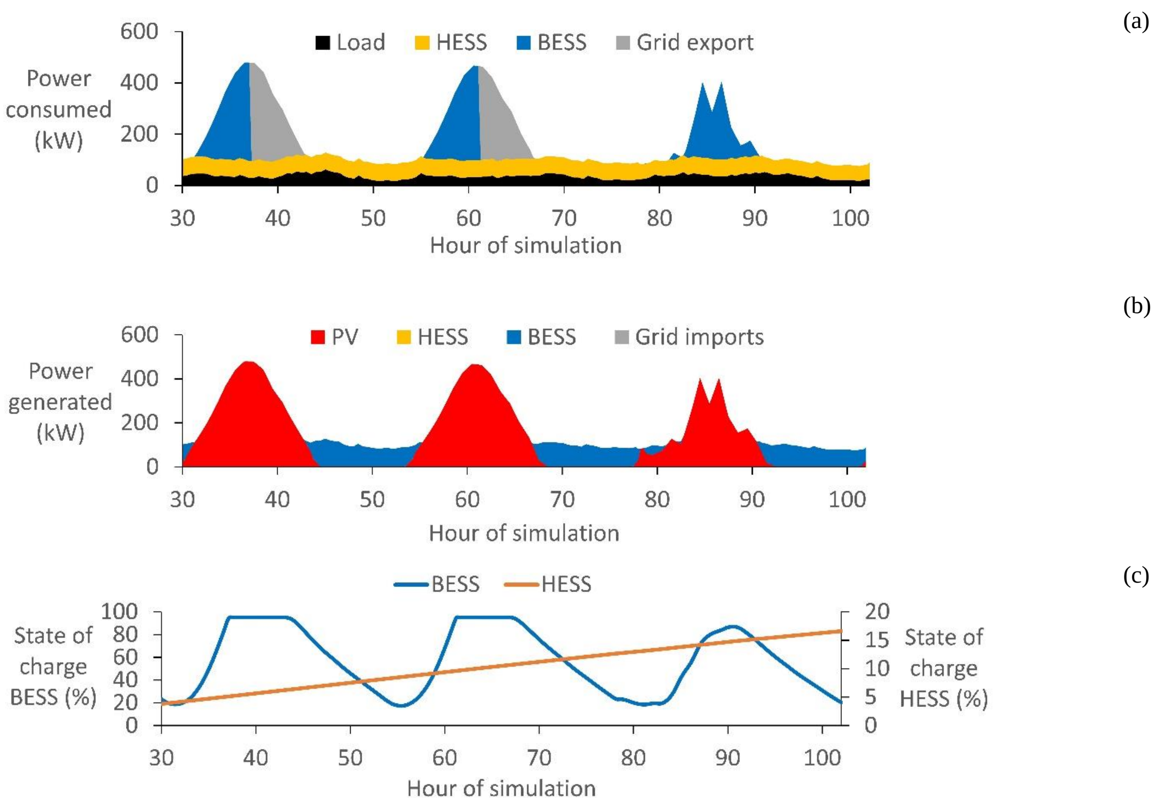

Figure 4.4. Example dispatch of the microgrid with hybrid energy storage over three days in early May. 6 kW PV per dwelling; 50 kW rSOC; 1438 kWh battery.
(a): power consumed; (b) power generated; (c) state of charge of each energy storage.

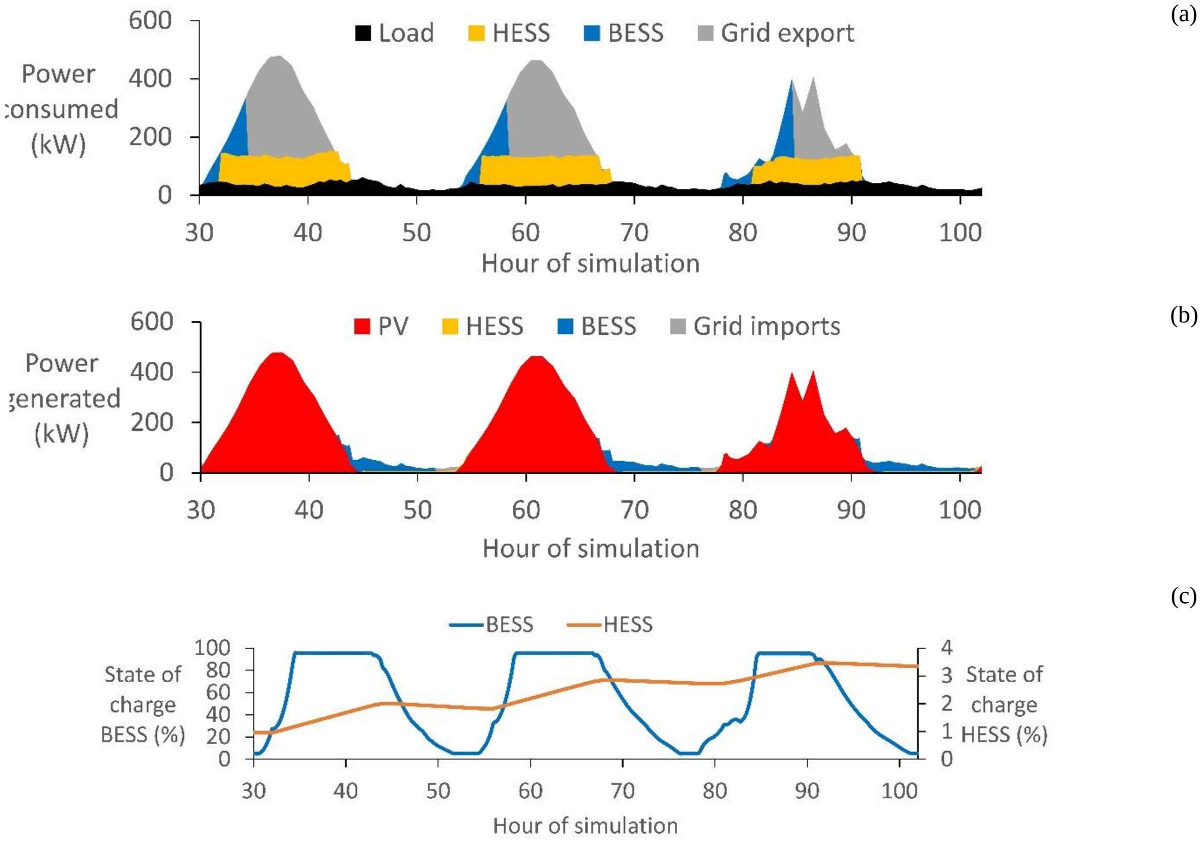

Figure 4.5. Example dispatch of the microgrid with hybrid energy storage over three days in early May. 6 kW PV per dwelling; 75 kW rSOC; 300 kWh battery.
(a): power consumed; (b) power generated; (c) state of charge of each energy storage.

4.2.7 Performance metrics; scenarios for cost and efficiency; optimisation of technology choice and sizing

Table 4.4. Estimates for installed CAPEX (two cost scenarios)

Technology	Symbol	Cost scenario 1 (Baseline estimate)	Cost scenario 2 (Low/future estimate)	References
rSOC	c_{rsoc}	£2000 / kW_{SOEC}	£750 / kW_{SOEC}	[35], [37]
PV	c_{pv}	£1750 / kW_p	£1000 / kW_p	[203]
H_2 storage	c_{H2}	£1000 / kg (£30 / kWh)	£333 / kg (£10 / kWh)	[24], [204], [205]
Li-ion battery storage	c_{BESS}	£500 / kWh	£500 / kWh	[206], [207]

Self-sufficiency ratio (SSR) for the community is defined to be the annual energy consumed which is *not* imported from the grid, as a proportion of total energy consumption:

$$SSR = \frac{(energy\ consumption) - (grid\ imports)}{(energy\ consumption)}$$

(Eqn. 4.14)

As well as quantifying the microgrid's grid-independence, SSR gives a basic measure of environmental benefit; under the simplifying assumption that grid emissions are constant, SSR is equal to the percentage reduction in emissions per unit of electricity consumed by the microgrid. In fact, SSR may give an underestimate of emissions curtailment, since the HESS and BESS are most likely to discharge in the early evening, when grid emissions are often above average. To give a rough idea for the cost of the energy system, based on the installed capacities of PV, rSOC and hydrogen storage, estimates for these technologies' installed CAPEX costs are used as shown in Table 4.4. Initial work uses the higher 'baseline' figures; we then consider a more optimistic future scenario (although the installed cost of battery storage is the same for both). Accordingly, the installed cost for the microgrid is estimated as:

$$c_{total} = c_{pv} \cdot n \cdot C_{pv} + a_{HESS} \cdot \left(c_{rsoc} \cdot P_{SOEC} + c_{H2} \cdot m_{full} \right) + a_{BESS} \cdot c_{BESS} \cdot C_{BESS}$$ (Eqn. 4.15)

Here, *n* represents the number of houses; C_{pv} the mean kW of installed PV per house; and m_{full} the capacity of the hydrogen storage in kg. a_{HESS} and a_{BESS} are binaries expressing whether each form of storage is installed.

Annual savings achieved by the microgrid are considered equal to the avoided cost of grid-imported power. The retail price of electricity c_{grid} is estimated to be £0.144 / kWh for the SE England study, and $0.127 / kWh for Texas. Simple payback periods are then calculated simply as CAPEX divided by annual savings:

$$payback\ period = \frac{c_{total}}{c_{grid} \cdot SSR \cdot E_{year}}$$ (Eqn. 4.16)

where E_{year} is the microgrid's annual electricity consumption in kWh, and c_{grid} is the cost of imported power per kWh.

For comparison between the case studies, an approximate exchange rate of \$1.25 to £1 is assumed. Two scenarios are considered for the efficiency of rSOC technology. The first (baseline) scenario is based on technology already demonstrated at scale by Sunfire [24], [46], achieving round-trip efficiency just under 35%. The second scenario assumes round-trip efficiency of 60%. Balance-of-plant level simulation work seen in the literature suggests that this may be realistic for rSOC technology in the future.

Table 4.5**.** Scenarios for efficiency of rSOC technology.

	Efficiency scenario 1 (Baseline estimate)	**Efficiency scenario 2 (High/future estimate)**
η_{SOEC}	172.5 MJ/kg$_{H2}$	120 MJ/kg$_{H2}$
η_{SOFC}	60 MJ/kg$_{H2}$	72 MJ/kg$_{H2}$
rSOC round-trip	34.8%	60%

All optimisations are conducted using the OptQuest global optimisation engine [188], [208]. In this work, optimisation of microgrid design has the minimisation of payback period (see Equation 4.16) as the objective, subject to constraints on the SSR to be achieved. Decision variables are summarised in Table 4.6:

Table 4.6. Decision variables for the optimisation of the microgrid design.

Variable	**Type**	**Description**
a_{HESS}	Binary	Installation of HESS
a_{BESS}	Binary	Installation of BESS
C_{pv}	Continuous	Capacity of PV (kW$_p$ per house)
P_{SOEC}	Continuous	Capacity of rSOC (kW)
m_{full}	Continuous	Capacity of H_2 storage (kg)
C_{BESS}	Continuous	Capacity of BESS (kWh)

4.3 Results

This section falls into the following parts. Firstly, the two case studies are introduced. Secondly, rSOC energy storage is considered for both of these, with optimisation of microgrid design under different scenarios. Thirdly, hybrid energy storage with battery and rSOC is considered (for the England case study only).

4.3.1 Case Studies

The model described above has been employed for two case studies. In both cases the scenario is a small residential community, each house equipped with rooftop PV, with the rSOC energy storage serving the whole community. The location for case study 1 is the south-east of England. Electrical load data comes from a smart-meter trial in London carried out by UK Power Networks and has half-hourly resolution [209]. Climate data was recorded by the UK Environmental Change Network at Rothamsted (near London) and has hourly resolution [28]. Rooftop PV installations are assumed to average 3 kW_p [210]. Simulations begin on May 1st, around the time of year that daily surpluses of solar power begin.

The second case study is located in Austin, Texas, USA. Two factors motivate this choice. Firstly, Pecan Street Inc. have a rich set of freely available data for many houses in Austin, with measured time series data for both electrical load and PV generation [211]. Secondly, the location provides a good contrast to the UK case study: peak electricity demand is in summer (owing to air-conditioning loads) rather than winter; PV installations tend to be larger and have higher capacity factor, and overall domestic electricity consumption is also much higher. These differences may be seen in Figure 4.6 and Table 4.7. Simulations for this case study begin with the calendar year, since solar surplus is experienced in late winter and early spring.

Table 4.7. Details of the two case studies. All parameters are for the microgrid as an aggregate whole.

	SE England	**Austin, Texas**
No. of dwellings	92	92
Annual electricity consumption	384 MWh	1090 MWh
PV installed	276 kW_p	508 kW_p
Annual PV generation	267 MWh	633 MWh
Capacity factor	11.0%	14.2%
SSR	33.4%	36.1%
Annual cost of imported power	£36830	$88494

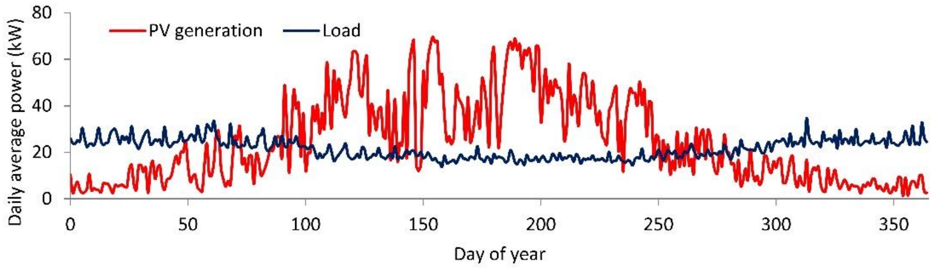

(a)

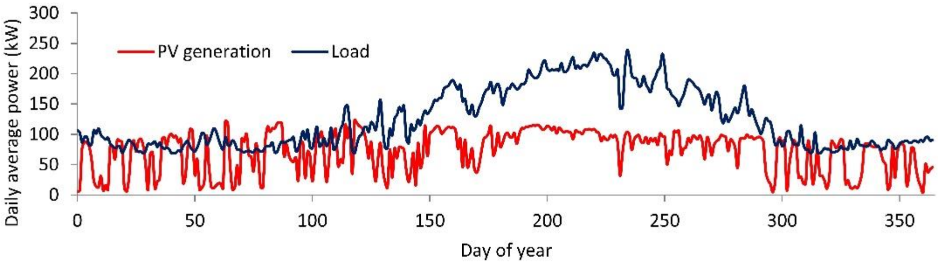

(b)

Figure 4.6. Average daily load and PV generation for the community of 92 dwellings, for (a) SE England and (b) Austin, Texas, over one year, prior to deployment of any energy storage. Clear differences between the case studies are evident. Electrical load is higher throughout the year in the Austin study, and peaks dramatically during the summer, rather than the winter. PV output is also more constant over the course of a year (due to both climate and latitude, it is assumed). PV output is modelled for England case study, but comes from Pecan Street Inc. data for Texas.

4.3.2 Initial results with existing PV capacity

Firstly, we explored what the rSOC energy storage could achieve alongside the baseline amount of installed PV. To determine the maximum possible impact, the rSOC capacity P_{SOEC} was optimised to achieve maximum SSR (with H_2 storage volume unlimited and PV capacity fixed). Correct sizing of the rSOC is important, since its partial load capability is limited. Table 4.8 gives a summary of the results for each case study. For both locations, the rSOC + H_2 storage system would enable SSR to increase to about 42% (up from 33% and 36% for the UK and Texas respectively). This is the maximum SSR achievable without installing additional PV capacity.

The storage profile over the year (in terms of mass of stored H_2) is shown in Figure 4.7, for each location. For the Texas case study, only short term cycles of at most a week's duration are observed. This is unsurprising, since a daily surplus of solar energy is rare (see Figure 4.6) and it tends to suggest that long term storage using hydrogen is hard to justify here, without an increase in PV capacity. For the UK study, surpluses of solar power are common enough in the summer that the storage profile does display a long-duration cycle.

The increase in SSR achieved by the storage results in lower payments for imported grid power. When comparing to the microgrid equipped with PV only, the rSOC + H_2 storage saves around £5000 p.a. in the UK, or $8000 p.a. in Texas. These savings are far from sufficient to offset the extra investment; in both locations, payback periods for the addition of storage exceed 60 years – far beyond the system lifetime. The addition of the HESS energy storage is thus hard to justify here, with poor economics and only a small increase in SSR to improve environmental credentials.

Table 4.8. Summary of rSOC impact on microgrid with baseline solar PV capacity & optimised rSOC capacity

	SE England		**Austin, Texas**	
	PV only	**PV + rSOC**	**PV only**	**PV + rSOC**
SSR achieved	0.334	0.423	0.361	0.418
PV per dwelling (kW_p)	3	3	5.52	5.52
rSOC capacity (kW)	0	91.5	0	168.4
Max required H_2 storage (m^3)	0	14.12	0	4.86
Max required H_2 storage (MWh)	0	5.03	0	1.73
Estimated CAPEX	£0.483m	£0.817m	$1.111m	$1.597m
Grid imports (MWh)	255.7	221.6	696.4	634.4
Annual savings	£18466	£23369	$49963	$57838
Payback time (years)	26.2	35.0	22.2	27.6
Payback time versus PV (years)	N.A.	68.1	N.A.	61.7

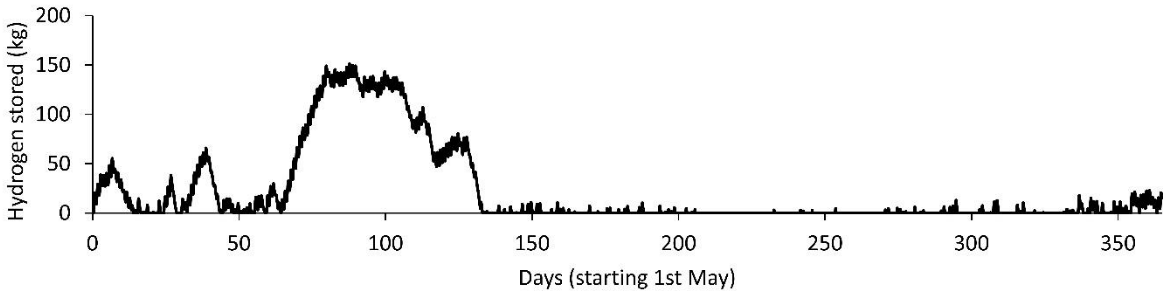

(a)

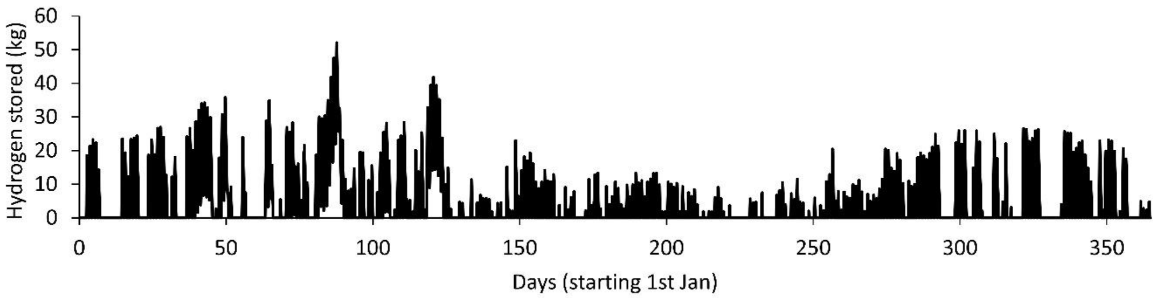

(b)

Figure 4.7. Annual hourly storage profiles for each case study, with baseline PV capacity and optimally sized rSOC. (a) SE England, (b) Austin, Texas. A long term cycle does emerge for SE England. For Texas, the longest storage cycles are of about a week's duration for this system. Note that cycling is deepest in spring and autumn, when surpluses of solar power are more common.

4.3.3 Optimisation of installed capacity for each component

Next, the optimiser was permitted to vary the installed capacity of all three components (rSOC, H_2 storage and PV). The intention was to explore scenarios with greater capacity of installed PV, perhaps providing more incentive for long term energy storage. The optimiser searched for the microgrid design achieving lowest CAPEX cost, whilst constrained to achieve a particular SSR. Payback periods were calculated for the microgrid as a whole, relative to a baseline scenario with all power imported from the grid (0% SSR). Results are shown in Figure 4.8 and Tables 9 and 10.

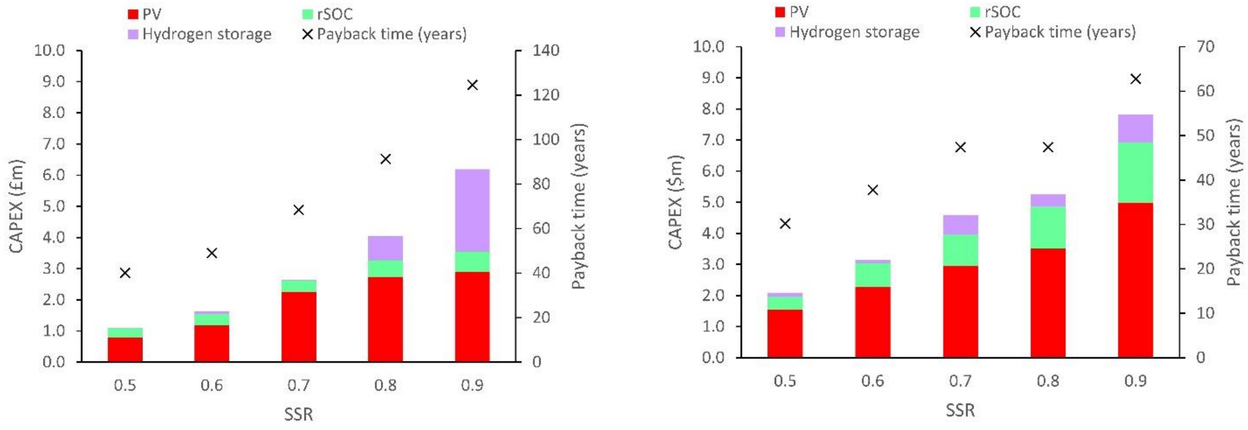

(a) (b)

Figure 4.8. Estimated CAPEX costs and payback times for systems optimised to achieve specified SSR. (a) SE England, (b) Austin, Texas.

Table 4.9. Summary of microgrid energy systems for SE England, with CAPEX minimised to achieve given SSR.

SSR requirement	**0.5**	**0.6**	**0.7**	**0.8**	**0.9**
PV per dwelling (kW_p)	4.90	7.30	14.00	16.99	17.98
rSOC capacity (kW)	132.8	149.0	182.0	268.0	329.2
H_2 storage (m^3)	2.1	8.0	2.7	71.6	246.9
H_2 storage (MWh)	0.75	2.85	0.96	25.53	88.03
Estimated CAPEX (£m)	1.077	1.559	2.647	4.037	6.194
Grid imports (MWh)	192.0	153.6	115.2	76.8	38.4
Annual savings (£)	27643	33172	38700	44229	49757
Approx payback time (years)	38.9	47.0	68.4	91.3	124.5

Table 4.10. Summary of microgrid energy systems for Texas, with CAPEX minimised to achieve given SSR.

SSR requirement	**0.5**	**0.6**	**0.7**	**0.8**	**0.9**
PV per dwelling (kW_p)	7.66	11.32	14.69	17.40	24.80
rSOC capacity (kW)	168.7	305.2	400.0	541.5	773.1
H_2 storage (m^3)	9.6	7.0	47.5	29.5	66.8
H_2 storage (MWh)	3.42	2.50	16.93	10.52	23.82
Estimated CAPEX ($m)	2.090	3.135	4.590	5.250	7.816
Grid imports (MWh)	544.9	435.9	326.9	218.0	109.0
Annual savings ($)	69201	83041	96881	110722	124562
Approx payback time (years)	30.2	37.8	47.4	47.4	62.8

For both case studies, it was possible to design systems achieving SSR of 90% or somewhat above. (100% SSR is not possible without the addition of more flexible, shorter term storage.) In every case, significant capacity of rSOC and H_2 storage was installed by the optimiser (i.e. the required SSR could not be achieved simply by oversizing the PV component). Thus, the rSOC energy storage has value to boost SSR and as such, to boost environmental sustainability.

The high SSR systems would require very large capacities of PV, which is a consequence of the rSOC's low round-trip efficiency. Such large capacities of PV would likely need to be ground-mounted. It will be noticed from Figure 4.8 that the cost of PV is the most significant part of system CAPEX, until very high SSR is required. For the UK, the H_2 storage volume and cost balloons if SSR above 0.8 is required. For Texas, this does not happen to the same extent, which reflects the reasonable availability of solar power throughout the seasons, as compared to its extreme seasonality in the UK.

Payback periods exceed 30 years in all cases, indicating that the systems would not be financially viable; furthermore, payback time worsens with increasing SSR. Better payback times are achieved for Texas than for the UK, which may be ascribed to the higher PV capacity factor and better synchronisation of PV and load. Since the energy storage is clearly not financially viable at the high costs and low efficiencies initially assumed, the low cost and high efficiency scenarios are now explored (see Tables 4.4 and 4.5 above). As before, the optimiser constrains for SSR and sizes the components to minimise CAPEX. Results are shown in Figure 4.9 and Tables 4.11 and 4.12.

Highly (90%) self-sufficient systems remain too costly in all scenarios. This is especially true for the UK study, with payback times of 80 and 46 years for the two scenarios. Payback periods of < 30 years for the Texas study are more hopeful, although still in excess of the system's likely lifetime. Note that higher efficiency for the energy storage allows for reduction in the required PV capacity, whilst the required rSOC capacity is similar. The impact of increasing rSOC efficiency has more impact in the UK, with the reduced requirement for H_2 storage allowing CAPEX to almost halve.

For systems with modest (50%) self-sufficiency, the results are more interesting. Payback periods of less than twenty years are suggested in both scenarios for Texas, and for the UK if cost and efficiency are both improved. These systems require only a few cubic metres of hydrogen storage, and PV capacities within realistic bounds for rooftop installations. At their present state of maturity, rSOCs cannot be expected to last even for 20 years. SOFCs are capable of running for at least ten years [96], but use in electrolysis mode causes accelerated degradation [28], [29], [34]. Ten years may be a reasonable lifetime for an rSOC stack in the medium term. This suggests that more detailed work is needed, taking the stack replacement cost into account, to establish whether a PV / rSOC / H_2 microgrid can really save versus grid imports over its lifetime.

It may be noted that the impact of increased efficiency is small for the 50% SSR systems; the system becomes 12% cheaper for the UK, and only 2.4% cheaper for Texas. The impact is greatest for the UK 90% SSR system, where the microgrid is 43% cheaper with enhanced efficiency. For the UK, achieving high SSR demands considerable use of storage because of the large seasonal mismatch between load and generation. By contrast, high SSR in Texas is achieved mainly by scaling up solar capacity, with less extra storage capacity needed.

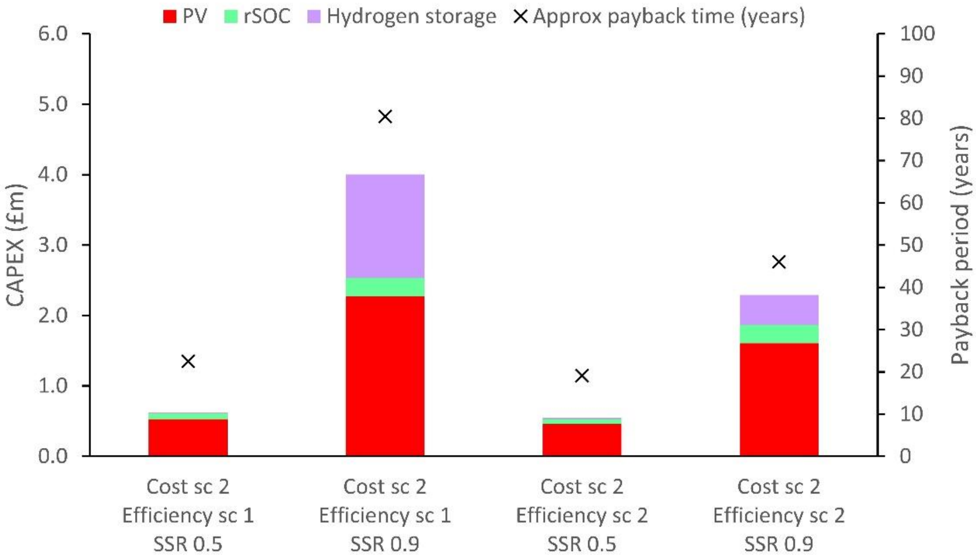

(a)

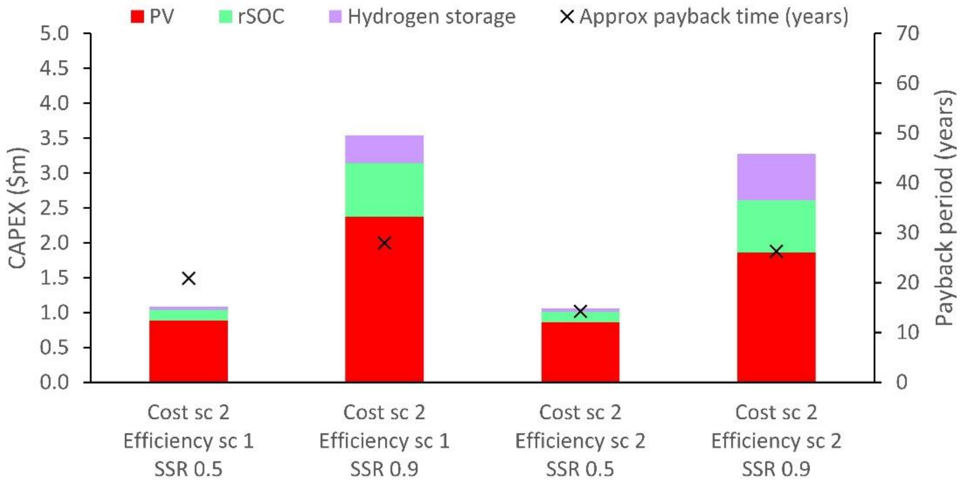

(b)

Figure 4.9. Estimated CAPEX costs and payback times, under future scenarios. (a) SE England, (b) Austin, Texas.

Table 4.11. Summary of optimised microgrid energy systems for SE England: future scenarios.

Scenarios	**Efficiency 1, Cost 2**		**Efficiency 2, Cost 2**	
SSR requirement	0.5	0.9	0.5	0.9
PV per dwelling (kW_p)	5.71	24.70	4.99	17.49
rSOC capacity (kW)	110.9	348.0	91.1	346.1
H_2 storage (m^3)	3.9	412.2	5.0	118.3
H_2 storage (MWh)	1.39	146.96	1.78	42.18
Estimated CAPEX (£m)	0.622	4.003	0.545	2.291
Grid imports (MWh)	195.0	39.0	195.0	39.0
Annual savings (£)	27643	49757	27643	49757
Approx payback time (years)	20.9	80.4	18.4	46.0

Table 4.12. Summary of optimised microgrid energy systems for Texas: future scenarios.

Scenarios	**Efficiency 1, Cost 2**		**Efficiency 2, Cost 2**	
SSR requirement	0.5	0.9	0.5	0.9
PV per dwelling (kW_p)	7.70	20.63	7.50	16.17
rSOC capacity (kW)	163.9	822.7	160.8	801.4
H_2 storage (m^3)	9.7	89.5	9.7	148.6
H_2 storage (MWh)	3.46	31.91	3.46	52.98
Estimated CAPEX ($m)	1.082	3.542	1.056	3.273
Grid imports (MWh)	544.9	109.0	544.9	109.0
Annual savings ($)	69201	124562	69201	124562
Approx payback time (years)	15.6	27.9	14.3	26.3

4.3.4 Results for hybrid energy storage

In this section, results are presented for the SE England study, now with battery storage (BESS) available in addition to rSOC. Similarly to the previous section, four components of the microgrid (PV, BESS, rSOC and H_2 storage) were sized to achieve the specified SSR for minimal payback time. Binary decision variables a_{BESS} and a_{HESS} determined whether BESS and HESS were to be installed. Thus, these results say something about the conditions under which hybrid energy storage (HESS + BESS) is preferable to a system with battery storage only. Scenarios 1 and 2 for efficiency and cost are considered. Details of the optimised microgrid systems are given in Table 4.13 and in Figures 4.10-4.12.

The optimiser exhibited a notable preference to install very large over-capacity of PV, with battery storage, rather than installing HESS. This approach allows for sufficient daily solar generation even during the winter so that the need for long-term bulk energy storage is obviated. Under baseline scenarios for efficiency and cost, even a 90% SSR system is most cheaply achieved without HESS, with 15.25 kW of PV per house. Under the improved scenarios, HESS is not selected until requiring SSR above 85%. It is worth noting that a 90% SSR system using hybrid storage has a payback period of about 37 years; with pure hydrogen based storage the figure was 46 years (see Table 4.11).

Such large PV installations will not often be feasible in the built environment. Therefore, further results were taken with PV per household constrained below 6 kW. This restriction increases the chance that the HESS is part of the optimal design: the optimiser now selects HESS whenever SSR above 75% is required. This was the case regardless of cost and efficiency scenario. It can be concluded that HESS using rSOC can be an optimal choice when high SSR is desired, whether to achieve high independence from the national grid, or to showcase environmental benefits. These systems are probably not economical, with simple payback period ranging from 20 to 100 years (according to the scenario and the SSR required). Nonetheless, the use of rSOC to obtain the higher SSR and emissions curtailment is implied to be more economical than the use of battery storage alone, if SSR is above the 75% SSR threshold.

Table 4.13. SE England case study; optimisations with battery / hybrid storage

Scenarios		**Constraints**		**Optimal system design**					**Finances**	
Price Scenario	**Efficiency scenario**	**SSR constraint**	**PV constraint (kW / house)**	**PV (kW / house)**	**BESS (kWh)**	**HESS?**	**rSOC (kW)**	**H_2 storage (m^3)**	**CAPEX (£m)**	**Payback (years)**
1	1	0.9	<20	15.25	1798	No	-	-	3.354	67.2
2	2	0.8	< 20	9.83	1016	No	-	-	1.412	31.9
2	2	0.85	< 20	9.97	651	**Yes**	165.1	42.6	1.518	32.2
2	2	0.9	< 20	13.34	787	**Yes**	138.7	28.7	1.827	36.8
1	1	0.7	< 6	6.00	898	No	-	-	1.415	36.5
1	1	0.75	< 6	6.00	1438	**Yes**	50.0	64.7	2.478	59.6
1	1	0.8	< 6	5.86	1267	**Yes**	56.2	217	4.007	89.6
1	1	0.9	< 6	6.00	2810	**Yes**	169.3	685	10.035	204
2	2	0.6	< 6	4.76	450	No	-	-	0.662	19.8
2	2	0.65	<6	5.40	612	No	-	-	0.803	22.2
2	2	0.7	<6	6.00	929	No	-	-	1.017	26.1
2	2	0.75	<6	5.97	728	**Yes**	64.1	174	1.582	35.6
2	2	0.8	<6	6.00	1106	**Yes**	172.4	202	1.955	42.5
2	2	0.9	< 6	6.00	1815	**Yes**	162.9	331	2.763	54.8

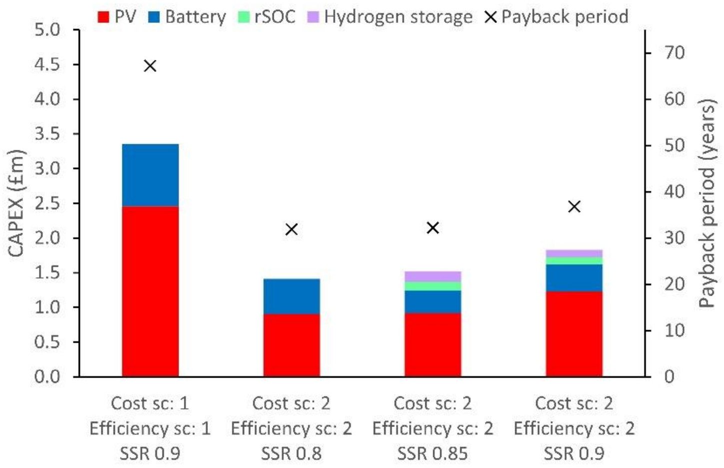

Figure 4.10. Costs and payback times of optimised microgrid energy systems, with PV capacity constrained below 20 kW.

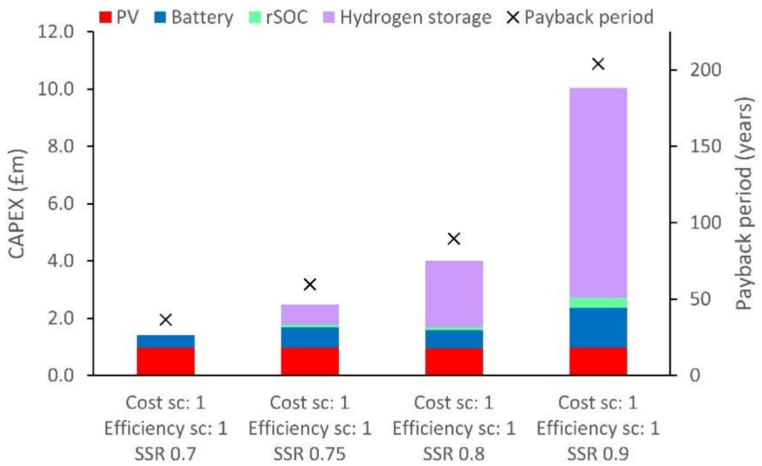

Figure 4.11. Costs and payback times of optimised microgrid energy systems, with PV capacity constrained below 6 kW. Scenario 1 for cost and efficiency. HESS is selected when SSR above 75% is required.

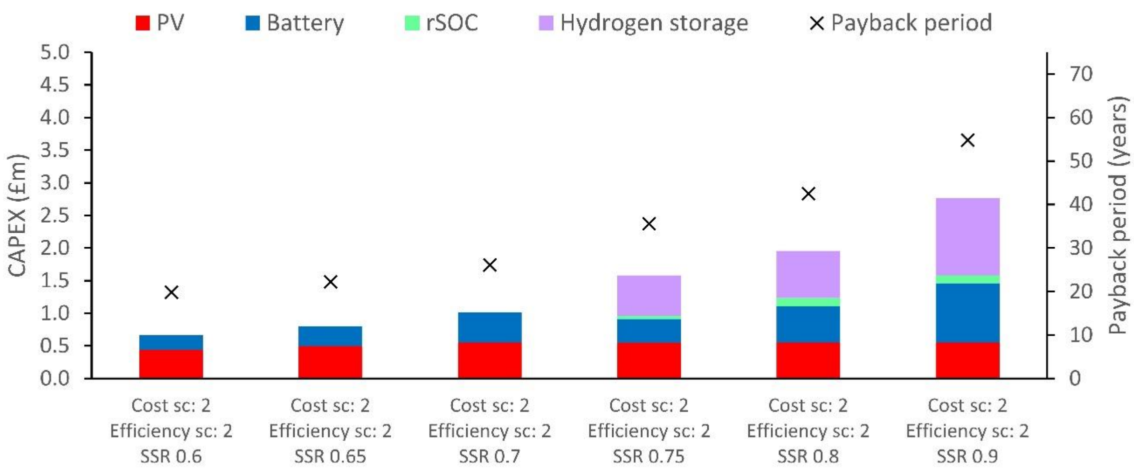

Figure 4.12. Costs and payback times of optimised microgrid energy systems, with PV capacity constrained below 6 kW. Scenario 2 for cost and efficiency. HESS is selected when SSR above 75% is required.

4.4 Conclusions and future work

In this paper we have presented an agent-based simulation model for a microgrid equipped with rooftop PV generation, and an rSOC + H_2 storage enabling long term energy storage. This model has been used to quantify the level of grid-independence that such a system could attain, and the consequent cost savings. These benefits have been set against the estimated CAPEX for the microgrid. Two locations have been considered, the south-east of the UK, and Texas, which exhibit differences in both scale and seasonality of solar resource and electricity demand.

Initial simulation work considered households with average-sized PV installations, for each location, and the possible impact of adding the energy storage. In both locations, it was found that the energy storage could allow the microgrid to achieve a self-sufficiency ratio of around 42% over a year, a fairly modest increase from SSR achievable by PV without storage. The cost saving associated with this would not be sufficient to make the energy storage system a viable investment, with payback periods of over six decades indicated. The moderate impact of the storage is partly due to the fact that typical residential PV installations do not generate long-term surpluses of power, in either location. Therefore, subsequent work allowed for PV capacity to be scaled higher.

Next, the capacity of the microgrid's three main components (PV, rSOC, H_2 storage) were optimised in order to achieve given SSR. It was possible to design systems with SSR of 90% or higher. A high SSR is expected to imply similarly high percentage curtailment of the emissions associated with electricity consumption. However, costs increase faster than savings as SSR is increased, with payback times between 30 and 120 years. Systems designed for Texas can be more conservative in scale (relative to the size of annual demand); this is thanks to the solar resource being less seasonal and better synchronised with the load. Consequently, cost-effectiveness is closer to being attainable for Texas. It is also worth noting that the low round-trip efficiency leads to large requirements for PV capacity in order to obtain high SSR.

Two further scenarios were then considered, with lower CAPEX costs and higher rSOC round-trip efficiency. In these scenarios, it was found that a microgrid designed to achieve SSR of 50% could be cost effective over 20 years relative to grid-imported power. Such a design would incorporate hydrogen storage below 10 m^3 volume, providing the equivalent of 10's of kWh of storage per household (about an order of magnitude higher than typical household batteries). Increasing the efficiency of the storage had only a minor effect on system cost for a 50% self-sufficient system; efficiency becomes important if high SSR is required. Accordingly, we conclude that if the lower CAPEX costs shown in Table 4.4 can be realised, a microgrid designed for 50% self-sufficiency, using rSOC for energy storage, could be cheaper than grid imported power. In addition to reduced costs, rSOC lifetime will need to increase towards (or beyond) the 10-year lifetime currently achievable by SOFCs. (It is worth noting, though, that replacement costs for degraded rSOC stacks would likely only be 20-30% of original CAPEX, since the majority of expense is for balance of plant equipment [105].)

Further work considered the possibilities of using the rSOC in tandem with battery storage for a 'hybrid' energy storage, and the degree to which this can compete with standalone battery storage. It was found that battery storage is in fact preferred to the hybrid storage in many circumstances. However, there is a threshold SSR above which the installation of the rSOC becomes cost-optimal; this threshold appears to be at least 75%, and is higher if the installation of very large capacity PV systems is an option. If it is wished to have a system with SSR above this threshold, to obtain very high environmental benefits and grid independence, the addition of rSOC is advised for the cheapest possible microgrid design. At very high SSR, investment cost and payback period grow very large;

financial viability is most plausible for the microgrid with hybrid energy storage with SSR near to the 75% threshold.

The challenging nature of the economics for rSOC energy storage is a common theme in these results, however certain recommendations can be made: firstly, it is notable from Section 4.3.4 that when HESS is selected, the hydrogen storage component becomes the single most significant cost. It is also known that rSOC efficiency indirectly impacts this (see Figure 4.9a). Thus, reduction of H_2 storage cost and improvement of rSOC efficiency are priorities. Secondly, payback time may also be improved if the rSOC can realise value in other ways: for instance, by deferring grid upgrades or by supplying heat.

Various directions are suggested for future work:

- Promising microgrid designs should be considered in more detail, with assessment for operating expenditure and equipment replacement costs, as well as possible degradation of equipment.
- The role of mass electric vehicle uptake and its effect on the microgrid's load will be considered.
- The possibility of extracting additional value from the rSOC through utilisation of its waste heat will be considered.
- This work has considered only a flat price for imported electricity, and has not considered the possibility of export tariffs, variable or otherwise. Future work could consider variable import and export tariffs, including under future energy scenarios (where these are expected to fluctuate more dramatically).
- CO_2 abatement has only been considered indirectly via the microgrid's SSR. Future work could quantify CO_2 abatement directly, again with consideration of future scenarios for grid electricity.
- The model should be run at higher time resolution, to allow better study of constraints on rSOC ramp-rate.
- Alternative forms of renewable generation, notably wind, may need to be considered. With less seasonal variation than solar power, the relative advantages of different energy storage technologies may change.
- The agent-based nature of the simulation will be used to study the interaction of individual households with the microgrid and the extent to which they might benefit financially by participating in peer-to-peer energy trading or a bill-sharing scheme.

4.5 Acknowledgements

Grateful acknowledgement is made of the financial support of the Engineering and Physical Sciences Research Council (EPSRC) in the form of the 'Energy Storage and its Applications' Centre for Doctoral Training under grant code EP/L0168/18; also of the Electric Power Research Institute.

This research makes use of data from the UK Environmental Change Network, UK Power Networks, and Pecan Street Inc.

4.6 Appendix – details on hybrid storage controller

Table 4.A1. Variables pertaining to the hybrid storage controller.

Symbol	Unit	Definition
$t \in \{0 \ldots 120\}$	-	Hour of forecast period
$d \in \{1 \ldots 5\}$	-	Day of forecast period
$P_{max,d}$	kW	Max AC power to be generated by SOFC during day d
$P_{min,d}$	kW	Max AC power to be consumed by electrolyser during day d
$P_{load,t}$	kW	Forecast electrical load for the microgrid at time t
$P_{gen,t}$	kW	Forecast PV generation for the microgrid at time t
$P_{net,t}$	kW	Forecast net generation for the microgrid at time t (positive sign indicates surplus generation)
$P_{HESS,t}$	kW	Scheduled power for the HESS at time t (positive sign indicates fuel cell mode)
$P_{BESS,t}$	kW	Scheduled power for the BESS at time t. (positive sign indicates discharge)
$P_{imp,t}$	kW	Power imported from grid at time t.
$P_{exp,t}$	kW	Power exported to grid at time t.
$m_{H2,t}$	kg	Mass of hydrogen stored at time t.
m_{full}	kg	Maximum quantity of storable hydrogen
$E_{BESS,t}$	kWh	Energy stored in battery at time t.
C_{BESS}	kWh	Nominal capacity of BESS
η_{comp}	MJ / kg	Energy required for compression of hydrogen
c_{grid}	£ / kWh $ / kWh	Price of grid imported electricity.
c_{store}	£ / kWh $ / kWh	Value assigned to stored energy at the end of the forecast period.

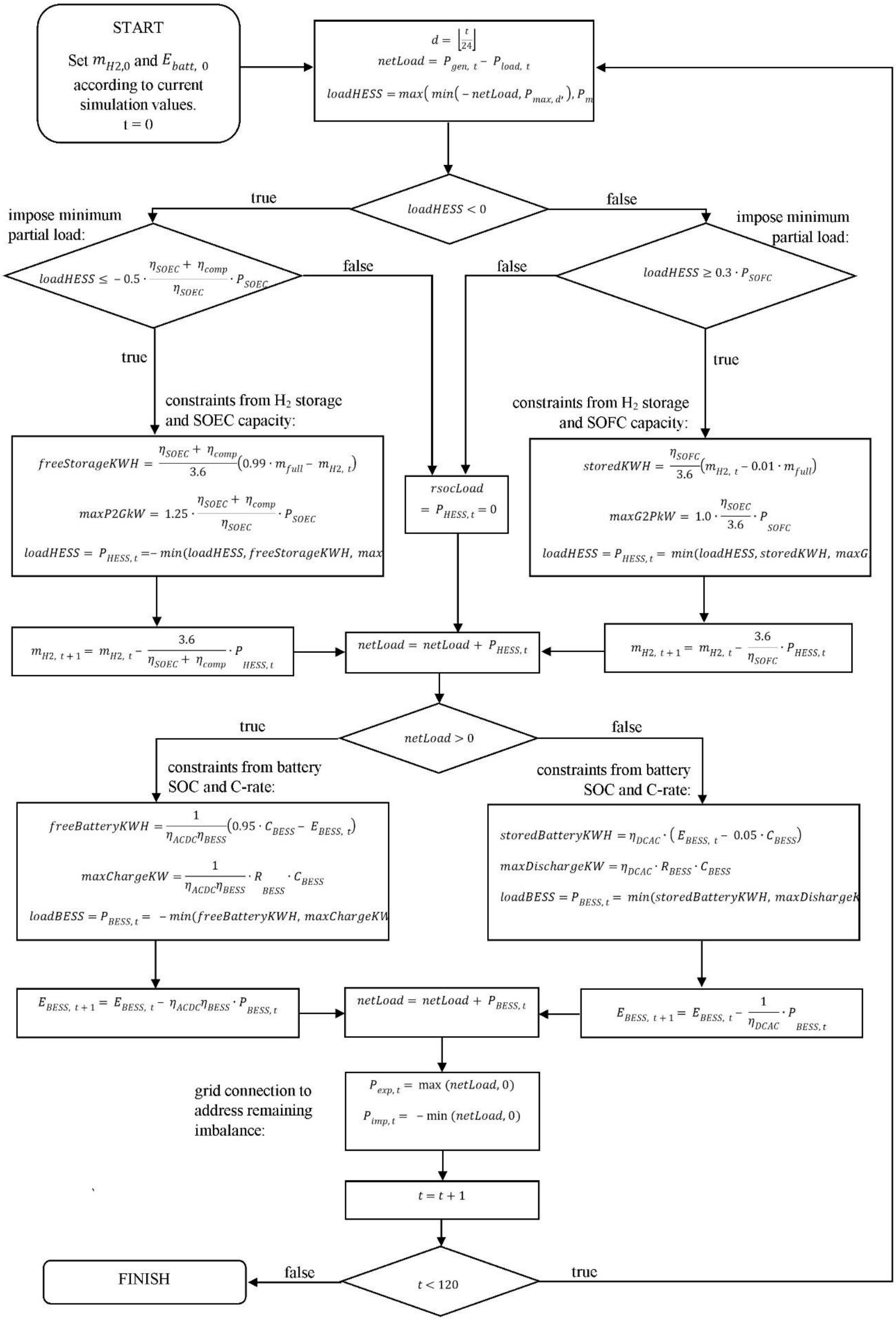

Figure 4.A1. Flowchart showing how a schedule $(P_{HESS,t,}, P_{BESS,t})_{0\le t<120}$ is created for the hybrid energy storage, for given values of $(P_{max,d})_{1\le d\le 5}$ and $(P_{min,d})_{1\le d\le 5}$.

5th Annual CDT Conference in Energy Storage and Its Applications, Professor Andrew Cruden, 2021, 01-21, University of Sheffield, UK

5. Long term energy storage with reversible solid oxide cells for microgrid applications

Timothy D Hutty[a], Siyuan Dong[a], Rachel Lee[a], Solomon Brown[a]

[a]*University of Sheffield, Dept. of Chemical and Biological Engineering, Sheffield, UK*

Abstract

Reversible solid oxide cells (rSOCs) offer the prospect of long term bulk energy storage using hydrogen or methane fuel. Whilst less mature than alkaline and PEM fuel cell / electrolysis technology, solid oxide cells offer superior efficiency: as high as 80 - 90%$_{LHV}$ at system level. Furthermore, the possibility of using the cells reversibly means that separate 'power-to-gas' and 'gas-to-power' components are not needed. Here, we consider the suitability of a hydrogen energy storage system (HESS) using rSOCs for a solar-powered residential microgrid. Battery energy storage (BESS) is considered as a competing (or complementary) energy storage technology. Since the electrification of transport is likely to be a major aspect of the transformation of domestic energy consumption, electric cars are also included in the microgrid model. The performance of the microgrid is evaluated in terms of its grid independence (self-sufficiency ratio, SSR) and economics (simple payback time and net present value). Optimisation is used to select and size the microgrid's components under different scenarios. Optimisation results suggest that battery storage is often preferred to HESS. However, two factors in particular can cause the selection of HESS to be favoured: (i) a requirement for high SSR and (ii) a lower constraint (6 kW) on the PV capacity per household. The economics for such systems remain very challenging.

Peer-review under responsibility of the scientific committee of the Name of the Conference, Conference Organizer Name, Year or Edition of Conference.

Keywords: energy storage; reversible solid oxide cell; microgrid; hybrid energy storage; self-sufficiency ratio; rSOC

5.1. Introduction

As the World's energy systems move towards greater dependence on renewable energy, the intermittent nature of solar and wind power may call for widespread use of energy storage. Electrical energy storage using batteries is already quite widespread; however, battery storage is not viable for storage of energy in bulk, or with discharge duration longer than 4 - 8 hours [9], [212], [213]. For bulk, long-duration energy storage, the conversion of electrical energy to a fuel such as hydrogen is a more viable option. The conversion of electrical power to hydrogen is accomplished by an electrolyser, whilst a fuel cell performs the reverse conversion of gas-to-power. The most prevalent technologies use alkaline and, increasingly, PEM electrolytes; the electrolyser for power-to-gas and fuel cell for gas-to-power are typically separate devices [30]. Reversible solid oxide cells (rSOCs), by contrast, achieve both functions within the same device, switching between solid oxide fuel cell 'SOFC' mode and solid oxide electrolyser cell 'SOEC' modes. These cells are also distinguished by their high temperature of operation (600 – 1000°C), and tend to be more efficient than the rival technologies: system level efficiency above 80%$_{LHV}$ may be possible, whereas 60-70%$_{LHV}$ is more typical for alkaline or PEM systems [34], [37], [43], [44]. However, rSOC technology is immature, suffering problems with material degradation [29], [34], [35], and also remains expensive [35], [37].

The work presented here considers the possible utility of energy storage using rSOC in a microgrid setting; that is, a small, localised electricity network, with its own generation and energy storage, seeking to achieve a degree of autonomy from the national grid. The possibilities of hydrogen energy storage for microgrids have received some attention in the academic literature (e.g. [118], [120]–

[126]) with common themes including concerns with high cost and the desirability of hybridisation with shorter term storage. rSOCs are rarely considered in these studies, which instead include separate gas-to-power and power-to-gas components. Notable exceptions include the work of Baldinelli et al [116] who considered an rSOC hybridised with flywheel energy storage to supply power to a number of homes, and Sorrentino et al [117], who considered an rSOC microgrid for an apartment complex. Nonetheless, most research on rSOCs considers balance-of-plant level detail, with little coverage of applications.

Here, we present a simulation of a microgrid with community energy storage, and the optimisation of the microgrid design. The work discussed here extends the modelling and optimisation work detailed in [214]. The main developments are (1) the inclusion of electric vehicles and (2) a more careful consideration of economics.

5.2. Methods

5.2.1. Microgrid model overview

This work employs a microgrid simulation model which has been implemented in the multi-paradigm simulation software AnyLogic [4]. This model has previously been reported in [214]; the key details are recapped here. The microgrid consists of a number of houses, equipped with rooftop PV generation. Shared community energy storage (CES) may be used; this consists of either a hydrogen energy storage system ('HESS'), with rSOC and storage of compressed hydrogen gas; or a battery energy storage system ('BESS'); or a hybrid system with both BESS and HESS. Additionally, each house has an electric car and a 7.2 kW charger. The overall setup of the microgrid is illustrated in Figure 5.1. Some details will now be given of the sub-models.

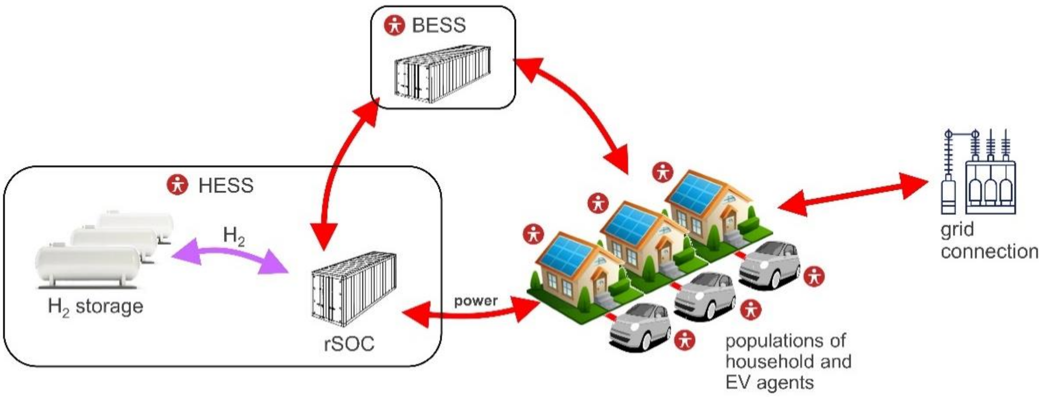

Figure 5.1. Schematic of simulated microgrid, incorporating houses with rooftop PV, electric cars, and community energy storage. (The figure symbol indicates that the component is modelled as an agent in AnyLogic.)

5.2.2. Solar model

The solar model calculates PV generation from measured irradiance data, for panels at arbitrary orientation. Erbs' correlation [197] is used to predict the diffuse component of irradiance. Solar installations vary in orientation between the different houses in the simulation; this results in an average capacity factor of 11.1% for the location under consideration (SE England). Validation of the PV model was conducted using hourly irradiance data for 2015 recorded at Rothamsted [200], and corresponding PV generation data for a 3.96 kW installation located 5.9 km to the south-west [201]. Comparing daily totals for generation over the year, mean absolute error was 0.769 kWh per day; comparing hourly generation over a summer fortnight, mean absolute error was 0.112 kWh/h.

5.2.3. Energy storage models

Table 5.1. Parameters used to characterise the rSOC system.

Parameter	**Symbol**	**Unit**	**Values from** [24], [46]
Electrolyser mode nominal capacity	P_{SOEC}	kW_{AC}	166
Electrolysis power consumption*	η_{SOEC}	MJ / kg_{H2}	172.5
Electrolyser partial load range	-	%	50 … 125%
Fuel cell mode nominal capacity	P_{SOFC}	kW_{AC}	30
Fuel cell power generation*	η_{SOFC}	MJ / kg_{H2}	60
Fuel cell partial load range	-	%	30 … 100%
Ramp rate	Δ	% of nominal capacity per minute	5%

*including steam production and all BoP other than H_2 compression

The rSOC system is characterised in terms of its capacity and power consumption/generation in each mode, and its maximum and minimum partial load. The ramp rate is also constrained to 5% of nominal capacity per minute, in each mode; however, at the half-hourly time resolution used in this work, this is not restrictive. It is assumed that the coupling of HESS with BESS would allow for shorter term oscillations in load to be evened out; future work using a higher time resolution will verify this. The baseline values for rSOC parameters are based on trials of Sunfire's rSOC technology [24], [46]. These values give a round-trip efficiency η_{rsoc} of 0.348. Hydrogen is assumed to be compressed to 150 bar for storage and the energy cost for compression is calculated accordingly.

Battery storage is assumed to be Li-ion technology. DC efficiency is 94%, with further 5% losses incurred by power converters in each direction, for total round-trip efficiency of 84.8%. The C-rate R_{BESS} is the reciprocal of the time in hours to charge or discharge the battery system. R_{BESS} is assumed never to exceed 2; lower values can allow for cheaper power conversion equipment (see 5.2.6).

5.2.4. Dispatch of hybrid storage

Here, rather than the control method detailed in [214], we use a simple greedy approach. For every half-hour, the net load on the microgrid is calculated. If BESS is installed, the BESS is prioritised to absorb as much of the net load as possible, as constrained by its C-rate and state of charge. If the microgrid is still unbalanced, and HESS is installed, the HESS will then absorb as much as possible of the remaining surplus or deficit. Grid import / export of power addresses any imbalance still remaining.

5.2.5. Electric vehicles

The present work extends the work reported in [214] by incorporating electric vehicles (EVs) into the simulation. This is approached in a similar way to reference [215], using trip data from the UK National Travel Survey [216] to determine when cars are at home, and the energy consumed on trips. A sample of 100 cars from the 2017 survey is used, with one car assigned to each house in the simulation. The sample is restricted to cars belonging to single-car households in a location classified as urban. Furthermore (and unlike in [215]), trip profiles are excluded if they cannot be achieved by EVs with 30 kWh batteries charging exclusively at home, on a 7.2 kW charger. In practice, only eight of 100 datasets needed to be substituted to satisfy this restriction. The cars in the final sample travel a mean weekly distance of 80.5 miles (median 65.5); the number of weekly trips averages 16.9 (median 15). Energy consumption is assumed to be a constant 3 miles / kWh.

It is the intention that the cars in the simulation will eventually charge their batteries smartly, in response to conditions on the microgrid, and perhaps discharge them to offset the load of the house (vehicle-to-home, 'V2H') or the microgrid (vehicle-to-grid, 'V2G'). However, in this present work the cars simply plug in to charge upon reaching home, and continue charging until their batteries are full. Figure 5.2 shows the contribution to the microgrid's load that results. The average weekly profiles are shown for standard domestic load, and PV generation (3 kW_p per house) for comparison with the EV load. There is clear potential for the EV load to be moved away from the domestic peak load, and synchronised better with the solar generation. This will be explored in future work.

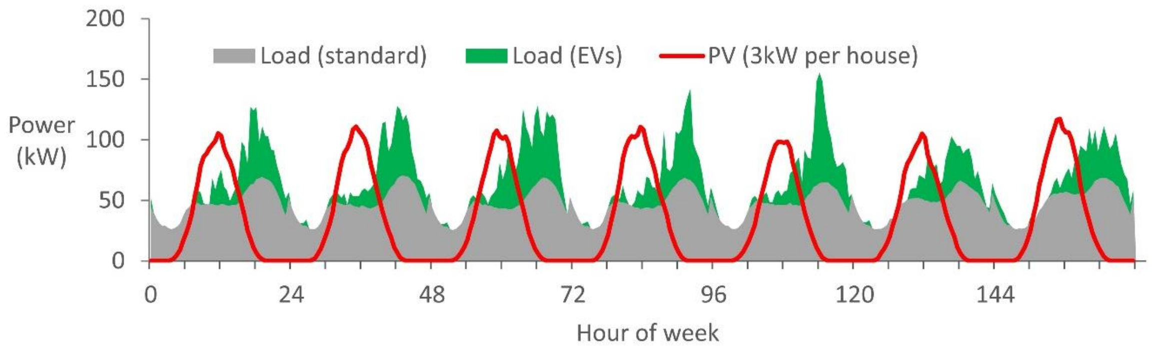

Figure 5.2. Impact of electric car charging on the microgrid's load.

5.2.6. Economics

5.2.6.1 CAPEX calculation

The investment costs for the microgrid are calculated according to the capacities of installed PV, rSOC, H2 storage and BESS. Cost assumptions are given in Table 5.2 with references.

Table 5.2. Installed cost for microgrid components.

Symbol	Unit	Description	Value range, with sources
c_{rsoc}	£/kW	rSOC system level installed cost, per kW capacity in electrolysis mode	750 – 2000 [35], [37], [118]
c_{pv}	£/kW$_p$	Installed cost of PV per kW$_p$	1000 – 1750 [203]
c_{H2}	£/kWh$_{LHV}$	Installed cost of hydrogen storage, per kWh$_{LHV}$. (Lower heating value 'LHV' of H_2 is 33.32 kWh/kg.)	10 – 30 [205], [217]
$c_{BESS,KW}$	£/kW	Installed cost of BESS per kWh energy capacity.	210 - 336 [218]
$c_{BESS,KWH}$	£/kWh	Installed cost of BESS per kW power capacity.	318 – 404 [218]

Accordingly, total CAPEX in GBP is given as:

$$c_{total} = 100 \cdot c_{pv} \cdot P_{pv} + a_{HESS} \cdot \left(c_{rsoc} \cdot P_{SOEC} + 33.32 \cdot c_{H2} \cdot m_{full} \right) + a_{BESS} \cdot P_{BESS} \cdot \left(c_{BESS,KWH} + R_{BESS} \cdot c_{BESS,KW} \right)$$

(Eqn. 5.1)

Here, 100 is the number of houses, and 33.32 kWh/kg is the lower heating value of hydrogen. a_{HESS} and a_{BESS} are binary variables for the installation of HESS and BESS.

5.2.6.2 Operational costs

References [105], [217], [219] suggest that annual OPEX for an rSOC of ca. 100 kW would be in the low £1000s. In particular, reference [105] suggests $0.03 per kWh generated for a SOFC; to allow for operation in both modes, we double this figure, giving ca. £0.048 per kWh generated. For the 70% SSR system detailed in the first row of Table 5.5, this would amount to £2150/a. For H_2 storage, we follow reference [219] in assuming annual OPEX equal to 1% of CAPEX. For the BESS system, we assume £8 per kW per annum [218]. Operational costs for PV are not considered.

5.2.6.3 Equipment replacement costs

The lifetime of the rSOC is assumed to be 40 000 operational hours [28]. It should be noted that a lifetime of this duration hasn't yet been demonstrated for rSOC, although the lifetime of SOFC can already exceed this [96]. It is assumed that replacement cost equates to the CAPEX of the rSOC stack, which is assumed to be 20% of total rSOC system CAPEX (the cost of the rSOC system is dominated by balance of plant costs). Operational hours per year are calculated by the simulation, enabling identification of the years where stack replacement will be necessary. The lifetime of the Li-ion battery storage is assumed to be 3000 cycles [220], with the replacement costs assumed equal to the energy component of the BESS CAPEX.

5.2.6.4 Performance metrics; net present value (NPV)

The self-sufficiency ratio 'SSR' of the microgrid is defined to be the proportion of annual energy consumed E_{cons} which is not imported from the grid. This is evaluated through running the simulation.

$$SSR = \frac{E_{cons} - E_{grid}}{E_{cons}}$$

(Eqn. 5.2)

SSR gives an indication of the microgrid's level of grid independence, as well as a crude indication of its environmental benefit. The annual savings achieved by the microgrid are assumed equal to the avoided costs of imported power:

$$annual\ savings = 0.144 \cdot \left(E_{cons} - E_{grid}\right)$$

(Eqn. 5.3)

where £0.144 / kWh is the assumed cost of grid electricity. The simple payback period is calculated as the number of years required for the annual savings to offset the initial CAPEX investment:

$$payback\ period = \frac{c_{total}}{annual\ savings}$$

(Eqn. 5.4)

The payback period for the microgrid gives a rough indication of its economic value but neglects ongoing costs and the time value of money. Accordingly, net present value (NPV) is also calculated, taking into account CAPEX, OPEX, equipment replacement costs, and annual savings, over a system lifetime of 25 years. Inflation of 2% and a discount rate of 12% are assumed.

5.2.7 Optimisation; scenario definitions

Multi-objective optimisation is carried out using the OptQuest optimisation engine [208], with SSR and payback period as the two objectives. The decision variables are given in Table 5.3. Binary variables determine whether BESS and HESS are to be installed; the five continuous variables determine sizing of microgrid components. The optimiser is permitted up to 10000 iterations of the simulation in order to construct a Pareto front for payback period versus SSR. SSR above 50% is set as a requirement for all solutions, as the threshold SSR for installation of the HESS is always above this, and restricting the width of the Pareto front improves the quality of results.

Table 5.3. Decision variables for the optimisation of the microgrid design.

Variable	Type	Description	Lower bound	Upper bound
a_{HESS}	Binary	Installation of HESS	0	1
a_{BESS}	Binary	Installation of BESS	0	1
P_{pv}	Continuous	Capacity of PV (kW_p per house)	0.25	$P_{pv,max}$
P_{SOEC}	Continuous	Capacity of rSOC in electrolysis mode (kW)	10	1000
m_{full}	Continuous	Capacity of H_2 storage (kg)	10.7 (1 m^3 @ 150 bar; 350 kWh_{LHV})	10700 (1000 m^3 @ 150 bar; 350 MWh_{LHV})
E_{BESS}	Continuous	Capacity of BESS (kWh)	100	10000
R_{BESS}	Continuous	C rate of BESS system (h^{-1})	0.01	2

The optimisation problem has been solved 15 times for different scenarios with varying costs and efficiencies, as detailed in Table 5.4. For every scenario, the optimiser designs microgrids with SSR in the range 50 – 100%.

Table 5.4. Definition of different scenarios considered. Where cells are blank, the value is as per the baseline scenario.

Scenario	$P_{pv,max}$	c_{rsoc}	c_{H2}	$c_{BESS,KW}$	$c_{BESS,KWH}$	c_{pv}	η_{rsoc}
1. Baseline	6.0	2000	15	361	273	1750	34.8
2. Allow large PV	12.0						
3. BESS cost low				318	210		
4. BESS cost high				404	336		
5. rSOC cost mid		1500					
6. rSOC cost low		750					
7. H_2 storage cost high			30				
8. H_2 storage cost low			10				
9. rSOC efficiency high							60.0
10. Scenarios 9 and 6		750					60.0
11. Scenarios 9, 6 and 8		750	10				60.0
12. Cheaper PV						1000	
13. Favourable BESS; unfavourable HESS			30	318	210		
14. Unfavourable BESS; favourable HESS		750	10	404	336		60.0
15. All favourable values		750	10	318	210	1000	60.0

5.3. Results

5.3.1. Case study

The microgrid considered in this work is notionally located in the SE of England, and consists of 100 houses with rooftop PV, as well as shared BESS and/or HESS. Electrical load data comes from a smart-meter trial in London carried out by UK Power Networks and has half-hourly resolution [209]. Domestic electricity load excluding EVs is 412 MWh annually, with peak half-hourly load of 103.4 kW. The addition of EVs as described in Section 5.2.5 adds 150 MWh / a, and increases peak load to 184.4 kW. Climate data was recorded by the UK Environmental Change Network at Rothamsted (near London) and has hourly resolution [28]. Installed PV has a capacity factor of 11.1% after allowing for diversity in orientation; so with 3 kW per household (the average installation size in the UK) annual generation is 291 MWh.

Each run of the simulation lasts for one year, beginning 1st May, which is the approximate time of year when typical PV systems begin producing a daily energy surplus for this location. Figure 5.3 compares the shape of the load (excluding EVs) with the solar resource, over one year.

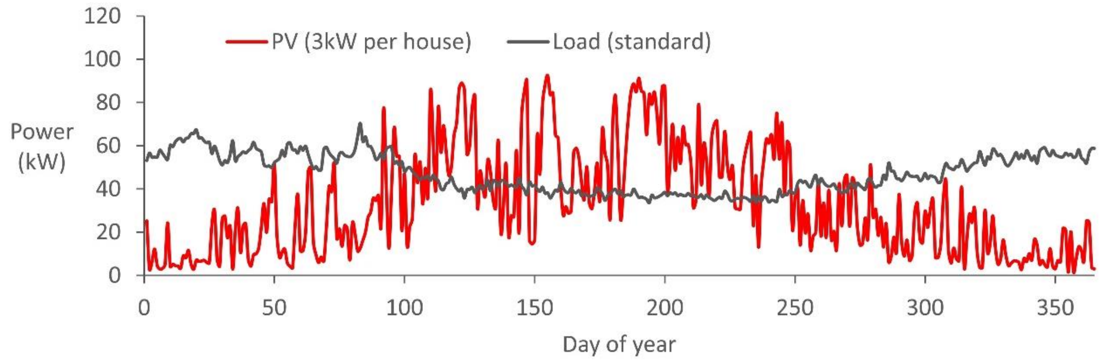

Figure 5.3. Contrast of electrical load with PV resource for the SE England location. (Daily resolution over one calendar year.)

5.3.2. Results of multi-objective optimisation

In all scenarios considered, BESS is installed by the optimiser in order to achieve the minimum SSR of 50%, and continues to be installed for all SSR up to the maximum achieved. For HESS, there is a higher threshold SSR above which installation of HESS becomes optimal, resulting in a hybrid energy storage system. The optimiser does not ever choose to install HESS without BESS. This threshold SSR tends to be around 60%, and in fact this value is relatively unchanging across almost all the different scenarios explored. Further, some of the variation that is seen is counterintuitive, suggesting that it should be regarded as noise. This threshold value is given in Table 5.5 for each of the scenarios. The table also gives the details for a microgrid design achieving 70% SSR in each scenario. Figures 5.4 and 5.5 show the Pareto front of payback time versus SSR for two of the scenarios, along with the CAPEX contribution per component. It is worth noting that the Pareto front appears chaotic at the highest SSR, but this may be due to shortcomings of the optimiser rather than a real effect.

The one scenario which does alter the 60% threshold is Scenario 2, in which a larger capacity of installed PV is permitted. In this case, energy storage with BESS alone is preferred right up to SSR of

80%. This is because significant overcapacity of PV can almost eliminate the seasonal deficit in generation. Thus, only the day night cycle, and shorter term weather fluctuations, need to be addressed by storage, and battery storage is preferred for these short term cycles. This agrees with our previous conclusion in [214]: overcapacity of generation is often cheaper than long term energy storage to achieve high SSR.

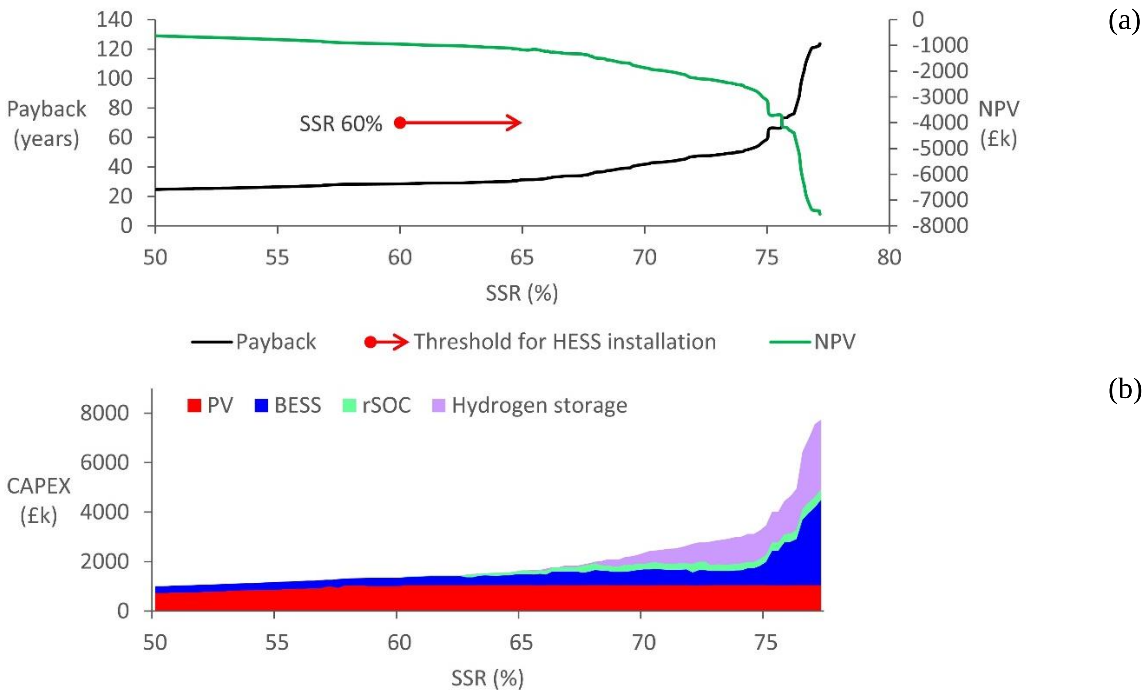

Figure 5.4. Results of multi-objective optimisation for Scenario 1 ('baseline'). (a) Pareto front for payback period against SSR, also showing NPV. (b) Contribution of each component to CAPEX cost.

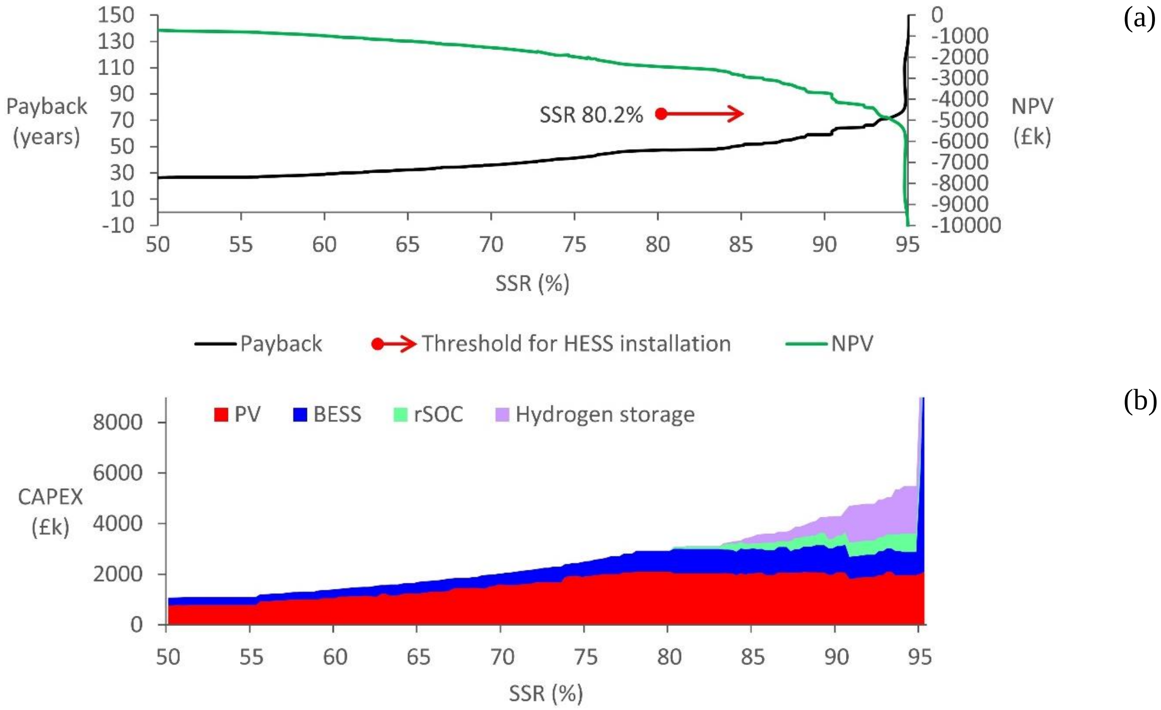

Figure 5.5. Results of multi-objective optimisation for Scenario 2 ('Allow large PV'). (a) Pareto front for payback period against SSR, also showing NPV. (b) Contribution of each component to CAPEX cost.

As will be seen from Figures 5.4 and 5.5, payback period rises and NPV falls as SSR increases. The payback time for the 60% SSR system in Scenario 1 (the first system to install HESS) is 28.5 years, longer than the expected system lifetime. The lowest payback time for a system with HESS installed is 15.9 years for a 58% SSR system under Scenario 15 (the most optimistic scenario). However, NPV is still negative (-£300k) for this system once OPEX and equipment replacement are accounted for. Indeed, negative NPV is found for all systems with SSR above 50%, even the BESS only systems. On this basis it cannot be concluded that the hydrogen storage with rSOC is an economical investment. Nonetheless, if high SSR is desired and overcapacity is not possible, it forms part of the cheapest possible microgrid design.

Another point worth highlighting is the size of H_2 storage required. For 70% SSR, this tends to be of the order 1000 kg (ca. 30 MWh, ca. 100 m^3), which is fairly substantial. The volume balloons quickly with increasing SSR; for Scenario 1, m_{full} = 948 kg for 70% SSR, and 2700 kg for 75% SSR. It is also worth commenting on the C-rates for the battery storage which tend to indicate discharge times between three and eight hours. These C-rates are easily achievable by the batteries and would enable smaller scale power electronics to be installed.

Table 5.5. Optimisation results for all scenarios. Shown is the threshold SSR above which the optimiser chooses to install HESS. Also shown are the details for a system with 70% SSR for each scenario (this includes HESS in all but one case) with the calculated NPV and simple payback time.

Scenario	Threshold SSR for HESS installation	Details for a 70% SSR system						
		P_{pv}	E_{BESS}	R_{BESS}	P_{SOEC}	m_{full}	NPV (£k)	Payback (years)
1. Baseline	60.0%	6.00	2001	0.15	116	948	-1904	42.3
2. Allow large PV	80.2%	9.09	1335	0.18	-	-	-1543	36.0
3. BESS cost low	58.2%	6.00	1898	0.13	143	802	-1702	39.0
4. BESS cost high	58.9%	6.00	1177	0.38	125	1287	-2093	44.3
5. rSOC cost mid	59.9%	6.00	1309	0.29	140	1040	-1822	40.1
6. rSOC cost low	62.0%	5.99	1721	0.20	137	860	-1675	38.4
7. H_2 storage cost high	59.3%	5.97	1314	0.21	171	1070	-2510	51.4
8. H_2 storage cost low	59.4%	6.00	1340	0.32	119	1155	-1729	38.6
9. rSOC efficiency high	68.5%	6.00	1978	0.10	143	287	-1547	36.8
10. 9 and 6	62.4%	6.00	1238	0.23	125	924	-1571	35.4
11. 9, 6 and 8	59.2%	5.95	1458	0.13	179	454	-1251	31.6
12. Cheaper PV	63.2%	6.00	1413	0.14	167	352	-1028	27.6
13. Favourable BESS; unfavourable HESS	64.7%	5.91	2644	0.20	141	873	-2029	43.5
14. Unfavourable BESS; favourable HESS	60.0%	6.00	2001	0.15	116	948	-1904	42.3
15. All favourable values	58.2%	5.75	1239	0.23	119	964	-841	23.4

5.4. Conclusions and future work

This work has considered the utility of hydrogen energy storage, using an rSOC, alongside Li-ion battery storage, to improve the self-sufficiency of a residential microgrid. Results suggest that such microgrids are not economical in terms of NPV. However, if high SSR is desired for greater grid autonomy or environmental credentials, the community energy storage becomes a cost optimal selection. In particular, hybrid energy storage with BESS + HESS is often the cheapest design once SSR above ca. 60% is required. The role of the HESS is then to engage in long duration storage cycles which can alleviate the seasonal mismatch between demand and solar generation (see Figure 5.3), whilst the battery carries out shorter term cycling with discharge duration invariably below ten hours. This threshold SSR is higher if there is an option to install larger PV systems (> 6 kW per house) which can start to obviate the winter deficit in generation.

This work still requires considerable further development. A priority is to improve the control strategy of EVs, so that charging is scheduled more intelligently; V2G may also need to be considered. These improvements should allow higher SSR perhaps with less community energy storage. Additionally, the possibility of distributing the rSOC's waste heat to supply the houses' thermal load will be investigated [220]. Since heat is generally a cheap commodity, distribution of heat is not expected to increase NPV much for a given microgrid design - but it would increase SSR. It is also possible that the value of the energy storage may increase if it can perform other applications, such as peak shaving, perhaps avoiding the need for distribution grid upgrades, or avoiding capacity charges - another topic for future work. Further work should also improve the accuracy of the rSOC model by accounting for energy consumption to sustain a 'hot idle' state.

Finally, it is intended to study more closely the interaction of households trading energy peer-to-peer, and the extent to which the energy storage could be financially beneficial to individual households.

5.5 Acknowledgements

Grateful acknowledgement is made of the financial support of the Engineering and Physical Sciences Research Council (EPSRC) in the form of the 'Energy Storage and its Applications' Centre for Doctoral Training under grant code EP/L0168/18; also of the Electric Power Research Institute.

This research makes use of data from the UK Environmental Change Network and UK Power Networks.

5.6 Appendix: Further details of EV model

The EV agents in Chapter 5 comprise the following key components: **trip schedule**, **trip statechart**, **battery model** and **charge schedule**.

The **trip schedule** is loaded as an AnyLogic Schedule object, which can robustly handle periodicity (weekly in this work), as well as details like Daylight Saving Time. Schedules specify the day and time of trip departure and arrival, as well as the trip distance and the classification of start and finish location. In this work, the trip schedule is viewed as deterministic, although stochastic elements could readily be introduced. The trip schedule can be disrupted if the EV battery runs out during a trip, causing a delay in the timings while rapid charging occurs. In the present work (chapters 5 – 7) trip schedules are constructed by sampling the UK National Travel Survey, as described in Section 5.2.5. Locations of cars in the sample over a seven day schedule are shown in Figure 5.7. Note the high proportion of time parked 'at home' – 78.7% in this sample, comparable to the 73% figure from the RAC [221].

The **trip statechart** monitors the status of the vehicle during simulation time (see Figure 5.6). It is responsible for controlling rapid charging if needed, and for triggering any other actions that are required on arrival or departure. Rapid charging is assumed to take place at 50 kW_{DC}, and ends when the battery is full, or when stored energy equals the requirement to finish the current journey, plus 25%. Note that the cars' actually geographic location / route is not considered important for this work and is omitted.

The EV **battery** is a sub-agent of the EV agent. The battery model is almost identical in construction to the model described in Section 4.2.4, although the rate of charge is typically limited by the capacity of charger connected, rather than by the inherent c-rate of the battery. Equation 4.5 from 4.2.4 can be rewritten as:

$$\dot{E}_{batt} = \eta_{batt} \cdot \eta_{ACDC} \cdot P_{ch} - \frac{v_{EV}}{FE_{EV}} - \Lambda \cdot E_{batt} \qquad [*]$$

where E_{batt} is the energy stored in the EV battery in kWh, P_{ch} is AC charge power in kW, v_{EV} is the speed in miles per hour (typically assumed constant for the duration of each trip), FE_{EV} is the fuel economy of the EV in miles per kWh, and Λ is the self-discharge rate with units h^{-1}. In Chapter 5, fuel economy is assumed constant; in Chapter 6 the model is improved by allowing for the effect of temperature (see Section 6.2.1).

Different approaches to **charge scheduling** are possible. In Chapter 5, a naïve approach is taken wherein cars plug in and charge until full as soon as they return home. In chapters 6 and 7, charging is scheduled according to the trades agreed in P2P electricity markets.

EV characteristics in Chapters 5 - 7 are based on the Nissan Leaf [222]. The diversity of behaviour across the modelled EV agents thus arises from their different trip schedules, since fuel economies and battery characteristics are assumed homogenous. Future work could allow for varying car / battery characteristics.

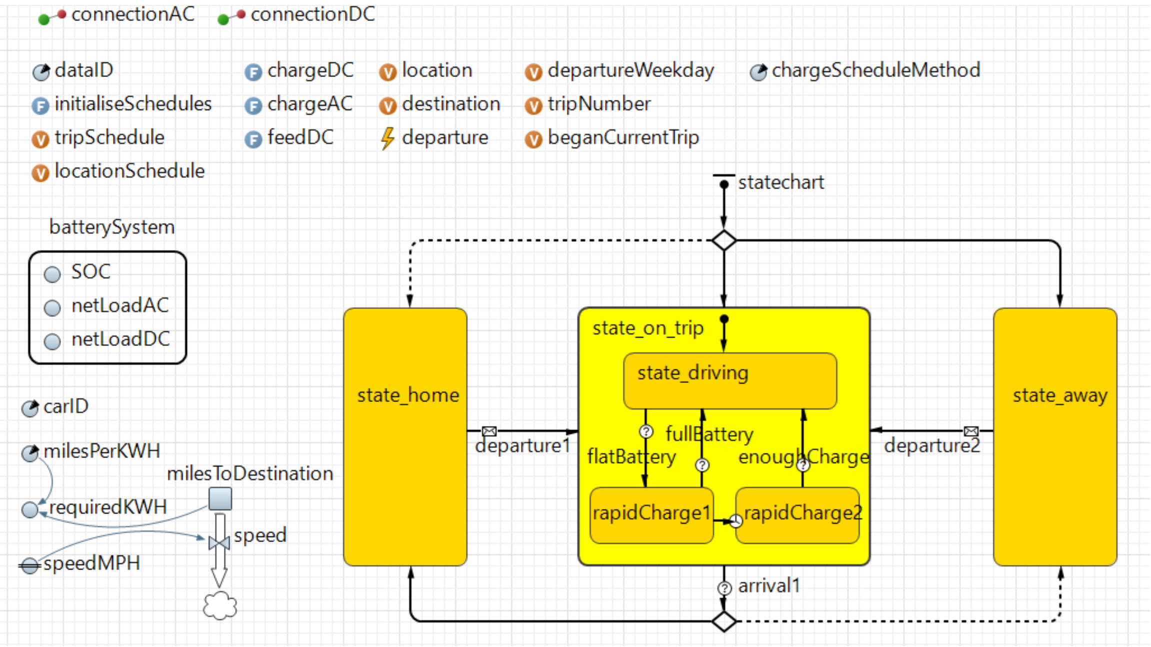

Figure 5.6. Main view of EV agent in AnyLogic, showing some of the key components.

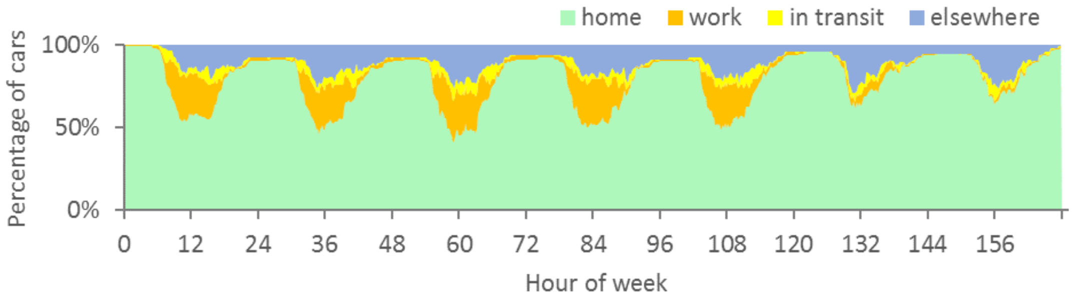

Figure 5.7. Locations of the cars from the NTS sample, across one week Monday to Sunday. Note the high proportion of time parked ‘at home’, suggesting the potential to synchronise some EV charging with solar generation.

6. Peer-to-peer electricity trading as an enabler of increased PV and EV ownership

Timothy D Hutty[a], Alejandro Pena Bello[b], Siyuan Dong[a], David Parra[b], Rachael Rothman[a], Solomon Brown[a]*

[a]*Department of Chemical and Biological Engineering, University of Sheffield, UK*
[b]*Energy Efficiency Group, Institute for Environmental Sciences, University of Geneva, Switzerland*

Abstract

Peer-to-peer (P2P) energy trading enables households to trade electricity with one another, rather than just with their supplier. This can help to incentivise the shifting of electrical loads to align with local renewable generation, which leads to decreased dependence on grid electricity and can bring financial savings for households. P2P is expected to be particularly suitable to complement embedded PV generation and electrical vehicles (EVs), two key technologies for grid decarbonisation. In this work we simulate P2P energy sharing for a local microgrid of 50 households with PV and EV ownership at various penetrations. In particular, we consider the merits of P2P in combination with uni-directional EV chargers ('V1G), and with chargers that can discharge EV battery energy to the home ('V2H') or the grid ('V2G'); we also consider the use of community energy storage ('CES') as an alternative to storage of energy in EV batteries. We simulate the interactions of the households with the P2P energy market over one week, for each of three seasons, and evaluate the microgrid's energy independence and the financial savings for households. Results suggest that P2P trading with V1G can effect an increase in shared energy, modest improvements to microgrid self-sufficiency, and improvements to household bills. However, the combination of P2P with V2H brings advantages substantially greater than either innovation individually. The typical household can save approaching £100/a (compared to an average bill of ca. £540 with no P2P), with savings exceeding £200/a in some situations. Importantly, we find that the P2P can achieve savings regardless of technology penetration, and furthermore, all types of household can benefit, including households that own both PV and EV. Under the market mechanism considered, we find only negligible impact for allowing V2G in addition to V2H.

Keywords: Peer-to-peer electricity trading; vehicle-to-house V2H; vehicle-to-X V2X; solar PV; microgrid; community energy storage

*Corresponding author.
E-mail address: s.f.brown@sheffield.ac.uk

6.1. Introduction

6.1.1 Outline and key definitions

Two significant aspects of energy decarbonisation that impact the electricity grid at a local level are the proliferation of embedded renewable generation (especially PV) and the electrification of transport. In the UK there are currently almost a million small scale solar PV installations, still leaving immense scope for growth [223]; and whilst electric vehicles (EVs) currently account for around 1% of vehicles on UK roads, the government plans to impose a ban on combustion vehicles by 2030 [224], [225] and it has been suggested that the UK fleet will need to be 55% electric by that date [225]. These technologies come with challenges and opportunities. High take-up of EVs will require considerable extra electrical energy for charging, and existing distribution grid infrastructure may struggle to meet peak charging demand [140]. Meanwhile, solar PV is a fluctuating, non-dispatchable resource, and generation is not guaranteed to align well with electrical demand (self-consumption for a UK household is typically below 50% annually [141]). Exports of solar power from multiple houses simultaneously pose a threat to distribution grids, potentially giving rise to voltage violations and line overload [142].

Clearly, PV and EVs offer a potential synergy, with EV batteries absorbing surplus power from nearby PV installations. However, the conventional energy system, wherein households can only trade power with their electricity supplier, provides no incentive for this (unless PV and EV are behind the same meter) [8], [226], [227]. The formation of local energy communities, with energy traded between households (as for instance in [8], [174]) could help to address this. An EV using a neighbour's surplus energy to charge would need to pay a price above the supplier's feed-in tariff but below the retail electricity price; both parties to the transaction would then benefit. We term such an exchange of energy a peer-to-peer (P2P) trade. As well as bringing financial savings, communities with P2P trading can achieve environmental benefits and reduce stress on the distribution grid [8], [147].

'Smart' scheduling of EV charging (for instance, to absorb renewable generation as described above) is generally termed V1G, denoting a one-way flow of power from grid to vehicle [228]. If a two-way charger is available, the vehicle can also discharge power to supply its own household (vehicle-to-home, V2H) or to export (vehicle-to-grid, V2G); the EV thereby becomes an energy storage device, shifting renewable energy to the time when it is required [228].

This work considers the benefits of P2P in combination with PV and V1G/V2H/V2G, in a local community of residential households. We will refer to this community as a 'microgrid', the term commonly applied to a local group of electrical loads and generation capable of a degree of autonomy from the main grid. We combine a realistic model for EV usage with a simulation of an iteratively settled P2P market. We compare the relative merits of V1G, V2H and V2G, evaluating performance in terms of the savings achieved by households, as well as the increased energy autonomy of the microgrid as a whole. Additionally, we consider the combination of the P2P market with community energy storage (CES) as an alternative to the use of EV batteries for energy storage.

The remainder of this section will discuss existing work on P2P energy trading, and V2H/V2G.

6.1.2 P2P energy markets

In traditional energy systems, households are purely consumers of energy, which is bought exclusively from a large-scale supplier; thus P2P energy trading represents a disruptive shake-up of this paradigm. Whilst in its strictest sense, P2P refers to trades of energy that are negotiated bilaterally between parties, here we use the term in its broader sense to denote any energy tariff or market that can incentivise and remunerate the sharing of electricity between households, a definition consistent with [8], [174]. Interest in P2P is growing, with companies including Centrica and EDF carrying out pilot schemes in recent years [143], [144]; a number of platforms for the P2P exchange of energy have also been designed, including among others Piclo and Vandebron [229].

In terms of the actual market mechanism through which P2P exchange of power is agreed and paid for, the literature covers a number of different possibilities. These include **centralised control**; **centrally issued price signals**; **auctions** and **iterative markets** – where these categories are not exhaustive and may also overlap. Under **centralised control**, optimisation is carried out centrally to determine which microgrid participants should trade energy, and how all the microgrid's flexible devices are to be scheduled. For instance, in [153] central optimisation is used to determine P2P energy trades between EVs. Centralised control raises concerns about participants' privacy and autonomy, and may also be computationally intensive unless the number of devices is small. Several researchers [148]–[151] pose a centralised optimisation problem, before going on to discuss distributed optimisation methods whereby participants need not surrender as much control or data. Another approach is for microgrid participants to retain full autonomy and plan their behaviour in response to **centrally issued price signals**. The problem then is for the operator to set the best prices to incentivise desirable behaviour; this problem may be interpreted as a Stackelberg game as in [155], [156], whilst in [154] a reinforcement learning approach is used. A natural approach to P2P markets is through the use of **auctions** – which may be designed to emulate traditional energy markets, as in

[157]. Double auctions, wherein buyers of energy submit ‘ask’ prices and sellers submit ‘bid’ prices are typically of most interest. In an auction market the chief problem is for individual participants to set their strategies intelligently; the literature includes approaches such as adaptive learning [159], the adaptive aggressive strategy [160], ‘eyes on best price’ [158] and ‘zero intelligence’ [158]. Literature covering P2P electricity auctions with flexible loads includes [147], [161]. In **iteratively settled markets**, feedback from each round of bidding is used by participants to update their new bids, and the market is settled if and when it converges, otherwise requiring an exit mechanism of some kind. Iterative market mechanisms of various kinds are employed in [8], [148], [158], [173], [174].

Liu et al [174] contrived an iterative pricing mechanism for an energy-sharing zone consisting of buildings with PV generation and some adjustable loads. The internal tariffs for import and export of power were functions of the supply-demand ratio (SDR), i.e. the total of all exported power over all buildings, divided by the total of imported power. As such, this pricing mechanism will henceforth be referred to as the SDR tariff; it is the mechanism adopted in the present work. When SDR > 1, prices are low (equal to the grid feed-in tariff), incentivising demand to be increased or supply reduced. For SDR < 1, prices increase towards the cost of grid power, incentivising demand to be reduced or supply increased. Prices are designed so that the operator operates a balanced budget – i.e. all payments effectively flow between households and the utility grid, or between different households, with the operator not profiting. The final prices and load schedules are decided iteratively; in each round, participants optimise their load schedule relative to the most recently issued internal prices. The process repeats until convergence is achieved: viz. prices do not significantly change between iterations. In [174], this market mechanism was implemented in a case study with a number of residential and commercial/office buildings, and was found to achieve modest technical and economic benefits. Zhou et al [8] also consider the SDR tariff. This work was focused on (i) possible approaches to improving the convergence of the iterative market mechanism; and (ii) the comparison of the SDR tariff to alternatives (mid-market rate and bill-sharing). Simulations involved 20 households equipped with PV and flexible loads, with one day simulated at a time. Flexible loads considered were water heaters and washing / drying machines in addition to EVs. The methods to improve convergence were found to be effective, and the SDR pricing tariff was considered to outperform the alternative pricing formulas.

In this work the SDR tariff with iterative bidding is adopted. Reasoning for this choice is as follows:

(i) The approach is amenable to use with energy storage. By contrast, strategies for energy storage in auction markets can be complex, and the auctioneer may need to process complex bids (as also in large scale power markets [230]).

(ii) Fairness: all households are offered the same prices at each timeslot.[1]

(iii) Autonomy: except for the constraints imposed by the convergence aids, houses are free to optimise their schedules in their own interests.

(iv) Confidentiality: only the planned net power of a household needs to be shared with the market, and no other details.

6.1.3 EVs in P2P power markets

Existing studies on P2P markets are often preoccupied with demonstrating the feasibility of a particular market mechanism; they tend to confine themselves to small scale, ‘proof-of-concept’ case studies. These may involve various different technologies, as shown in Table 6.1. The use of flexible load (either in the abstract, or pertaining to appliances like washers/dryers) in case studies is more

[1] This might be considered a limited definition of fairness; some further discussion of the distribution of benefits is found in Section 6.3.2.

common than either EVs or energy storage. Kim et al [173] performed a case study with eight households, with a mixture of EVs of three types – capable of V2H, V2G, or V1G only. PV generation was not included. El-Baz et al [147] carried out a case study for their double auction model, wherein ten households all possess PV, an EV and a heat pump; household savings up to 23% were achieved. Zhang et al [161] carried out a study where 10 PV systems were matched with 100 flexible loads including EVs. The emphasis of this work was the use of flexibility to address inaccuracy in PV forecasting; it was found that 78% of forecasting error was able to be absorbed locally in the case study. V2H/V2G were not considered. Alvaro-Hermana et al [153] considered the P2P exchange of power between EVs in Belgium, employing a detailed data-driven model for EV power consumption and availability. For those EVs requiring charging during the daily travel schedule, costs were reduced by 71%. Renewable generation was not modelled: the motivation to trade relied on a time-variable grid tariff. Finally, Zhou et al [8], as already noted, include EVs in their work comparing the SDR tariff to alternatives. This work is more far-reaching in its consideration of EVs than previous references; in particular, it includes sensitivity analysis of EV and PV technology penetration in the community of 20 households. This work does not, however, discuss possible household savings in absolute terms. Also, although V2H/V2G are available to the EVs in the model, the paper does not discuss the value of these options versus V1G.

Table 6.1. Aspects included in P2P studies from the literature. N.B. This signifies whether such aspects have been used in an actual case study, not whether the P2P system could theoretically accommodate them.

Reference(s)	Aspects modelled					
	P2P / local energy market	Flexible load	PV	Stationary energy storage	EV	V2H/V2G
[148], [154]–[156]	✓	✓	-	-	-	-
[159]	✓	-	-	✓	-	-
[153]	✓	-	-	-	✓	✓
[173]	✓	✓	-	-	✓	✓
[231]	✓	✓	✓	✓	-	-
[166], [232]	✓	-	✓	✓	-	-
[149], [233]	✓	✓	✓	-	-	-
[158]	✓	-	✓	-	-	-
[161]	✓	✓	✓	-	✓	-
[147]	✓	✓	✓	✓	✓	-
[8]	✓	✓	✓	-	✓	✓

6.1.4 Contribution of this work

The aim of this work is specifically to consider the possible advantages of a P2P energy market to complement PV generation and EVs, in the setting of a community of households forming a grid-connected microgrid. For this purpose, we adopt the SDR tariff introduced in [174]. We are interested in quantifying the possible real-world financial benefits for households, as well as the impact on the microgrid's overall energy autonomy. Additionally, since community energy storage (CES) has been proposed in the literature as an interesting alternative to household level energy storage [234], [235], we introduce shared CES as an alternative / complementary technology, and compare this to the use of the EV batteries for energy storage.

This paper's contributions can be summarised as follows:

- Comparison of the impact of V1G, V2H and V2G operating within a P2P energy sharing market, which to the authors' knowledge has not been addressed before.
- Estimation of annual savings for households (rarely covered by existing work), and comparison between households of different categories.
- Adaption of the SDR market mechanism to work in tandem with community energy storage (CES); comparison of CES to V2H / V2G.

6.2. Method

6.2.1 Model overview

In this work we model an energy community consisting of a number of households. These are assumed to be proximately located and to share the same distribution transformer, so as to form a grid-connected microgrid. The houses may each own an EV and / or a PV system. We consider different combinations of a P2P tariff with the options of V1G, V2H and V2G, and compare these to a baseline with the standard grid tariff. We also consider the use of the P2P tariff in tandem with CES. This forms an interesting comparison with the use of EV batteries for energy storage: the latter are dispersed, sometimes unavailable, and under the direct control of a subset of individual households; whereas the former is always available, and interacts with all the households via the market. Figure 6.1 gives a high-level schematic of the model.

The various sub-models will now be discussed.

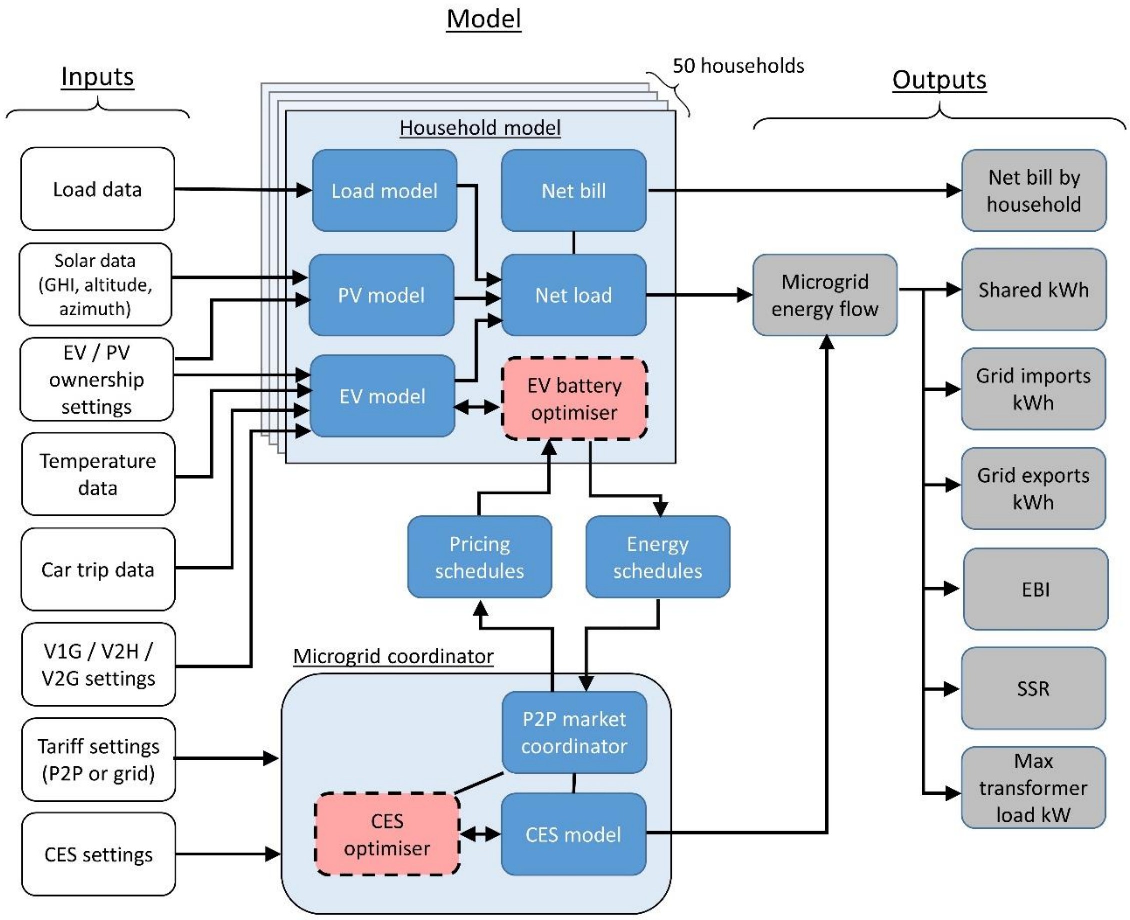

Figure 6.1. Overall schematic of model. All model aspects are implemented in AnyLogic [48], except optimisers which use Pyomo [236], [237] with the GLPK solver [238]. Key to note is the exchange of information between the coordinator and the households: the coordinator sends prices and receives energy schedules back.[2]

[2] The ‘coordinator’ is regarded as running all centralised activities of the microgrid, including CES if any. In the simplest case the coordinator is simply software which mediates the P2P market. It is not specified in this work which real life parties would take on these activities; it could be the energy supplier, the DNO or some kind of energy cooperative.

6.2.1.1 Solar model

The solar model utilised here is reported in [214], and uses measured data for global horizontal irradiance to predict the radiation incident on an inclined plane. A constant efficiency of 15.4% is then applied to calculate generation; this efficiency is calibrated so that a south-facing system with 40° tilt, located in the London area, would have capacity factor of 11.8% [202].

6.2.1.2 EV model

EVs in the model follow week-long travel schedules recorded in the UK National Travel Survey, 2017 – 2019 [216]. The survey includes 27,516 vehicles for these years. Here, we restrict to cars belonging to single-car households in an urban location, of which there are 8,948. Further, we restrict to vehicle schedules that can be completed by EVs with a 30 kWh battery and 7.2 kW charger, assuming a constant fuel economy of 3.75 miles/kWh: this is 7,769 vehicles. The final sample of vehicles is then taken as a stratified sample by number of trips in the week (vehicles with data inconsistencies are excluded). It is worth noting that around 18% of vehicles make no trips at all over the course of a week.

Table 6.2. Details of vehicle sample.

Sample	Number of vehicles	Distance driven (miles)		Trips taken	
		Mean	Median	Mean	Median
Urban cars	21,189	99.7	63.7	12.4	12
Urban cars, one car household	8,948	94.7	61.5	13.3	12
Urban cars; one car household; viable for 30 kWh EV battery	7,769	84.0	54	12.2	11
Final sample	50	78.1	53.3	12.4	12

The 30 kWh Nissan Leaf is taken as the template for the modelled EVs. It is assumed that actual available battery capacity is 28.5 kWh, and that average fuel economy is 3.75 miles / kWh [222], [239]. This fuel economy is then adjusted according to the temperature, as shown in Figure 6.2.

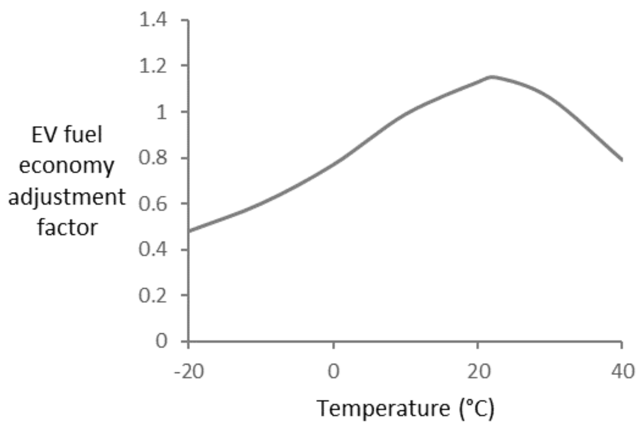

Figure 6.2. Adjustment to EV fuel economy according to outdoor temperature [239].

We use the same trip schedules regardless of the time of year, as the seasonal variation of weekly mileage / number of trips in the source data is negligible. The significant seasonal effect comes via the impact of temperature on fuel economy, rather than vehicle usage.

V2X efficiency

In this work we allow for energy losses of 5% for power conversion between AC and DC, and for 6% losses from the battery itself [192], [193]. Thus, the V2G storage efficiency is 84.9%. Although [240], [241] suggest that V2G round-trip efficiency may only be 50 – 70%, experimental work published more recently by Schram et al [242] suggests a range of 79.2 to 87% is realistic. Schram et al also found that the effects of state-of-charge or temperature on charging efficiency are relatively small, so these are neglected here.

6.2.2 Microgrid internal pricing and iterative bidding process

For this work, we adapt the P2P mechanism laid out in Liu et al [174]. This is not a P2P mechanism in the strictest sense (trades that are negotiated bilaterally) but in the broader sense that it incentivises and remunerates power sharing between peers. Houses receive prices from the microgrid coordinator and plan their battery schedules accordingly. The new energy schedules are submitted to the microgrid operator, and new prices are calculated. The process iterates until convergence is achieved (or the maximum number of iterations is reached). The microgrid operator operates a balanced budget. Details of the process will now be given.

6.2.2.1 Pricing formula

The prices for household import and export of power are set according to the SDR formula [174]. Eqns. 6.1 – 6.5 give the details. If $E_{h,t}$ is the net energy flow for household *h* during time period *i*, then the total of all household energy surpluses is:

$$E_{surplus,i} = \sum_{h \epsilon H} max\left(0, E_{h,i}\right) \qquad \text{(Eqn. 6.1)}$$

whereas the total of energy deficits is:

$$E_{deficit,i} = \sum_{h \epsilon H} max\left(0, -E_{h,i}\right) \qquad \text{(Eqn. 6.2)}$$

The supply demand ratio may then be defined:

$$SDR_i = \frac{E_{surplus,i}}{E_{deficit,i}} \quad \text{(Eqn. 6.3)}$$

The prices that will be applied to the households' bills are then calculated in terms of the SDR, and fixed costs π_{high} and π_{low} in £/kWh [174]:

$$\pi_{export}(SDR_i) = \begin{cases} \frac{\pi_{high} \cdot \pi_{low}}{(\pi_{high} - \pi_{low}) \cdot SDR + \pi_{low}} & , SDR < 1 \\ \pi_{low} , & SDR \geq 1 \end{cases} \quad \text{(Eqn. 6.4)}$$

$$\pi_{import}(SDR_i) = \begin{cases} SDR \cdot \pi_{export} + (1 - SDR) \cdot \pi_{high} & , SDR < 1 \\ \pi_{low} & SDR \geq 1 \end{cases} \quad \text{(Eqn. 6.5)}$$

In general, π_{high} and π_{low} are respectively equal to the retail price and the feed-in tariff, that is, $\pi_{grid,imp}$ and $\pi_{grid,exp}$; however, they may take different values when CES is used, as detailed below. Note that, as SDR rises to 1, import and export prices fall towards π_{low}, whereas they rise towards π_{high} when SDR approaches 0.

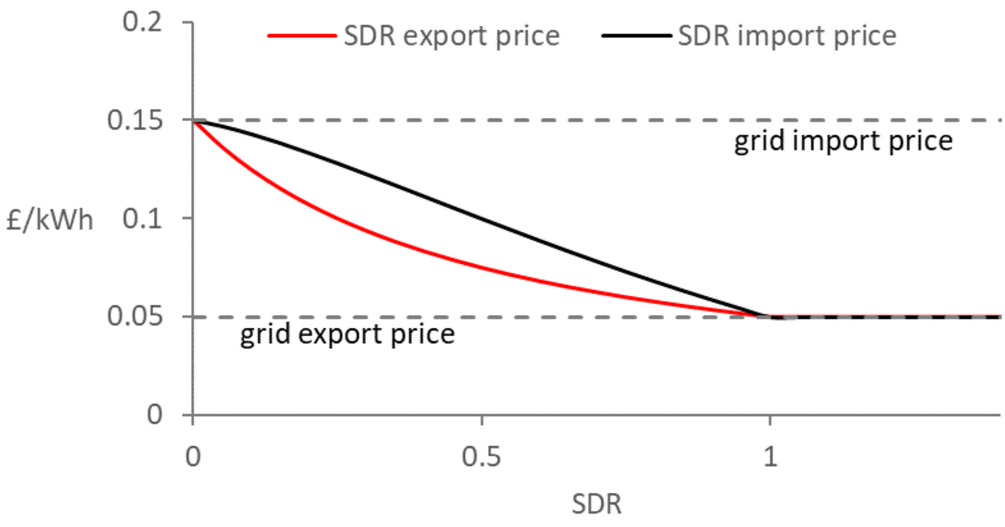

Figure 6.3. Internal microgrid prices as a function of SDR.

6.2.2.2 Iterative bidding process

The P2P market in this work is for periods of one day at half hour resolution. Days run from 5.30am, since very few cars have trips earlier than this; this time can be regarded as the 'beginning of the EV day'. *k* is used to index the iterations of the bidding process, whereas *i* is used to index the day's 48 time periods. Thus, $E_{h,i}^{k}$ is the signed net energy production of house *h* for time interval *i*, as scheduled at iteration *k* of the market mechanism (where a positive sign indicates power export).

$SDR_{PRE,i}^{k}$ is the SDR corresponding to the prices issued to households for bidding round *k*. $SDR_{POST,i}^{k}$ is the SDR resulting from the re-optimisation of household schedules at round *k*.

For each household, $E_{h,i}^{0}$ is initialised according to the inelastic demand $E_{load,i}$ and generation $E_{PV,i}$, i.e.

$$E_{h,i}^{0} \; = \eta_{inv} \cdot E_{PV,i} - E_{load,i} \qquad \text{(Eqn. 6.6)}$$

(η_{inv} represents the efficiency of the household's inverter.) From this, $SDR_{PRE,i}^{1}$ can be calculated, and hence prices $\pi_{import,i}^{1}$, $\pi_{export,i}^{1}$. For each subsequent iteration, $k \geq 1$, each household with an EV optimises its EV battery schedule in response to the latest prices $\{\pi_{export,i}^{k}, \pi_{import,i}^{k}\}$. The optimisation model employed by households uses MILP and is detailed in Section 6.2.5. The new values of $E_{h,i}^{k}$ are then used to calculate the resulting supply demand ratio $SDR_{POST,i}^{k}$.

For the next round, $SDR_{PRE,i}^{k+1}$ is calculated as

$$SDR_{PRE,i}^{k+1} = 0.5 \cdot SDR_{PRE,i}^{k} + \; 0.5 \cdot SDR_{POST,i}^{k} \qquad (\forall k \geq 1) \qquad \text{(Eqn. 6.7)}$$

An alternative would be to set $SDR_{PRE,i}^{k+1} = \; SDR_{POST,i}^{k}$ as in [174] but we find that the approach given in Eqn. (6.7) can achieve better convergence. New prices are then calculated according to the SDR and the iteration continues. To improve convergence, we impose a maximum adjustment ΔE_{max} to the net household energy flow at each time interval; this applies from the second iteration onward, and the value of ΔE_{max} is reduced in subsequent rounds:

$$\left|E_{h,i}^{k} - \; E_{h,i}^{k-1}\right| \leq \Delta E_{max,k} \coloneqq \begin{cases} 0.5\ \text{kWh} & , \quad 2 \leq \text{k} < 6 \\ 0.1\ \text{kWh} & , \quad 6 \leq \text{k} < 12 \\ 0.05\ \text{kWh} & , \quad 12 \leq \text{k} \end{cases} \qquad \text{(Eqn. 6.8)}$$

6.2.2.3 Convergence criteria

Satisfactory convergence is considered to be achieved at round $\hat{k}$ if the following hold:

1. SDR has converged to a fixed point so that values before and after the round of optimisations are close:

$$\left|SDR_{PRE,i}^{\hat{k}} - SDR_{POST,i}^{\hat{k}}\right| < 0.02 \qquad \text{(Eqn. 6.9)}$$

2. No household has incremented its energy flow by the maximum permitted amount, and in the same direction, for two consecutive steps. This can be expressed as:

$$\left(E_{h,i}^{\hat{k}} - E_{h,i}^{\hat{k}-1}\right)\left(E_{h,i}^{\hat{k}-1} - E_{h,i}^{\hat{k}-2}\right) < 0.05^2, \quad \forall h, i \qquad \text{(Eqn. 6.10)}$$

When convergence is achieved, households are committed to the energy bids submitted at the last iteration. The final prices will be calculated according to $SDR_{POST,i}^{\hat{k}}$. If convergence has not been achieved after 25 iterations, the prices and schedules for the 25th iteration are implemented.

6.2.2.4 Adaption of process for community energy storage

When CES is present, it is scheduled by the microgrid operator to benefit the whole microgrid as a collective. The iterative bidding process is adapted to incorporate CES as follows. At each iteration, dispatch of the CES is optimized immediately after households submit their own newly optimised schedules. The objective function for minimisation is the total cost of energy exchanged with the grid, plus a penalty term to encourage peak shaving:

$$\sum_i \left\{-\pi_{grid,exp} \cdot max\left(E_{CES,i} + \sum_h E_{h,i}, 0\right) + \pi_{grid,imp} \cdot max\left(-E_{CES,i} - \sum_h E_{h,i}, 0\right)\right\}$$
$$+ \pi_{capacity} \cdot max_i\left(2\left|E_{CES,i} + \sum_h E_{h,i}\right|\right) \qquad \text{(Eqn. 6.11)}$$

where $E_{CES,i}$ is the net energy from the CES at time interval i (with positive sign corresponding to energy generation) and $\pi_{capacity}$ is a nominal cost per kW for the peak usage of the grid connection (N.B. this does not actually form part of the retail tariff).

The contribution of CES is excluded from the calculation of SDR as specified in Eqn. 6.3. The discharge of CES does not make energy cheaper to buy for households at the specific time it occurs (conversely, when the CES charges, the households do not get an increased export tariff at that specific time). Instead, the value gained by use of the CES is distributed to households throughout the day, by adjusting the value of π_{high} and π_{low} in Eqns. 6.4 and 6.5:

$$\pi_{high} = \pi_{grid,imp} - \lambda$$
$$\pi_{low} = \pi_{grid,exp} + \lambda \qquad \text{(Eqn. 6.12)}$$

The value of λ is chosen to ensure that the microgrid operator has a balanced budget – i.e. net cash flow of zero for the day. Prices for the next bidding iteration are then calculated as per Eqns. 6.12, 6.4

and 6.5. This approach ensures that the dispatch of CES is not detrimental to the convergence of the bidding process.

6.2.3 Case study

We consider a grid-connected microgrid consisting of 50 households, notionally located in the south-east of England. The number of households is intentionally larger than in most previous literature; this is to help ensure that the model captures the diversity between demand profiles and vehicle schedules for different households, since such diversity is a motivating factor for P2P. These households are assumed to share a single distribution transformer, and may each have an EV, a 3 kW PV installation, or both. 3 kW is the average capacity for small-scale solar installations in the UK [223]. The houses' basic electrical load comes from half-hourly measured data recorded by UK Power Networks in 2013 [209]. Measured irradiance data used for the PV model was recorded at Rothamsted in 2013, by UK Environmental Change Network [243]. PV systems are assumed to be split roughly evenly between south-facing, east-facing and west-facing systems; tilt angle of 40° is assumed in each case. The retail price of electricity is assumed to be £0.15/kWh and the feed-in tariff £0.05/kWh. Sizes of CES considered are 100 kWh, corresponding to ca. five hours of storage with respect to the load, and 500 kWh, corresponding to roughly a day of storage.

6.2.3.1 Representative climate weeks

We simulate the microgrid over one week for each of three seasons, with low, medium and high irradiance. Thus, 21 days are simulated overall (more than in most extant work), enabling estimation of annual performance. Details of the representative weeks are given in Table 6.3. Estimation of annual household savings is done by assuming 52 weeks to a year, and giving double weighting to the Autumn week. This weighting corresponds to annual insolation of 982 kWh / m^2, which is reasonable given that insolation for Southern England is typically 950 – 1100 kWh / m^2 / a (equivalently, 108 - 126 W/m^2) [244].

Table 6.3. Representative weeks for three seasons.

Season	Dates	Average irradiance (W/m^2)	Load excluding EVs (kWh/house/day)	Weighting
Winter	23rd – 30th Nov 2013	26.3	13.7	0.25
Autumn	22nd – 29th Sept 2013	97.7	10.0	0.5
Summer	4th – 11th June 2013	226.7	10.0	0.25

6.2.3.2 Systems and scenarios

We compare seven different microgrid setups, or ‘systems’; these are shown in Table 6.4. G_V1G is the baseline system, whereby households are billed according to the grid tariff. EVs cannot engage in V2H or V2G; however, households with an EV and PV can optimise EV charging against their own generation. Subsequent systems allow different combinations of tariff with V2H or V2G. Note that all EV households are assumed to have the same capability regarding V2H / V2G. In the final two systems, CES sized at respectively 100 kWh (ca. five hours of storage) and 500 kWh (ca. one day of storage) is used for energy storage, but there is no V2H or V2G.

Table 6.4. Microgrid systems.

System name	Description
G_V1G	Grid tariff; V1G.
G_V2H	Grid tariff; V2H.
P2P_V1G	P2P tariff; V1G.
P2P_V2H	P2P tariff; V2H.
P2P_V2G	P2P tariff; V2G.
P2P_CES_100	P2P tariff; V1G, community energy storage 100 kWh
P2P_CES_500	P2P tariff; V1G, community energy storage 500 kWh

We consider penetrations of EV and PV ownership of 10%, 20%, 40%, 60%, 80% and 90%, so that there are 36 penetration scenarios overall. We do not consider 0% or 100% penetration, since it is more interesting to observe the performance of households that are in a minority, rather than completely eliminate a type of household. For some of the analysis in Section 6.3, we also group aggregate scenarios into four quadrants Q1 – Q4; see Figure 6.4.

Penetration scenarios assume that EV and PV ownership are statistically independent. Thus, for instance, if EV and PV penetration are respectively 60% and 20%, then 12% of houses will have both technologies.

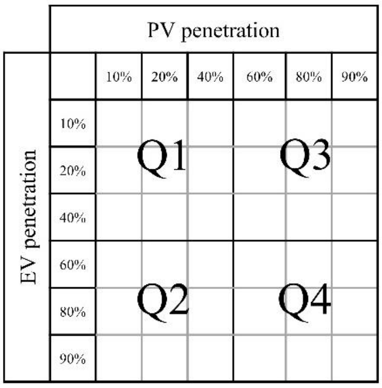

Figure 6.4. Shows the 36 technology penetration scenarios. These are also grouped into four quadrants Q1 – Q4.

6.2.4 Performance metrics

Self-sufficiency ratio (SSR) is defined as the proportion of load which is procured locally within the microgrid, i.e. not procured from grid imports. As such this provides a measure of the microgrid’s energy independence, and a rough indication of emissions curtailment:

$$SSR = \frac{total\ energy\ consumed - total\ grid\ imports}{total\ energy\ consumed} \quad \text{(Eqn. 6.13)}$$

Here, ‘total energy consumed’ includes energy charged to cars, as well as energy required for the basic household load.

Energy balance index (EBI) is a measure introduced in [8]. Like SSR, it is a measure of grid independence, but penalises exports to the grid as well as imports:

$$SSR = 1 - \frac{total\ grid\ imports + total\ grid\ exports}{total\ energy\ consumed + total\ energy\ generated} \quad \text{(Eqn. 6.14)}$$

We also consider the total energy shared between households:

$$total\ shared\ energy = \sum_i min\left(E_{surplus,i}, E_{deficit,i}\right) \quad \text{(Eqn. 6.15)}$$

We also consider the maximum power flow through the transformer at the microgrid’s grid coupling in either direction. The grid connection is assumed to balance the microgrid’s net energy demand, whenever sharing energy / CES cannot wholly do so.

6.2.5 Optimisation of a household’s EV dispatch

The optimisation model employed by households for scheduling of EV batteries is based on the ‘BASOPRA’ model reported in [190]. The model has been adapted to represent an EV battery by introducing parameters to represent battery availability and battery discharge to the EV. Unlike in [190], the battery may be permitted to export power to the grid. Additional constraints can also impose a minimum state-of-charge for the battery at the end of the optimisation time frame (one day), and a minimum state-of-charge at which V2X can take place. A variable is also introduced to allow rapid charge of EV batteries while the car is away from home. This energy is priced at £0.30/kWh [245], [246]. The availability of rapid charge ensures that individual optimisations are always feasible, although the high cost of this energy means that use of rapid charging will always be as minimal as possible. Optimisation is conducted using the GLPK solver.

Table 6.5. Nomenclature for EV battery optimisation

Description	Symbol	Unit	Set, or default value
Optimisation parameters			
Time parameters			
Time instant	t	-	$T = \{0,1, \ldots 48\}$
Time step	i	-	$I = \{1,2, \ldots 48\}$
Length of time step	dt	hours	0.5
Settings			
Permit EV battery discharge (V2X)	B_{V2X}	-	$\{0, 1\}$
Permit household power export	B_{exp}	-	$\{0, 1\}$
Valuation of final energy stored	π_{final}	£ / kWh	0.06
Price for rapid charge during trip	$\pi_{rapid,i}$	£ / kWh	0.30
Capacity tariff	$\pi_{capacity}$	£ / kW	0
Battery and inverter			
Battery nominal capacity	C_{batt}^{nom}	kWh	30
Battery DC efficiency	η_{batt}	-	0.94
Battery initial energy stored	E_{stored_init}	kWh	$[0, \infty)$
Minimum final energy stored	$E_{stored\_\min\_final}$	kWh	$[0, \infty)$
Minimum battery energy for V2X	$E_{stored\_\min\_V2X}$	kWh	$[0, \infty)$
Battery maximum charge power	$P_{max-char}$	kW	7.2
Battery maximum discharge power	$P_{max-disch}$	kW	7.2
Battery maximum state of charge	SOC_{max}	-	0.95
Batter minimum state of charge	SOC_{min}	-	0.05
Inverter efficiency	η_{inv}	-	0.95
Inverter power	P_{inv}	kW	10
Time series inputs			
Price for household power import	$\pi_{import,i}$	£ / kWh	$[0, \infty)^{\|I\|}$
Price for household power export	$\pi_{export,i}$	£ / kWh	$[0, \infty)^{\|I\|}$
Household load	$E_{load,i}$	kWh	$[0, \infty)^{\|I\|}$
PV generation	$E_{PV,i}$	kWh	$[0, \infty)^{\|I\|}$
Energy required for driving	$E_{drive,i}$	kWh	$[0, \infty)^{\|I\|}$
Availability of EV battery	α_i	-	$[0, 1]^{\|I\|}$
Optimisation decision variables			
Energy stored in battery	$E_{stored,t}$	kWh	$[0, \infty)^{\|T\|}$
DC kWh for battery charge	$E_{char,i}$	kWh	$[0, \infty)^{\|I\|}$
DC kWh from battery discharge	$E_{disch,i}$	kWh	$[0, \infty)^{\|I\|}$
Binary variable for battery charge	$B_{char,i}$	-	$\{0, 1\}^{\|I\|}$
Binary variable for battery discharge	$B_{dis,i}$	-	$\{0, 1\}^{\|I\|}$
Net AC energy for inverter	$E_{inv\_net,i}$	kWh	$\mathbb{R}^{\|I\|}$
Net energy flow for household	$E_{house\_net,i}$	kWh	$\mathbb{R}^{\|I\|}$
Energy from rapid charger	$E_{rapid,i}$	kWh	$[0, \infty)^{\|I\|}$
Net cashflow	CF_i	£	$\mathbb{R}^{\|I\|}$
Max powerflow	$P_{house,max}$	kW	$[0, \infty)$

$B_{char,i}$ and $B_{dis,i}$ are initialised to random values before solving. This encourages households to find different solutions, aiding convergence of prices.

6.2.5.1 Optimisation Constraints
Constraints on EV battery

Eqns. 6.16 to 6.19, below, describe the stored energy in the EV battery $E_{stored,i}$, including the initial and final values.

$$E_{stored,0} = E_{stored\_init} \qquad \text{(Eqn. 6.16)}$$

$$E_{stored,i} = E_{stored,i-1} + \eta_{batt} \cdot E_{char,i} - E_{disch,i} - E_{drive,i} + E_{rapid,i}\ , i > 0 \qquad \text{(Eqn. 6.17)}$$

$$SOC_{min} \cdot C_{batt}^{nom} \leq E_{stored,i} \leq SOC_{max} \cdot C_{batt}^{nom} \qquad \text{(Eqn. 6.18)}$$

$$E_{stored,48} \geq E_{stored\_\mathrm{min}\_final} \qquad \text{(Eqn. 6.19)}$$

Eqns. 6.20 and 6.21 impose the availability of the EV battery, the maximum charge/discharge power; and the binary on/off state for charge/discharge. Eqn. 6.22 ensures that charge and discharge are not simultaneous.

$$E_{char,i} \leq \alpha_i \cdot P_{max-char} \cdot B_{char,i} \cdot dt \qquad \text{(Eqn. 6.20)}$$

$$E_{disch,i} \leq \alpha_i \cdot P_{max-disch} \cdot B_{disch,i} \cdot dt \qquad \text{(Eqn. 6.21)}$$

$$B_{char,i} + B_{disch,i} \leq 1 \qquad \text{(Eqn. 6.22)}$$

Eqn. 6.23 prevents discharge of the battery if V2X is not permitted; Eqn. 6.24 imposes the minimum battery state-of-charge for V2X. Eqn. 6.25 ensures that rapid charging only occurs while the vehicle is away from home.

$$E_{disch,i} \leq B_{V2X} \cdot 10^6 \qquad \text{(Eqn. 6.23)}$$

$$E_{disch,i} \leq E_{stored,i-1} - E_{stored\_\mathrm{min}\_V2X} \cdot B_{disch,i} \qquad \text{(Eqn. 6.24)}$$

$$E_{rapid,i} \leq (1 - \alpha_i) \cdot 10^6 \qquad \text{(Eqn. 6.25)}$$

Inverter constraints

Eqns. 6.26 and 6.27 constrain the net power on the AC side of the inverter; Eqn. 6.26 covers the case of power export through the inverter, whilst Eqn. 6.27 covers the case of power import. Eqn. 6.28 imposes the inverter capacity. The inverter can curtail power if necessary.

$$E_{inv\_net,i} \leq \eta_{inv} \cdot \left(E_{disch,i} - E_{char,i} + E_{PV,i}\right) \qquad \text{(Eqn. 6.26)}$$

$$E_{inv\_net,i} \leq \frac{1}{\eta_{inv}} \left(E_{disch,i} - E_{char,i} + E_{PV,i}\right) \qquad \text{(Eqn. 6.27)}$$

$$-P_{inv} \cdot dt \leq E_{inv\_net,i} \leq \eta_{inv} \cdot P_{inv} \cdot dt \quad \text{(Eqn. 6.28)}$$

Household constraints

Eqn. 6.29 gives the overall net load for the household; Eqn. 6.30 controls whether export of power is allowed. Eqns. 6.31 and 6.32 control the net payments for export / import of energy.

$$E_{house\_net,i} = E_{inv\_net,i} - E_{load,i} \quad \text{(Eqn. 6.29)}$$

$$E_{house\_net,i} \leq B_{exp} \cdot 10^6 \quad \text{(Eqn. 6.30)}$$

$$CF_i \leq E_{house\_net,i} \cdot \pi_{export,i} \quad \text{(Eqn. 6.31)}$$

$$CF_i \leq E_{house\_net,i} \cdot \pi_{import,i} \quad \text{(Eqn. 6.32)}$$

Objective function

This consists of the nominal value assigned to final energy stored, the payment for rapid charging, and the net bill for import and export of power.

$$OBJ = \pi_{final} \cdot E_{stored,48} - \pi_{rapid} \cdot \sum_i E_{rapid,i} + \sum_i CF_i \quad \text{(Eqn. 6.33)}$$

6.3. Results

This section is organised as follows. We first present results for the operation of the microgrid over the summer week, and consider the overall performance in terms of the technical performance indicators, and household savings. We then assess the impact of season on the microgrid's performance, before focusing specifically on the annual savings for households, and how these are distributed to households of different classifications.

6.3.1 Results for summer

To illustrate the operation of the microgrid, Figure 6.5 shows simulation results for system P2P_V2G over the course of the summer week, for a scenario with 80% PV penetration and 40% EV penetration. Shown are energy production, energy consumption, self-consumed vs. shared power, and internal microgrid prices. By comparison of Figures 6.5 (a) and 6.5 (b), it will be seen that the charging of EVs tends to track the rise and fall of solar generation. Conversely, the discharging of EVs at night time tracks the standard (inflexible) electric load. As shown in Figure 6.5 (c), this flexibility is accomplished both by self-consumption within houses, and also to a significant extent by power sharing via the P2P market. The total shared energy over the week was 1681 kWh, compared to 619 kWh for the baseline system G_V1G at the same technology penetration levels. Grid imports across the week are reduced by 59%, from 1714 to 701 kWh; grid exports by 55% from 2012 kWh to 908 kWh; self-sufficiency increases from 55% to 86%. Consequently the average household is £3.19 better off across the week compared to the baseline system.

(a)
(b)
(c)
(d)

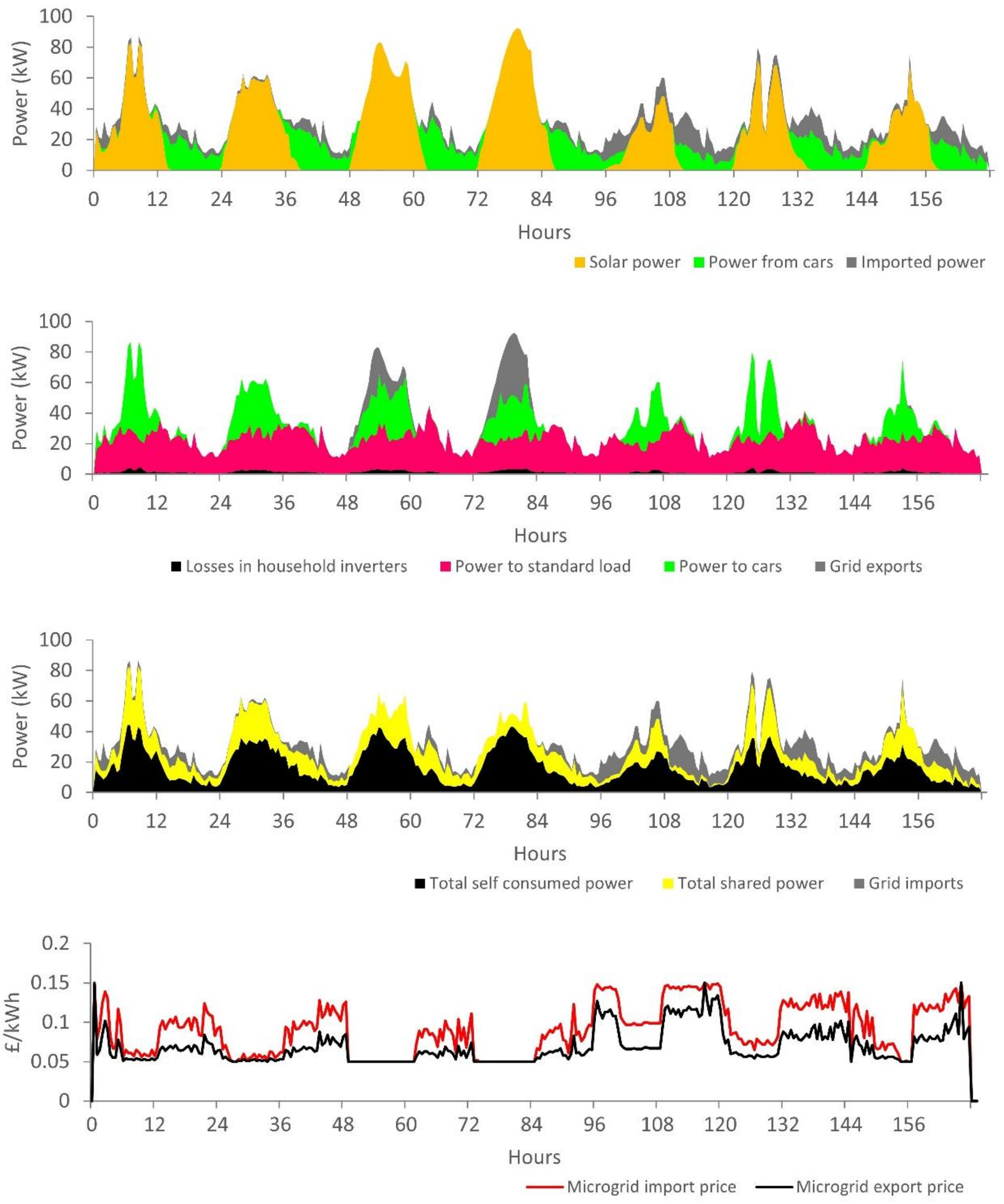

Figure 6.5. Operation of microgrid P2P_V2G over the simulated week, with 80% PV penetration and 40% EV penetration. (Hour zero is Monday 5.30am.)

(a) Power generation
(b) Power consumption
(c) Power self-consumed by households / shared between households / imported from grid
(d) Internal microgrid prices

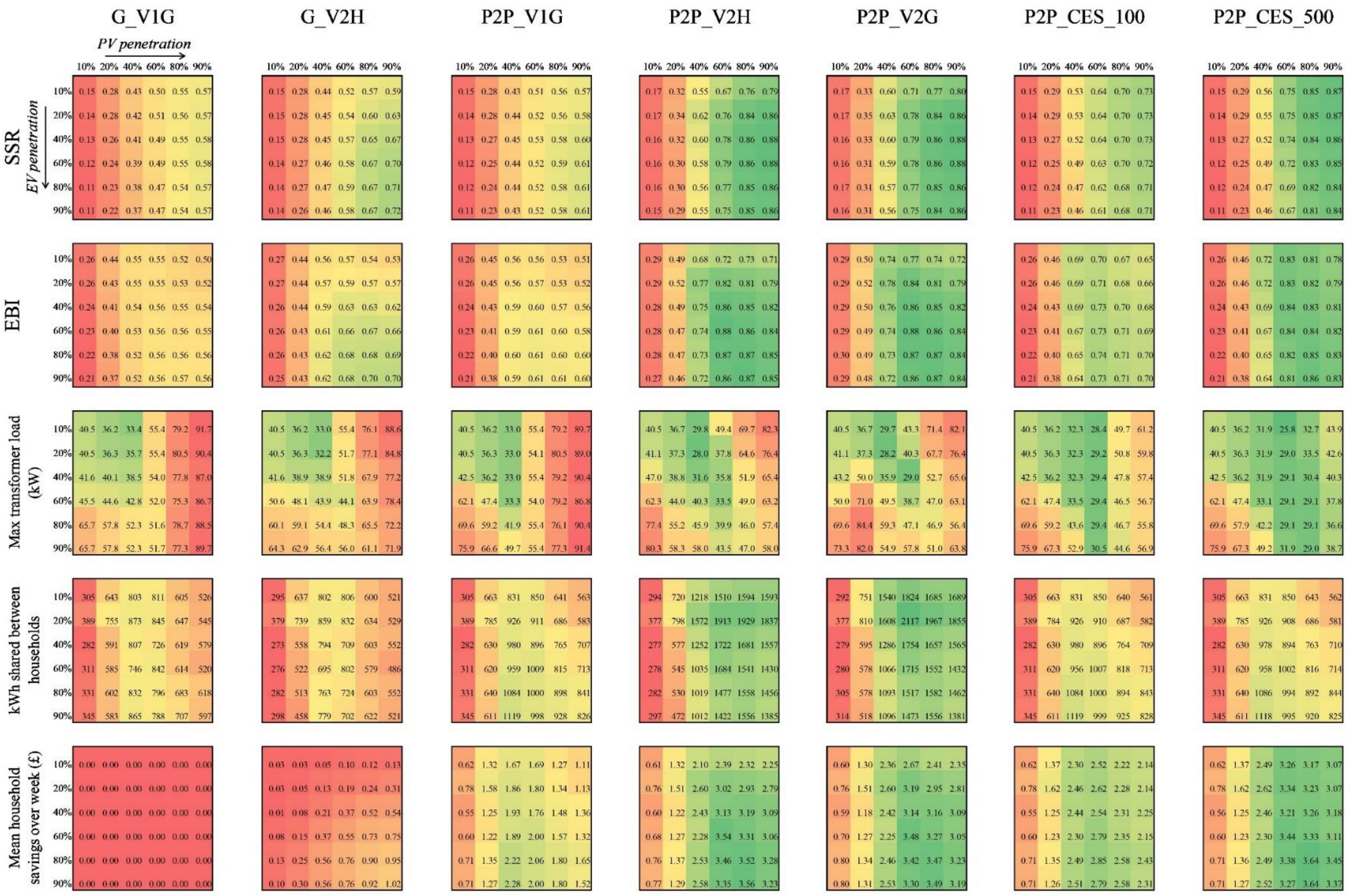

Figure 6.6 Performance indicators for the microgrid, for the various systems and scenarios, over the summer week. In each block, PV penetration increases from left to right, and EV penetration increases from top to bottom. Shading has highest values coloured green and lowest values red, except for 'Max transformer load' where this colour scheme is reversed.

Figure 6.6 summarises the performance of the microgrid over all systems and technology penetration levels for the summer week. Performance indicators shown are SSR, EBI, maximum transformer loading at the grid connection, shared kWh and average household savings (versus the baseline scenario, G_V1G). Certain broad observations can be made: the impact of PV penetration on these metrics is generally strong, whereas the impact of EV penetration tends to be more subtle, even when V2H / V2G are permitted. Whilst SSR naturally climbs with increasing PV penetration, shared energy and household savings (relative to the grid tariff) tend to peak at middling PV penetration. Peak transformer loading and EBI also achieve their best values for middling PV penetration.

In G_V1G (the baseline system) SSR for the week varies between 11% and 58%, EBI between 21% and 57%, and maximum transformer loading between 40.5 kW and 91.7 kW, according to the technology penetration. Power shared varies between 282 and 873 kWh (N.B. this is power which is physically shared, although not traded). SSR and EBI improve strongly as PV penetration increases. Increasing EV penetration tends to have a more modest, downward impact on these metrics. However, additional EVs can improve EBI if PV penetration is high, owing to the reduction in grid exports.

In G_V2H, EV households are permitted to discharge their batteries as V2H. Without a P2P trading system or time-of-use tariff, only the households in possession of EV and PV can profit by this. Thus the impact is negligible unless PV and EV penetration are high. With high enough penetration, we see moderate improvements in the microgrid's SSR and EBI, and decreased transformer loading; the highest SSR and EBI achieved are now 72% and 70%. Shared power decreases somewhat under G_V2H, since PV households can store surplus power for later use.

P2P_V1G introduces the P2P market mechanism (but does not allow V2H). There is now an incentive for households with EVs, but no PV, to schedule their charging to synchronise with peaks in solar generation. The effect is best demonstrated by observing the increase in energy shared between households, relative to the baseline G_V1G. This increase is typically at least 20%, representing up to 250 additional shared kWh across the week; across all technology penetration scenarios, the maximum shared energy is now 1,119 kWh (for 40% PV, 90% EV penetration). The increases in shared power correspond to modest improvements in SSR and EBI, although less than the improvements effected by G_V2H. No improvement is seen in the maximum transformer loading. The P2P tariff achieves household savings averaging up to £2.28 for the week; the best savings are seen when EV penetration is high and PV penetration is medium.

For most penetration scenarios, performance indicators for P2P_V2H are significantly improved versus G_V1G, G_V2H and P2P_V1G. Thus, the combination of V2H and a P2P tariff achieves much more than either innovation individually, a point we wish to emphasize. (However, for PV penetration below 20%, performance is similar to P2P_V1G, as there is insufficient surplus energy to store for V2H.) The increase in shared power versus the baseline is often several hundred kWh, with the largest increases of over 1 MWh additional shared power, occurring for PV penetration ≥ 60% and EV penetration 10 – 40%. Imported power is much reduced; for instance at 60% PV, 40% EV penetration, imports fall from 1,952 kWh baseline to 1,071 kWh under P2P_V2H (-45%). The reduced grid interaction is also reflected in improved SSR and EBI scores, with the best values now 88% and 87% respectively. Further, the maximum loading on the microgrid's transformer is also reduced; for instance, 90% penetration of both PV and EV can be accommodated with a peak loading of 58 kW, compared to 90 kW under G_V1G; a 36% reduction (although it should be remembered that this peak reduction is just over a one-week duration). The savings for households across the week can average up to £3.54.

P2P_V2G additionally allows all EV households to export power from EV batteries (V2G). In these results, the impact of allowing V2G is minimal to non-existent, so that P2P_V2G and P2P_V2H have very similar performance across all performance indicators. At middling PV penetration, V2G does result in an increase in shared power, but this increase is small. A possible explanation would be that households prefer to expend all energy stored in the EV battery on offsetting their own local electrical load. However, the average daily load for a household is only ca. 10 kWh, compared to 15 kWh of EV battery storage made available for V2X. Thus, the average household carrying out V2X should have enough battery capacity for V2G as well as V2H. The other explanation is simply that the iterative market mechanism is not good at incentivising V2G. Specifically, the SDR approach cannot allow a large proportion of supply to be exported from EV batteries, as the price paid for household export inevitably falls as the power exported from EVs increases. To incentivise V2G, some form of double auction is preferable, since this allows owners of EV batteries (or other flexible generation / storage) to make energy bids contingent on securing a given price. This power to dictate prices is absent from the market mechanism used here.

The final two systems introduce stationary CES (respectively 100, 500 kWh) but do not allow V2H or V2G. The energy independence measures, SSR and EBI, are improved substantially versus the baseline, reaching SSR = 73%, EBI = 74% for P2P_CES_100; and SSR = 87%, EBI = 86% for P2P_CES_500. The 500 kWh CES outperforms the 100 kWh CES only when PV penetration exceeds 60%; this is reflected in the scores for SSR, EBI and transformer loading, as well as the household savings. Thus it seems that for the lower PV penetration, 100 kWh of community storage is adequate. Broadly speaking, P2P_CES_500 achieves similar levels of energy independence to P2P_V2H across most technology penetration scenarios. On the other hand, the CES is significantly more successful at reducing peak transformer load. For example, P2P_CES_500 can accommodate 90% penetration of both EV and PV ownership, with a peak load of 39 kW – compared to 58 kW under P2P_V2H and 90 kW under G_V1G. This is expected since the CES is controlled with peak shaving as an explicit objective, whereas for previous systems, any peak shaving is an incidental consequence of households pursuing their self-interest.

Besides the clear advantages of combining P2P with V2H, a further point to emphasize is that doing so can achieve benefits regardless of EV and PV penetration. This contradicts a result of Zhou et al [8] who suggested that P2P becomes redundant when PV and EV penetrations are both high, as households can charge their own EV with their own generation. In our results, the average household saves £3.23 when EV and PV penetration are at 90% thanks to the P2P system.

6.3.1.1 Seasonal variation

The results up to this point have been for the typical summer week; we now introduce the impact of seasons. Figure 6.7 shows SSR and mean household savings for the various microgrid systems, across three seasons, with the penetration scenarios averaged into four quadrants (see Section 6.2.3). Season has a pronounced effect on both measures. In autumn, the P2P systems can still achieve notable improvements to SSR and to bills, although the improvements are reduced in magnitude. Generally, the relative performance of the different systems in summer and autumn is very similar; in particular, P2P_V2H still clearly outperforms G_V2H and P2P_V1G in autumn. For winter, savings and SSR are around an order of magnitude less than in summer, and the P2P systems can make only negligible impact. In the next section, we discuss the annual savings for households, which are estimated as a weighted combination of weekly savings in summer, autumn and winter.

(a)

(b)

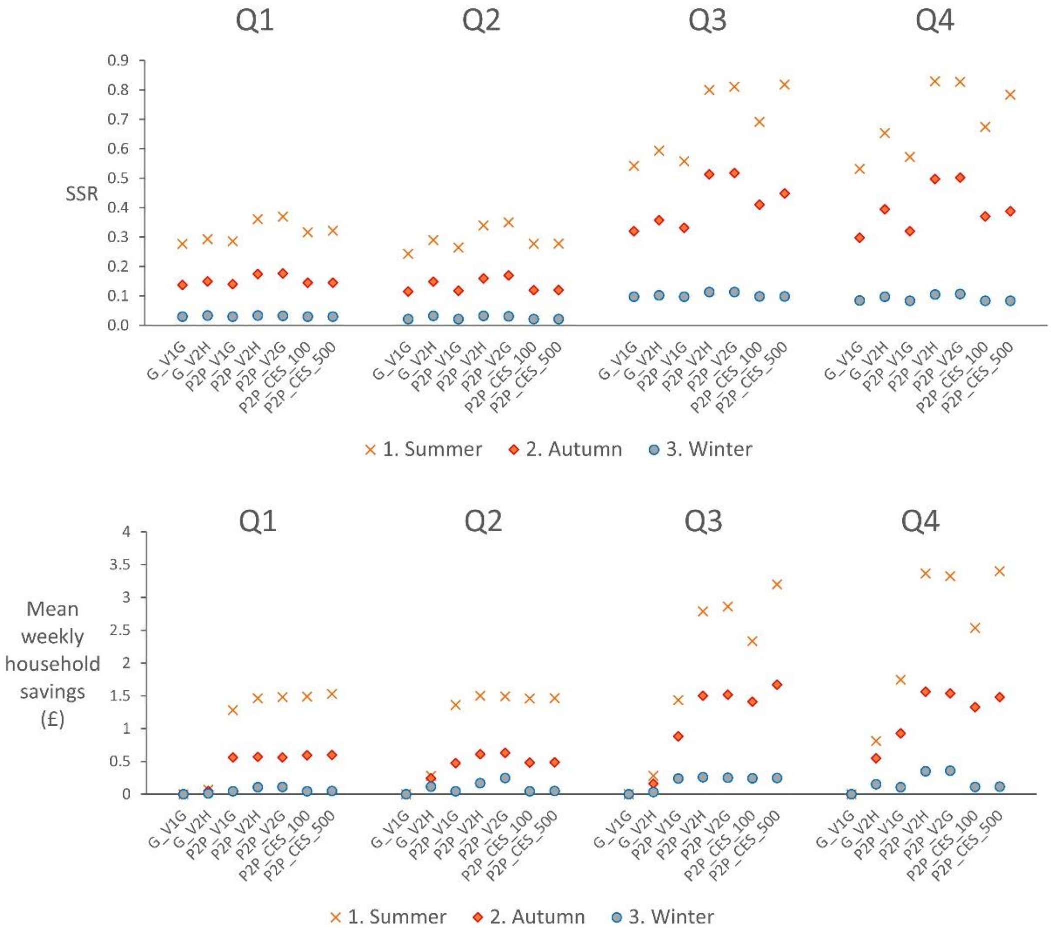

Figure 6.7. Impact of season on (a) SSR and (b) weekly household savings, for each of the seven microgrid systems. Household savings are relative to the baseline system with no P2P (G_V1G). Quadrants Q1 – Q4 are used for technology penetration (see Section 6.2.3).

6.3.2 Household savings and distribution of benefits

In this section we discuss the possible annual savings for households participating in the microgrid's market. Under G_V1G the average annual bill is £590 for a household with no EV or PV, £770 for a household with an EV; £380 for a household with PV; £440 for a household with both technologies. Figure 6.8 shows estimated annual savings across all microgrid systems and penetration scenarios, with households classified according to ownership of PV / EV. Figure 6.9 uses additional classifications of households (commuter / non-commuter; PV orientation), and shows results for P2P_V1G, P2P_V2H and P2P_CES_500.

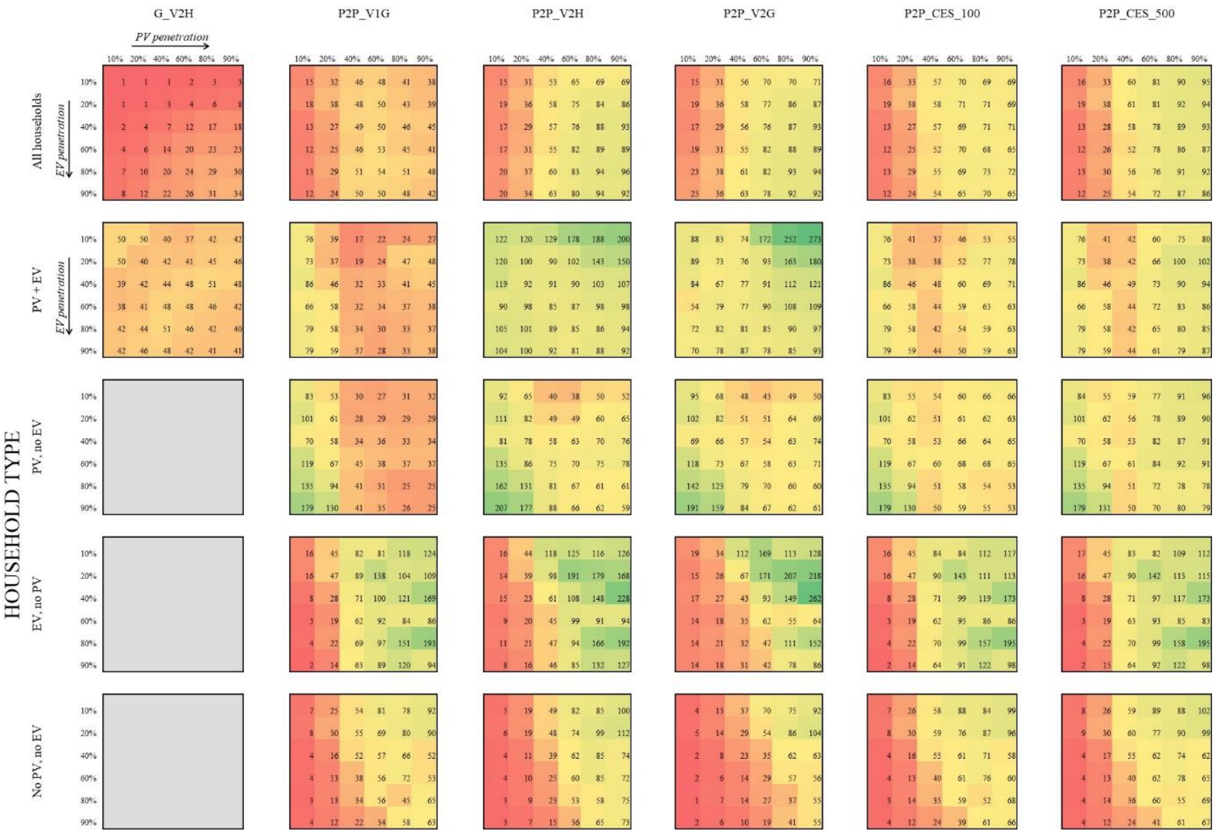

Figure 6.8. Average improvement in annual household bill, relative to G_V1G, for different household types and scenarios. In each block, PV penetration increases from left to right, and EV penetration increases from top to bottom. Blocks with no possibility of households making a saving are left blank. Unit is GBP.

Annual bill savings enabled by the various P2P systems tend to average up to £100, but can be over £200 for some household types in some scenarios. It is important to note that *all* types of households can benefit from the P2P. For instance, even for households with both PV and EV, P2P_V2H achieves markedly higher savings than G_V2H. Thus, these households evidently benefit from the ability to trade energy with neighbours, despite possessing their own generation and energy storage. This even remains true even at 90% penetration of the technologies. Households with neither PV nor EV can also benefit, although usually to a lesser extent than households with EV/PV. The largest savings (>£200/a) from P2P are enjoyed by households with an EV but no PV of their own, in scenarios with high PV penetration creating a buyer's market. Conversely, large benefits can also be felt by households with PV but no EV, especially when low PV penetration and high EV penetration create a seller's market.

Under G_V2H (given that the grid tariff is assumed constant) households must have both PV and EV in order to benefit economically; for these households, the benefits to the annual bill average ca. £44. Under P2P_V1G, household savings average £38/a across all household types and technology penetrations; savings are greatest at middling PV penetration, reaching a maximum of £54/a. Middling PV penetration allows that different households can simultaneously be in deficit or surplus, so that the P2P is most beneficial.

As with the technical performance measures, P2P_V2H achieves notably greater household savings than either G_V2H or P2P_V1G; the average across all household types and scenarios is £60/a. The savings are most significant at middling to high PV penetration, which allows households to charge cheap power to their vehicles during the day for use after sunset. Unlike P2P_V1G, savings do not peak at mid-range PV penetration, suggesting that more generation can always be put to use; savings reach ca. £90/a when PV penetration is high. Again, the biggest savings versus G_V1G (sometimes >£200) are made by households with EVs but no PV. Interestingly though, the jump in savings from P2P_V1G to P2P_V2H is actually less for the EV owners than the PV owners, who evidently benefit from the competition to buy power for V2H.

As already discussed, the market mechanism is not well-designed to incentivise V2G. Thus savings under P2P_V2G are very similar to P2P_V2H, with the average benefit again being £60/a across all tech penetration levels. Household savings for P2P_CES_100 and P2P_CES_500 average respectively £51 and £60. Because the CES enables microgrid prices to be smoother throughout the day, avoiding extreme values, distribution of benefits to different classes of households is somewhat more even than under P2P_V2H (see also Figure 6.9). The magnitude of household savings is broadly comparable for systems P2P_V2H and P2P_CES_500.

6.3.2.1 EV usage and PV orientation

For an EV owner, pay-off from the P2P systems comes from charging the vehicle when power is cheap, i.e. when PV generation is high. Thus it would be expected that commuter vehicles, that are often away at work during the daytime, will benefit less. This does indeed prove to be the case in our results (wherein we define a commuter household to be any household with four or more trips to work in the morning, over the week-long travel schedule). For instance, under P2P_V1G, average annual benefits for commuter EV households are £29, but £47 for non-commuters; under P2P_V2H the discrepancy is £60 to £77. Figure 6.9 shows that the discrepancy in earnings between commuters and non-commuters is greater when EV penetration is higher (3.5 (b) and (d)); whereas higher PV penetration is beneficial to both groups of EV drivers (3.5 (c) and (d)).

Additionally, we consider the orientation of PV systems (east, west, or south). Overall the benefits of the P2P mechanisms for each orientation appear very similar (see Figure 6.9). There is some indication that high PV penetration in the microgrid is more detrimental to the households with south-facing PV (see particularly Figure 6.9 (c)). However, it’s important to note that the bills for households with south-facing systems are already lower in absolute terms (average £362/a for south-facing PV, versus £431/a for the other orientations, under G_V1G).

(a) Q1

(b) Q2

(c) Q3

(d) Q4

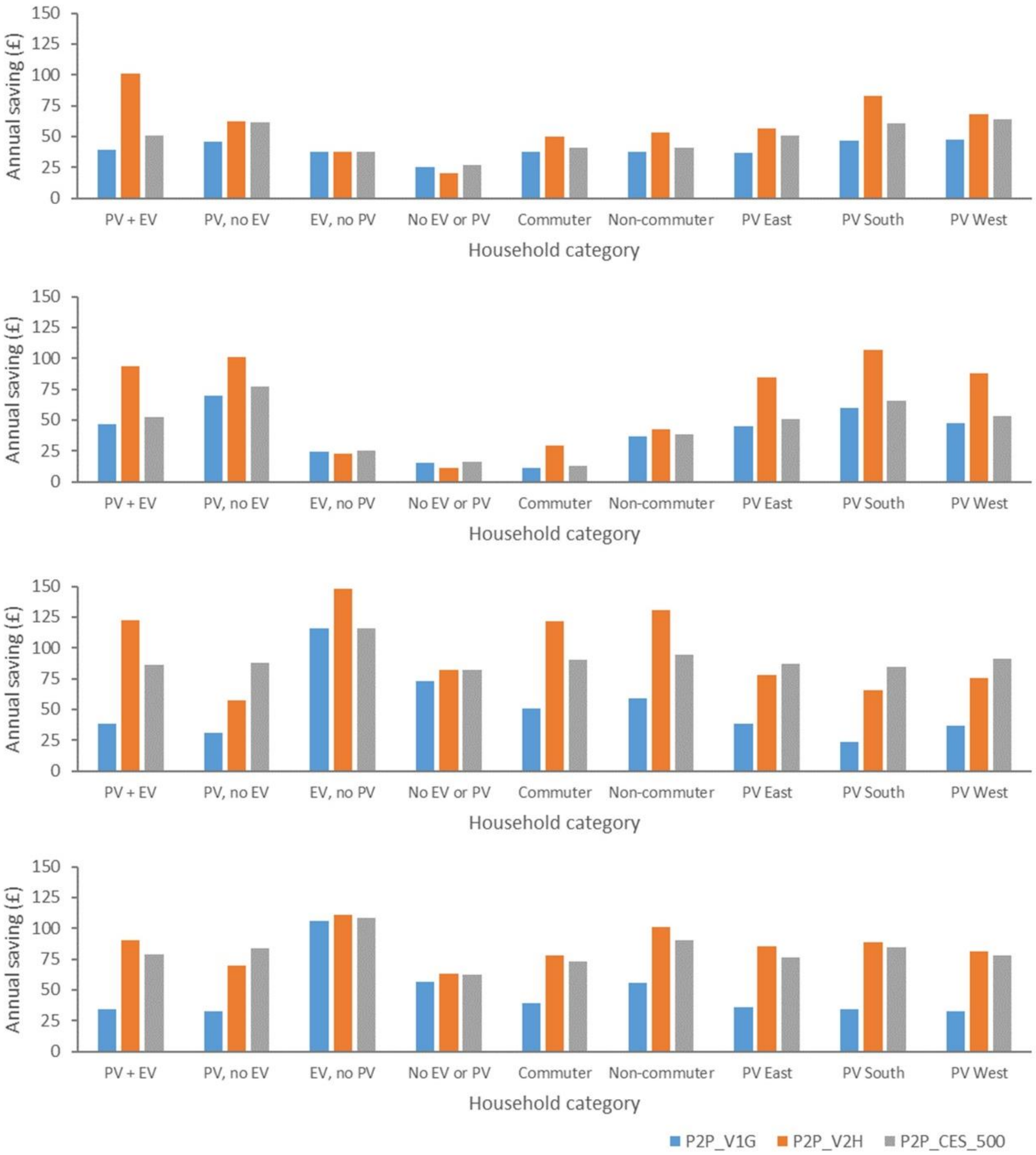

Figure 6.9. Average improvement in household net daily bill relative to G_V1G, for different household categories and microgrid systems. Estimated for one full year. Systems shown are P2P_V1G, P2P_V2H and P2P_CES_500.

6.4. Discussion

This work has developed a simulation model to investigate a P2P market mechanism based on iterative bidding, in combination with realistic models for EV usage and PV generation. We have confirmed that P2P trading can achieve significant benefits, both technical and economic. These are particularly interesting when the P2P market is combined with V2H technology. For instance, at 40% penetration for EV and PV ownership, average bills over a summer week improve by £2.42 (around 33% of the average summer weekly bill) and SSR increases from 41 to 60%. The benefits of V2H and P2P in tandem exceed the benefits of either in isolation. Perhaps counter-intuitively, this is still true when PV penetration and EV penetration are both high, so that most households possess both: for 90% penetration of each, V2H alone achieves average weekly savings of £1.02; P2P achieves £1.52; but the two in combination save households an average of £3.23. That P2P trading is profitable even when most households have PV and EV makes sense when considering two factors (i) EVs are not always available and (ii) they can charge at higher power than the output of typical rooftop solar (respectively 7.2 kW and 3 kW in this work). Thus, an available vehicle can utilise all the surplus PV from its own household, and still benefit from buying additional power from a neighbour whose car is unavailable.

We find some indication that the benefits of the P2P market for commuters, whose cars are likely to be unavailable during the day, may be less than for non-commuters. For the system with V2H and P2P, the annual benefits for non-commuters are 28% greater, averaged over all scenarios. We also compared the usage of EVs for energy storage with shared, stationary CES. This was controlled to minimise the microgrid's aggregate net bill, whilst also peak shaving for the grid connection. Because the CES schedule is controlled directly – whereas the schedules of EV batteries can only be influenced by market conditions – CES proved more successful at reducing peak loads than V2H; whereas household cost savings and improvements in energy autonomy were similar for V2H / CES.

The iterative bidding market mechanism used for this study has various strengths and weaknesses. Optimisation of household schedules in response to published prices is a simple and intuitive problem. Unlike in other market mechanisms, energy bids are never declined – rather, adjustments are encouraged by the price changes for the next iteration. Thus, there are no 'lucky' or 'unlucky' participants in the daily market. On the other hand, the need for constraints to encourage convergence of prices means that a level of central control is still present – the households are not fully free in their decision making. Pricing can tend to favour consumers more than generators. In particular, this market mechanism would need adapting in order to incorporate generation with non-zero marginal cost (V2G, CHP) as the mechanism currently assumes prices must be low whenever most supply is procured internally. Thus in this work, making V2G available achieved negligible benefits versus V2H – but there is no reason why this has to be true in general. Future work could compare this iterative market mechanism with other mechanisms: for instance, full central control; one-shot double auction; continuous double auction.

It is worth noting that passive participants in the microgrid (who have neither an EV or a PV) still benefit from the P2P market, especially in a buyer's market scenario (see Figures 6.8, 6.9). These benefits are always less than households with flexible load, but can sometimes be greater than the benefits to PV households. This is not necessarily reasonable, as these households are essentially profiting at the energy supplier's expense whilst taking no actions to benefit the community. The rationale for allowing these households to participate is that the market mechanism should not necessarily be aware of, or care about, what is 'behind' a household's meter. However, it might be worthwhile to consider market designs that more explicitly reward flexibility in demand. One possibility could be to reward load adjustments which are made to alleviate forecasting uncertainty or unforeseen fluctuations – see for instance [161]. Another possibility might be to impose a fee to join the P2P market, and thus recoup the average benefit of passive participants. It's also worth noting that participants without EV or PV could still contribute to the microgrid through control of smaller flexible loads (e.g. dishwashers, fridges) although these have not been modelled here.

6.5. Conclusions and future work

The authors believe that this work has demonstrated P2P to be a very interesting innovation that could greatly assist the integration of a high penetration of PV and EVs in the built environment. It can enable significant gains in energy independence (which should correspond to a reduction in emissions) and significant reduction of household bills, especially when PV penetration is high (see Figure 6.7). In particular, the coupling of P2P with V2H chargers is of interest, bringing greater benefits than either innovation individually.

Suggested topics for future work include:

- P2P market mechanisms that can take account of forecasting uncertainty. Uncertainty in forecasting generation / demand has received some attention; in contrast, forecasting of EV usage / availability has received little if any.
- Simulation of P2P mechanisms at higher time resolution. Existing work, including the present work, tends to use hourly or half-hourly resolution. Real life management of a microgrid demands attention to shorter term fluctuations.
- Coupling of markets for heat and power. Some proposals have been made for this (e.g. [162]) but such work is rare.

6.6. Acknowledgements

Grateful acknowledgement is made of the financial support of the Engineering and Physical Sciences Research Council (EPSRC) in the form of the 'Energy Storage and its Applications' Centre for Doctoral Training under grant code EP/L0168/18; also of the Electric Power Research Institute. The final author would like to acknowledge the support of the Royal Academy of Engineering through the Industrial Fellowship (Reference: IF\192046).

This research makes use of data from the UK Environmental Change Network and UK Power Networks.

7. P2P trading of heat and power via a continuous double auction

Timothy D Hutty[a], Solomon Brown[a]*

[a]*Department of Chemical and Biological Engineering, University of Sheffield, UK*

Abstract

Peer-to-peer (P2P) energy trading, whereby customers can trade energy with one another rather than the energy supplier only, has the potential to save money for consumers whilst also incentivising more efficient and environmentally beneficial behaviour. Many existing models for P2P only consider a real-time or hour-ahead market, which does not allow proper scope for the planning of flexible demand or for energy storage. Accordingly, in this model we employ a day-ahead continuous double auction, in which all the upcoming timeslots are simultaneously open for trading. This allows schedules for device dispatch to be developed properly. Furthermore, we consider the trade of heat as well as power, via a low temperature heat network. Heat and power trading interact due to the use of air source heat pumps (ASHPs) as well as reversible solid oxide cells (rSOCs) which can provide combined heat and power, or alternatively produce hydrogen via water electrolysis. In our case study, the P2P market is simulated with 25 houses participating, for two week long periods in different climate conditions. P2P electricity trading is found to bring a marked reduction in reliance on grid electricity, and a reduction in peak grid load. This is brought about mainly by the incentive for rSOCs to generate at a higher average load factor, and the average house makes savings of ca. £10 / week in winter weather. Trading of heat brings a further decrease in reliance on grid electricity, and largely eliminates the use of inefficient resistive heat. However, the heat trading may not be financially worthwhile in all conditions.

7.0 Nomenclature and terminology

Table 7.1. Acronyms.

ASHP	Air source heat pump
CDA	Continuous double auction
CHP	Combined heat and power
COP	Coefficient of performance (of heat pump)
EV	Electric vehicle
G_ONLY	Market paradigm where only grid trade of electricity is available.
LHV	Lower heating value
MILP	Mixed integer linear programming
P2P	Peer-to-peer
P2P_P	Peer-to-peer market allowing trading of electrical power only
P2P_H_P	Peer-to-peer market allowing trading of both heat and power
rSOC	Reversible solid oxide cell
SOEC	Solid oxide electrolyser cell [mode of rSOC]
SOFC	Solid oxide fuel cell [mode of rSOC]
TES	Thermal energy storage
TR	Truthful [bidder]
V2X; V2H; V2G	Vehicle to anything; vehicle to house; vehicle to grid
ZI	Zero intelligence [bidder]

Table 7.2. Symbols.

Symbol	Unit	Description
t	-	Timeslot, typically in {1…24}
t_{last}	-	Final timeslot, typically 24.
Δt	s	Duration of a timeslot.
b	-	Binary variable
v_{V2X}	£/kWh	Estimated financial benefit of 1 kWh charged to the EV battery for V2X.
C	kWh/°K	Heat capacity
C_{EV}	kWh	Capacity of EV battery
c_{V2X}	£/kWh	Estimated cost of discharging 1 kWh from the EV battery for V2X.
c_{rapid}	£/kWh	Cost of rapid charging.
$\mathcal{D}$		Set of devices owned by auction participant
p	£/kWh £/kg	Price; £ / kWh for energy, £ / kg for H_2.
p_{cl}	£/kWh	Clearing price for double auction
H	kWh	Thermal energy
H2	kg	Hydrogen
K	kW/°K	Thermal transfer coefficient
E	kWh	Electrical energy
E_{min_final}	kWh	Minimum kWh for the final storage state of the EV battery.
P	kW	Power
PEN	£	Penalty term in objective function

T	°C	Temperature
VAL	£	Valuation of a device's stored energy
η_{inv}		Efficiency of inverter
η_{SOFC}	kWh/kg$_{H2}$	For rSOC in SOFC mode, kWh electricity generated per kg H_2.
η_{SOFCth}	kWh$_{th}$/kg$_{H2}$	For rSOC in SOFC mode, kWh heat generated per kg H_2.
η_{SOEC}	kWh/kg$_{H2}$	For rSOC in SOEC mode, kWh electricity consumed per kg H_2.
		Subscripts
buy		Energy to buy via future trades
sell		Energy to sell via future trades
bought		Energy already bought via successful offers
sold		Energy already sold via successful asks
imp		Imported
exp		Exported
cl		Cleared in auction
P2P		peer-to-peer
res		reserve price
rh		resistive heat
st		energy storage
tes		Thermal energy storage
grid_retail		Grid retail tariff for electricity import
grid_FI		Grid feed-in tariff for electricity export

7.1. Introduction

As the world seeks to decarbonise its energy systems, some of the changes will be seen at a local and household level. These changes will be felt across the key sectors of power, transport and heat. They include the growth of embedded generation, both solar PV and combined heat and power (CHP) systems [223]; the proliferation of electric vehicles (EVs) [247]; and the decarbonisation of heating systems. Peer-to-peer (P2P) energy trading, whereby consumers are able to trade energy with one another, rather than the energy supplier only, can help to incentivise the efficient use of these new technologies [8], [248]. In particular, P2P can incentivise the synchronisation of flexible loads with surpluses in renewable generation; a simple example of this is the scheduling of EV charging to make use of a peer's surplus solar power. The net effect is increased local self-sufficiency in energy, decreased environmental impact and a reduction in bills [248]. Whilst current market regulations in the UK do not permit peer-to-peer trading, interest is growing, with companies including Centrica and EDF carrying out trial schemes in recent years [143], [144].

Decarbonisation of heat, which is often neglected in studies of P2P trading, can lead to additional motivations to trade energy [249], [250]. For instance, air source heat pumps (ASHPs) can make use of peers' surplus electricity generation, storing heat either in the fabric of buildings or in dedicated thermal storage. Meanwhile, CHP systems which typically produce heat and power in a fixed ratio [251], can benefit by exporting surplus power to peers while tracking heat demand. The possibility of local trading in heat between peers, rather than power only, has received a limited amount of attention in the literature. Such trading requires connection to a heat network, likely operating at a moderate temperature [250]. In theory, this enables the extra flexibility to procure heat from different sources, depending on what is most cost-effective at a given time, achieving additional savings.

In this work, we consider a continuous double auction (CDA) for P2P trading of energy in a small residential community, and present an agent-based simulation of this setup. The CDA resembles the continuous trading which takes place, for instance, in stock and currency markets, as well as intraday electricity markets, with prices on the market being determined purely by competition on the supply and demand sides. No information is required to be shared by peers beyond the volume of energy they wish to trade, and the reserve price. CDAs for each timeslot of the upcoming day run simultaneously; this is key to enable scheduling of flexible loads and energy storage. We present results both for the trading of power only, and for the trading of both heat and power.

The next section discusses in more detail the literature and background surrounding the topic of P2P trading.

7.2. Literature Review

7.2.1 P2P trading and double auctions

By enabling peers to trade with one another, rather than the energy supplier, P2P trading can be advantageous for both consumers and generators (often termed ‘prosumers’); for electricity, trades agreed at prices between the grid retail cost and the feed-in tariff (if any) are profitable to both parties [226]. In the absence of flexible demand, generation or energy storage, P2P can still be profitable, as it simply provides fairer recompense for energy that would be physically shared anyway – as in [158]. The real power of P2P, however, lies in its ability to incentivise smart coordination of flexible devices between peers, where these incentives do not exist under the traditional market paradigm. For instance, this can include the scheduling of a flexible load, or energy storage, to absorb surplus solar generation from a peer [8], [231]. It is this aspect of P2P which can bring technical and environmental benefits, rather than financial only [248].

Existing literature on P2P includes both a variety of market structures, and a variety of approaches to their simulation and study. In some cases, flexible devices and energy sharing transactions are optimised centrally [148], [149], [153] although for real-world implementations this would often be unviable [147]. Central optimisation methods can be reposed as distributed optimisation problems, with the alternating method of mixed multipliers (ADMM) a popular approach, as in [252]. Game theoretic approaches are frequently seen, as in [154], [163]–[166]; and many researchers have considered various forms of iterative market, where peers repeatedly adjust their strategies on the basis of feedback from the previous iteration, until convergence is achieved [8], [173], [174], [248].

In this work the focus is on a **double auction** as the basis of the P2P market; this is an auction where buyers and sellers of a commodity are simultaneously in competition. One of the merits of this approach is the analogy with the operation of utility scale markets [230], as well as existing P2P schemes like the Brooklyn microgrid [158]. Participants submit bids to buy or sell consisting of a volume of energy and a reserve price; an equilibrium price is established and as many trades are cleared as possible. The clearing of the market may be one-off, as in [163], or may happen on a rolling basis as in [159], [253]; the latter case is termed a continuous double auction (CDA).

There is a reasonable amount of previous work on double auctions for P2P energy trading, covering such issues as secure, distributed implementation [160], use of Blockchain [159], and comparison of price setting strategies [158]. Zhang et al [161] contrived a novel auction system wherein flexible loads were explicitly paired with the forecasting uncertainty of renewable generation. Chen et al [254] used a data-driven machine learning method to integrate price predictions with the strategy formation of auction participants in a CDA electricity market; the focus here was on the benefits to the single prosumer using the machine learning method, rather than the benefits of the market overall. Thakur et al [255] consider a novel distributed double auction market in which any peer can act as the auctioneer; the focus here is on the reduction of computational overhead via use of the distributed algorithm, and flexible load / generation appears not to have been considered. Haggi et al [256] consider a hierarchical double auction, with nodal, zonal and distribution network stages. The auction mechanism is able to ensure that physical network constraints are not violated; again, flexible load / generation is not considered, and only one timeslot is settled at a time. Zhang et al [257] present an iterated double auction wherein agents may adjust their prices to increase profits with successive rounds.

The inclusion of flexible devices / energy storage in P2P markets brings particular challenges, owing to the coupling that these devices introduce between different timeslots. For instance, a battery may seek to buy additional energy at 12pm, contingent on being able to sell this energy at 7pm; an EV may prefer to charge at 6pm *unless* cheaper energy will be available at 11pm. El-Baz et al [147] note that these issues mean that the real-time or hour-ahead trading most commonly seen in literature is not adequate when flexible devices and energy storage are involved. It is important that multiple timeslots of an upcoming day are simultaneously available for trading. It is worth noting that in utility scale double auctions, the potential interdependence of bids between timeslots can be addressed by the use of complex bids: these include linked block orders, flexible hourly orders and exclusive block orders [230]. These were instituted more for the benefit of pumped hydropower energy storage, as opposed to newer forms [258]; their use adds considerable complexity to the auction clearing algorithm, and is only appropriate for auctions that are cleared one time, as opposed to the CDA.

7.2.2 Heat and power

The consideration of heat in studies of P2P energy trading can take two forms. Firstly, without actual trading of heat, but with consideration of household devices that couple electricity and heat demand: that is, principally heat pumps or CHP. Secondly, with P2P trading of heat as well as power. In the first category, Gan et al [259] considered P2P electricity trading between multiple energy ‘hubs’ equipped with 200 kW CHP generators; an increase in profits of up to 19% was obtained. Zhu et al [249] studied synergies between power, heat and hydrogen energy flows, with only power traded; P2P trading and hydrogen storage were both found to be important in cutting costs. The work of Nguyen et al [252] is particularly relevant to the present work, as it involves P2P power trading between fuel cells providing CHP. The motivation to trade stemmed partly from the variable efficiency of the fuel cell at different partial loads. Heat from the fuel cells was used for DHW tanks – this system was the sole flexible device involved in the trading. Detailed consideration of bill savings is not included. The work of Block et al [162] is also of interest; here a two-dimensional auction for heat and power was contrived, allowing for dependency between bids in the two energy types.

In the second category, Davoudi et al [260] considered a trading of both heat and power, albeit with the price for heat assumed to be fixed and constant. An iterative approach was employed where peers had the ability to form both fixed-price and variable-price contracts. The P2P market was found to be profitable with respect to grid trading. Shi et al [261] studied an integrated energy system with trading in heat, power and hydrogen. ADMM was used to optimise transactions between peers, and it was found that P2P together with a demand response programme was more profitable than either in isolation. Jing et al [262] considered the trading of heat and power between commercial and residential prosumers, with an emphasis on finding fair prices for transactions – although they do not appear to have allowed the P2P prices to vary across timeslots. Daryan et al [263] consider trading of heat and power between Smart Energy Hubs; the settlement of trading is broken down into optimisation of the trades which should take place, followed by identification of fair prices to incentivise these trades; the total social cost sees a 14% reduction. Finally, Wang et al [250] employed coalition game theory to study a double auction market for heat and power. Trading was motivated by slightly undersized heat pumps in dwellings, the varying COPs of these, and varying willingness to compromise on comfort.

7.2.3 Contribution of this work

In this work, we consider a continuous double auction for P2P trading of both heat and power. The CDA is chosen as one of the most simple, generic and flexible forms of market [254], and because of its resemblance to utility scale markets. The market has a day-ahead format, with all timeslots simultaneously available to trade, improving the ability of peers to schedule flexible devices and energy storage. To our knowledge, an auction of this form which also extends to both heat and power has not been covered in the literature before.

We include in our case study reversible solid oxide fuel cells (rSOCs) which can convert power to hydrogen, as well as converting hydrogen to heat and power. Although the participation of fuel cell CHPs in P2P has occasionally been studied, we believe this has not in the past extended to rSOC.

7.3. Method

7.3.1 Overview

The day-ahead P2P energy market consists of a continuous double auction for each timeslot of the upcoming day, and where applicable each energy type (heat and power). Figure 7.1 gives a high-level overview of this, and a simplified view of household strategy. MILP optimisations are carried out using Pyomo [236] with the GLPK solver [238]; all other aspects of the market simulation are modelled in AnyLogic software [4].

Essential issues that need to be considered include the following:

- flexibility of bids in time
- interdependence of bids between energy types (e.g. sale of heat and power from the rSOC)
- interdependence of bids between timeslots (as for energy storage charge and discharge)

The CDA market structure does not allow ‘complex’ bids with inherent interdependence or flexibility in time, and so here, these issues have to be handled principally by the strategies of the bidders themselves. To facilitate this, it is enforced that the auctions for different timeslots and energy types never clear simultaneously; thus, participants always have opportunity to respond to their success or failure in a particular auction by adjusting bids in other auctions.

We adopt the following conventions for terminology:

Bid – any order whether to buy or sell energy. **Offer** – a bid to buy energy. **Ask** – a bid to sell energy.

Timeslot – A future time period during which power is traded, typically half an hour or one hour in duration.

Round – an iteration of the market wherein CDA’s are cleared for every timeslot for both heat and power.

We define *D* to be the set of devices available to an auction participant. ‘Device’ is to be interpreted broadly, as for instance the inflexible electrical load of a house and the space heating demand are both regarded as ‘devices’.

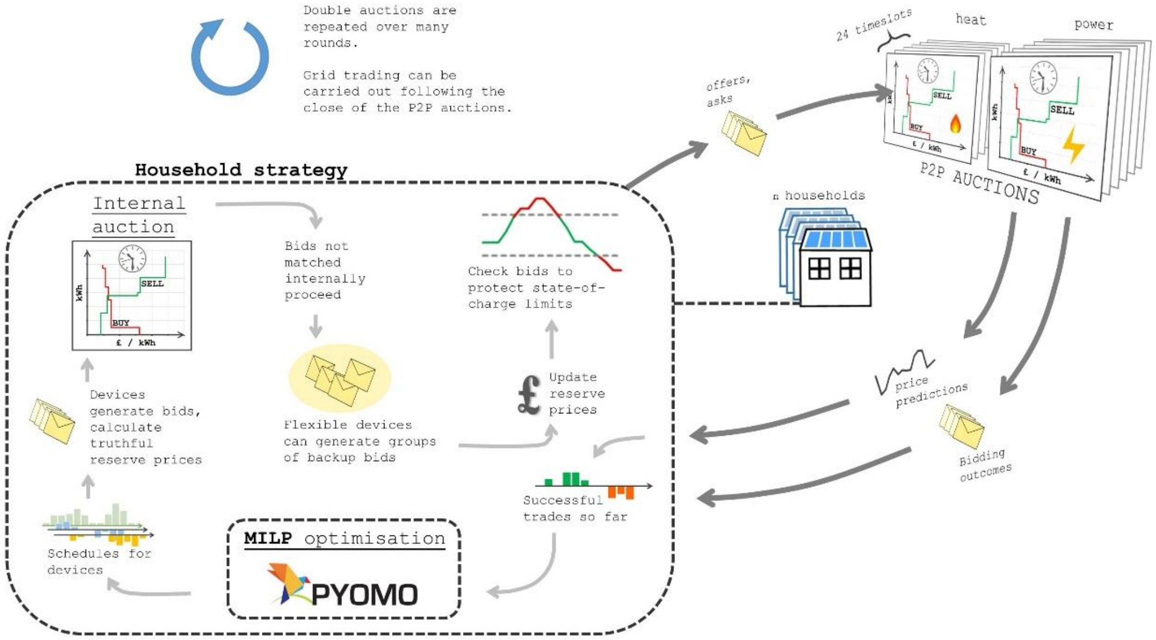

Figure 7.1. A simplified overview of the market structure and household strategisation process.

7.3.2 Markets

As in [147], [264], offers and asks are not submitted to the auctions in truly continuous time, but rather in a sequence of rounds. Multiple bids will typically arrive at each auction every round, after which the auction is cleared. The separate auctions for different timeslots clear in chronological order every round, with the auction for heat following the auction for power, for each timeslot, where applicable. Auction clearing entails ordering the offers in descending order of the submitted price, and the asks in ascending order. Offers are matched to asks until either the current ask price exceeds the current offer price, or there are no more asks to process, or there are no more offers to process. The clearing price p_{cl} is midway between the price of the final ask and offer to be cleared. Typically, either the final offer or final ask is only partially fulfilled. The auctions implement a 'pay-as-cleared' rule, meaning that all the cleared trades are transacted at the same price p_{cl}. Figure 7.2 illustrates how the auction is cleared, showing the supply / demand curves as a function of price, with the intersection of these curves giving the clearing price.

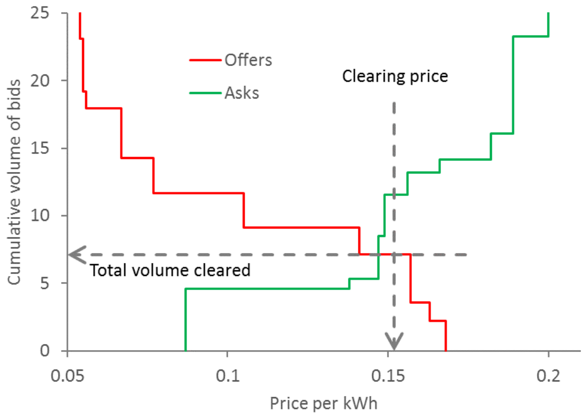

Figure 7.2. Illustrates how the clearing price is found when a double auction is resolved. Note that each vertical step corresponds to a bid.

7.3.3 Determination of bidding strategy

A bidding strategy is defined as the full set of asks and offers that a participant wishes to submit, across all timeslots of the auction, incorporating both the quantities to trade and the reserve prices. Participants may theoretically update strategies at any time; for the purposes of this work strategies are only updated between rounds, and in general only every few rounds. Smaller adjustments may be made more frequently; these typically involve the interdependence of bids (see Section 7.3.3.4) – and could involve the activation / deactivation / cancelling of bids, as well as adjustments to reserve prices.

When the final round of auctions is completed, all households optimise their devices one final time, with respect to the trades they have successfully closed. Grid prices are available for further trade of power; further trade of heat is not allowed.

7.3.3.1 Categories of bid

Table 7.3. Categories of bids.

Name	Description
	Offers (power)
INFLEXIBLE_LOAD	Standard electrical load of the house, assumed inflexible
EV_ESSENTIAL	EV charging that is essential for travel.
EV_ARBITRAGE	EV charging for V2X, or to carry energy into the next day.
ASHP_BUY	Power required for the ASHP to meet the heat demand
ASHP_FOR_TES	Power required for the ASHP to charge thermal storage.
ASHP_FOR_EXPORT	Power required for the ASHP to export heat (P2P_H_P only)
RESISTIVE_BUY	Power for resistive heat
RSOC_BUY	Power required to run SOEC mode of the rSOC
	Asks (power)
PV_EXPORT	Exported solar PV power
EV_V2X	Power exported from the EV battery
RSOC_SELL	Power from SOFC mode of the rSOC
	Offers (heat)
HEAT_DEMAND	Heat required to meet household demand

HEAT_FOR_TES	Heat to charge thermal storage
	Asks (heat)
HEAT_FROM_RSOC	Heat from the rSOC
HEAT_FROM_ASHP	Heat from the ASHP
HEAT_FROM_RH	Heat from the resistive heater

7.3.3.2 Price prediction

For simplicity, the initial price prediction at the start of trading is equal to the mid-market rate halfway between grid retail and feed-in price. Initial heat price predictions are £0.10 / kWh or £0.08 / kWh, dependent on season, where this is based on experience running the model. A truer picture of prices emerges after a few rounds of bidding. Subsequent price predictions at each timeslot are the mean of the two most recent clearing prices. If no trading is occurring for the timeslot in question, the price predictions start to 'decay' exponentially towards limiting prices given by top-of-book prices, if outstanding bids exist, or otherwise the utility prices. A decay constant of 0.22 is used based on experience. Note that in the absence of trading, price predictions can still improve if top-of-book prices improve. The price of hydrogen is considered fixed, at least over the one day time horizon of an auction.

7.3.3.3 Optimisation and internal auction

A full update to bidding strategy employs MILP optimisation of a household's energy flow, combined with rules to generate additional backup bids.

Electricity purchased to charge the EV battery may be required either for essential travel, or for V2H / V2G, and this affects the valuation per kWh. To enable these bids to be separated, the optimiser runs twice, with V2X disabled the first time.

For each timeslot *t* the MILP optimisation receives information on the energy that has already been traded, i.e. $E_{bought,t}$, $E_{sold,t}$, $H_{bought,t}$, and $H_{sold,t}$, as well as the latest price forecasts for each timeslot. The optimiser calculates schedules for all devices and the amount of energy to be imported / exported. At each timeslot, the net energy required by the devices must balance with the energy already bought / sold, and the energy to be bought / sold in the future, as expressed in equations 7.1 and 7.2.

$$E_{sold,t} - E_{bought,t} = -E_{sell,t} + E_{buy,t} + \sum_{d\in\mathcal{D}} \left(E_{gen,d,t} - E_{cons,d,t}\right) \quad \text{(Eqn. 7.1)}$$

$$H_{sold,t} - H_{bought,t} = -H_{sell,t} + H_{buy,t} + \sum_{d\in\mathcal{D}} \left(H_{gen,d,t} - H_{cons,d,t}\right) \quad \text{(Eqn. 7.2)}$$

Note that the left hand side of each equations consists of fixed parameters, whereas the right hand side consists of non-negative decision variables.

For simplicity, P2P trades that have previously been made are not reversed; i.e. participants do not sell / buy back energy that they have previously bought / sold. Thus, participants will never have both asks and offers agreed for the same energy type at the same timeslot. (The exception is at the very end of the trading, when trade with the utility electricity supplier, at retail tariff, may be used to reverse P2P trades if wished.) Accordingly, the following constraints apply:

$$\begin{cases} E_{bought,t} > 0 \ : \ E_{sell,t} = 0 \\ E_{sold,t} > 0 \ : \ E_{buy,t} = 0 \end{cases} \quad \text{(Eqn. 7.3)}$$

$$\begin{cases} H_{bought,t} > 0 \ : \ H_{sell,t} = 0 \\ H_{sold,t} > 0 \ : \ H_{buy,t} = 0 \end{cases} \quad \text{(Eqn. 7.4)}$$

The objective function for the household optimisation is given as the net earnings; plus the value attached to any energy stored at the close of the day; minus any penalty terms arising from individual device models. Note that this is expressed as a maximisation problem:

$$\begin{aligned} obj = & \sum_t \left(E_{sell,t} \cdot p_{power,exp,t} - E_{buy,t} \cdot p_{power,imp,t}\right) \\ & + \sum_t \left(H_{sell,t} \cdot p_{heat,exp,t} - H_{buy,t} \cdot p_{heat,imp,t}\right) \\ & + p_{H2,exp} \sum_t H2_{sell,t} - p_{H2,imp} \sum_t H2_{buy,t} \\ & + \sum_{d \in \mathcal{D}} VAL_{d,t_{last}} - \sum_{d \in \mathcal{D}} \sum_t PEN_{d,t} \end{aligned} \quad \text{(Eqn. 7.5)}$$

The variables, constraints and penalty terms that describe the specific behaviour of each device $d \in \mathcal{D}$ are given in Section 7.3.4.

The optimisation model is expressed in terms of net energy generation / consumption; thus it does not explicitly specify which devices in a house share energy with each other, nor which devices are assigned to use (supply) energy previously bought (sold) on the P2P market. However, for the assignment of reserve prices in the P2P market, it is necessary to know which device is seeking to buy / sell energy. Therefore, before bids are submitted to the P2P auctions, the devices in each household participate in an internal auction. Each device places offers for the amounts $E_{cons,d,t}$ and asks for the amounts $E_{gen,d,t}$; these may be broken down into separate bids with differing reserve price. Prices submitted to the internal auction are always truthful (see Table 7.4). Additionally, the amounts $E_{bought,t}$ and $E_{sold,t}$ enter the internal auction respectively as asks and offers; they are assigned respectively very low and very high prices, to ensure that they are cleared. The internal auctions are cleared in identical fashion to the P2P auction (see Section 7.3.2). Bids cleared in the internal auction are stamped with a nominal valuation that corresponds either to the current predicted P2P price (when the bid has been matched with another household device) or, if matched with a previously successful P2P bid, the traded price of this bid. Bids not cleared in the internal auction proceed to the P2P auction.

7.3.3.4 Interdependence of bids

As has been already mentioned, bids to buy and sell energy can be interdependent in two ways. Firstly, in the heat and power market, there is interdependence between bids for the two types of energy. For the rSOC (in SOFC mode) to export both heat and power at a particular timeslot, it is fundamentally required that:

$$\eta_{SOFC} \cdot \eta_{inv} \cdot p_{power} + \eta_{SOFCth} \cdot p_{heat} \geq p_{H2} \quad \text{(Eqn. 7.6)}$$

Where heat (power) from the rSOC is matched in the internal auction, the corresponding power (heat) can immediately be assigned a reserve price and sent to the P2P market. The P2P reserve price in this case is obtained by substituting the valuation assigned by the internal auction into Equation 7.6. Where neither heat nor power are matched in the internal auction, so that both are to be sold to peers, the following approach is taken:

1. The bulk of the energy for export is assigned a reserve price that guarantees a profit, i.e. $p_{H2} \,/\, \eta_{SOFCth}$ for heat and $p_{H2} \,/\, \eta_{SOFC}$ for power.

2. Incremental amounts of heat / power corresponding to 10% of the rSOC capacity are assigned more aggressive reserve prices that still mutually satisfy Equation 7.6.

3. Whenever a P2P bid to sell rSOC heat or power is matched, the corresponding quantity of power / heat receives a new price obtained by substituting the clearing price into Equation 7.6.

4. When the aggressively priced incremental amounts are matched, they are replaced, until there is no more capacity to sell, or the auction ends.

For the ASHP to import power in order to export heat, it is required that:

$$COP \cdot p_{heat} \geq p_{power} \qquad \text{(Eqn. 7.7)}$$

This is addressed in a similar manner to the rSOC. Where power is to be imported in order to export heat, only 10% of the ASHP capacity is entered into the P2P electricity auction at one time. This is priced at $COP \cdot \tilde{p}_{heat}$ where $\tilde{p}_{heat}$ is the predicted price to sell heat. 100% of the ASHP thermal capacity can be entered into the P2P heat market with a price of $p_{grid\_retail} \,/\, COP$, as the grid retail price is guaranteed to be available. If a bid to buy power is matched, the price of the corresponding heat can be updated as $p_{cl} \,/\, COP$. Note that the incremental bidding of 10% capacity prevents excessive purchase of electricity when the sale of corresponding heat may not be achieved.

The second type of interdependence is between bids to charge and discharge energy storage. For instance, for the EV, the fundamental requirement in order to buy energy at t_1 and sell at t_2 is:

$$\eta_{inv}^2 \cdot \eta_{st}\left(p_{power,t_2} - c_{V2X}\right) \geq p_{power,t_1} \qquad \text{(Eqn. 7.8)}$$

where c_{V2X} represents the cost of cycling the EV battery, η_{st} is the DC round-trip battery efficiency, and η_{inv} is the inverter efficiency. As with the ASHP and rSOC, the approach is to only allow small increments of energy to be submitted to the P2P auction at one time. For the EV, the total volume of bids to charge the storage (i.e. type EV_ARBITRAGE) should not exceed the volume of matched V2X energy by more than 10% of battery capacity. Conversely, the total volume of bids to discharge storage does not exceed the volume of matched EV_ARBITRAGE bids by more than 10%. As with the interdependence of heat and power bids, matching of a P2P bid to charge / discharge the EV will trigger adjustment of the price for a corresponding volume of discharged / charged energy. Bids to charge and discharge the TES are dealt with in analogous fashion.

It is worth noting that the model also allows heat energy to be stored in the fabric of the house, by exceeding the minimum thermostat demand temperature. The interaction of timeslots induced by this energy storage is handled by the optimiser, but we have not attempted to explicitly address it in the bidding strategy and reserve prices.

Interdependent bids are updated after the clearing of every timeslot in every round, even if the house does not perform a full strategy update that round (this detail is omitted from Figure 7.1).

7.3.3.5 Pricing strategy

Truthful reserve prices

It is important for bidders to assign a value to the energy they are seeking to trade; i.e. a minimum acceptable price for asks and a maximum acceptable price for offers. The assumptions made for these reserve prices are shown in Table 7.4.

Table 7.4. Truthful reserve prices (i.e. limit prices) assumed for different applications.

Category	Truthful reserve price (£/kWh)
Offers to buy power	
INFLEXIBLE_LOAD	p_{grid_retail}
EV_ESSENTIAL	p_{grid_retail}
ASHP_BUY	p_{grid_retail}
ASHP_FOR_EXPORT	$COP \cdot \tilde{p}_{heat}$ where $\tilde{p}_{heat}$ is the predicted price to sell heat
RESISTIVE_BUY	p_{grid_retail}
RSOC_BUY	$min\left(p_{grid\_retail}, \frac{p_{H2} \cdot \eta_{inv}}{\eta_{SOEC}}\right)$
EV_ARBITRAGE	**For an amount corresponding to the EV_V2G bids that have been matched (internally or externally) at an average value of p_{V2X}:** $(p_{V2X} - c_{V2X}) \cdot \eta_{inv}^2 \cdot \eta_{st}$ **For a further amount not exceeding 10% of battery capacity in each auction round:** $(\tilde{p}_{V2X} - c_{V2X}) \cdot \eta_{inv}^2 \cdot \eta_{st}$ (where $\tilde{p}_{V2X}$ is the *predicted* average value of corresponding EV_V2X.)
Asks to sell power	
PV_EXPORT	p_{grid_FI}
RSOC_SELL	**No heat trading:** ***For the power corresponding to heat used in the house:*** $\frac{p_{H2}}{\eta_{SOFC} \cdot \eta_{inv} + \eta_{SOFCth}}$ ***For any further power:*** $\frac{p_{H2}}{\eta_{SOFC} \cdot \eta_{inv}}$ **With heat trading:** ***Where corresponding heat is unmatched:*** $\frac{p_{H2}}{\eta_{SOFC} \cdot \eta_{inv}}$ ***Where corresponding heat is matched at price p_{heat}:*** $\frac{p_{H2}}{\eta_{SOFC} \cdot \eta_{inv}} - \frac{p_{heat} \cdot \eta_{SOFCth}}{\eta_{SOFC} \cdot \eta_{inv}}$
EV_V2G	**For an amount corresponding to the EV_ARBITRAGE bids that have been**

	matched (internally or externally) at an average value of p_{ARB}: $$\frac{p_{ARB}}{\eta_{inv}^2 \cdot \eta_{st}} + c_{V2X}$$ **For a further amount not exceeding 10% of battery capacity in each auction round:** $$\frac{\tilde{p}_{ARB}}{\eta_{inv}^2 \cdot \eta_{st}} + c_{V2X}$$ where $\tilde{p}_{ARB}$ is the average predicted price of the EV_ARBITRAGE bids not yet matched.
Offers to buy heat	
HEAT_DEMAND	$min(\tilde{p}_{power}, p_{heat,marginal})$ where $\tilde{p}_{power}$ is predicted power price and $p_{heat,marginal}$ is the price to generate more heat locally.
Asks to sell heat	
HEAT_FROM_RSOC	***Where corresponding power is unmatched:*** $$\frac{p_{H2}}{\eta_{SOFCth}}$$ ***Where corresponding power is matched at price p_{power}:*** $$\frac{p_{H2}}{\eta_{SOFCth}} - \frac{p_{power} \cdot \eta_{SOFC} \cdot \eta_{inv}}{\eta_{SOFCth}}$$
HEAT_FROM_ASHP	***Where corresponding power has not been obtained:*** $$\frac{p_{grid\_retail}}{COP}$$ ***Where corresponding power has been obtained at price p_{power}:*** $$\frac{p_{power}}{COP}$$

Submitted prices

Some auction participants submit their truthful valuations (or 'limit' prices) with their bids, as per Table 7.4. This is termed an 'aggressive' strategy, since it maximises the chance of making a trade, possibly at the expense of obtaining a less favourable price. Other participants are 'zero-intelligence' (Z.I.) bidders. Z.I. bidders submit a reserve price uniformly distributed between their truthful reserve price and an upper or lower bound price. For bids to buy power, this means:

$$p_{res} \sim U(p_{grid\_FI}, p_{tr}) \qquad \text{(Eqn. 7.9)}$$

For bids to sell power:

$$p_{res} \sim U(p_{tr}, p_{grid\_retail}) \qquad \text{(Eqn. 7.10)}$$

For bids to buy heat:

$$p_{res} \sim U(0, p_{tr}) \qquad \text{(Eqn. 7.11a)}$$

For bids to sell heat:

$$p_{res} \sim U(p_{tr},\ p_{grid\_retail}) \qquad \text{(Eqn. 7.11b)}$$

7.3.3.6 Flexible bidding by the EV

For the charge and discharge of the EV battery, it is assumed that bidding can be more flexible than the strategy dictated by optimisation. The timeslots are partitioned into availability periods A_i representing distinct periods when the vehicle is available (long availability periods may also be subdivided). The amount to buy or sell from the battery is then calculated for the period as a whole, using the optimisation output, as per equations 7.12 and 7.13.

$$E_{buy,EV}^{A_i} = \sum_{t \in A_i} E_{buy,EV,t} \qquad \text{(Eqn. 7.12)}$$

$$E_{sell,EV}^{A_i} = \sum_{t \in A_i} E_{sell,EV,t} \qquad \text{(Eqn. 7.13)}$$

The bidder then places a 'group' of offers or asks across multiple timeslots of the availability period. These include the bids specified by the optimiser, as well as backup bids with a total volume of up to $r_{bu} \cdot E_{buy,EV}^{A_i}$ or $r_{bu} \cdot E_{sell,EV}^{A_i}$ where r_{bu} is a backup ratio randomly chosen by each auction participant. Since the total volume of the bids is now greater than required, superfluous bids must be cancelled once the targeted amount is secured for the availability periods. Because the timeslots of the auction are settled sequentially, there is opportunity after the settlement of each timeslot to make these adjustments. Note again that the market does *not* allow the submission of bids that are flexible by time. Instead, the flexibility is achieved entirely by the bidder's strategy of placing additional bids and cancelling those which become superfluous.

Since the 'backup' bids have not been specified by the optimiser, the headroom to charge or discharge the battery has to be checked at each timeslot, against any bids to buy or sell that have already succeeded, and any energy planned to exchange between EV and house.

7.3.3.7 Protecting state-of-charge limits

Bids to supply energy from energy storage (the EV battery or TES) may be contingent on bids to buy energy at a separate timeslot. If only a subset of the bids placed are successful, then the state-of-charge limits of the storage could be infringed (in practice this could be prevented via last-minute trading at the grid tariffs, but this would be financially unattractive). To avoid this situation, the volume of bids can be trimmed to ensure that the future state-of-charge remains within limits.

Following the settlement of the internal auctions, the 'achieved' storage profile $\hat{E}_{stored,t}$ is obtained for the EV battery (or any other energy storage device). That is, the profile achievable with energy already bought / sold on the P2P market, and energy shared within the house, that the internal market has assigned to the storage. $\hat{E}_{cons,st,t} \in (0, E_{cons,st,t})$ and $\hat{E}_{gen,st,t} \in (0, E_{gen,st,t})$ are respectively the amounts of power consumption and generation cleared by the internal auction for the storage device *d*. The achieved storage profiles is then defined as follows:

$$\hat{E}_{stored,\hat{t}} = E_{stored,0} + \sum_{t=1}^{\hat{t}} \left\{ \eta_{inv} \cdot \eta_{st} \cdot \hat{E}_{cons,d,t} - \frac{1}{\eta_{inv}} \hat{E}_{gen,d,t} + E_{drive,t} - E_{drive,t} \right\} \quad \text{(Eqn. 7.14)}$$

Before the auction for timeslot t is settled, each participant checks the headroom for charge and discharge:

$$BUY_{max} = \min_{\hat{t} \geq t} \left(C_{st} - \hat{E}_{stored,\hat{t}} \right) \cdot \frac{1}{\eta_{inv} \cdot \eta_{st}} \quad \text{(Eqn. 7.15)}$$

$$SELL_{max} = \min \left(\min_{\hat{t} \geq t} \left(\hat{E}_{stored,\hat{t}} \right), \hat{E}_{stored,t_{last}} - E_{min\_final} \right) \cdot \eta_{inv}$$

Note that, if there is a constraint E_{min_final} on the final amount of energy stored, this must also be factored in. The volume of bids for energy to charge the storage are then compared to the value of BUY_{max} and reduced if necessary; asks are compared to $SELL_{max}$ in the same way. Conversely, bids that were previously reduced in this way may be restored to their original value following the success of 'dependent' bids. Bids with volume reduced to zero are not submitted to the auction, but still retained in case they can be activated in future rounds.

7.3.4 MILP models for devices

In this section details of the constraints that describe particular devices are given. Recall that H_{gen}, E_{gen}, H_{cons} and E_{cons} are the main variables interfacing the rest of the model.

7.3.4.1 ASHP

COP is assumed dependent only on the outdoor temperature, with no dependence on the load point. For simplicity, full modulation to arbitrary partial load is assumed to be possible.

$$H_{gen,ashp,t} = COP_t \cdot E_{cons,ashp,t} \quad \text{(Eqn. 7.16)}$$

$$0 \leq E_{cons,ashp,t} \leq \Delta t \cdot P_{ashp}^{max} \quad \text{(Eqn. 7.17)}$$

7.3.4.2 EV battery

Optimisation of the EV battery includes two important time series inputs: the energy required for driving $E_{drive,t}$ and the availability α_t which takes a value in [0,1] for every timeslot. Decision variables are the AC power consumed by the battery $E_{cons,EV,t}$, AC power generated $E_{gen,EV,t}$, and power consumed from rapid charging while away from the house, $E_{rapid,t}$. Penalty terms include the cost of rapid charging and the assumed cost for discharging the battery V2X. Generally V2X discharge will not happen except when $p_{power,exp,t} > c_{V2X}/\eta_{inv}$.

$$E_{stored,t+1} = E_{stored,t} + \eta_{inv} \cdot \eta_{st} \cdot E_{cons,EV,t} + \eta_{st} \cdot E_{rapid,t} - \frac{1}{\eta_{inv}} \cdot E_{gen,EV,t} - E_{drive,t} \quad \text{(Eqn. 7.18)}$$

$$0 \leq E_{stored,t+1} \leq C_{EV} \quad \text{(Eqn. 7.19)}$$

$$E_{stored,t_{last}} \geq E_{min\_final} \quad \text{(Eqn. 7.20)}$$

$$E_{rapid,t} \leq 50 \cdot (1 - \alpha_t) \quad \text{(Eqn. 7.21)}$$

$$PEN_{EV,t} = c_{rapid} \cdot E_{rapid,t} + c_{V2X} \cdot E_{gen,EV,t} \quad \text{(Eqn. 7.22)}$$

7.3.4.3 rSOC

The rSOC may operate in either SOFC or SOEC mode. Operation is described principally by decision variables $E_{gen,rSOC,t}$, $E_{cons,rSOC,t}$ and $H_{gen,rSOC,t}$ with hydrogen consumption / production derived from these. Binary variables b_{SOFC} and b_{SOEC} describe the mode of the rSOC, and enable minimum partial loads to be imposed. Switching between modes incurs a penalty described by $PEN_{rSOC,t}$ It is assumed that 'hot idle' operation corresponds to the lowest possible partial load for SOFC mode or SOEC mode; full cycling of the rSOC to a cold, fully off state is not considered in the context of the MILP formulation. Note that the rSOC is assumed to be able to dump heat if necessary.

$$\Delta t \cdot P_{SOFC}^{min} \cdot b_{SOFC,t} \leq E_{gen,rSOC,t} \leq \Delta t \cdot P_{SOFC}^{max} \cdot b_{SOFC,t} \quad \text{(Eqn. 7.23)}$$

$$\Delta t \cdot P_{SOEC}^{min} \cdot b_{SOEC,t} \leq E_{cons,rSOC,t} \leq \Delta t \cdot P_{SOEC}^{max} \cdot b_{SOEC,t} \quad \text{(Eqn. 7.24)}$$

$$b_{SOFC,t} + b_{SOEC,t} = 1 \quad \text{(Eqn. 7.25)}$$

$$0 \leq H_{gen,rSOC,t} \leq \frac{\eta_{SOFCth}}{\eta_{SOFC}} E_{gen,rSOC,t} \quad \text{(Eqn. 7.26)}$$

$$H2_{gen,rSOC,t} = E_{cons,rSOC,t}/\eta_{SOEC} \quad \text{(Eqn. 7.27)}$$

$$H2_{cons,rSOC,t} = E_{gen,rSOC,t}/\eta_{SOFC} \quad \text{(Eqn. 7.28)}$$

$$PEN_{rSOC,t+1} \geq c_{switch} \cdot \left(b_{SOFC,t+1} - b_{SOFC,t}\right) \quad \text{(Eqn. 7.29)}$$

$$PEN_{rSOC,t+1} \geq c_{switch} \cdot \left(b_{SOEC,t+1} - b_{SOEC,t}\right) \quad \text{(Eqn. 7.30)}$$

7.3.4.4 Space heating

Buildings consist of two thermal masses, representing the building interior and building walls. Building archetypes consist of the thermal masses of these C_i and C_w, and heat transfer coefficients $K_{i\leftrightarrow w}$, $K_{i\leftrightarrow e}$, $K_{w\leftrightarrow e}$, between the thermal masses and the environment. Heat $H_{sh,t}$ representing space heating output is added to the building interior. A trapezoidal method is used to discretize the resulting system of ODEs. Demand temperature is given by $T_{dem,t}$ while $T_{max,t}$ gives an upper temperature limit. Penalty terms $PEN_{sh,t}$ are defined for infringing these limits, with c_{sh} representing the cost per degree-hour of temperature infringement.

$$H_{i\leftrightarrow w,t} = 0.5 \cdot \Delta t \cdot K_{i\leftrightarrow w}\left(T_{i,t} + T_{i,t+1} - T_{w,t} - T_{w,t+1}\right) \quad \text{(Eqn. 7.31)}$$

$$H_{i\leftrightarrow e,t} = 0.5 \cdot \Delta t \cdot K_{i\leftrightarrow e}\left(T_{i,t} + T_{i,t+1} - T_{e,t} - T_{e,t+1}\right) \quad \text{(Eqn. 7.32)}$$

$$H_{w\leftrightarrow e,t} = 0.5 \cdot \Delta t \cdot K_{w\leftrightarrow e}\left(T_{w,t} + T_{w,t+1} - T_{e,t} - T_{e,t+1}\right) \quad \text{(Eqn. 7.33)}$$

$$T_{i,t+1} = T_{i,t} + \left(H_{sh,t} + H_{gain,t} - H_{i\leftrightarrow w,t} - H_{i\leftrightarrow e,t}\right)/C_i \quad \text{(Eqn. 7.34)}$$

$$T_{w,t+1} = T_{w,t} + \left(H_{i\leftrightarrow w,t} - H_{w\leftrightarrow e,t}\right)/C_w \quad \text{(Eqn. 7.35)}$$

$$PEN_{sh,t} \geq 0 \quad \text{(Eqn. 7.36)}$$

$$PEN_{sh,t} \geq \Delta t \cdot c_{sh} \cdot \left(T_{dem,t} - T_{i,t}\right) \quad \text{(Eqn. 7.37)}$$

$$PEN_{sh,t} \geq \Delta t \cdot c_{sh} \cdot \left(T_{i,t} - T_{max,t}\right)(\quad \text{(Eqn. 7.38)}$$

7.3.4.5 TES

Sensible thermal storage with hot water is modelled as a single thermal mass. This is described by variables $T_{tes,t}$, $H_{cons,tes,t}$ and $H_{gen,tes,t}$. Losses $H_{loss,tes,t}$ are assumed proportional to the difference in temperature $T_{tes} - T_i$ between the storage and the house interior. These losses are added to the gains term $H_{gain,t}$ of the space heating model. C_{tes} gives the constant heat capacity of the storage in kWh/°C. Using a trapezoidal method to account for any variation in T_i over a timestep, the temperature of the storage evolves as specified in equations 7.39 and 7.40. Imposing a minimum usable temperature T_{tes}^{usable} requires the introduction of binary variables $b_{gen,tes,t}$ and $b_{cons,tes,t}$ together with the constraints given in equations 7.42 – 7.44 and 7.46.

$$\Lambda \coloneqq exp\left(-\frac{\Delta t \cdot K_{tes\leftrightarrow i}}{C_{tes}}\right) \quad \text{(Eqn. 7.39)}$$

$$T_{tes,t+1} = \Lambda \cdot T_{tes,t} + (1 - \Lambda) \cdot \left(\frac{H_{cons,tes,t} - H_{gen,tes,t}}{\Delta t \cdot K_{tes\leftrightarrow i}} + 0.5 \cdot T_{i,t} + 0.5 \cdot T_{i,t+1}\right) \quad \text{(Eqn. 7.40)}$$

$$H_{loss,tes,t} = C_{tes} \cdot \left(T_{tes,t} - T_{tes,t+1}\right) - H_{gen,tes,t} + H_{cons,tes,t} \quad \text{(Eqn. 7.41)}$$

$$b_{gen,tes,t} + b_{cons,tes,t} \leq 1 \quad \text{(Eqn. 7.42)}$$

$$H_{cons,tes,t} \leq b_{cons,tes,t} \cdot \Delta t \cdot P_{tes}^{max} \quad \text{(Eqn. 7.43)}$$

$$H_{gen,tes,t} \leq b_{gen,tes,t} \cdot \Delta t \cdot P_{tes}^{max} \quad \text{(Eqn. 7.44)}$$

$$T_{tes}^{min} \leq T_{tes,t} \leq T_{tes}^{max} \quad \text{(Eqn. 7.45)}$$

$$T_{tes,t+1} \geq b_{gen,tes,t} \cdot T_{tes}^{usable} \quad \text{(Eqn. 7.46)}$$

7.3.4.6 Resistive heater

A resistive heater in the model converts electrical power to heat with 100% efficiency.

$$H_{cons,rh,t} = E_{cons,rh,t} \quad \text{(Eqn. 7.47)}$$

$$0 \leq E_{cons,rh,t} \leq \Delta t \cdot P_{rh}^{max} \quad \text{(Eqn. 7.48)}$$

7.4. Results

7.4.1 Case study

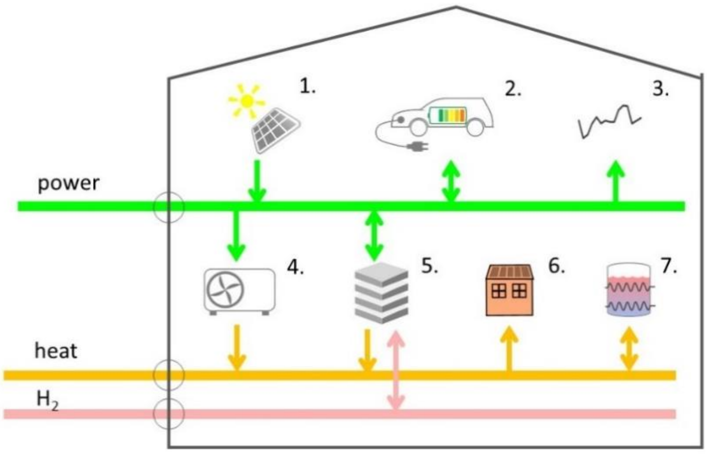

Figure 7.3. Shows the possible devices included in houses (not all houses contain all devices). 1. PV generation. 2. EV. 3. Inflexible electric load. 4. ASHP. 5. rSOC. 6. Heat demand model. 7. TES. 25 houses with varying devices are included in the case-study.

To investigate the efficacy of the P2P market, we employ a case study of 25 houses, containing various devices (see Figure 7.3). These are assumed to share the same circuit in the electrical distribution grid. Where heat trading is considered, the houses are assumed linked by a small 4th generation heat network.

The energy sharing neighbourhood is notionally located in south-east England with climate data drawn from UKECN [265] and inflexible load data from UKPN [209]. 15 houses are randomly assigned to have 6 kW$_p$ solar PV systems; these are evenly split between east-, south- and west-facing systems. Generation is calculated from irradiance data and the azimuth and tilt of the panels, using the model reported in [214].

All houses have one EV, with a trip schedule drawn from the UK National Travel Survey 2017 – 2019 [189]. The fuel economy of the vehicles is assumed to depend strongly on outdoor temperature; for more details of the data sample and EV model, see [248]. EV chargers have 7 kW capacity and for simplicity are assumed operable at any partial load. Furthermore, the possibility to discharge the EV battery V2H or V2G is always permitted.

Heat demand is modelled by adopting the CREST building archetype for improved semi-detached buildings, with building parameters varied by ± 20% for additional diversity [266]. Space heating demand temperatures are uniformly distributed between 17.5°C and 22°C; 50% of houses are assigned morning and evening heating patterns, while 50% are assigned all day heating patterns. 13 houses are assigned to have ASHP heating systems, and 12 have rSOCs. ASHPs have capacity 3 kW$_e$; COP is assumed to be 38% of the ideal COP operating between the outdoor air temperature and a flow temperature of 55°C, an assumption based on reference [267]. The heat pumps are assumed to be accompanied with TES consisting of 300 litres of hot water, operating between an upper temperature of 80°C and a minimum usable temperature of 40°C. Insulation is 10cm thick with conductivity 0.03 W/mK; thermal losses are assumed to flow into the internal node of the space heating model; see also the MILP model in Section 7.3.4.5.

The rSOC is assigned a capacity in SOFC mode of 2.5 kW_e. We assign η_{SOFC} as 16.7 kWh_e/kg_{H2} and η_{SOFCth} as 13.3 kWh_e/kg_{H2}, for a total CHP efficiency of $90\%_{LHV}$. η_{SOEC} is assigned as 48 kWh_e/kg_{H2}, so that used as an energy storage device, the rSOC has round-trip efficiency of just under 35%. Capacity in SOEC mode is taken as 7.5 kW_e. In both modes, the rSOC is assumed to have a partial load range of 10 – 100%. The rSOC is sized as a compromise between the peak electrical load and the peak space heating load of around 5 kW; for peaks in heat demand, either resistive heat or the heat network connection must be employed. See also the MILP rSOC model in Section 7.3.4.3.

Simulations were run over the duration of one week. The first week simulated was a spring week with moderate heat demand and moderate solar resource; the second was a winter week with high heat demand and low solar resource. The specifics are given in Table 7.5. Note that a 'heating degree day' (HDD) is calculated as the gap between a day's mean temperature and 15.5°C.

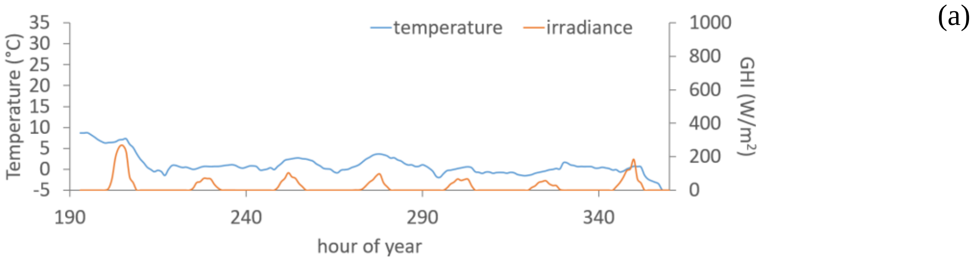

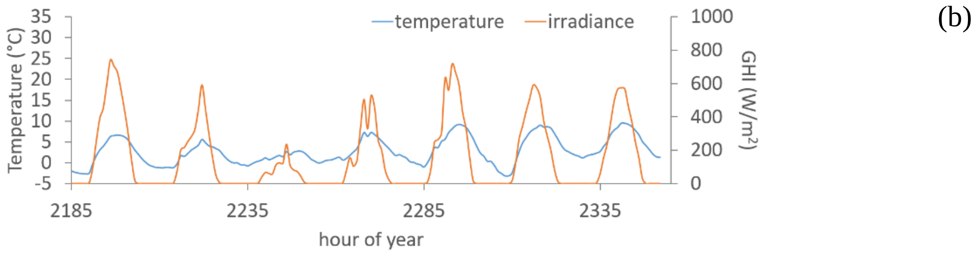

Figure 7.4. Irradiance and temperature for (a) the winter week and (b) the spring week.

Table 7.5. Climate weeks for simulation.

Season	Sample week start date	Mean GHI (W/m^2)	Mean HDD (°C)
Winter	9th Jan 2013	22.1	14.5
Spring	2nd April 2013	159.2	12.7

Three scenarios are considered: G_ONLY, where only grid trade of electricity is possible, and no trading in heat; P2P_P, where P2P trading of power only occurs, using the double auction approach detailed in the previous section; and P2P_H_P, where P2P trading of both heat and power is available.

The grid retail tariff in this work is assumed to be a constant £0.28 / kWh [268]; the grid feed-in tariff is £0.075 / kWh [269]. The cost of rapid charging for EVs is set at £0.0446 / kWh [246], [270]. We assume that the price of hydrogen is fixed in the case study, at £3.50 / kg [271], [272].

7.4.2 Results

We focus initially on the **spring** week in order to explore and showcase the functioning of the market. Figure 7.5 shows the volume of (a) power and (b) heat traded on April 2nd under P2P_H_P. The day's timeslots are shown vertically, and the rounds of the auction horizontally. Importantly, trading comes to an end after finite time; this is expected, since re-trading of energy already bought / sold is not considered for this work. Here, no transactions are taking place by the 25th round of trading; a similar outcome was observed for all days and seasons. Note that heat trading continues for longer than power trading. One reason for this is that ASHP heat becomes available on the market *after* the corresponding power has been acquired.

(a)

(b)

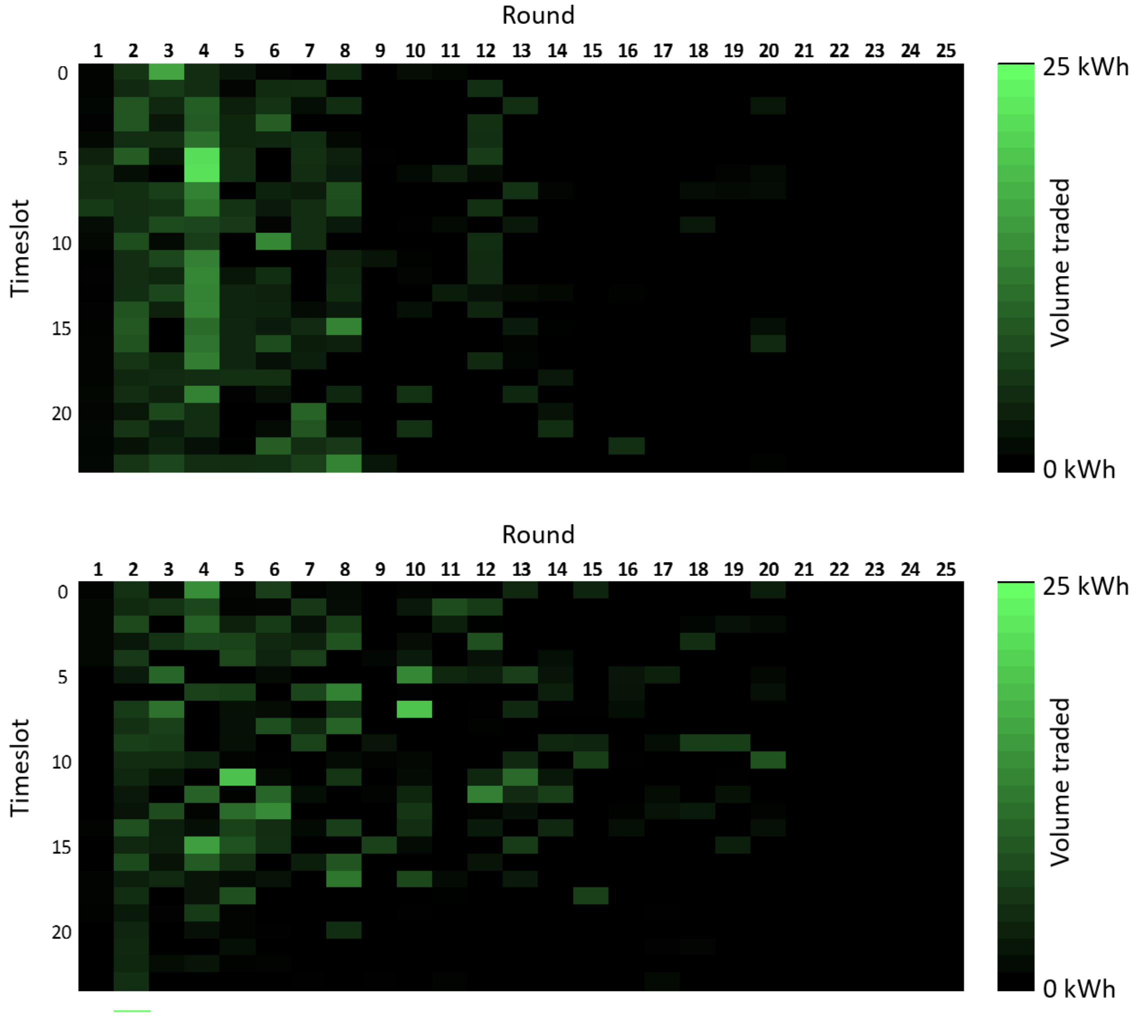

Figure 7.5. Shows progress of the double auction for April 2nd, the first day of the spring week, under P2P_H_P. Rounds of the auction are shown left to right, and timeslots of the day from top to bottom. (a) power trading; (b) heat trading. Timeslot 0 corresponds to 5 a.m.

For the spring week under P2P_P, 9400 bids to trade power were matched by the P2P auction, representing a turnover of 2.95 MWh, with an average price of £0.220 / kWh. Figure 7.6 (a) shows the diurnal P2P price variation, with heat demand and inflexible electrical load shown for comparison. The variation in electricity price is relatively modest; the price peak is roughly coincident with peak inflexible demand at 7 p.m, whilst availability of solar power depresses the price during the daytime.

Figure 7.7 shows the volume of (a) offers and (b) asks matched by the P2P_P market, by category, averaged over the spring week. The purchase of power for EV charging clearly peaks during the lowest priced period, particularly for the non-essential ('arbitrage') charging. ASHPs also purchase power to charge TES during the low price period. Transactions to supply inflexible load and essential EV charging continue all day, with generation from the rSOC dominating the supply side. Figure 7.9 shows the energy flows for P2P_P in the second column. When comparing with G_ONLY, the following observations can be made:

1. The quantity of grid imports is greatly reduced, with generation from the rSOC filling the gap.

2. Use of the rSOC's SOEC mode is decreased. Houses with solar surpluses find it more profitable to sell power to peers rather than manufacture H_2.

3. EV charging increases during the peak in solar generation, replacing the SOEC use.

4. Use of resistive heat is decreased. This is because the rSOCs in SOFC mode can now follow their household heat load, exporting the corresponding power to peers.

For the spring week under P2P_H_P, 9100 bids to trade power were successful, representing a turnover of 3.6 MWh; for heat, 8200 bids representing 2.9 MWh were matched (compare the total heat demand of 5.9 MWh). The average price of power was virtually unchanged from P2P_P at £0.226 / kWh; the average heat price was £0.078 / kWh. Figure 7.6 (b) shows the diurnal price variation for P2P power and heat; variations in heat price clearly respond to the demand.

Figure 7.8 shows the volumes of successful asks and offers under P2P_H_P. As before, EV charging increases in response to peak solar generation. Large amounts of power are purchased by ASHPs in order to re-export the heat. ASHP dominates the supply side of heat market during the day, whereas rSOCs are more likely to export heat at night when (a) COP is lower for the ASHPs, making them less competitive and (b) local heat demand is more likely to be low. 1.97 MWh of ASHP heat was exported overall, at an average price of £0.077 / kWh; for rSOC the corresponding figures were 0.90 MWh, and £0.081 / kWh. Note that the cost of rSOC heat is well below the cost of the corresponding hydrogen, which is possible thanks to the high average value (£0.228 / kWh) of the corresponding power on the P2P market. Some import of heat in order to charge TES occurs during price troughs; this heat is always discharged locally, as no heat is observed to be sold back to the network. The impact of heat trading on the energy flows can be seen in Figure 7.9; the most significant impact is that the use of resistive heat now almost completely ceases, as heat that cannot be generated locally can instead be imported. Heat trading also appears to have enabled increased V2X discharge from the EVs, the reasons for which are not wholly clear. Use of TES is decreased, as exporting heat P2P may be more profitable than storing it.

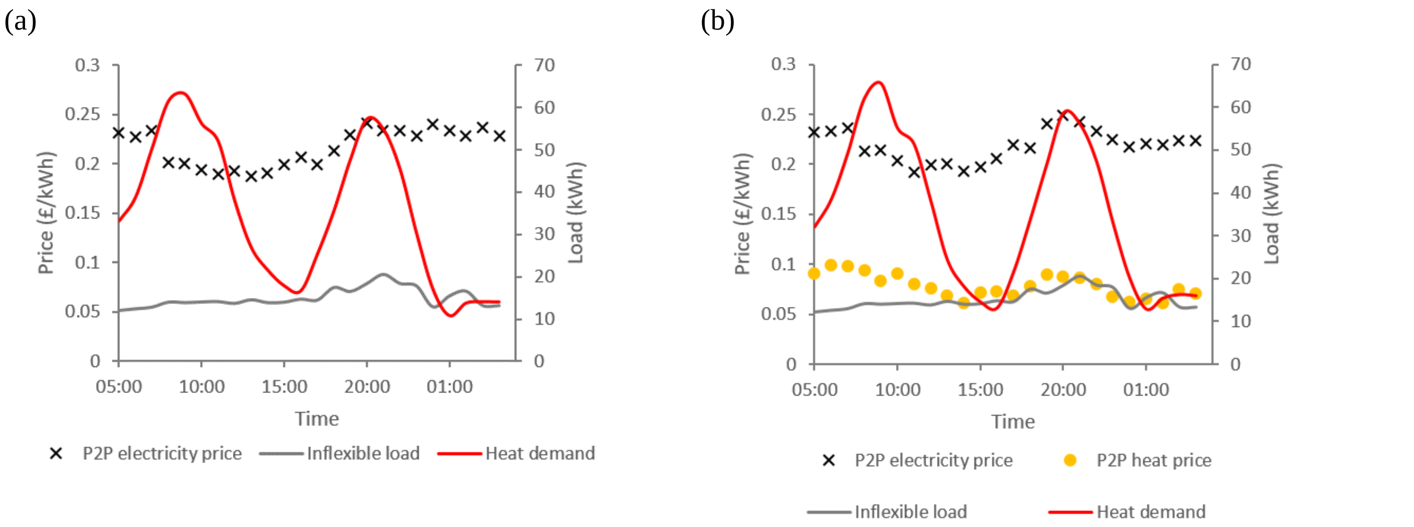

Figure 7.6. Daily P2P price variations averaged across the spring week. (a) P2P_P (b) P2P_H_P

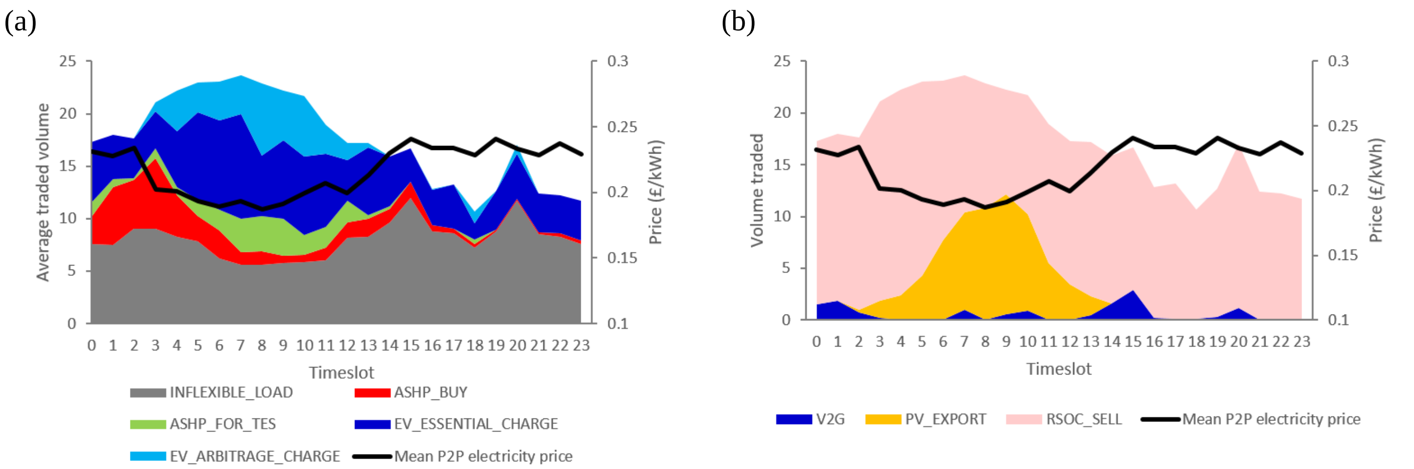

Figure 7.7. Electricity trades matched under **P2P_P** for the spring week. (a) offers (b) asks. Shown are the volumes transacted as a daily profile averaged across the week, with the average P2P prices for comparison.

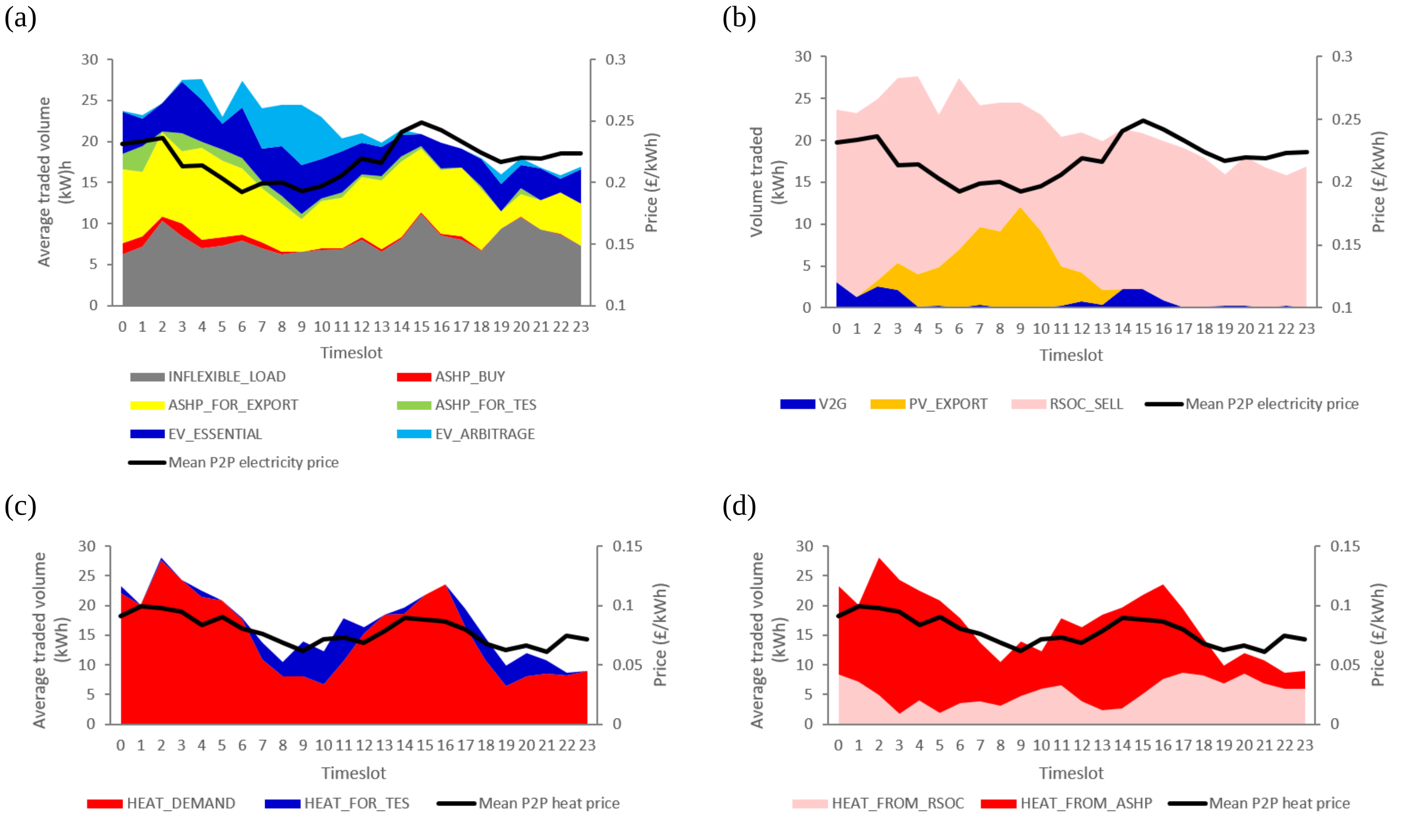

Figure 7.8. Trades matched under **P2P_H_P** for the spring week. Shown are the volumes transacted as a daily profile averaged across the week, with the average P2P prices for comparison. (a) electricity offers (b) electricity asks (c) heat offers (d) heat asks.

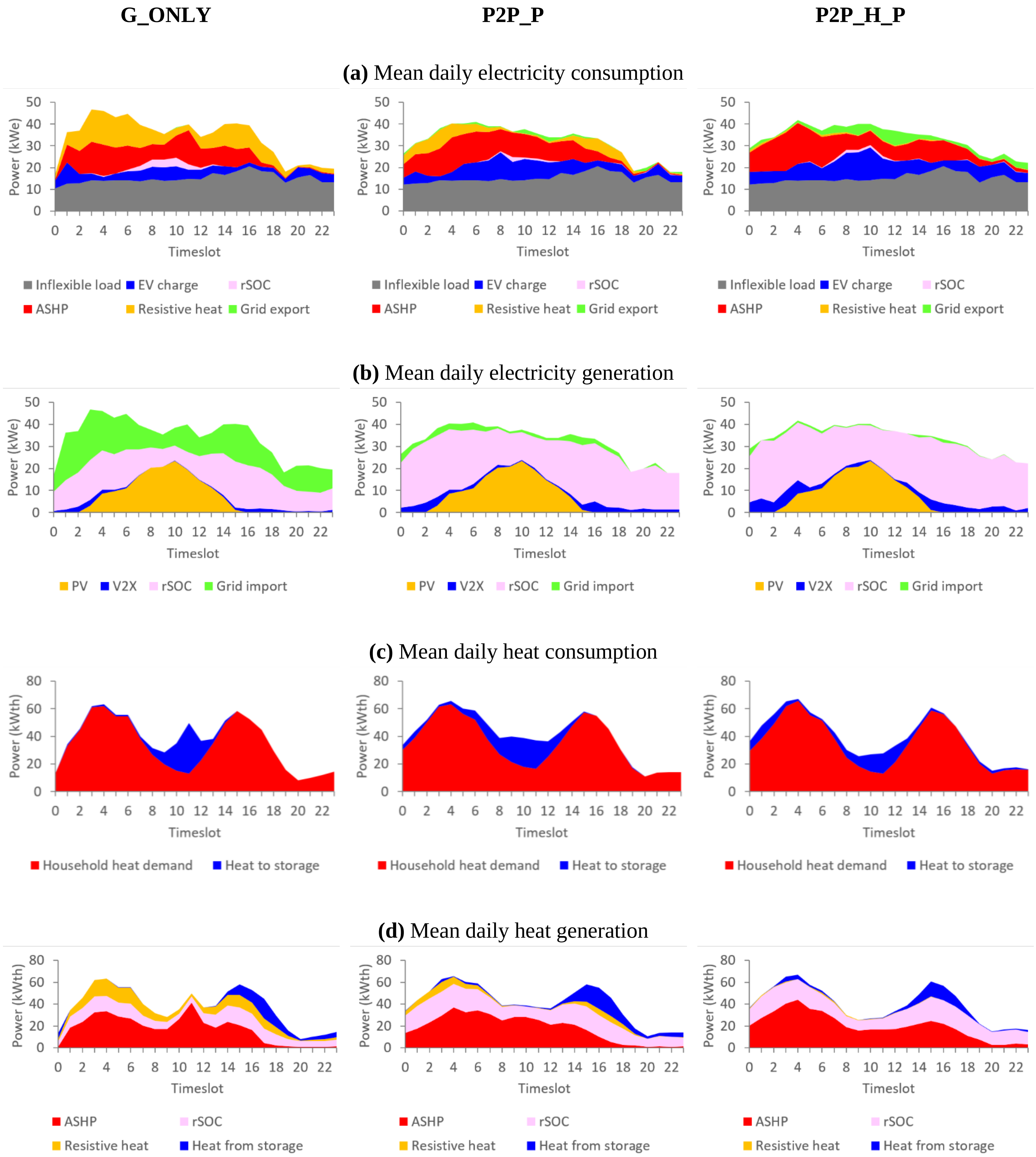

Figure 7.9. Average daily energy flow during the spring week, for G_ONLY (left), P2P_P (centre) and P2P_H_P (right). Shown are the generation and consumption of both heat and electricity.
Note that timeslot 0 corresponds to 5 a.m.

7.4.3 Savings and participant willingness

We now evaluate the economic advantages of the P2P markets; results from both spring and winter are considered. Figure 7.10 gives the average net bill for houses over (a) the winter week, and (b) the spring week; net bills comprise net P2P payments, net grid payments, and net hydrogen payments. Both trading systems enable the average house to save money relative to G_ONLY. For the winter week, the mean saving is £9.52 under P2P_P and £19.59 under P2P_H_P, and participant willingness is 84% and 88% respectively. rSOC houses appear to enjoy the greater financial benefits, but ASHP houses also profit. For the spring week, the mean saving is £16.99 under P2P_P and £16.69 under P2P_H_P, with participant willingness of 100% and 84%. From this it appears that the possibility to trade heat may not achieve additional financial savings during the spring weather conditions, although there may still be technical benefits.

7.4.4 Technical and environmental impact

Figure 7.13 shows the impact of the trading systems on the load duration curve for electrical grid interaction. For both winter and spring, P2P_P achieves a notable decrease in peak load, and P2P_H_P achieves a further reduction. Specifically, under G_ONLY, grid imports peak at 44.5 kW in winter and 35.3 kW in spring. P2P_P sees decreases of 20% (to 35.5 kW) and 44% (to 20.0 kW) for winter and spring respectively. P2P_H_P sees decreases of 44% (to 24.8 kW) and 66% (to 12.0 kW) for winter and spring respectively. Conversely, export of electricity to the grid becomes somewhat more common under P2P trading. This is especially the case under P2P_H_P, where for the rSOC, the opportunity to earn money by exporting heat P2P means that exporting power at the feed-in tariff is more viable. Under P2P_P the export of power to grid is more questionable and may indicate imperfections in houses' bidding strategies.

Note that grid interaction is a relatively small proportion of overall energy flow (see Figure 7.9); energy is principally obtained from hydrogen. P2P trading increases the usage of hydrogen, as the rSOCs are able to export energy to peers, and therefore run at a higher average load factor (see Figures 7.14, 7.12 (a)). The UK marginal GHG intensity for grid electricity is estimated at 0.269 $kgCO_2e$ / kWh for 2022 [273]. Under the assumption that all hydrogen purchased is green hydrogen, the GHG emissions for the 25 houses are proportional to the grid imports. The highest GHG intensity occurs during the winter week under G_ONLY, averaging 5.93 $kgCO_2e$ per house per day. P2P_P cuts this to 2.81 $kgCO_2e$ (-53%), P2P_H_P to 1.88 $kgCO_2e$ (-68%). The respective figures for spring are 3.29 $kgCO_2e$ under G_ONLY; 0.447 $kgCO_2e$ (-86%) and 0.134 $kgCO_2e$ (-96%).

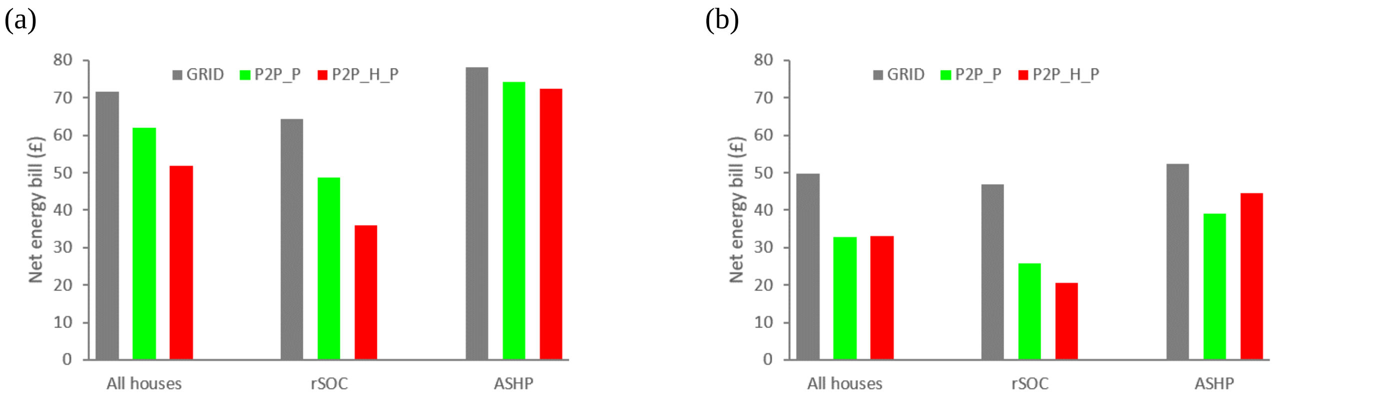

Figure 7.10. Average net household bills for (a) the winter week and (b) the spring week; these consist of net P2P payments, net grid payments, and net hydrogen payments.

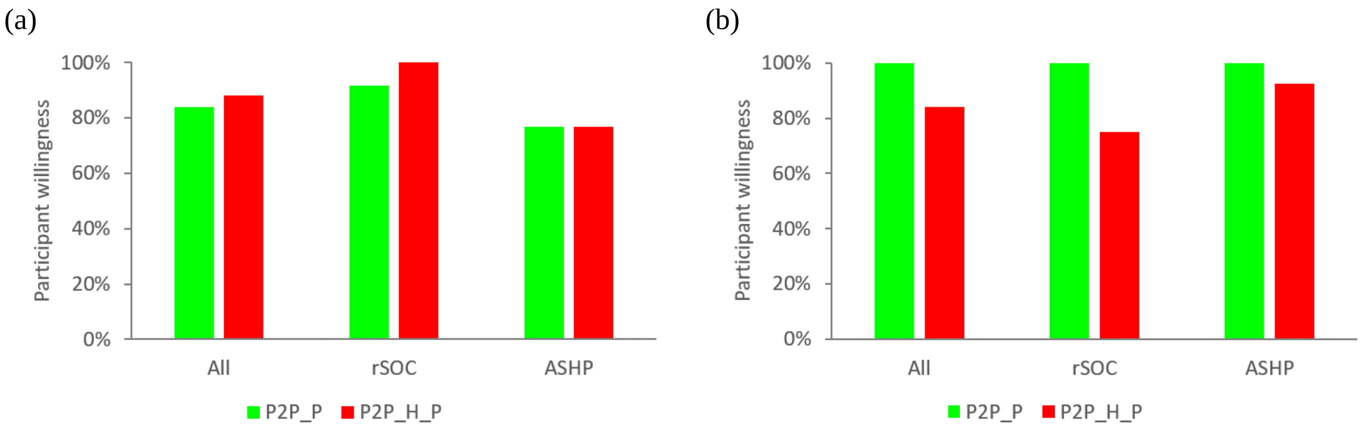

Figure 7.11. Participant willingness for (a) the winter week and (b) the spring week.

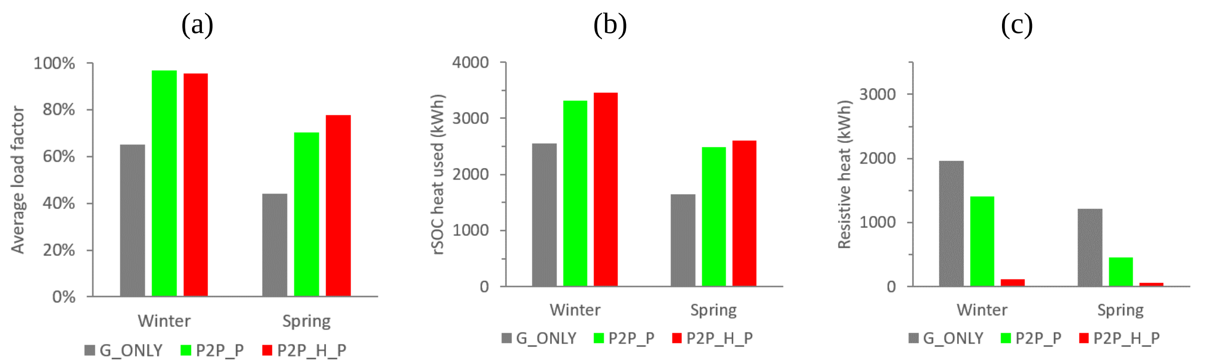

Figure 7.12. Impact of P2P trading on the rSOC and resistive heat use. (a) Average load factor for SOFC mode over one week. (b) rSOC heat used. (c) Resistive heat used.

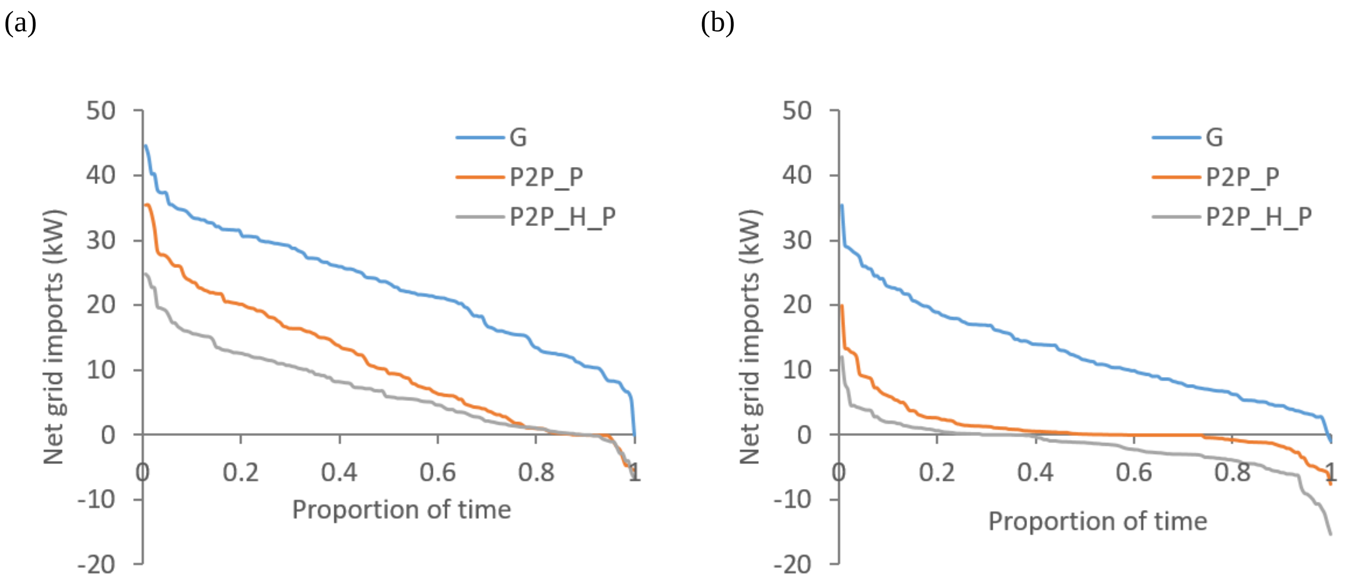

Figure 7.13. Load duration curves for the grid connection in (a) winter and (b) spring, for the three trading setups.

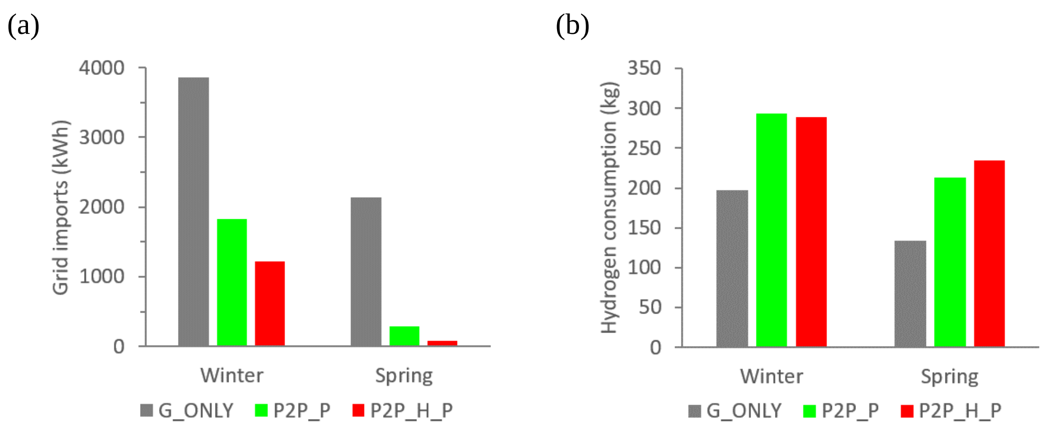

Figure 7.14. Imports of energy to the neighbourhood. (a) Grid electricity; (b) hydrogen.

7.5. Discussion and future work

The advantages of the P2P power trading market (P2P_P) are clear from these results, with the average house making significant weekly savings in both the climate weeks. Whilst PV and EVs play a part (see Figure 7.9) the rSOC is clearly the driving force, consuming more hydrogen in order to export power to peers at the P2P market price. The merits of the heat trading are more nuanced. In the cold winter week, P2P_H_P almost doubled the savings of an average house compared to P2P_P; however, in the spring week additional savings were not obtained. On the other hand, the burden on the grid connection was reduced both in terms of total and peak energy import.

Participant willingness for engagement with the P2P market was generally under 100%, indicating that it was possible for households to lose money via their attempts to trade energy. This possibility is somewhat inevitable, given that actual clearing prices may always differ from predicted prices. Also, whenever passive bidding takes place, there is the possibility of sub-optimal outcomes – for instance, an offer of type ESSENTIAL_LOAD could be outbid by an offer of type EV_ARBITRAGE. More sophisticated price prediction could perhaps help with participant willingness, and it may be that the bidding and pricing strategies could be further improved. A possible extension of the model could see the CDA preceded by a one-off double auction, allowing complex orders as found on the Nordpool and EPEX exchanges.

It is worth noting that the P2P power market in this work experienced almost universal 'seller's market' conditions, indicating an overall scarcity of power, and resulting in a P2P price closer to the retail tariff than the feed-in tariff. 6 kW_p PV generation in houses was clearly insufficient to cause major downward pressure on prices, despite the 6 kW_p figure being towards the upper end of what is viable for average UK housing stock (the actual average is 3 kW_p [1]). The addition of wind power into the generation mix might add interesting dynamics to the market – however, wind power is not generally very feasible in proximity to the built environment. Perhaps of more interest would be to use a variable grid tariff (the grid tariff was constant in this work) which could reflect the abundance of wind power on the wider electricity network.

A related issue to the prevailing seller's market conditions was the negligible use of SOEC mode of the rSOC. For manufacture of hydrogen to be optimal, there needs to be an abundance of cheap energy generation. For the spring week under G_ONLY, only 2.6 kg of hydrogen was produced via water electrolysis, compared to 133 kg consumed by SOFC mode. With the introduction of P2P trading, even this hydrogen production was mainly eliminated, as it became more profitable to export energy surpluses to peers. Even when we tried a run of the model over a high irradiance summer week with negligible heat demand, demand for hydrogen was still an order of magnitude higher than production. This seems to indicate that it is difficult to have enough generation in a distributed energy setting to justify running electrolysis.

All energy trading in this work was carried out on a day-ahead basis. In reality, trading would need to continue throughout the day, to balance imperfections in forecasting. The extension of the model to include such real-time trading should be relatively straightforward. Voltage constraints have also not been considered in this work (nor the analogous temperature constraints in the heat network); previous work such as [256] has explored such issues.

We have not modelled the possibility of storing hydrogen locally in this work, nor the possible fluctuations in hydrogen price over time. This is a topic worthy of interest. The fluctuating availability / price of hydrogen could provide additional incentives for P2P trading, as the relative desirability of procuring heat from ASHP and SOFC would see additional variation.

7.5.1 Conclusions

This work presented a continuous double auction P2P market for trading of power and heat in the day ahead. Both forms of market were successful in reducing reliance on grid electricity, and significant household savings were observed of the order of £10 / week; however some participants in the auction also incurred losses, and the availability of heat trading did not always provide an advantage over trading purely in power.

Reversible solid oxide fuel cells (rSOCs) were particularly advantaged by the P2P energy markets; it is clear that the availability of P2P energy trading could help to incentivise the take-up of such devices for CHP in houses. However, the 'reversible' aspect of the rSOC proved insignificant, with little hydrogen manufactured.

7.6. Acknowledgements

Grateful acknowledgement is made of the financial support of the Engineering and Physical Sciences Research Council (EPSRC) in the form of the ‘Energy Storage and its Applications’ Centre for Doctoral Training under grant code EP/L0168/18; also of the Electric Power Research Institute.

This research makes use of data from the UK Environmental Change Network and UK Power Networks.

8. Conclusions

This work centred on the possible energy storage applications of reversible solid oxide cells (rSOCs). As seen in Chapter 2, rSOCs have some notable characteristics distinct from other electrolyser and fuel cells - PEM and alkaline cells being the main rival technologies. Specifically, rSOCs can operate electrolysis and fuel cell modes within just one device; the conversion efficiency is higher; and the high operational temperature leads to the possibility of combined heat and power applications. A sizeable body of academic work already existed considering plant design for rSOC, but higher-level work on applications and techno-economic analysis was found to be very rare. This work therefore aimed to address some of this research gap, with the rSOC in tandem with hydrogen storage considered as a provider of electrical energy storage. The work aimed to assess the technical and economic benefits of the rSOC, including in comparison with other energy storage, with an approach combining simulation, optimisation and agent-based modelling.

A particular aim of the work was to consider the rSOC alongside distributed generation, electrified transport and electrified heat, since these three represent significant ongoing changes to the energy system that should not be omitted from any assessment of future technologies. Consideration of these also motivated the study of peer-to-peer (P2P) trading to be incorporated into the work. P2P can help to incentivise the shifting of demand (or generation) to allow more efficient energy use in a locality. Since P2P and energy storage both aim to address the problem of temporally matching energy supply and demand, studying both in conjunction seemed a logical approach. The various features were added progressively to the model, with embedded generation from Chapter 4 onwards; electric vehicles (EVs) from Chapter 5 onwards; P2P in chapters 6 and 7; and heat electrification in chapter 7.

The first two publications included here (chapters 4 and 5) considered the rSOC as an electrical energy storage to supply residential demand for power, with rooftop PV as the embedded energy generation. The construction of a microgrid simulation model was detailed in these chapters, and this model was combined with a global optimiser in order to explore technology choice and sizing, and to assess techno-economics. In both chapters, the rSOC is compared to a more conventional energy storage technology, namely the Li-ion battery; such comparison with alternative energy storage devices is missing from much of the extant literature. Electric vehicles were added to the simulation in Chapter 5. Both publications reached a similar conclusion: the economics for energy storage using rSOC, whether measured as payback period or net present value, are not attractive. Only when requiring the highest possible self-sufficiency is the hydrogen storage an optimal technology selection; even then, oversizing of generation is generally preferred where possible (for rooftop PV, of course, the sizing *is* generally constrained). For moderate increases in self-sufficiency, battery storage is generally preferred, and even battery storage systems will struggle to achieve positive NPV. The largest storage duration for the battery appears to be around 8 to 10 hours; addressing generation fluctuations on longer timescales did require the rSOC.

The third publication (Chapter 6) presented an introductory exploration of P2P electricity trading. The P2P trading was simulated in tandem with energy storage (although the latter was provided by EV batteries in this chapter, with the rSOC returning only in Chapter 7). The academic literature contains many approaches to the design of, or simulation of, P2P markets, and it was not the objective of this chapter to improve on these, but rather to quantify the technical and economic benefits of the P2P market working with EV batteries. In fact, provision of estimates for annual household savings attainable from P2P is rather rare in the literature. Here these were found to be of the order £100/a, or approaching 20% of pre-existing annual electricity bills. An important outcome of the work was the identification of a particularly strong synergy between P2P and V2H (that is, vehicle-to-home, where the EV battery stores energy for meeting household power requirements). Another notable outcome was the finding that P2P is beneficial even at very high penetrations of PV generation and EV ownership, somewhat contradicting results from earlier research, likely owing to the use of more realistic data inputs here.

The fourth publication (Chapter 7) reunited the P2P topic with the rSOC technology. It also introduced the use of heat from the rSOC to supply space heating demand. A novel P2P auction was designed that could accommodate flexible loads (like EV charging) and energy storage, also allowing for trading of heat as well as power across multiple future timeslots. It was clear from this final piece of work that for a household scale rSOC system providing CHP the availability of a P2P trading market is highly beneficial, significantly reducing net running costs. The possibility of trading heat as well as power also showed promise, although more work is needed to confirm or refute this.

The overarching conclusions of this work are that energy storage using rSOC is hard to justify financially, but that it may be a competitive solution if a high degree of self-sufficiency is required. P2P electricity trading, meanwhile, has undoubted potential to save money and increase the energy independence of localities. Furthermore, P2P markets - in addition to working well alongside EVs and rooftop PV - can notably increase the profitability of energy storages such as rSOC.

9. Discussion and future work

The potential advantages of P2P electricity trading should be considered established, in the light of a large body of literature, even if the details of implementation are not agreed. Whether P2P trading of heat could become significant is more questionable. Where the construction of heat networks makes such trading a possibility, it seems more likely that centralised heat generation will be in use. Even so, an efficient system is likely to have a variety of different heat supplies to suit different circumstances – such as the CHP and heat pumps considered in Chapter 7. Whilst in this work, the P2P trading model was only employed for trading between houses – which all had comparable assets with which to trade, and similar market power – the model should be readily adaptable for a situation where houses can bid to purchase heat from a variety of centralised sources.

The clear next step for the work, which unfortunately was not reached within the project timescale, is to take the P2P energy trading model and use it to answer the sort of questions that the first two results chapters attempted to address: specifically the questions related to technology choice and sizing for a distributed energy system. Under what conditions would an rSOC be a profitable investment in the context of an energy sharing neighbourhood such as discussed in chapters 6 and 7? How should it be sized, and could hydrogen storage be sited locally? How important is the possible integration with heat networks to make the technology more financially attractive? The market model would be impossible to incorporate directly in the sort of global optimisation method employed in chapters 4 and 5, being computationally far too slow. However, it should be possible to employ the market model to create some ‘design days’ (or weeks) which could then be employed in an optimisation model. Two paradigms that would be of interest to compare would be rSOCs in individual houses, able to supply heat directly without the overhead costs of a heat network, with P2P trading of power only; versus a centralised community system, where heat from the rSOC would have to be shared via a network.

The ‘reversible’ nature of the rSOC did not have great impact in the market model presented in Chapter 7. This reflects the fact that, once demand for power, heat and transport are all accounted for, it is rather difficult to generate a surplus of energy in a distributed setting. Reference to Figure 6.5 is a good demonstration of this; even with 80% penetration of PV generation, and during a very sunny week, there is little surplus energy for grid export once the local demands for power and transport have both been addressed. Notwithstanding, there could be other incentives to store and use hydrogen in a distributed energy setting, even without large surpluses of local generation, and these could be the subject of future work. Even supposing that the future of renewable generation is centralised (e.g. offshore wind) there could still be an argument for transmitting wind power surpluses to downstream locations in the grid for electrolysis. One such argument would come from the possibility to distribute heat from the plant when running in the opposite (i.e. fuel cell) mode, which would be less practical with utility scale energy storage. A straightforward way to leverage the existing work to consider the local storage of national energy surpluses would be to consider a variable grid electricity tariff, which would fluctuate in accordance with the level of wind power as well as other market forces. A variable price for hydrogen could likewise be of interest in coupling the dispatch of local energy storage to the wider picture of energy supply and demand.

We emphasised only the comparison between the rSOC and short-term (battery) energy storage in this work. It would be of interest in future to run models where alternative electrolysers and fuel cells (i.e. most likely PEM, the preferred technology at present) could compete for selection by an optimiser.

This work did not consider fuel cell electric vehicles (FCEVs). This decision was made on the basis that the adoption of EVs has far greater momentum at present; but it could be of interest to consider the design of a microgrid energy system with a choice between EVs and FCEVs, along with the possible use of the rSOC and P2P trading. The travel model would be relatively easy to adopt for this purpose.

The possibility of using industrial waste heat to boost SOEC efficiency has not been explored in detail in this work, other than implicitly in ‘high efficiency’ scenarios for the rSOC. The UK does in fact have significant quantities of waste industrial heat: 391 TWh in 2018 [274], which for context can be compared to 434 TWh of residential heat demand [275]. An interesting avenue of research would be to consider the benefits of the rSOC and hydrogen storage in the vicinity of an industrial waste heat source. In summer, the industrial waste heat would be used to boost the efficiency of hydrogen production; in winter when SOEC mode is less likely to run, the waste heat could be distributed via a heat network. The work completed in Chapter 7 concerning markets for heat and power could help to support such an investigation.

Epilogue

At the commencement of this project, the average retail electricity price in the UK was around £0.13 / kWh, whilst gas was around £0.03 / kWh. These prices remained relatively stable, and were not considered by the author even to be a major source of uncertainty for calculation of economic indicators. The current year (2022) has proven this to be complacency. The UK price cap for electricity going into October is to be £0.52 / kWh, for gas, £0.15 / kWh [268].

The relative merits of rSOC energy storage versus battery storage or other alternatives will not necessarily have changed much. In chapters 4 and 5, systems were sized according to the minimisation of CAPEX and maximisation of self-sufficiency. The conditions under which rSOC is preferable to a battery are likely similar to before. However, in absolute terms, the economic metrics for rSOC and hydrogen storage will be looking much attractive – and this will be true for a host of green technologies. PV uptake is already increasing [276]. Will prices remain at their elevated levels in the long-term? ICAEW predicts that prices will peak around the second quarter of 2023, but a fall back to 2021 levels is not yet foreseen [277]. If the age of cheap fossil fuels is over then many conclusions on the viability of renewable technologies will need to be rewritten – and not only in this present work.

References

[1] F. Zhang, P. Zhao, M. Niu, and J. Maddy, “The survey of key technologies in hydrogen energy storage,” *Int. J. Hydrogen Energy*, vol. 41, no. 33, pp. 14535–14552, 2016, doi: 10.1016/j.ijhydene.2016.05.293.

[2] S. B. Walker, U. Mukherjee, M. Fowler, and A. Elkamel, “Benchmarking and selection of Power-to-Gas utilizing electrolytic hydrogen as an energy storage alternative,” *Int. J. Hydrogen Energy*, vol. 41, no. 19, pp. 7717–7731, 2016, doi: 10.1016/j.ijhydene.2015.09.008.

[3] J. Auer, J. Keil, and a Stobbe, “State-of-the-art electricity storage systems,” *Frankfurt am Main, …*, p. 16, 2012, doi: 1612-3158.

[4] The AnyLogic Company, “AnyLogic,” 2019. https://www.anylogic.com/.

[5] A. Hirsch, Y. Parag, and J. Guerrero, “Microgrids: A review of technologies, key drivers, and outstanding issues,” *Renew. Sustain. Energy Rev.*, vol. 90, pp. 402–411, Jul. 2018, doi: 10.1016/j.rser.2018.03.040.

[6] H. Æ. Sigurjonsson and L. R. Clausen, “Solution for the future smart energy system: A polygeneration plant based on reversible solid oxide cells and biomass gasification producing either electrofuel or power,” *Appl. Energy*, vol. 216, pp. 323–337, Apr. 2018, doi: 10.1016/j.apenergy.2018.02.124.

[7] Z. Zhang, J. Zhou, Z. Zong, Q. Chen, P. Zhang, and K. Wu, “Development and modelling of a novel electricity-hydrogen energy system based on reversible solid oxide cells and power to gas technology,” *Int. J. Hydrogen Energy*, vol. 44, no. 52, pp. 28305–28315, 2019, doi: 10.1016/j.ijhydene.2019.09.028.

[8] Y. Zhou, J. Wu, and C. Long, “Evaluation of peer-to-peer energy sharing mechanisms based on a multiagent simulation framework,” *Appl. Energy*, vol. 222, no. November 2017, pp. 993–1022, 2018, doi: 10.1016/j.apenergy.2018.02.089.

[9] P. D. Lund, J. Lindgren, J. Mikkola, and J. Salpakari, “Review of energy system flexibility measures to enable high levels of variable renewable electricity,” *Renew. Sustain. Energy Rev.*, vol. 45, pp. 785–807, 2015, doi: 10.1016/j.rser.2015.01.057.

[10] H. Ibrahim, A. Ilinca, and J. Perron, “Energy storage systems-Characteristics and comparisons,” *Renew. Sustain. Energy Rev.*, vol. 12, no. 5, pp. 1221–1250, 2008, doi: 10.1016/j.rser.2007.01.023.

[11] T. M. Gür, “Review of electrical energy storage technologies, materials and systems: challenges and prospects for large-scale grid storage,” *Energy Environ. Sci.*, vol. 11, no. 10, pp. 2696–2767, 2018, doi: 10.1039/C8EE01419A.

[12] M. Aneke and M. Wang, “Energy storage technologies and real life applications – A state of the art review,” *Appl. Energy*, vol. 179, pp. 350–377, 2016, doi: 10.1016/j.apenergy.2016.06.097.

[13] U.S. Energy Information Administration, “Electricity storage technologies can be used for energy management and power quality,” 2011. .

[14] M. Faisal, M. A. Hannan, P. J. Ker, A. Hussain, M. Bin Mansor, and F. Blaabjerg, “Review of energy storage system technologies in microgrid applications: Issues and challenges,” *IEEE Access*, vol. 6, pp. 35143–35164, 2018, doi: 10.1109/ACCESS.2018.2841407.

[15] Y. Ohki, “Commencement of operation of the world’s largest storage battery facility [News from Japan],” *IEEE Electr. Insul. Mag.*, vol. 33, no. 1, pp. 59–61, 2017, doi: 10.1109/MEI.2017.7804322.

[16] X. Luo, J. Wang, M. Dooner, and J. Clarke, “Overview of current development in electrical energy storage technologies and the application potential in power system operation,” *Appl. Energy*, vol. 137, pp. 511–536, 2015, doi: 10.1016/j.apenergy.2014.09.081.

[17] M. King, A. Jain, R. Bhakar, J. Mathur, and J. Wang, “Overview of current compressed air energy storage projects and analysis of the potential underground storage capacity in India and the UK,” *Renew. Sustain. Energy Rev.*, vol. 139, p. 110705, Apr. 2021, doi: 10.1016/j.rser.2021.110705.

[18] C. R. Matos, P. P. Silva, and J. F. Carneiro, “Overview of compressed air energy storage projects and regulatory framework for energy storage,” *J. Energy Storage*, vol. 55, p. 105862, Nov. 2022, doi: 10.1016/j.est.2022.105862.

[19] J. Moore and B. Shabani, “A critical study of stationary energy storage policies in Australia in an international context: The role of hydrogen and battery technologies,” *Energies*, vol. 9, no. 9, 2016, doi: 10.3390/en9090674.

[20] J. B. Hansen, “Fuel processing for fuel cells and power to fuels as seen from an industrial perspective,” *J. Catal.*, vol. 328, pp. 280–296, 2015, doi: 10.1016/j.jcat.2015.04.014.

[21] S. H. Jensen, P. H. Larsen, and M. Mogensen, “Hydrogen and synthetic fuel production from renewable energy sources,” *Int. J. Hydrogen Energy*, vol. 32, no. 15 SPEC. ISS., pp. 3253–3257, 2007, doi: 10.1016/j.ijhydene.2007.04.042.

[22] B. Zakeri and S. Syri, “Electrical energy storage systems: A comparative life cycle cost analysis,” *Renew. Sustain. Energy Rev.*, vol. 42, no. 3, pp. 569–596, Feb. 2015, doi: 10.1016/j.rser.2014.10.011.

[23] California Hydrogen Business Council, “Power-to-Gas : The Case for Hydrogen White Paper,” *White Pap.*, pp. 1–17, 2015, doi: 10.1097/01.ju.0000077558.48257.3d.

[24] J. Mermelstein and O. Posdziech, “Development and Demonstration of a Novel Reversible SOFC System for Utility and Micro Grid Energy Storage,” *Fuel Cells*, vol. 17, no. 4, pp. 562–570, 2017, doi: 10.1002/fuce.201600185.

[25] ERP, “Managing Flexibility Whilst Decarbonising the GB Electricity System The Energy Research Partnership,” no. August, 2015.

[26] P. C. Ghosh, B. Emonts, H. Janßen, J. Mergel, and D. Stolten, “Ten years of operational experience with a hydrogen-based renewable energy supply system,” *Sol. Energy*, vol. 75, no. 6, pp. 469–478, 2003, doi: 10.1016/j.solener.2003.09.006.

[27] M. Little, M. Thomson, and D. Infield, “Electrical integration of renewable energy into stand-alone power supplies incorporating hydrogen storage,” *Int. J. Hydrogen Energy*, vol. 32, no. 10–11, pp. 1582–1588, 2007, doi: 10.1016/j.ijhydene.2006.10.035.

[28] I. Dincer and C. Acar, “Review and evaluation of hydrogen production methods for better sustainability,” *Int. J. Hydrogen Energy*, vol. 40, no. 34, pp. 11094–11111, 2014, doi: 10.1016/j.ijhydene.2014.12.035.

[29] A. Ursúa, L. M. Gandía, and P. Sanchis, “Hydrogen production from water electrolysis: Current status and future trends,” *Proc. IEEE*, vol. 100, no. 2, pp. 410–426, 2012, doi: 10.1109/JPROC.2011.2156750.

[30] G. Gahleitner, “Hydrogen from renewable electricity: An international review of power-to-gas pilot plants for stationary applications,” *Int. J. Hydrogen Energy*, vol. 38, no. 5, pp. 2039–2061, 2013, doi: 10.1016/j.ijhydene.2012.12.010.

[31] Y. Wang, D. Y. C. Leung, J. Xuan, and H. Wang, “A review on unitized regenerative fuel cell technologies, part-A: Unitized regenerative proton exchange membrane fuel cells,” *Renew.*

Sustain. Energy Rev., vol. 65, pp. 961–977, 2016, doi: 10.1016/j.rser.2016.07.046.

[32] B. Paul and J. Andrews, “PEM unitised reversible/regenerative hydrogen fuel cell systems: State of the art and technical challenges,” *Renew. Sustain. Energy Rev.*, vol. 79, no. February, pp. 585–599, 2017, doi: 10.1016/j.rser.2017.05.112.

[33] R. M. Ormerod, “Solid oxide fuel cells,” *Chem. Soc. Rev.*, vol. 32, no. 1, pp. 17–28, Dec. 2003, doi: 10.1039/b105764m.

[34] R. Bhandari, C. A. Trudewind, and P. Zapp, “Life cycle assessment of hydrogen production via electrolysis - A review,” *J. Clean. Prod.*, vol. 85, pp. 151–163, 2014, doi: 10.1016/j.jclepro.2013.07.048.

[35] O. Schmidt, A. Gambhir, I. Staffell, A. Hawkes, J. Nelson, and S. Few, “Future cost and performance of water electrolysis: An expert elicitation study,” *Int. J. Hydrogen Energy*, vol. 42, no. 52, pp. 30470–30492, 2017, doi: 10.1016/j.ijhydene.2017.10.045.

[36] Ø. Ulleberg, T. Nakken, and A. Eté, “The wind/hydrogen demonstration system at Utsira in Norway: Evaluation of system performance using operational data and updated hydrogen energy system modeling tools,” *Int. J. Hydrogen Energy*, vol. 35, no. 5, pp. 1841–1852, 2010, doi: 10.1016/j.ijhydene.2009.10.077.

[37] A. Buttler and H. Spliethoff, “Current status of water electrolysis for energy storage, grid balancing and sector coupling via power-to-gas and power-to-liquids: A review,” *Renew. Sustain. Energy Rev.*, vol. 82, no. September 2017, pp. 2440–2454, 2018, doi: 10.1016/j.rser.2017.09.003.

[38] M. Bertoldi, O. Bucheli, and A. Ravagni, “Development, Manufacturing and Deployment of SOFC-Based Products at SOLIDpower,” *ECS Trans.*, vol. 68, no. 1, pp. 117–123, Jul. 2015, doi: 10.1149/06801.0117ecst.

[39] Battelle Memorial Institute, “Manufacturing cost analysis of 1, 5, 10 and 25 kW Fuel Cell Systems for Primary Power and Combined Heat and Power Applications,” 2017.

[40] S. Y. Gómez and D. Hotza, “Current developments in reversible solid oxide fuel cells,” *Renew. Sustain. Energy Rev.*, vol. 61, pp. 155–174, 2016, doi: 10.1016/j.rser.2016.03.005.

[41] V. Venkataraman *et al.*, “Reversible solid oxide systems for energy and chemical applications – Review & perspectives,” *J. Energy Storage*, vol. 24, p. 100782, Aug. 2019, doi: 10.1016/j.est.2019.100782.

[42] M. A. Laguna-Bercero, “Recent advances in high temperature electrolysis using solid oxide fuel cells: A review,” *J. Power Sources*, vol. 203, no. 2, pp. 4–16, Apr. 2012, doi: 10.1016/j.jpowsour.2011.12.019.

[43] Fuel cells and hydrogen joint undertaking, “Development of water electrolysis in the European Union,” 2014.

[44] Sunfire GmbH, “Steam Electrolysis as the Core Technology for Sector Coupling in the Energy Transition,” 2017. .

[45] S. P. S. Badwal, S. S. Giddey, C. Munnings, A. I. Bhatt, and A. F. Hollenkamp, “Emerging electrochemical energy conversion and storage technologies,” *Front. Chem.*, vol. 2, no. September, pp. 1–28, 2014, doi: 10.3389/fchem.2014.00079.

[46] K. Schwarze, O. Posdziech, J. Mermelstein, and S. Kroop, “Operational Results of an 150/30 kW RSOC System in an Industrial Environment,” *Fuel Cells*, p. fuce.201800194, Apr. 2019, doi: 10.1002/fuce.201800194.

[47] “Jülich scientists report efficiency record for reversible fuel cell,” *Fuel Cells Bull.*, vol. 2019, no. 1, p. 15, Jan. 2019, doi: 10.1016/S1464-2859(19)30036-7.

[48] Sylfen, "MAJOR TECHNICAL PROGRESS WITH DEMONSTRATOR SMARTHYES," 2018. .

[49] K. Schwarze, O. Posdziech, S. Kroop, N. Lapeña-Rey, and J. Mermelstein, "Green Industrial Hydrogen via Reversible High-Temperature Electrolysis," *ECS Trans.*, vol. 78, no. 1, pp. 2943–2952, 2017, doi: 10.1149/07801.2943ecst.

[50] K. Kendall and M. Kendall, *High-Temperature Solid Oxide Fuel Cells for the 21st Century*. Elsevier, 2016.

[51] Tractebel and Hinicio, "STUDY ON EARLY BUSINESS CASES FOR H2 IN ENERGY STORAGE AND MORE BROADLY POWER TO H2 APPLICATIONS," 2017.

[52] TESLA, "Powerpack - Commercial & Utility Energy Storage Solutions," 2019. .

[53] Makridis, "Hydrogen storage and compression," *Methane Hydrog. Energy Storage*, no. June, pp. 1–28, 2016, doi: 10.1049/PBPO101E_ch1.

[54] J. Zheng, X. Liu, P. Xu, P. Liu, Y. Zhao, and J. Yang, "Development of high pressure gaseous hydrogen storage technologies," *Int. J. Hydrogen Energy*, vol. 37, no. 1, pp. 1048–1057, 2012, doi: 10.1016/j.ijhydene.2011.02.125.

[55] D. J. Durbin and C. Malardier-Jugroot, "Review of hydrogen storage techniques for on board vehicle applications," *Int. J. Hydrogen Energy*, vol. 38, no. 34, pp. 14595–14617, 2013, doi: 10.1016/j.ijhydene.2013.07.058.

[56] S. Dutta, "A review on production, storage of hydrogen and its utilization as an energy resource," *J. Ind. Eng. Chem.*, vol. 20, no. 4, pp. 1148–1156, 2014, doi: 10.1016/j.jiec.2013.07.037.

[57] M. Lototskyy *et al.*, "A concept of combined cooling, heating and power system utilising solar power and based on reversible solid oxide fuel cell and metal hydrides," *Int. J. Hydrogen Energy*, vol. 43, no. 40, pp. 18650–18663, 2018, doi: 10.1016/j.ijhydene.2018.05.075.

[58] S. Niaz, T. Manzoor, and A. H. Pandith, "Hydrogen storage: Materials, methods and perspectives," *Renew. Sustain. Energy Rev.*, vol. 50, pp. 457–469, 2015, doi: 10.1016/j.rser.2015.05.011.

[59] Siemens, "'Green' ammonia is the key to meeting the twin challenges of the 21st century.," 2017. .

[60] C. H. Wendel, P. Kazempoor, and R. J. Braun, "Novel electrical energy storage system based on reversible solid oxide cells: System design and operating conditions," *J. Power Sources*, vol. 276, pp. 133–144, 2015, doi: 10.1016/j.jpowsour.2014.10.205.

[61] C. H. Wendel and R. J. Braun, "Design and techno-economic analysis of high efficiency reversible solid oxide cell systems for distributed energy storage," *Appl. Energy*, vol. 172, pp. 118–131, 2016, doi: 10.1016/j.apenergy.2016.03.054.

[62] C. H. Wendel, Z. Gao, S. A. Barnett, and R. J. Braun, "Modeling and experimental performance of an intermediate temperature reversible solid oxide cell for high-efficiency, distributed-scale electrical energy storage," *J. Power Sources*, vol. 283, pp. 329–342, 2015, doi: 10.1016/j.jpowsour.2015.02.113.

[63] S. H. Jensen *et al.*, "Large-scale electricity storage utilizing reversible solid oxide cells combined with underground storage of CO<inf>2</inf> and CH<inf>4</inf>," *Energy Environ. Sci.*, vol. 8, no. 8, pp. 2471–2479, 2015, doi: 10.1039/c5ee01485a.

[64] E. Reznicek and R. J. Braun, "Techno-economic and off-design analysis of stand-alone, distributed-scale reversible solid oxide cell energy storage systems," *Energy Convers. Manag.*, vol. 175, no. August, pp. 263–277, 2018, doi: 10.1016/j.enconman.2018.08.087.

[65] G. Butera, S. H. Jensen, and L. R. Clausen, “A novel system for large-scale storage of electricity as synthetic natural gas using reversible pressurized solid oxide cells,” *Energy*, vol. 166, pp. 738–754, Jan. 2019, doi: 10.1016/j.energy.2018.10.079.

[66] A. B. Stambouli and E. Traversa, “Solid oxide fuel cells (SOFCs): A review of an environmentally clean and efficient source of energy,” *Renew. Sustain. Energy Rev.*, vol. 6, no. 5, pp. 433–455, 2002, doi: 10.1016/S1364-0321(02)00014-X.

[67] N. Q. Minh and M. B. Mogensen, “Reversible Solid Oxide Fuel Cell Technology,” *Electrochem. Soc. Interface*, no. Winter, pp. 55–62, 2013.

[68] Y. Wang, D. Y. C. Leung, J. Xuan, and H. Wang, “A review on unitized regenerative fuel cell technologies, part B: Unitized regenerative alkaline fuel cell, solid oxide fuel cell, and microfluidic fuel cell,” *Renew. Sustain. Energy Rev.*, vol. 75, no. January 2016, pp. 775–795, 2017, doi: 10.1016/j.rser.2016.11.054.

[69] S. Santhanam, M. P. Heddrich, M. Riedel, and K. A. Friedrich, “Theoretical and experimental study of Reversible Solid Oxide Cell (r-SOC) systems for energy storage,” *Energy*, vol. 141, pp. 202–214, 2017, doi: 10.1016/j.energy.2017.09.081.

[70] J. F. McElroy, D. B. Hickey Fred Mitlitsky, and M. Field, “Optimization & Demonstration of a Solid Oxide Regenerative Fuel Cell System DE-FC26-03NT41854 Ion America Corporation,” no. October 2003, 2003.

[71] Green Industrial Hydrogen, “GrInHy 2.0 Project Overview,” 2021. https://www.green-industrial-hydrogen.com/ (accessed Nov. 12, 2021).

[72] B. Radowitz, “Linde to build ‘world’s largest electrolyser’ to produce green hydrogen,” *rechargenews.com*, 2021. https://www.rechargenews.com/transition/linde-to-build-world-s-largest-electrolyser-to-produce-green-hydrogen/2-1-944080 (accessed Nov. 12, 2021).

[73] Air Liquide, “Inauguration of the world’s largest PEM electrolyzer,” *airliquide.com*, 2021. https://www.airliquide.com/magazine/energy-transition/inauguration-worlds-largest-pem-electrolyzer (accessed Nov. 12, 2021).

[74] S. Patel, “Shell Starts Up 10-MW REFHYNE Hydrogen Electrolyzer, Eyes Expansion to 100 MW,” *powermag.com*, 2021. https://www.powermag.com/shell-starts-up-10-mw-refhyne-hydrogen-electrolyzer-eyes-expansion-to-100-mw/ (accessed Nov. 12, 2021).

[75] V. Saarinen *et al.*, “Design, manufacturing, and operation of movable 2 × 10 kW size rSOC system,” *Fuel Cells*, Oct. 2021, doi: 10.1002/fuce.202100021.

[76] A. Nechache and S. Hody, “Test and Evaluation of an Hybrid Storage Solution for Buildings, Based on a Reversible High-Temperature Electrolyzer,” *ECS Trans.*, vol. 91, no. 1, pp. 2485–2494, Jul. 2019, doi: 10.1149/09101.2485ecst.

[77] R. Peters *et al.*, “Long-Term Experience with a 5/15kW-Class Reversible Solid Oxide Cell System,” *J. Electrochem. Soc.*, vol. 168, no. 1, p. 014508, Jan. 2021, doi: 10.1149/1945-7111/abdc79.

[78] J. Mougin, “Reversible solid oxide Electrolyzer and Fuel cell for optimized Local Energy miX,” *fch.europa.eu*. .

[79] O. Lindholm, R. Weiss, A. Hasan, F. Pettersson, and J. Shemeikka, “A MILP Optimization Method for Building Seasonal Energy Storage: A Case Study for a Reversible Solid Oxide Cell and Hydrogen Storage System,” *Buildings*, vol. 10, no. 7, p. 123, Jul. 2020, doi: 10.3390/buildings10070123.

[80] G. Buffo, D. Ferrero, M. Santarelli, and A. Lanzini, “Energy and environmental analysis of a flexible Power-to-X plant based on Reversible Solid Oxide Cells (rSOCs) for an urban

district," *J. Energy Storage*, vol. 29, p. 101314, Jun. 2020, doi: 10.1016/j.est.2020.101314.

[81] J. Aicart, S. Di Iorio, M. Petitjean, P. Giroud, G. Palcoux, and J. Mougin, "Transition Cycles during Operation of a Reversible Solid Oxide Electrolyzer/Fuel Cell (rSOC) System," *Fuel Cells*, p. fuce.201800183, May 2019, doi: 10.1002/fuce.201800183.

[82] M. Lamagna, B. Nastasi, D. Groppi, C. Rozain, M. Manfren, and D. Astiaso Garcia, "Techno-economic assessment of reversible Solid Oxide Cell integration to renewable energy systems at building and district scale," *Energy Convers. Manag.*, vol. 235, p. 113993, 2021, doi: 10.1016/j.enconman.2021.113993.

[83] N. Rispoli *et al.*, "Constrained optimal design of a reversible solid oxide cell-based multiple load renewable microgrid," *J. Energy Storage*, vol. 31, no. June, p. 101570, 2020, doi: 10.1016/j.est.2020.101570.

[84] O. Posdziech, K. Schwarze, and J. Brabandt, "Efficient hydrogen production for industry and electricity storage via high-temperature electrolysis," *Int. J. Hydrogen Energy*, vol. 44, no. 35, pp. 19089–19101, Jul. 2019, doi: 10.1016/j.ijhydene.2018.05.169.

[85] Green Industrial Hydrogen, "GrInHy Project Overview," 2019. .

[86] Sunfire, "RENEWABLE HYDROGEN FOR INDUSTRIAL APPLICATIONS SUNFIRE-HYLINK SOEC," *sunfire.de*. https://www.sunfire.de/files/sunfire/images/content/Sunfire.de (neu)/Sunfire-Factsheet-HyLink-SOEC-20210108.pdf (accessed Oct. 12, 2021).

[87] Sunfire, "PROVIDING CLEAN POWER AND HEAT FOR RESIDENTIAL BUILDINGS SUNFIRE-HOME," *sunfire.de*. https://www.sunfire.de/files/sunfire/images/content/Produkte_Technologie/factsheets/Sunfire-Factsheet-Home-en.pdf (accessed Oct. 12, 2021).

[88] M. Hanasaki *et al.*, "SOFC Durability against Standby and Shutdown Cycling," *J. Electrochem. Soc.*, vol. 161, no. 9, pp. F850–F860, Jun. 2014, doi: 10.1149/2.0421409jes.

[89] L. Nousch, M. Hartmann, and A. Michaelis, "Improvements of Micro-CHP SOFC System Operation by Efficient Dynamic Simulation Methods," *Processes*, vol. 9, no. 7, p. 1113, Jun. 2021, doi: 10.3390/pr9071113.

[90] M. Dokiya, "SOFC system and technology," *Solid State Ionics*, vol. 152–153, pp. 383–392, Dec. 2002, doi: 10.1016/S0167-2738(02)00345-4.

[91] C. Walter, K. Schwarze, M. Boltze, K. Herbrig, and A. Surrey, "Status of Stack and System Development at Sunfire," Lucerne, 2020. [Online]. Available: https://iopscience.iop.org/article/10.1149/MA2021-031187mtgabs/meta.

[92] O. S. Jeon, H. J. Hwang, O. Chan Kwon, J. G. Lee, and Y. G. Shul, "Next-generation flexible solid oxide fuel cells with high thermomechanical stability," *J. Mater. Chem. A*, vol. 6, no. 37, pp. 18018–18024, 2018, doi: 10.1039/C8TA03573C.

[93] P. Mottaghizadeh, M. Fardadi, F. Jabbari, and J. Brouwer, "Thermal Management of a Reversible Solid Oxide System for Long-Term Renewable Energy Storage," in *Volume 8: Energy*, Nov. 2020, doi: 10.1115/IMECE2020-24153.

[94] P. Mottaghizadeh, M. Fardadi, F. Jabbari, and J. Brouwer, "Dynamics and control of a thermally self-sustaining energy storage system using integrated solid oxide cells for an islanded building," *Int. J. Hydrogen Energy*, vol. 46, no. 49, pp. 24891–24908, Jul. 2021, doi: 10.1016/j.ijhydene.2021.03.136.

[95] X. Zhang, J. E. O'Brien, R. C. O'Brien, and G. K. Housley, "Durability evaluation of reversible solid oxide cells," *J. Power Sources*, vol. 242, pp. 566–574, Nov. 2013, doi: 10.1016/j.jpowsour.2013.05.134.

[96] “SOFC reaches 11 years in Jülich lifetime test,” *Fuel Cells Bull.*, vol. 2019, no. 3, p. 14, 2019, doi: 10.1016/S1464-2859(19)30125-7.

[97] M. Andersson and B. Sunden, “Technology review – Solid Oxide Fuel Cell,” 2017. [Online]. Available: https://energiforskmedia.blob.core.windows.net/media/22411/technology-review-solid-oxide-fuel-cell-energiforskrapport-2017-359.pdf.

[98] C. Graves, S. D. Ebbesen, S. H. Jensen, S. B. Simonsen, and M. B. Mogensen, “Eliminating degradation in solid oxide electrochemical cells by reversible operation,” *Nat. Mater.*, vol. 14, no. 2, pp. 239–244, Feb. 2015, doi: 10.1038/nmat4165.

[99] K. Chen, S. S. Liu, N. Ai, M. Koyama, and S. P. Jiang, “Why solid oxide cells can be reversibly operated in solid oxide electrolysis cell and fuel cell modes?,” *Phys. Chem. Chem. Phys.*, vol. 17, no. 46, pp. 31308–31315, 2015, doi: 10.1039/c5cp05065k.

[100] J. Mougin, “Reversible solid oxide Electrolyzer and Fuel cell for optimized Local Energy miX,” *fch.europa.eu*. https://www.fch.europa.eu/sites/default/files/3. Mougin_REFLEX.pdf (accessed Oct. 05, 2021).

[101] T. L. Cable, J. A. Setlock, S. C. Farmer, and A. J. Eckel, “Regenerative performance of the NASA symmetrical solid oxide fuel cell design,” *Int. J. Appl. Ceram. Technol.*, vol. 8, no. 1, pp. 1–12, 2011, doi: 10.1111/j.1744-7402.2009.02477.x.

[102] M. B. Choi, B. Singh, E. D. Wachsman, and S. J. Song, “Performance of La0.1Sr0.9Co0.8Fe 0.2O3-δ and La0.1Sr0.9Co 0.8Fe0.2O3-δ-Ce0.9Gd 0.1O2 oxygen electrodes with Ce0.9Gd 0.1O2 barrier layer in reversible solid oxide fuel cells,” *J. Power Sources*, vol. 239, pp. 361–373, 2013, doi: 10.1016/j.jpowsour.2013.03.154.

[103] J. Hong *et al.*, “Electrochemical performance and long-term durability of a 200 W-class solid oxide regenerative fuel cell stack,” *Int. J. Hydrogen Energy*, vol. 39, no. 35, pp. 20819–20828, Dec. 2014, doi: 10.1016/j.ijhydene.2014.06.114.

[104] P. Mottaghizadeh, S. Santhanam, M. P. Heddrich, K. A. Friedrich, and F. Rinaldi, “Process modeling of a reversible solid oxide cell (r-SOC) energy storage system utilizing commercially available SOC reactor,” *Energy Convers. Manag.*, vol. 142, pp. 477–493, 2017, doi: 10.1080/00140139.2017.1329939.

[105] R. Scataglini *et al.*, “A Total Cost of Ownership Model for Solid Oxide Fuel Cells in Combined Heat and Power and Power-Only Applications,” no. September, p. 197, 2015.

[106] Bloomberg New Energy Finance, “Electric Vehicles,” 2018. .

[107] D. M. Bierschenk, J. R. Wilson, and S. A. Barnett, “High efficiency electrical energy storage using a methane-oxygen solid oxide cell,” *Energy Environ. Sci.*, vol. 4, no. 3, pp. 944–951, 2011, doi: 10.1039/c0ee00457j.

[108] J. Ren, S. R. Gamble, A. J. Roscoe, J. T. S. Irvine, and G. Burt, “Modeling a reversible solid oxide fuel cell as a storage device within ac power networks,” *Fuel Cells*, vol. 12, no. 5, pp. 773–786, 2012, doi: 10.1002/fuce.201100185.

[109] M. Frank, R. Deja, R. Peters, L. Blum, and D. Stolten, “Bypassing renewable variability with a reversible solid oxide cell plant,” *Appl. Energy*, vol. 217, no. January, pp. 101–112, 2018, doi: 10.1016/j.apenergy.2018.02.115.

[110] A. Perna, M. Minutillo, and E. Jannelli, “Designing and analyzing an electric energy storage system based on reversible solid oxide cells,” *Energy Convers. Manag.*, vol. 159, no. September 2017, pp. 381–395, 2018, doi: 10.1016/j.enconman.2017.12.082.

[111] R. K. Akikur, R. Saidur, H. W. Ping, and K. R. Ullah, “Performance analysis of a co-generation system using solar energy and SOFC technology,” *Energy Convers. Manag.*, vol.

79, pp. 415–430, 2014, doi: 10.1016/j.enconman.2013.12.036.

[112] P. Di Giorgio and U. Desideri, "Potential of Reversible Solid Oxide Cells as Electricity Storage System," *Energies*, vol. 9, no. 8, p. 662, Aug. 2016, doi: 10.3390/en9080662.

[113] V.-T. Giap, S. Kang, and K. Y. Ahn, "HIGH-EFFICIENT reversible solid oxide fuel cell coupled with waste steam for distributed electrical energy storage system," *Renew. Energy*, vol. 144, pp. 129–138, Dec. 2019, doi: 10.1016/j.renene.2018.10.112.

[114] Y. Wang, A. Banerjee, L. Wehrle, Y. Shi, N. Brandon, and O. Deutschmann, "Performance analysis of a reversible solid oxide cell system based on multi-scale hierarchical solid oxide cell modelling," *Energy Convers. Manag.*, vol. 196, pp. 484–496, Sep. 2019, doi: 10.1016/j.enconman.2019.05.099.

[115] N. C. Ullvius and M. Rokni, "A study on a polygeneration plant based on solar power and solid oxide cells," *Int. J. Hydrogen Energy*, vol. 44, no. 35, pp. 19206–19223, 2019, doi: 10.1016/j.ijhydene.2018.04.085.

[116] A. Baldinelli, L. Barelli, and G. Bidini, "Progress in renewable power exploitation: reversible solid oxide cells-flywheel hybrid storage systems to enhance flexibility in micro-grids management," *J. Energy Storage*, vol. 23, pp. 202–219, Jun. 2019, doi: 10.1016/j.est.2019.03.018.

[117] M. Sorrentino, A. Adamo, and G. Nappi, "Optimal Sizing of an rSOC-Based Renewable Microgrid," *Energy Procedia*, vol. 159, pp. 237–242, Feb. 2019, doi: 10.1016/j.egypro.2018.12.063.

[118] M. Patterson, N. F. Macia, and A. M. Kannan, "Hybrid microgrid model based on solar photovoltaic battery fuel cell system for intermittent load applications," *IEEE Trans. Energy Convers.*, vol. 30, no. 1, pp. 359–366, 2015, doi: 10.1109/TEC.2014.2352554.

[119] HOMER Energy LLC, "HOMER Energy," 2018. .

[120] M. J. Khan and M. T. Iqbal, "Pre-feasibility study of stand-alone hybrid energy systems for applications in Newfoundland," *Renew. Energy*, vol. 30, no. 6, pp. 835–854, May 2005, doi: 10.1016/j.renene.2004.09.001.

[121] H. Shahinzadeh, M. Moazzami, S. H. Fathi, and G. B. Gharehpetian, "Optimal sizing and energy management of a grid-connected microgrid using HOMER software," *2016 Smart Grids Conf. SGC 2016*, pp. 13–18, 2017, doi: 10.1109/SGC.2016.7882945.

[122] A. Maroufmashat *et al.*, "Optimization of renewable powered hydrogen micro-grid; Taking in to account economic criteria," *2016 4th IEEE Int. Conf. Smart Energy Grid Eng. SEGE 2016*, pp. 252–256, 2016, doi: 10.1109/SEGE.2016.7589534.

[123] G. Kyriakarakos, A. I. Dounis, S. Rozakis, K. G. Arvanitis, and G. Papadakis, "Polygeneration microgrids: A viable solution in remote areas for supplying power, potable water and hydrogen as transportation fuel," *Appl. Energy*, vol. 88, no. 12, pp. 4517–4526, 2011, doi: 10.1016/j.apenergy.2011.05.038.

[124] D. B. Nelson, M. H. Nehrir, and C. Wang, "Unit sizing and cost analysis of stand-alone hybrid wind/PV/fuel cell power generation systems," *Renew. Energy*, vol. 31, no. 10, pp. 1641–1656, 2006, doi: 10.1016/j.renene.2005.08.031.

[125] C. Wang and M. H. Nehrir, "Power management of a stand-alone wind/photovoltaic/fuel cell energy system," *IEEE Trans. Energy Convers.*, vol. 23, no. 3, pp. 957–967, 2008, doi: 10.1109/TEC.2007.914200.

[126] P. Gabrielli, M. Gazzani, E. Martelli, and M. Mazzotti, "Optimal design of multi-energy systems with seasonal storage," *Appl. Energy*, vol. 219, no. July 2017, pp. 408–424, 2018, doi:

10.1016/j.apenergy.2017.07.142.

[127] R. Gammon, A. Roy, J. Barton, and M. Little, “Hydrogen and Renewables Integrations (HARI),” *Renew. Energy*, no. March, 2006.

[128] R. Gazey, S. K. Salman, and D. D. Aklil-D’Halluin, “A field application experience of integrating hydrogen technology with wind power in a remote island location,” *J. Power Sources*, vol. 157, no. 2, pp. 841–847, 2006, doi: 10.1016/j.jpowsour.2005.11.084.

[129] Sunfire, “About Sunfire,” 2019. .

[130] O. Posdziech, K. Schwarze, and J. Brabandt, “Efficient hydrogen production for industry and electricity storage via high-temperature electrolysis,” pp. 1–13, 2018, doi: 10.1016/j.ijhydene.2018.05.169.

[131] M. Gruber *et al.*, “Power-to-Gas through thermal integration of high-temperature steam electrolysis and carbon dioxide methanation - Experimental results,” *Fuel Process. Technol.*, vol. 181, pp. 61–74, Dec. 2018, doi: 10.1016/j.fuproc.2018.09.003.

[132] Sylfen, “SYLFEN ANNOUNCES THE FIRST HIGH TEMPERATURE REVERSIBLE ELECTROLYSIS DEMONSTRATOR,” 2018. .

[133] Sylfen, “THE EUROPEAN PROJECT REFLEX,” 2018. .

[134] D. J. L. Brett, A. Atkinson, N. P. Brandon, and S. J. Skinner, “Intermediate temperature solid oxide fuel cells,” *Chem. Soc. Rev.*, vol. 37, no. 8, pp. 1568–1578, 2008, doi: 10.1039/b612060c.

[135] M. Dillig and J. Karl, “Thermal management of high temperature solid oxide electrolyser cell/fuel cell systems,” *Energy Procedia*, vol. 28, pp. 37–47, 2012, doi: 10.1016/j.egypro.2012.08.038.

[136] J. Kim *et al.*, “Hybrid-solid oxide electrolysis cell: A new strategy for efficient hydrogen production,” *Nano Energy*, vol. 44, no. December 2017, pp. 121–126, 2018, doi: 10.1016/j.nanoen.2017.11.074.

[137] J. B. Goodenough, “Electrochemical energy storage in a sustainable modern society,” *Energy Environ. Sci.*, vol. 7, no. 1, pp. 14–18, 2014, doi: 10.1039/c3ee42613k.

[138] Department for Business Energy and Industrial Strategy, “Energy Consumption in the UK (ECUK) 2018 Data Tables,” 2018. .

[139] G. Wilson, R. Taylor, and P. Rowley, “Challenges for the decarbonisation of heat: local gas demand vs electricity supply Winter 2017/2018,” London, 2018.

[140] P. Papadopoulos, S. Skarvelis-Kazakos, I. Grau, L. M. Cipcigan, and N. Jenkins, “Electric vehicles’ impact on British distribution networks,” *IET Electr. Syst. Transp.*, vol. 2, no. 3, pp. 91–102, Sep. 2012, doi: 10.1049/iet-est.2011.0023.

[141] E. McKenna, J. Pless, and S. J. Darby, “Solar photovoltaic self-consumption in the UK residential sector: New estimates from a smart grid demonstration project,” *Energy Policy*, vol. 118, no. April, pp. 482–491, 2018, doi: 10.1016/j.enpol.2018.04.006.

[142] R. Gupta *et al.*, “Spatial analysis of distribution grid capacity and costs to enable massive deployment of PV, electric mobility and electric heating,” *Appl. Energy*, vol. 287, no. December 2020, p. 116504, 2021, doi: 10.1016/j.apenergy.2021.116504.

[143] Centrica, “Centrica joins community energy blockchain trial,” *centrica.com*, 2018. https://www.centrica.com/media-centre/news/2018/centrica-joins-community-energy-blockchain-trial (accessed Feb. 20, 2021).

[144] P. Gordon, “EDF launches blockchain-enabled renewables trading pilot,” *smart-energy.com*, 2019. https://www.smart-energy.com/industry-sectors/distributed-generation/edf-launches-blockchain-p2p-solar-and-storage-trading-pilot/ (accessed Feb. 20, 2021).

[145] “Piclo Flex.” .

[146] “Vandebron.” .

[147] W. El-Baz, P. Tzscheutschler, and U. Wagner, “Integration of energy markets in microgrids: A double-sided auction with device-oriented bidding strategies,” *Appl. Energy*, vol. 241, no. November 2018, pp. 625–639, 2019, doi: 10.1016/j.apenergy.2019.02.049.

[148] Z. Guo, P. Pinson, S. Chen, Q. Yang, and Z. Yang, “Chance-Constrained Peer-to-Peer Joint Energy and Reserve Market Considering Renewable Generation Uncertainty,” *IEEE Trans. Smart Grid*, vol. 12, no. 1, pp. 798–809, 2021, doi: 10.1109/TSG.2020.3019603.

[149] J. Li, C. Zhang, Z. Xu, J. Wang, J. Zhao, and Y. J. A. Zhang, “Distributed transactive energy trading framework in distribution networks,” *IEEE Trans. Power Syst.*, vol. 33, no. 6, pp. 7215–7227, 2018, doi: 10.1109/TPWRS.2018.2854649.

[150] P. Samadi, A.-H. Mohsenian-Rad, R. Schober, V. W. S. Wong, and J. Jatskevich, “Optimal Real-Time Pricing Algorithm Based on Utility Maximization for Smart Grid,” in *2010 First IEEE International Conference on Smart Grid Communications*, Oct. 2010, vol. 2015-March, no. March, pp. 415–420, doi: 10.1109/SMARTGRID.2010.5622077.

[151] E. Oh and S. Y. Son, “Peer-to-Peer Energy Transaction Mechanisms Considering Fairness in Smart Energy Communities,” *IEEE Access*, vol. 8, pp. 216055–216068, 2020, doi: 10.1109/ACCESS.2020.3041838.

[152] N. B. G. Brinkel, W. L. Schram, T. A. AlSkaif, I. Lampropoulos, and W. G. J. H. M. van Sark, “Should we reinforce the grid? Cost and emission optimization of electric vehicle charging under different transformer limits,” *Appl. Energy*, vol. 276, no. July, p. 115285, 2020, doi: 10.1016/j.apenergy.2020.115285.

[153] R. Alvaro-Hermana, J. Fraile-Ardanuy, P. J. Zufiria, L. Knapen, and D. Janssens, “Peer to Peer Energy Trading with Electric Vehicles,” *IEEE Intell. Transp. Syst. Mag.*, vol. 8, no. 3, pp. 33–44, Sep. 2016, doi: 10.1109/MITS.2016.2573178.

[154] B. Kim, Y. Zhang, M. van der Schaar, and J. Lee, “Dynamic Pricing and Energy Consumption Scheduling With Reinforcement Learning,” *IEEE Trans. Smart Grid*, vol. 7, no. 5, pp. 2187–2198, Sep. 2016, doi: 10.1109/TSG.2015.2495145.

[155] C. Chen, S. Kishore, and L. V. Snyder, “An innovative RTP-based residential power scheduling scheme for smart grids,” *ICASSP, IEEE Int. Conf. Acoust. Speech Signal Process. - Proc.*, pp. 5956–5959, 2011, doi: 10.1109/ICASSP.2011.5947718.

[156] P. Yang, G. Tang, and A. Nehorai, “A game-theoretic approach for optimal time-of-use electricity pricing,” *IEEE Trans. Power Syst.*, vol. 28, no. 2, pp. 884–892, 2013, doi: 10.1109/TPWRS.2012.2207134.

[157] C. Zhang, J. Wu, Y. Zhou, M. Cheng, and C. Long, “Peer-to-Peer energy trading in a Microgrid,” *Appl. Energy*, vol. 220, no. December 2017, pp. 1–12, 2018, doi: 10.1016/j.apenergy.2018.03.010.

[158] Z. Li and T. Ma, “Peer-to-peer electricity trading in grid-connected residential communities with household distributed photovoltaic,” *Appl. Energy*, vol. 278, no. July, p. 115670, 2020, doi: 10.1016/j.apenergy.2020.115670.

[159] J. Wang, Q. Wang, N. Zhou, and Y. Chi, “A novel electricity transaction mode of microgrids based on blockchain and continuous double auction,” *Energies*, vol. 10, no. 12, pp. 1–22,

2017, doi: 10.3390/en10121971.

[160] A. M. C. Marufu, A. V. D. M. Kayem, and S. D. Wolthusen, “A distributed continuous double auction framework for resource constrained microgrids,” *Lect. Notes Comput. Sci. (including Subser. Lect. Notes Artif. Intell. Lect. Notes Bioinformatics)*, vol. 9578, pp. 183–196, 2016, doi: 10.1007/978-3-319-33331-1_15.

[161] Z. Zhang, R. Li, and F. Li, “A Novel Peer-to-Peer Local Electricity Market for Joint Trading of Energy and Uncertainty,” *IEEE Trans. Smart Grid*, vol. 11, no. 2, pp. 1205–1215, 2020, doi: 10.1109/TSG.2019.2933574.

[162] C. Block, D. Neumann, and C. Weinhardt, “A market mechanism for energy allocation in micro-CHP grids,” *Proc. Annu. Hawaii Int. Conf. Syst. Sci.*, no. May 2006, pp. 1–11, 2008, doi: 10.1109/HICSS.2008.27.

[163] C. Zhang, J. Wu, M. Cheng, Y. Zhou, and C. Long, “A Bidding System for Peer-to-Peer Energy Trading in a Grid-connected Microgrid,” *Energy Procedia*, vol. 103, no. April, pp. 147–152, 2016, doi: 10.1016/j.egypro.2016.11.264.

[164] M. Marzband, M. Javadi, S. A. Pourmousavi, and G. Lightbody, “An advanced retail electricity market for active distribution systems and home microgrid interoperability based on game theory,” *Electr. Power Syst. Res.*, vol. 157, pp. 187–199, 2018, doi: 10.1016/j.epsr.2017.12.024.

[165] M. Sabounchi and J. Wei, “A decentralized real-time electricity market mechanism for autonomous microgrids,” in *2017 IEEE Power & Energy Society General Meeting*, Jul. 2017, pp. 1–5, doi: 10.1109/PESGM.2017.8273727.

[166] W. Tushar *et al.*, “A coalition formation game framework for peer-to-peer energy trading,” *Appl. Energy*, vol. 261, no. January, p. 114436, 2020, doi: 10.1016/j.apenergy.2019.114436.

[167] C. Chen, S. Kishore, and L. V. Snyder, “An innovative RTP-based residential power scheduling scheme for smart grids,” in *2011 IEEE International Conference on Acoustics, Speech and Signal Processing (ICASSP)*, May 2011, pp. 5956–5959, doi: 10.1109/ICASSP.2011.5947718.

[168] E. F. Bompard and B. Han, “Market-Based Control in Emerging Distribution System Operation,” *IEEE Trans. Power Deliv.*, vol. 28, no. 4, pp. 2373–2382, Oct. 2013, doi: 10.1109/TPWRD.2013.2277576.

[169] Ni Zhang, Yu Yan, Shengyao Xu, and Wencong Su, “Game-theory-based electricity market clearing mechanisms for an open and transactive distribution grid,” in *2015 IEEE Power & Energy Society General Meeting*, Jul. 2015, pp. 1–5, doi: 10.1109/PESGM.2015.7285598.

[170] Wencong Su and A. Q. Huang, “Proposing a electricity market framework for the Energy Internet,” in *2013 IEEE Power & Energy Society General Meeting*, 2013, pp. 1–5, doi: 10.1109/PESMG.2013.6672224.

[171] F. Wei, Z. X. Jing, P. Z. Wu, and Q. H. Wu, “A Stackelberg game approach for multiple energies trading in integrated energy systems,” *Appl. Energy*, vol. 200, pp. 315–329, Aug. 2017, doi: 10.1016/j.apenergy.2017.05.001.

[172] W. Tushar, T. K. Saha, C. Yuen, P. Liddell, R. Bean, and H. V. Poor, “Peer-to-Peer Energy Trading With Sustainable User Participation: A Game Theoretic Approach,” *IEEE Access*, vol. 6, pp. 62932–62943, 2018, doi: 10.1109/ACCESS.2018.2875405.

[173] B. G. Kim, S. Ren, M. Van Der Schaar, and J. W. Lee, “Bidirectional energy trading and residential load scheduling with electric vehicles in the smart grid,” *IEEE J. Sel. Areas Commun.*, vol. 31, no. 7, pp. 1219–1234, 2013, doi: 10.1109/JSAC.2013.130706.

[174] N. Liu, X. Yu, C. Wang, C. Li, L. Ma, and J. Lei, “Energy-Sharing Model with Price-Based Demand Response for Microgrids of Peer-to-Peer Prosumers,” *IEEE Trans. Power Syst.*, vol. 32, no. 5, pp. 3569–3583, 2017, doi: 10.1109/TPWRS.2017.2649558.

[175] P. Ringler, D. Keles, and W. Fichtner, “Agent-based modelling and simulation of smart electricity grids and markets – A literature review,” *Renew. Sustain. Energy Rev.*, vol. 57, pp. 205–215, 2016, doi: 10.1016/j.rser.2015.12.169.

[176] E. Kremers, *Modelling and Simulation of Electrical Energy Systems Through a Complex Systems Approach Using Agent-Based Models*. KIT Scientific Publishing, 2013.

[177] I. Grigoryev, *AnyLogic in Three Days*. 2016.

[178] J. M. Gonzalez De Durana, O. Barambones, E. Kremers, and L. Varga, “Agent based modeling of energy networks,” *Energy Convers. Manag.*, vol. 82, pp. 308–319, 2014, doi: 10.1016/j.enconman.2014.03.018.

[179] L. Ponta, M. Raberto, A. Teglio, and S. Cincotti, “An Agent-based Stock-flow Consistent Model of the Sustainable Transition in the Energy Sector,” *Ecol. Econ.*, vol. 145, no. October 2017, pp. 274–300, 2018, doi: 10.1016/j.ecolecon.2017.08.022.

[180] A. Mittal, C. C. Krejci, and M. C. Dorneich, “An agent-based approach to designing residential renewable energy systems,” *Renew. Sustain. Energy Rev.*, vol. 112, no. June, pp. 1008–1020, 2019, doi: 10.1016/j.rser.2019.06.034.

[181] E. Kuznetsova, Y. F. Li, C. Ruiz, and E. Zio, “An integrated framework of agent-based modelling and robust optimization for microgrid energy management,” *Appl. Energy*, vol. 129, pp. 70–88, 2014, doi: 10.1016/j.apenergy.2014.04.024.

[182] J. Gonzalez de Durana and O. Barambones, “Technology-free microgrid modeling with application to demand side management,” *Appl. Energy*, vol. 219, no. December 2017, pp. 165–178, 2018, doi: 10.1016/j.apenergy.2018.03.024.

[183] E. Kremers, J. Gonzalez De Durana, and O. Barambones, “Multi-agent modeling for the simulation of a simple smart microgrid,” *Energy Convers. Manag.*, vol. 75, pp. 643–650, 2013, doi: 10.1016/j.enconman.2013.07.050.

[184] E. Kremers, P. Viejo, O. Barambones, and J. G. De Durana, “A complex systems modelling approach for decentralised simulation of electrical microgrids,” *Proc. IEEE Int. Conf. Eng. Complex Comput. Syst. ICECCS*, pp. 302–311, 2010, doi: 10.1109/ICECCS.2010.46.

[185] J. M. G. De Durana, O. Barambones, E. Kremers, and P. Viejo, “Complete agent based simulation of mini-grids,” *Proc. 9th IASTED Eur. Conf. Power Energy Syst. Eur. 2009*, 2009.

[186] P. Bazan and R. German, “HYBRID SIMULATION OF RENEWABLE ENERGY GENERATION AND STORAGE GRIDS,” in *Proceedings of the 2012 Winter Simulation Conference*, 2012.

[187] Department for Business Energy and Industrial Strategy, “Digest of UK Energy Statistics (DUKES) 2022,” *gov.uk*, 2022. https://www.gov.uk/government/statistics/digest-of-uk-energy-statistics-dukes-2022.

[188] M. Laguna, “OptQuest: Optimization of Complex Systems,” pp. 1–15, 2011.

[189] UK Government, “National Travel Survey ,” Jul. 2020. .

[190] A. Pena-Bello, E. Barbour, M. C. Gonzalez, M. K. Patel, and D. Parra, “Optimized PV-coupled battery systems for combining applications: Impact of battery technology and geography,” *Renew. Sustain. Energy Rev.*, vol. 112, no. May, pp. 978–990, 2019, doi: 10.1016/j.rser.2019.06.003.

[191] J. O. Jensen, Q. Li, and N. J. Bjerrum, “The energy efficiency of onboard hydrogen storage,” 2008.

[192] B. Gundogdu, D. T. Gladwin, and D. A. Stone, “Battery SOC Management Strategy for Enhanced Frequency Response and Day-Ahead Energy Scheduling of BESS for Energy Arbitrage,” in *IECON 2017 - 43rd Annual Conference of the IEEE Industrial Electronics Society*, 2017.

[193] T. Feehally *et al.*, “Battery energy storage systems for the electricity grid: UK research facilities,” *IET Conf. Publ.*, vol. 2016, no. CP684, pp. 1–6, 2016, doi: 10.1049/cp.2016.0257.

[194] Spirit Energy, “Battery Storage Knowledge Bank - Understanding Batteries,” *https://www.spiritenergy.co.uk/*, 2020. .

[195] B. Lawson, “Battery Performance Characteristics,” *Electropaedia*, 2005. .

[196] D. Dusabe, J. Munda, and A. Jimoh, “Modelling of cloudless solar radiation for pv module performance analysis,” *J. Electr. Eng.*, vol. 60, no. 4, pp. 192–197, 2009.

[197] D. G. Erbs, S. A. Klein, and J. A. Duffie, “Estimation of the diffuse radiation fraction for hourly, daily and monthly-average global radiation,” *Sol. Energy*, vol. 28, no. 4, pp. 293–302, 1982, doi: 10.1016/0038-092X(82)90302-4.

[198] Sandia National Laboratories, “PVPerformance Modeling Collaborative,” 2018. .

[199] The Green Age, “How many solar panels can I fit on my roof?,” 2014. .

[200] UK Environmental Change Network, “UK Environmental Change Network.”

[201] PVOutput, “PVOutput,” 2020. .

[202] N. B. Mason, “Solar PV yield and electricity generation in the UK,” *IET Renew. Power Gener.*, vol. 10, no. 4, pp. 456–459, 2016, doi: 10.1049/iet-rpg.2015.0550.

[203] National Statistics, “Solar photovoltaic (PV) cost data,” *gov.uk*, 2019. .

[204] E. Rivard, M. Trudeau, and K. Zaghib, “Hydrogen storage for mobility: A review,” *Materials (Basel).*, vol. 12, no. 12, 2019, doi: 10.3390/ma12121973.

[205] B. D. James, C. Houchins, J. M. Huya-Kouadio, and D. A. Desantis, “Final Report: Hydrogen Storage System Cost Analysis,” no. September, pp. 1–54, 2016.

[206] NREL, “Costs Continue to Decline for Residential and Commercial Photovoltaics in 2018,” *nrel.gov*, 2018. .

[207] KPMG LLP, “Development of decentralised energy and storage systems in the UK. A report for the Renewable Energy Association,” 2016.

[208] OptTek Systems Inc., “OptQuest,” 2019. .

[209] UK Power Networks, “SmartMeter Energy Consumption Data in London Households,” 2015. .

[210] National Statistics, “Monthly feed-in tariff commissioned installations,” 2019. .

[211] Pecan Street Inc., “Dataport,” 2019. .

[212] Environmental and Energy Study Institute, “Fact Sheet: Energy Storage (2019),” 2019. https://www.eesi.org/papers/view/energy-storage-2019 (accessed Dec. 01, 2020).

[213] J. Spector, “So, What Exactly Is Long-Duration Energy Storage?,” *greentechmedia.com*, 2020. https://www.greentechmedia.com/articles/read/so-what-exactly-is-long-duration-storage-explained (accessed Dec. 01, 2020).

[214] T. D. Hutty, S. Dong, and S. Brown, "Suitability of energy storage with reversible solid oxide cells for microgrid applications," *Energy Convers. Manag.*, vol. 226, p. 113499, Dec. 2020, doi: 10.1016/j.enconman.2020.113499.

[215] R. Lee, S. Yazbeck, and S. Brown, "Validation and application of agent-based electric vehicle charging model," *Energy Reports*, vol. 6, pp. 53–62, 2020, doi: 10.1016/j.egyr.2020.02.027.

[216] Department for Transport, "National Travel Survey," *gov.uk*, 2020. https://www.gov.uk/government/collections/national-travel-survey-statistics (accessed May 01, 2020).

[217] D. Steward *et al.*, "Lifecycle Cost Analysis of Hydrogen Versus Other Technologies for Electrical Energy Storage Lifecycle Cost Analysis of Hydrogen Versus Other Technologies for Electrical Energy Storage," no. November, 2009.

[218] K. Mongird *et al.*, "Energy Storage Technology and Cost Characterization Report | Department of Energy," no. July, 2019.

[219] J. Gorre, F. Ruoss, H. Karjunen, J. Schaffert, and T. Tynjälä, "Cost benefits of optimizing hydrogen storage and methanation capacities for Power-to-Gas plants in dynamic operation," *Appl. Energy*, vol. 257, no. August 2019, 2020, doi: 10.1016/j.apenergy.2019.113967.

[220] V. Authors, "Commercialisation of Energy Storage," 2015.

[221] E. Nagler, "Standing Still," *racfoundation.org*, 2021. https://www.racfoundation.org/wp-content/uploads/standing-still-Nagler-June-2021.pdf.

[222] EV Database, "Nissan Leaf 30 kWh," *Electric Vehicle Database*, 2021. .

[223] Department for Business Energy & Industrial Strategy, "Feed-in Tariff statistics," *gov.uk*, 2021. https://www.gov.uk/government/collections/feed-in-tariff-statistics (accessed Apr. 15, 2021).

[224] R. Harrabin, "Ban on new petrol and diesel cars in UK from 2030 under PM's green plan - BBC News," Nov. 2020. .

[225] T. Wills, "The UK's transition to electric vehicles," 2020. [Online]. Available: https://www.theccc.org.uk/wp-content/uploads/2020/12/The-UKs-transition-to-electric-vehicles.pdf.

[226] W. Tushar, T. K. Saha, C. Yuen, D. Smith, and H. V. Poor, "Peer-to-Peer Trading in Electricity Networks: An Overview," *IEEE Trans. Smart Grid*, vol. 11, no. 4, pp. 3185–3200, Jul. 2020, doi: 10.1109/TSG.2020.2969657.

[227] Z. Li and T. Ma, "Peer-to-peer electricity trading in grid-connected residential communities with household distributed photovoltaic," *Appl. Energy*, vol. 278, p. 115670, Nov. 2020, doi: 10.1016/j.apenergy.2020.115670.

[228] N. S. Pearre and H. Ribberink, "Review of research on V2X technologies, strategies, and operations," *Renewable and Sustainable Energy Reviews*, vol. 105. Elsevier Ltd, pp. 61–70, May 2019, doi: 10.1016/j.rser.2019.01.047.

[229] C. Zhang, J. Wu, C. Long, and M. Cheng, "Review of Existing Peer-to-Peer Energy Trading Projects," in *Energy Procedia*, May 2017, vol. 105, pp. 2563–2568, doi: 10.1016/j.egypro.2017.03.737.

[230] NEMO Committee, "EUPHEMIA Public Description," 2019. [Online]. Available: https://www.nordpoolgroup.com/globalassets/download-center/single-day-ahead-coupling/euphemia-public-description.pdf.

[231] Y. Liu, K. Zuo, X. (Amy) Liu, J. Liu, and J. M. Kennedy, "Dynamic pricing for decentralized

energy trading in micro-grids," *Appl. Energy*, vol. 228, no. June, pp. 689–699, 2018, doi: 10.1016/j.apenergy.2018.06.124.

[232] M. H. Cintuglu, H. Martin, and O. A. Mohammed, "Real-time implementation of multiagent-based game theory reverse auction model for microgrid market operation," *IEEE Trans. Smart Grid*, vol. 6, no. 2, pp. 1064–1072, Mar. 2015, doi: 10.1109/TSG.2014.2387215.

[233] A. Paudel and H. B. Gooi, "Pricing in Peer-to-Peer Energy Trading Using Distributed Optimization Approach," pp. 1–5, 2020, doi: 10.1109/pesgm40551.2019.8973868.

[234] D. Parra, S. A. Norman, G. S. Walker, and M. Gillott, "Optimum community energy storage system for demand load shifting," *Appl. Energy*, vol. 174, pp. 130–143, Jul. 2016, doi: 10.1016/j.apenergy.2016.04.082.

[235] S. Dong, E. Kremers, M. Brucoli, R. Rothman, and S. Brown, "Establishing the value of community energy storage: A comparative analysis of the UK and Germany," *J. Energy Storage*, vol. 40, p. 102709, Aug. 2021, doi: 10.1016/j.est.2021.102709.

[236] W. E. Hart *et al.*, *Pyomo — Optimization Modeling in Python*, vol. 67. Cham: Springer International Publishing, 2017.

[237] W. E. Hart, J.-P. Watson, and D. L. Woodruff, "Pyomo: modeling and solving mathematical programs in Python," *Math. Program. Comput.*, vol. 3, no. 3, pp. 219–260, Sep. 2011, doi: 10.1007/s12532-011-0026-8.

[238] A. Makhorin, "GLPK (GNU Linear Programming Kit)," 2012. https://www.gnu.org/software/glpk/ (accessed Apr. 06, 2021).

[239] C. Argue, "To what degree does temperature impact EV range?," *geotab.com*, 2020. https://www.geotab.com/blog/ev-range/ (accessed Jan. 28, 2021).

[240] E. Apostolaki-Iosifidou, P. Codani, and W. Kempton, "Measurement of power loss during electric vehicle charging and discharging," *Energy*, vol. 127, pp. 730–742, 2017, doi: 10.1016/j.energy.2017.03.015.

[241] E. Apostolaki-Iosifidou, W. Kempton, and P. Codani, "Reply to Shirazi and Sachs comments on 'Measurement of Power Loss During Electric Vehicle Charging and Discharging,'" *Energy*, vol. 142, pp. 1142–1143, 2018, doi: 10.1016/j.energy.2017.10.080.

[242] W. Schram, N. Brinkel, G. Smink, T. Van Wijk, and W. Van Sark, "Empirical evaluation of V2G round-trip efficiency," *SEST 2020 - 3rd Int. Conf. Smart Energy Syst. Technol.*, 2020, doi: 10.1109/SEST48500.2020.9203459.

[243] S. Rennie *et al.*, "UK Environmental Change Network (ECN) meteorology data: 1991-2015. Centre for Ecology & Hydrology (Natural Environment Research Council)," 2017.

[244] World Bank Group, ESMAP, and Solargis, "Map and data downloads," *globalsolaratlas.info*, 2019. https://globalsolaratlas.info/download (accessed Jun. 04, 2021).

[245] C. Moldrich, "How much does it cost to charge an electric car? Running costs explained," *carmagazine.co.uk*, 2020. https://www.carmagazine.co.uk/electric/how-much-ev-charging-and-running-cost/ (accessed Jun. 04, 2021).

[246] Pod Point, "Cost of charging an electric car," *pod-point.com*, 2021. https://pod-point.com/guides/driver/cost-of-charging-electric-car (accessed Jun. 04, 2021).

[247] J. Jolly, "UK electric car sales surge despite Covid lockdown," *theguardian.com*, 2021. https://www.theguardian.com/business/2021/apr/06/uk-electric-car-sales-covid-lockdown (accessed Apr. 15, 2021).

[248] T. D. Hutty, A. Pena-Bello, S. Dong, D. Parra, R. Rothman, and S. Brown, "Peer-to-peer

electricity trading as an enabler of increased PV and EV ownership," *Energy Convers. Manag.*, vol. 245, p. 114634, Oct. 2021, doi: 10.1016/j.enconman.2021.114634.

[249] D. Zhu *et al.*, "Energy trading in microgrids for synergies among electricity, hydrogen and heat networks," *Appl. Energy*, vol. 272, p. 115225, Aug. 2020, doi: 10.1016/j.apenergy.2020.115225.

[250] N. Wang, Z. Liu, P. Heijnen, and M. Warnier, "A peer-to-peer market mechanism incorporating multi-energy coupling and cooperative behaviors," *Appl. Energy*, vol. 311, p. 118572, Apr. 2022, doi: 10.1016/j.apenergy.2022.118572.

[251] Energy Saving Trust, "Micro combined heat and power," *energysavingtrust.org.uk*, 2022. https://energysavingtrust.org.uk/advice/micro-combined-heat-and-power/.

[252] D. H. Nguyen and T. Ishihara, "Distributed peer-to-peer energy trading for residential fuel cell combined heat and power systems," *Int. J. Electr. Power Energy Syst.*, vol. 125, p. 106533, Feb. 2021, doi: 10.1016/j.ijepes.2020.106533.

[253] P. Vytelingum, D. Cliff, and N. R. Jennings, "Strategic bidding in continuous double auctions," *Artif. Intell.*, vol. 172, no. 14, pp. 1700–1729, Sep. 2008, doi: 10.1016/j.artint.2008.06.001.

[254] K. Chen, J. Lin, and Y. Song, "Trading strategy optimization for a prosumer in continuous double auction-based peer-to-peer market: A prediction-integration model," *Appl. Energy*, vol. 242, pp. 1121–1133, May 2019, doi: 10.1016/j.apenergy.2019.03.094.

[255] S. Thakur, B. P. Hayes, and J. G. Breslin, "Distributed Double Auction for Peer to Peer Energy Trade using Blockchains," in *2018 5th International Symposium on Environment-Friendly Energies and Applications (EFEA)*, Sep. 2018, pp. 1–8, doi: 10.1109/EFEA.2018.8617061.

[256] H. Haggi and W. Sun, "Multi-Round Double Auction-Enabled Peer-to-Peer Energy Exchange in Active Distribution Networks," *IEEE Trans. Smart Grid*, vol. 12, no. 5, pp. 4403–4414, Sep. 2021, doi: 10.1109/TSG.2021.3088309.

[257] C. Zhang, T. Yang, and Y. Wang, "Peer-to-Peer energy trading in a microgrid based on iterative double auction and blockchain," *Sustain. Energy, Grids Networks*, vol. 27, p. 100524, Sep. 2021, doi: 10.1016/j.segan.2021.100524.

[258] I. Herrero, P. Rodilla, and C. Batlle, "Evolving Bidding Formats and Pricing Schemes in USA and Europe Day-Ahead Electricity Markets," *Energies*, vol. 13, no. 19, p. 5020, Sep. 2020, doi: 10.3390/en13195020.

[259] W. Gan, M. Yan, W. Yao, and J. Wen, "Peer to peer transactive energy for multiple energy hub with the penetration of high-level renewable energy," *Appl. Energy*, vol. 295, p. 117027, Aug. 2021, doi: 10.1016/j.apenergy.2021.117027.

[260] M. Davoudi and M. Moeini-Aghtaie, "Local energy markets design for integrated distribution energy systems based on the concept of transactive peer-to-peer market," *IET Gener. Transm. Distrib.*, vol. 16, no. 1, pp. 41–56, Jan. 2022, doi: 10.1049/gtd2.12274.

[261] M. Shi, H. Wang, P. Xie, C. Lyu, and Y. Jia, "Distributed Energy Scheduling for Integrated Energy System Clusters with Peer-to-Peer Energy Transaction," *IEEE Trans. Smart Grid*, pp. 1–1, 2022, doi: 10.1109/TSG.2022.3197435.

[262] R. Jing, M. N. Xie, F. X. Wang, and L. X. Chen, "Fair P2P energy trading between residential and commercial multi-energy systems enabling integrated demand-side management," *Appl. Energy*, vol. 262, p. 114551, Mar. 2020, doi: 10.1016/j.apenergy.2020.114551.

[263] A. G. Daryan, A. Sheikhi, and A. A. Zadeh, "Peer-to-Peer Energy sharing Among Smart Energy Hubs in an integrated Heat-Electricity Network," *Electr. Power Syst. Res.*, vol. 206, p.

107726, May 2022, doi: 10.1016/j.epsr.2021.107726.

[264] C. Preist and M. van Tol, "Adaptive agents in a persistent shout double auction," in *Proceedings of the first international conference on Information and computation economies - ICE '98*, 1998, pp. 11–18, doi: 10.1145/288994.288998.

[265] S. Rennie and J. Adamson, "UK Environmental Change Network (ECN) meteorology data: 1991-2015," *Centre for Ecology & Hydrology (Natural Environment Research Council)*, 2017. https://doi.org/10.5285/fc9bcd1c-e3fc-4c5a-b569-2fe62d40f2f5.

[266] E. McKenna and M. Thomson, "High-resolution stochastic integrated thermal–electrical domestic demand model," *Appl. Energy*, vol. 165, pp. 445–461, Mar. 2016, doi: 10.1016/j.apenergy.2015.12.089.

[267] M. Brunner, S. Tenbohlen, and M. Braun, "Heat pumps as important contributors to local demand-side management," in *2013 IEEE Grenoble Conference*, Jun. 2013, pp. 1–7, doi: 10.1109/PTC.2013.6652381.

[268] Ofgem, "Check if the energy price cap affects you," *ofgem.gov.uk*, 2022. https://www.ofgem.gov.uk/check-if-energy-price-cap-affects-you.

[269] Solar Energy UK, "Smart Export Guarantee League Table," *solarenergyuk.org*, 2022. https://solarenergyuk.org/resource/smart-export-guarantee/.

[270] RAC, "Cost to rapid charge an electric car rises by a fifth in eight months," *rac.co.uk*, 2022. https://www.rac.co.uk/drive/news/rac-news/cost-to-rapid-charge-an-electric-car-rises-by-a-fifth-in-eight-months/.

[271] KPMG, "The hydrogen trajectory," *KPMG*, 2022. https://home.kpmg/xx/en/home/insights/2020/11/the-hydrogen-trajectory.html#:~:text=Cost of green hydrogen from,-6 USD%2Fkg H2.

[272] L. Collins, "Green hydrogen to become cheaper than grey," *rechargenews.com*, 2022. https://www.rechargenews.com/energy-transition/violent-shakedown-green-hydrogen-to-become-cheaper-than-grey-within-two-years-says-analyst/2-1-1147440.

[273] BEIS, "Green Book supplementary guidance: valuation of energy use and greenhouse gas emissions for appraisal," *gov.uk*, 2021. https://www.gov.uk/government/publications/valuation-of-energy-use-and-greenhouse-gas-emissions-for-appraisal.

[274] M. D. A. Albert, K. O. Bennett, C. A. Adams, and J. G. Gluyas, "Waste heat mapping: A UK study," *Renew. Sustain. Energy Rev.*, vol. 160, p. 112230, May 2022, doi: 10.1016/j.rser.2022.112230.

[275] Ofgem, "The Decarbonisation of Heat," 2016. [Online]. Available: https://www.ofgem.gov.uk/sites/default/files/docs/2016/11/ofgem_future_insights_programme_-_the_decarbonisation_of_heat.pdf.

[276] S. Read, "Solar panel sales boom as energy bills soar," *bbc.co.uk*, 2022. https://www.bbc.co.uk/news/business-62524031.

[277] ICAEW Insights, "Chart of the week: energy price cap update," *icaew.com*, 2022. https://www.icaew.com/insights/viewpoints-on-the-news/2022/sept-2022/chart-of-the-week-energy-price-cap-update.